REINFORCED CONCRETE DEEP BEAMS

Edited by F. K. Kong

BLACKIE

Reinforced Concrete Deep Beams

Reinforced Concrete Deep Beams

Edited by

PROFESSOR F.K.KONG
Professor of Structural Engineering
Department of Civil Engineering
University of Newcastle-upon-Tyne

Blackie
Glasgow and London

Van Nostrand Reinhold
New York

Blackie and Son Ltd
Bishopbriggs, Glasgow G64 2NZ
and
7 Leicester Place, London WC2H 7BP

Published in the United States of America by
Van Nostrand Reinhold
115 Fifth Avenue
New York, New York 10003

This edition published in the Taylor & Francis e-Library, 2002.

Distributed in Canada by
Nelson Canada
1120 Birchmount Road
Scarborough, Ontario M1K 5G4, Canada

First published 1990

British Library Cataloguing in Publication Data

Reinforced concrete deep beams.
1. Structural components: Deep reinforced concrete beams. Design
I. Kong, F.K. (Fung Kew) *1935–*
624.1'83423

ISBN 0-216-92695-5 (Print Edition)

Library of Congress Cataloging-in-Publication Data

Reinforced concrete deep beams/edited by F.K.Kong.
p. cm.
Includes bibliographical references.
ISBN 0-442-30298-3 (Print Edition)
1. Concrete beams—Testing. 2. Reinforced concrete construction.
I. Kong, F.K.
TA683.5.B3R45 1990
624. 1′83423—dc20 89–70433
CIP

ISBN 0-203-03488-0 Master e-book ISBN
ISBN 0-203-19142-0 (Glassbook Format)

Preface

This book is designed as an international reference work on the behaviour, design and analysis of reinforced concrete deep beams. It is intended to meet the needs of practising civil and structural engineers, consulting engineering and contracting firms, research institutes, universities and colleges.

Reinforced concrete deep beams have many useful applications, particularly in tall buildings, foundations and offshore structures. However, their design is not covered adequately by national codes of practice: for example the current British Code BS 8110, explicitly states that 'for design of deep beams, reference should be made to specialist literature'. The major codes and manuals that contain some discussion of deep beams include the American ACI Building Code, the draft Eurocode EC/2, the Canadian Code, the CIRIA Guide No. 2, and Reynolds and Steedman's *Reinforced Concrete Designer's Handbook*. Of these, the CIRIA Guide No. 2: *Design of Deep Beams in Reinforced Concrete,* published by the Construction Industry Research and Information Association in London, gives the most comprehensive recommendations.

The contents of the book have been chosen with the following main aims: (i) to review the coverage of the main design codes and the CIRIA Guide, and to explain the fundamental behaviour of deep beams; (ii) to provide information on design topics which are inadequately covered by the current codes and design manuals: deep beams with web openings, continuous deep beams, flanged deep beams, deep beams under top and bottom loadings and buckling and stability of slender deep beams; (iii) to give authoritative reviews of some powerful concepts and techniques for the design and analysis of deep beams such as the softened-truss model, the plastic method and the finite element method.

The contributing authors of this book are so eminent in the field of structural concrete that they stand on their own reputation and I feel privileged to have had the opportunity to work with them. I only wish to thank them for their high quality contributions and for the thoroughness with which their chapters were prepared.

I wish to thank Mr A.Stevens, Mr J.Blanchard and Mr E.Booth of Ove Arup and Partners for valuable discussions, and to thank Emeritus Professor R.H.Evans, C.B.E., of the University of Leeds for his guidance over the years. Finally, I wish to thank Mrs Diane Baty for the much valued secretarial support throughout the preparation of this volume.

F.K.K.

Contributors

Dr M.W.Braestrup
Rambull and Hannemann, Taknikerbyen 38, Copenhagen virum, Denmark 2830.

Born in 1945, M.W.Braestrup obtained his M.Sc. in Structural Engineering from the Technical University of Denmark, where he completed his Ph.D. in 1970. After two years of voluntary service in the Peruvian Andes he was engaged in research and teaching on plastic analysis of structural concrete, including a year as a visitor at the Cambridge University Engineering Department. In the autumn of 1979 Dr Braestrup joined the consulting engineering company Rambøll & Hannemann, where he became an expert on submarine pipeline technology, whilst also continuing his activities in the concrete field. He is currently head of the department for Knowledge and Development, being responsible for the management and execution of R&D projects. Dr Braestrup is the author of many papers and reports on concrete plasticity and marine pipelines.

Dr H.C.Chan
Department of Civil Engineering, University of Hong Kong, Hong Kong.

Hon-Chuen Chan graduated in Civil Engineering from the University of Hong Kong and then received his Ph.D. degree from the Imperial College of Science and Technology of London University in 1965. After working for several years in consulting engineering firms in Britain and Hong Kong, he took up teaching at the University of Hong Kong and is now a senior lecturer in the Department of Civil and Structural Engineering, teaching subjects in structural theory, engineering mechanics and design of reinforced concrete structures. He has also practised as a consulting engineer in the capacity of a partner with Harris and Sutherland (Far East). His publication includes some fifty technical reports and papers in international journals and conference proceedings.

Dr M.Chemrouk
Department of Civil Engineering, University of Newcastle upon Tyne, Newcastle upon Tyne, NE1 7RU, UK.

M.Chemrouk is a lecturer at the Université des Sciènces et de la Technologie Houari Boumediene, Institut de Genie Civil, Algeria. He did his Ph.D. research at the University of Newcastle upon Tyne, under an Algerian Government Scholarship. He has co- authored several papers on the subject of reinforced concrete deep beams, including a paper published in *The Structural Engineer* which won a Henry Adams Award diploma from the Institution of Structural Engineers.

Professor Y.K.Cheung
Department of Civil Engineering, University of Hong Kong, Hong Kong.

Y.K.Cheung was born in Hong Kong and having obtained his B.Sc. degree at the South

China Institute of Technology was awarded a Ph.D. from the University of Wales in 1964. After two years as a lecturer at University College, Swansea, he became Associate Professor (1967) and then Professor of Civil Engineering (1970) at the University of Calgary. In 1974 he took up the chair of Civil Engineering in the University of Adelaide, returning to the University of Hong Kong in 1977 as Head of Civil Engineering and, for ten years, Dean of Engineering. He is at present the Pro-Vice- Chancellor and Head of Department of Civil and Structural Engineering, University of Hong Kong. His work has been recognised by the presentation of D.Sc. and D.Eng. degrees and by his election to the Fellowship of Engineering. He has also been awarded an Honorary Fellowship and three Honorary Professorships. Professor Cheung served as the first Senior Vice-President in the Hong Kong Institution of Engineers and is on the Editorial Advisory Board of eight international journals. His own publications include five books and over two hundred journal articles.

Professor A.R.Cusens
Department of Civil Engineering, University of Leeds, Leeds, LS2 9JT, UK.

A.R.Cusens is currently Professor and Head of Civil Engineering at the University of Leeds. His professional career began at University College London, and after short spells at Wexham Springs and RMCS Shrivenham, his interests took him to the University of Khartoum and the Asian Institute of Technology, Bangkok. He returned in 1965 to head the new Department of Civil Engineering at the University of Dundee and moved to his present position in Leeds in 1979. He has been involved in research on concrete technology and concrete structures for many years. In particular he has carried out comprehensive analytical and experimental studies of bridge decks. His interest in deep beams stems from unanswered questions arising from a specific building design he worked upon some years ago and subsequent research studies.

Dr A.Gogate
Gogate Engineers, 2626 Billingsley Road, Worthington, Ohio 43085, USA.

A.Gogate is President of the Gogate Engineering Firm, Ohio, USA. He was Associate Professor of Architecture at the Ohio State University from 1981–84. He has been in practice designing all types of building structures for 28 years. He earned his B.Eng. degree at Poona University in India in 1958, his M.S. degree at Iowa University in 1963, and his Ph.D. at Ohio State University. He has won several engineering awards including the ASCE Raymond C.Reese Award, the ASCE 'State of the Art' award for work related to shear strength of concrete members, and the OSPE award for obtaining the highest P.E. examination grade in 1968. He has published several papers in various concrete journals. Dr Gogate is a Fellow of the American Concrete Institute and of the American Society of Civil Engineers.

Professor T.C.Hsu
Department of Civil Engineering, University of Houston, 4800 Calhoun Road, Houston, Texas 77004, USA.

T.C.Hsu is Professor and former Chairman in the Civil and Environmental Engineering Department, University of Houston. He was Development Engineer at Portland Cement Association from 1962 to 1968, and a Professor and Chairman in the Civil Engineering

Department, University of Miami from 1968 to 1980. A fellow of the American Society of Civil Engineers and the American Concrete Institute, Dr Hsu was the recipient of ACI Wason Medal, ASEE Research Award, and ASCE Huber Prize. He is a member of ACI National Technical Committee 215, Fatigue, and 358, Concrete Guideways, and of joint ACI-ASCE Committee 343, Concrete Bridge Design, and 445, Shear and Torsion.

Professor F.K.Kong
Department of Civil Engineering, University of Newcastle upon Tyne, Newcastle upon Tyne, NE1 7RU, UK.

F.K.Kong, M.A., M.Sc., Ph.D., C.Eng., FICE, F.I.Struct.E. is Professor of Structural Engineering at the University of Newcastle upon Tyne in England. Professor Kong is a member of the Royal Society's National Committee for Theoretical and Applied Mechanics, and a member of the Structural Engineering Group Board of the Institution of Civil Engineers. He is a member of the Institution of Structural Engineers Council and Executive Committee, and was twice elected Chairman of the Northern Counties Branch of the Institution. He was appointed to the Chair at Newcastle in 1981, after nine years at Cambridge University, where he was a University Lecturer in Engineering, Fellow of Girton College, and Director of Engineering Studies. He had earlier done research work at Leeds University and taught at the Universities of Hong Kong and Nottingham, and worked for consulting engineers in Hong Kong and the United Kingdom. Professor Kong is the chief Editor of McGraw Hill's *International and University Series in Civil Engineering* and the chief Editor of Longman's new *Concrete Design and Construction Series* and has, jointly with ACI Past President Edward Cohen and Professor R.H.Evans and F.Roll, edited the 2000-page *Handbook of Structural Concrete* published by Pitman in London and McGraw Hill in New York. He has published many research papers, four of which have won awards from the Institution of Structural Engineers.

Dr M.D.Kotsovos
Department of Civil Engineering, Imperial College, London SW7 2BU, UK.

M.D.Kotsovos, D.Sc., Ph.D., DIC, M.I.Struct.E., C.Eng., is a lecturer in the Department of Civil Engineering at Imperial College of Science, Technology and Medicine in London. His interests and research activities cover a wide range of topics related to concrete structures and technology such as fracture processes, strength and deformation characteristics of concrete under multi-axial states of stress, constitutive relations of concrete under generalised stress, non-linear finite element analysis of concrete structures under static and dynamic loading conditions, and structural concrete design, with emphasis on earthquake resistant design of concrete structures.

Dr S.T.Mau
Department of Civil Engineering, University of Houston, 4800 Calhoun Road, Houston, Texas 77004, USA.

S.T.Mau, Ph.D., is Professor of Civil Engineering at the University of Houston where he has been since 1985. Prior to that he was Professor and Chairman of the Department of Civil Engineering at National Taiwan University, where he had received his B.S. and M.S.

degree. Dr Mau received his Ph.D. degree in structural engineering from Cornell University and was a Senior Research Engineer at MIT in the Department of Aeronautics and Astronautics. He has more than 50 publications in reinforced concrete, computational mechanics and structural dynamics. He is a co-recipient of the 1989 Mosseiff Award of the American Society of Civil Engineers.

Dr S.P.Ray
Department of Civil Engineering, Regional Institute of Technology, Jamshedpur, Bihar, India.

S.P.Ray obtained a first class BCE degree from Jadavpur University in 1965, ME (Civil) degree from Calcutta University in 1968 and Ph.D. degree from the Indian Institute of Technology, Karagpur, India in 1982. He worked on a pre-stressed concrete research project at Bengal Engineering College, Howrah, India, as a Senior Research Fellow of the University Grants Commission. He taught at Jalpaiguri Government Engineering College, North Bengal, India, as a Pool Officer of the Council of Scientific and Industrial Research. He has published a number of research papers on plain, reinforced and pre-stressed concrete in reputable journals. He received the Institution of Engineers' research award 'Certificate of Merit' in 1974. He is now a member of the teaching faculty of the Civil Engineering Department at Regional Institute of Technology, Jamshedpur, India. He is also actively involved in research and consultancy work on various Civil Engineering problems.

Dr D.M.Rogowsky
Underwood McLellan Ltd, 1479 Buffalo Place, Winnepeg, Manitoba, Canada R3T 1L7.

D.M.Rogowsky is Head of Special Developments for VSL International Ltd., Bern, Switzerland, a firm which specialises in post-tensioned concrete. He was formerly Chief Structural Engineer for UMA Engineering Ltd. in Winnipeg, Canada where he was involved in the design, assessment and repair of various industrial structures. His research interests inlcude the development of post-tensioning systems, water-retaining structures, material storage silos and concrete slab design. He was co-recipient of the American Concrete Institute Reese Structural Research Award for work related to deep beam design. As an active member of the Institute, Dr Rogowsky serves on various ACI technical committees.

Dr H.T.Solanki
Smally Wellford and Nalven, Inc., 3012 Bucida Drive, Sarasota, FL 34232, USA.

H.T.Solanki is a senior structural engineer in the engineering and architectural firm of Iffland Kavanagh Waterbury, New York, USA. His professional career includes over 22 years of design and construction practice in engineering. He was educated in Civil Engineering at the Gujarat University, Ahmedabad, India, where he received a bachelor degree. He has completed graduate and postgraduate course work at the University of South Florida, Tampa, Florida, and has published several papers in technical journals. He is a Registered Professional Engineer in the States of New York, Florida and Pennsylvania, and is a member of the American Concrete Institute, American Society of Civil Engineers,

Institution of Engineers (India) and International Society of Soil Mechanics and Foundation Engineering.

Dr H.H.A.Wong
Ove Arup and Partners, Consulting Engineers, London, UK.

H.H.A.Wong obtained his B.Sc. degree in 1983 and his Ph.D. in 1987, at the University of Newcastle upon Tyne. Formerly a Hong Kong Croucher Foundation Scholar at the University of Newcastle upon Tyne, Dr Wong has received the Institution of Structural Engineers Henry Adams Award for a research paper on slender deep beams, co-authored with Professor, F.K.Kong and others. Dr Wong's research interests are in the structural stability of concrete members and in the application of computers to the analysis and design of concrete structures. Since 1987 Dr Wong has been a structural engineer with Ove Arup and Partners and has worked on a number of building projects, and has been involved in the development of Arup's in-house computer system.

Contents

1 Reinforced concrete deep beams

F.K.KONG and M.CHEMROUK, University of Newcastle upon Tyne

Notation

A_h	area of horizontal web reinforcement with a spacing sh
A_r	area of reinforcement bar
A_s	area of main longitudinal reinforcement
A_v	area of vertical web reinforcement within a spacing s_v
b	beam thickness
c, c_1, c_2	support lengths
d	effective depth
f'_c	concrete cylinder compressive strength
f_{cu} (f_y)	characteristic strength of concrete (of reinforcement)
h	overall height of beam
h_a	effective height of beam
l	effective span
l_o	clear distance between faces of supports
M	moment
M_u	design ultimate moment; moment capacity
s_h	spacing of horizontal web reinforcement
s_v	spacing of vertical web reinforcement
V	shear force
V_c	shear strength provided by concrete
v_c	shear stress value
V_n	nominal shear strength
V_s	shear strength provided by steel
V_u	design ultimate shear force; shear capacity
v_u	ultimate shear stress value
v_x, v_{ms}, v_{wh}, v_{wv}	shear stress parameters
x	clear shear span; shear span
x_e	effective clear shear span
y_r	distances defined in Eqn (1.11)
z	lever arm
γm	partial safety factor for material (typically, γ_m=1.15 for reinforcement and 1.5 for concrete)
θ	angle
θr	angle defined in Eqn (1.11) and Figure 1.3
λ	coefficient
λ_1	coefficient
λ_2	coefficient
ρ	steel ratio A_s/bd
ϕ	capacity reduction factor; angle

1.1 Introduction

Recent lectures delivered at Ove Arup and Partners, London (Kong, 1986a), and at the Institution of Structural Engineers' Northern Counties Branch in Newcastle upon Tyne (Kong, 1985), have shown that reinforced concrete deep beams is a subject of considerable interest in structural engineering practice. A deep beam is a beam having a depth comparable to the span length. Reinforced concrete deep beams have useful applications in tall buildings, offshore structures, and foundations. However, their design is not yet covered by BS 8110, which explicitly states that 'for the design of deep beams, reference should be made to specialist literature'. Similarly, the draft Eurocode EC/2 states that 'it does not apply however to deep beams…' and

refers readers instead to the CEB-FIP Model Code. Currently, the main design documents are the American code ACI 318–83 (revised 1986), the Canadian code CAN-A23.3-M84, the CEB-FIP Model Code and the CIRIA Guide 2. Of these, the CIRIA Guide gives the most comprehensive recommendations and is the only one that covers the buckling strength of slender beams.

The transition from ordinary-beam behaviour to deep-beam behaviour is imprecise; for design purposes, it is often considered to occur at a span/depth ratio of about 2.5 (Kong, 1986b). Although the span/depth ratio *l/h* is the most frequently quoted parameter governing deep-beam behaviour, the importance of the shear-span/depth ratio *l/h* was emphasised many years ago (Kong and Singh, 1972) and, for buckling and instability, the depth/thickness ratio *l/h* and the load-eccentricity/thickness ratio *l/h* are both relevant (Garcia, 1982; Kong *et al.,* 1986).

1.2 History and development

Classic *literature reviews* have been compiled by Albritton (1965), the Cement and Concrete Association (C&CA) (1969) and Construction Industry Research and Information Association (CIRIA) (1977), which have been supplemented by the reviews of Tang (1987), Wong (1987) and Chemrouk (1988). These show that the early investigations were mostly on the elastic behaviour. Of course, elastic studies can easily be carried out nowadays, using the standard finite difference and finite element techniques (Coates *et al.,* 1988; Zienkiewicz and Taylor, 1989). However, a serious disadvantage of elastic studies is the usual assumption of isotropic materials obeying Hooke's law; hence they do not give sufficient guidance for practical design.

It was not until the 1960s that systematic *ultimate load tests* were carried out by de Paiva and Siess (1965) and Leonhardt and Walther (1966). These tests were a major step forward in deep beam research. They revealed a concern for empirical evidence which reflected the philosophy of the European Concrete Committee (CEB, 1964) which stated that 'the Comité Européen du Béton considered that the 'Principles' and 'Recommendations' should be fundamentally and solely based on experimental knowledge of the actual behaviour…' The lead provided by these pioneers was subsequently followed by many others in different parts of the world (reviews by CIRIA, 1977; Chemrouk, 1988).

In the late 1960s an extensive long-term programme was initiated by Kong and is still continuing at the University of Newcastle upon Tyne; tests to destruction have so far been carried out on over 490 deep beams, which included large specimens weighing 4.5 t. each (Figure 1.1 and Kong *et al.,* 1978; Kong and Kubik, 1991) and slender specimens of height/thickness ratio *h/b* up to 67 (Kong *et al.,* 1986).

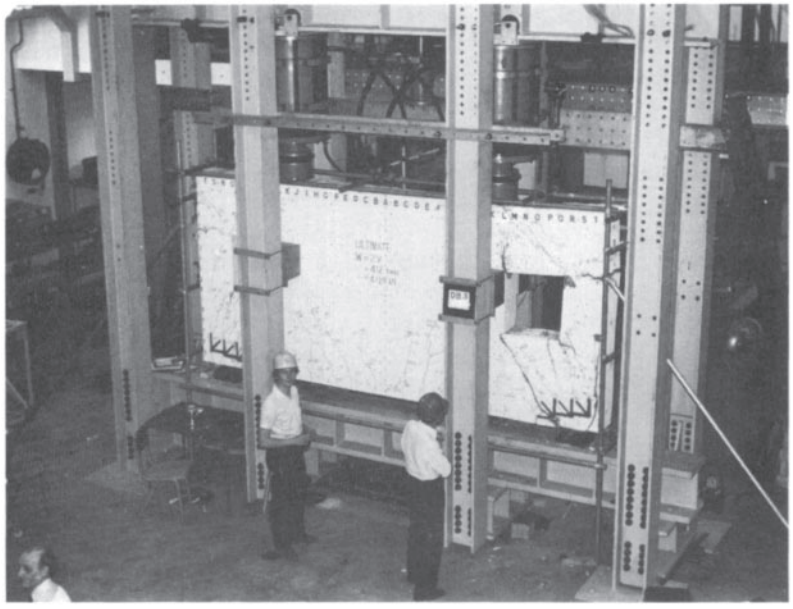

Figure 1.1 Test on a large deep beam (after Kong and Kubik, 1991)

The solution of deep-beam type problem using *plasticity concepts* was reported by Nielsen (1971) and Braestrup and Nielsen (1983); shear strength prediction by the plastic method is covered in Chapter 8 of this book. Kong and Robins (1971) reported that *inclined web reinforcement* was highly effective for deep beams; this was confirmed by Kong and Singh (1972) and Kong *et al.* (1972a) who also proposed a method for comparing quantitatively the effects of different types of web reinforcement (Kong *et al.,* 1972b). Kong and Sharp (1973) reported on the strength and failure modes of deep beams with *web openings;* the proposed formula for predicting the ultimate load was subsequently refined (Kong and Sharp, 1977; Kong *et al.,* 1978) and adopted by the *Reinforced Concrete Designer's Handbook* (Reynolds and Steedman, 1981 and 1988). The topic has been followed up by Ray (1980) and others and is the subject of Chapter 3. Robins and Kong (1973) used *the finite element method* to predict the ultimate loads and crack patterns of deep beams; Taner *et al.* (1977) reported that the finite element method gave good results when applied to flanged deep beams. The finite element method is now covered in Chapter 9 and *flanged deep beams* in Chapter 5. Serviceability and failure under *repeated loading* was studied by Kong and Singh (1974). Garcia (1982) was among the first to carry out *buckling tests* on a substantial series of slender concrete deep beams; these and the subsequent tests by Kong *et al.* (1986) and others are discussed in Chapter 10. The effects of *top and bottom loadings,* the subject of Chapter 6, was

studied by Cusens and Besser (1985) and, less systematically, by a few others earlier (CIRIA, 1977). Rogowsky *et al,* (1986) carried out extensive tests on *continuous deep beams,* which is the subject of Chapter 4. Mau and Hsu (1987) applied the *softened truss model theory* to deep beams; see Chapter 7 for details. Kotsovos (1988) studied deep beams in the light of a comprehensive investigation into the fundamental causes of shear failure; Chapter 2 gives further details.

The major contributions of other active workers are referred to elsewhere in this volume; mention need only be made here of Barry and Ainso (1983), Kubik (1980), Mansur and Alwis (1984), Regan and Hamadi (1981), Rasheeduzzafar and Al-Tayyib (1986), Roberts and Ho (1982), Shanmugan (1988), Singh *et al.* (1980), Smith and Vantsiotis (1982), Subedi (1988), and Swaddiwudhipong (1985).

With reference to Chapter 8, plastic methods have valuable applications in structural concrete. However, their more general acceptance has probably been hindered by the widespread confusion over the *fundamental plastic theorems* themselves (Kong and Charlton, 1983). For example, the plastic truss model proposed by Kumar (1976) could be shown to violate the *lower bound theorem* (Kong and Kubik, 1977). The difficulties are unlikely to be overcome until the currently widespread misunderstanding of the principle of virtual work can somehow be cured (Kong *et al.,* 1983b).

1.3 Current design practice

The subsequent sections of this chapter will summarise the main design recommendations of: the CIRIA Guide 2, the (draft) Eurocode and the CEBFIP Model Code, the ACI Code 318–83 (revised 1986) and the Canadian Code CAN-A23.3-M84

1.4 CIRIA Guide 2

The CIRIA Guide (CIRIA, 1977) applies to beams having an effective span/depth ratio l/h of less than 2 for single-span beams and less than 2.5 for continuous beams. The CIRIA Guide was intended to be used in conjunction with the British Code CP110:1972; however, the authors have done some comparative calculations (Kong *et al.,* 1986) and believe that the CIRIA Guide could safely be used with BS 8110:1985.

The Guide defines the *effective span* l and the *active height* h_a as follows (see meanings of symbols in Figure 1.2.)

$$l=l_o+[\text{lesser of } (c_1/2 \text{ and } 0.1\ l_o]+[\text{lesser of } (c_2/2) \text{ and } 0.1\ l_o] \qquad (1.1)$$

$$h_a=h \text{ or } l \text{ whichever is the lesser} \qquad (1.2)$$

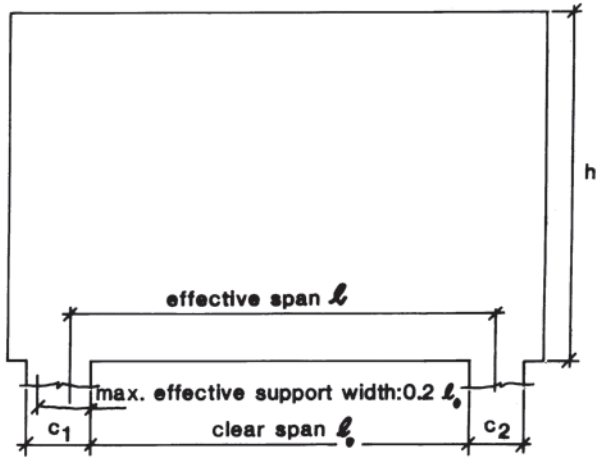

Figure 1.2 CIRIA Guide 2—meanings of symbols c_1, c_2, h, l and l_o

The CIRIA Guide considers that the active height h_a of a deep beam is limited to a depth equal to the span; that part of the beam above this height is taken merely as a load-bearing wall between supports.

1.4.1 *CIRIA Guide 'Simple Rules'*

CIRIA's 'Simple Rules' are intended primarily for uniformly loaded deep beams. They can be applied to both single-span and continuous beams.

1.4.1.1 Flexural strength

Step 1: Calculate the capacity of the concrete section.

$$M_u = 0.12 f_{cu} b h_a^2 \tag{1.3}$$

where f_{cu} is the concrete characteristic strength and b the beam thickness.

Step 2: If $l/h_a \leq .5$ go to step 3. If $l/h_a > 1.5$ check that the applied moment M does not exceed M_u of Eqn (1.3)

Step 3: Calculate the area A_s of the main longitudinal reinforcement:

$$A_s > M/0.87 f_y z \tag{1.4}$$

where M is the applied moment, f_y the steel characteristic strength and z the lever arm, which is to be taken as follows:

$$z = 0.2l + 0.4h_a \text{ for single-span beams} \tag{1.5}$$

$$z = 0.2l + 0.3h_a \text{ for continuous beams} \tag{1.6}$$

Step 4: Distribute the reinforcement A_s (Eqn (1.4)) over a depth of $0.2h_a$. Anchor the reinforcement bars to develop at least 80% of the maximum ultimate force beyond the face of the support. A proper

anchorage contributes to the confinement of the concrete at the supports and improves the bearing strength.

1.4.1.2 Shear strength: bottom-loaded beams

Step 1: Calculate the concrete shear capacity:

$$V_u = 0.75 b h_a v_u \tag{1.7}$$

where v_u is the maximum shear stress taken from Table 6 of CPI 10 (1972) for normal weight concrete and Table 26 for lightweight concrete (see also BS 8110: Part 1: clause 3.4.5.2 and Part 2: clause 5.4)

Step 2: Check that the applied shear force V does not exceed V_u of Eqn (1.7)

Step 3: Provide hanger bars in both faces to support the bottom loads, using a design stress of $0.87 f_y$. The hanger bars should be anchored by a full bond length above the active height h_a or, alternatively, anchored as links around longitudinal bars at the top.

Step 4: Provide nominal horizontal web reinforcement over the lower half of the active height h_a and over a length of the span equal to 0.4ha measured from each support. The area of this web reinforcement should not be less than 80% that of the uniformly distributed hanger steel, per unit length. The bar spacing and reinforcement percentage should also meet the requirements of Section 1.4.1.5.

1.4.1.3 Shear strength: top-loaded beams. The proven concept of the *clear shear span x*, as used by Kong *et al.* (1972b and 1975) has been adopted by the CIRIA Guide. The CIRIA Guide has also accepted the Kong *et al.* (1972b) proposal that, for uniformly distributed loading, the *effective clear shear span* xe may be taken as *l*/4.

Step 1: With reference to Figure 1.3, calculate the effective clear shear span x_e which is to be taken as the least of:

i) The clear shear span for a load which contributes more than 50% of the total shear force at the support.
ii) *l*/4 for a load uniformly distributed over the whole span.
iii) The weighted average of the clear shear spans where more than one load acts and none contributes more than 50% of the shear force at the support. The weighted average will be calculated as $\Sigma(V_r x_r)/\Sigma V_r$ where $\Sigma V_r = V$ is the total shear force at the face of the support, V_r=an individual shear force and x_r=clear shear span of V_r.

Step 2: Calculate the shear capacity V_u to be taken as the value given by Eqns (1.8) and (1.9)

$$V_u = 2 b h_a^2 v_c / x_e \quad \text{for} \quad h_a / b < 4 \tag{1.8a}$$

$$V_u = 1.2bh_a^2 v_c / x_e \quad \text{for} \quad h_a / b \geq 4 \tag{1.8b}$$

$$V_u = bh_a v_u \tag{1.9}$$

where the x_e is the effective clear shear span calculated from step 1, v_u is as defined for Eqn (1.7) and v_c is the shear stress value taken from Table 5 of CP1 10 (1972) for normal weight concrete and Table 25 for lightweight concrete (see also BS 8110: Part 1: clause 3.4.5.4 and Part 2: clause 5.4).

Step 3: Check that the applied shear force V does not exceed the shear capacity V_u calculated in step 2.

Step 4: Provide nominal web reinforcement in the form of a rectangular mesh in each face. The amount of this nominal reinforcement should not be less than that required for a wall by clauses 3.11 and 5.5 of CP1 10 (1972); this in effect means at least 0.25% of deformed bars in each direction (see also BS 8110: Part 1: clauses 3.12.5.3 and 3.12.11.2.9). The vertical bars should be anchored round the main bars at the bottom; the horizontal bars should be anchored as links round vertical bars at the edges of the beam. The bar spacings and minimum percentage should also meet the requirements of section 1.4.1.5.

1.4.1.4 Bearing strength For deeper beams (l/h<1.5), the bearing capacity may well be the governing design criterion, particularly for those having shorter shear spans. To estimate the bearing stress at the support, the reaction may be considered uniformly distributed over an area equal to (the beam width b)×(the effective support length) where the effective support length is to be taken as the actual support length c or $0.2l_o$ whichever is the lesser. The bearing stress so calculated should not exceed $0.4f_{cu.}$

1.4.1.5 Crack control The minimum percentage of reinforcement, in the horizontal or vertical direction, should comply with the requirements for a wall, as given in clauses 3.11 and 5.5 of CP110 (1972) (see also BS 8110: Part 1: clauses 3.12.5.3 and 3.12.11.2.9). The maximum bar spacing should not exceed 250 mm. In a tension zone, the steel ratio ρ, calculated as the ratio of the total steel area to the local area of the concrete in which it is embedded, should satisfy the condition

$$\rho > (0.52\sqrt{f_{cu}})/(0.87f_y) \tag{1.10}$$

The maximum crack width should not be allowed to exceed 0.3 mm in a normal environment; in a more aggressive environment, the maximum crack width may have to be limited to 0.1mm. To control maximum crack widths to within 0.3 and 0.1mm, bar spacings should not exceed those given in Tables 2 and 3, respectively, of the CIRIA Guide.

1.4.1.6 Web openings See comment vi) in Section 1.4.2.4.

1.4.2 *CIRIA Guide 'Supplementary Rules'*

CIRIA's 'Supplementary Rules' cover aspects of the design of deep beams which are outside the scope of the 'Simple Rules' (Section 1.4.1) and are to be read in conjunction with the latter. The 'Supplementary Rules' cover concentrated loading, indirect loading and indirect supports but, because of space limitation, we shall deal here only with single-span beams under top loading.

1.4.2.1 Flexural strength The 'Simple Rules' of Section 1.4.1.1 can be used without modification.

1.4.2.2 Shear strength: top-loaded beams (see also the comments in Section 1.4.2.4).

Step 1: If the beam is under uniformly distributed loading, go to Step 3 or else use the more conservative 'Simple Rules' given in Section 1.4.1.3

Step 2: If the beam is under concentrated loading, go to step 3.

Step 3: Check that the applied shear force V does not exceed the limit imposed by Eqn (1.11); for a beam with a system of orthogonal web reinforcement. Eqn (1.11) can be expressed in the more convenient form of Eqn (1.12). Eqns (1.11) and (1.12) apply over the range 0.23–0.70 for x_e/h (see comment (ii) in Section 1.4.2.4). In using these equations, ignore any web reinforcement which is above the active height h_a.

$$\frac{V}{bh_a} < \lambda_1 \left[1 - 0.35\frac{x_e}{h_a}\right]\sqrt{f_{cu}} + \lambda_2 \sum \frac{100A_r y_r \sin^2\theta_r}{bh_a^2} \qquad (1.11)$$

where (see comments in Section 1.4.2.4) λ_1 is 0.44 for normal weight concrete and 0.32 for lightweight concrete, λ_2 is 1.95 N/mm^2 for deformed bars and 0.85 N/mm^2 for plain bars, b is the beam thickness, h_a is the active height of the beam (Eqn 1.2), A_r is the area of a typical web bar (for the purpose of Eqn (1.11), the main longitudinal bars are considered also to be web bars), y_r is the depth at which the typical web bar intersects the critical diagonal crack, which is represented by the line Y-Y in Figure 1.3, θ_r is the angle between the bar being considered and the line Y-Y in Figure 1.3 ($\theta_r \leq p/\pi$) and x_e is effective clear shear span as defined in step 1 of Section 1.4.1.3.

On the right-hand side of Eqn (1.11) the term $\lambda_1 [1 - 0.35x_e/h_a] \sqrt{f_{cu}}$ is the concrete contribution to the shear capacity. It is clear that this quantity can be tabulated from various values of x_e/h_a and f_{cu}. The term $\lambda_2 \sum (100A_r\, y_r \sin^2\theta_r/bh_a^2)$ is the steel

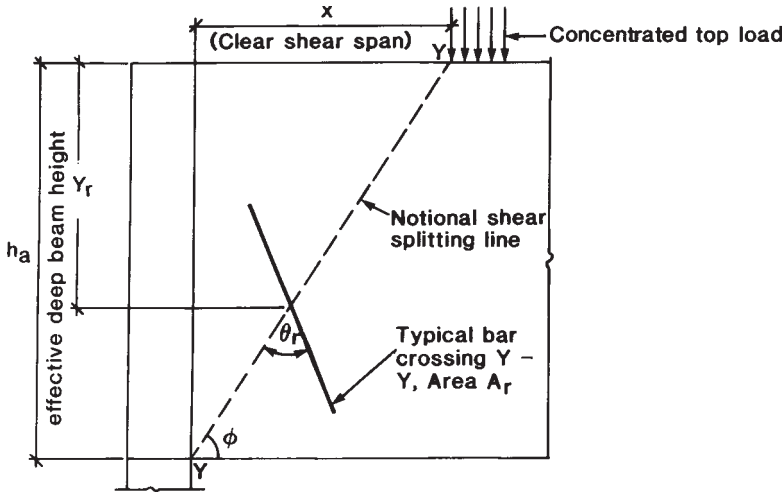

Figure 1.3 Meanings of symbols A_r. h_a, x, y_r, θ_r, ϕ (after CIRIA, 1977)

contribution to the shear capacity; for a beam with or thogonal web reinforcement; it can also be tabulated for various steel ratios and x_e/h_a ratios. In other words, for a beam with orthogonal web reinforcement, Eqn (1.11) can be expressed as Eqn (1.12), which is more convenient to use in design:

$$V/bh_a < \lambda_1 v_x + ß(v_{ms} + v_{wh} + v_{wv}) \tag{1.12}$$

where λ_1 is λ_1 in Eqn (1.11), v_x is the concrete shear stress parameter, as tabulated in Table 4 of the CIRIA Guide for various values of f_{cu} and the x_e/h_a ratio; ß is 1.0 for deformed bars and 0.4 for plain round bars; v_{ms} is the main steel shear stress parameter, as tabulated in Table 6 of the CIRIA Guide for various values of the main steel ratio and the x_e/h_a ratio; v_{wh} is the horizontal web steel shear stress parameter, as tabulated in Table 7 of the CIRIA Guide for various values of the horizontal web steel ratio and the x_e/h_a ratio; and v_{wv} is the vertical web steel shear stress parameter, as tabulated in Table 8 of the CIRIA Guide for various values of the vertical web steel ratio and the x_e/h_a ratio.

Step 4: From the calculations in step 3, check the total contribution of the (main and web) reinforcement to the shear capacity. The total contribution is given by the second term on the right-hand side of Eqn (1.11) (or Eqn (1.12)). If this is less than $0.2V$, increase the web reinforcement to bring the total steel contribution up to at least $0.2V$

Step 5: Check that the applied shear force V is less than the shear capacity of the concrete section:

$$V/bh_a < 1.3\lambda_1\sqrt{f_{cu}} \tag{1.13}$$

where λ_1 is as defined for Eqn. (1.11).

1.4.2.3 Bearing strength CIRIA's 'Supplementary Rules' allow the bearing stress limit (=$0.4f_{cu}$ in Section 1.4.1.4) to be increased to $0.6f_{cu}$ at the end supports and to $0.8f_{cu}$ under concentrated loads, provided the concrete in the stress zones is adequately confined, as specified in clause 3.4.3 of the CIRIA Guide.

1.4.2.4 Comments on Eqn (1.11) of Section 1.4.2.2

i) Eqn (1.11), taken from clause 3.4.2 of the CIRIA Guide (1977), is essentially the Kong *et al.* (1972b and 1975) equation. CIRIA, however, has modified the numerical values of the coefficients λ_1 and λ_2 to introduce the necessary factor of safety for the design purpose.

ii) According to the CIRIA Guide (1977), Eqns (1.11) and (1.12) apply only over the range 0.23 to 0.70 for x_e/h_a. This is because the test data then available (Kong *et al.,* 1972b; 1975) were limited to this range of x_e/h_a. However, as a result of more recent tests (Kong *et al.,* 1986), the authors believe that Eqns (1.11) and (1.12) can be applied to an extended range of x_e/h_a from 0 to 0.70.

iii) On the right-hand side of Eqn (1.11), the quantity $\lambda_1\sqrt{f_{cu}}\,bh_a$ is a measure of the load-carrying capacity of the concrete strut, along the line Y-Y in Figure 1.3. From the figure, it is seen that the capacity increases with the angle ϕ in Eqn (1.11), the factor $(1-0.35x_e/h_a)$ allows for the experimental observation of the way in which this capacity reduces with ϕ, (i.e. with an increase in the x_e/h_a ratio). When the load carried by the concrete strut is high enough, a splitting failure occurs, resulting in the formation of the diagonal crack along Y-Y in Figure 1.3. In Eqn (1.11), the quantity $\sqrt{f_{cu}}$ is a measure of the splitting strength of the concrete. After the formation of the diagonal crack, the concrete strut becomes in effect two eccentrically loaded struts. These eccentrically loaded struts are restrained against in-plane bending by the web reinforcement.

iv) On the right-hand side of Eqn (1.11), the second term represents the contribution of the reinforcement to the shear strength of the beam. The reinforcement helps the split concrete strut (iii)) to continue to carry loads, by restraining the propagation and widening of the diagonal crack. The beam has a tendency to fail in a mechanism in which the end portion of the beam moves outwards in a rotational motion about the loading point (Kong and Sharp, 1973). Thus, the lower down the reinforcement bar intersects the the diagonal crack, the more effective it would be in restraining this rotation. Hence in Eqn (1.11), the steel

contribution $\lambda_2 \Sigma (100A_r y_r \sin^2 \theta_r)/bh_a^2$ is proportional to y_r. The laws of equilibrium are unaware of the designer's discrimination between bars labelled as 'web reinforcement' and those labelled as 'main reinforcement'. Eqn (1.11) accepts any reinforcement bar (be it labelled as web bar or main bar) provided it effectively helps to preserve the integrity of the concrete web by restraining the propagation and widening of the diagonal crack. It judges the contribution of an individual bar by its area A_r, the depth y_r and the angle of intersection θ_r.

v) As explained earlier (Kong, 1986b) 'Eqn 1.11 focuses attention on the basic features of what in reality is a complex load-transfer mechanism; it does this by deleting quantities which are less important compared with the main elements—quantities whose inclusion will obscure the designer's understanding of the problem at the physical level. It is a useful tool in the hands of engineers who possess a sound understanding of statics, geometry and structural behaviour. Of course, the equation can be abused by indiscriminate application—as indeed can Codes of Practice be so abused. Consider, for example, a deep beam with a wide bottom flange, which contains two large-diameter longitudinal bars away from the plane of the web. These bars clearly do not effectively protect the integrity of the concrete web, though they have a large product $A_r y_r \sin^2 \theta_r$; hence it would be inappropriate to include such bars when using Eqn 1.11.'

vi) The CIRIA Guide (1977) does not in effect cover *web openings,* unless they are minor with little structural significance. Eqn (1.11), however, has successfully been extended to deep beams with web openings; this has been explained by Kong and Sharp (1977) and Kong *et al.* (1978). A brief description of the method is also given in Reynolds and Steedman's *Reinforced Concrete Designer's Handbook* (1981 and 1988). For a detailed discussion of web openings in deep beams, see Chapter 3.

1.5 Draft Eurocode and CEB-FIP Model Code

The (draft) Eurocode 2 (1984): *Common Unified Rules for Concrete Structures* does not directly provide guidelines for the design of deep beams. It refers instead to clauses 18.1.8 of the CEB-FIP Model Code (1978). The CEB-FIP Model Code applies to simply supported beams of span/depth ratio *l/h* less than 2 and to continuous beams of *l/h* less than 2.5.

1.5.1 *Flexural strength: simply supported deep beams*

The area of the longitudinal reinforcement is calculated from the equation

$$A_s = M/(f_y/\gamma_m)z \tag{1.14}$$

where M is the largest applied bending moment in the span, f_y is the reinforcement characteristic strength, γ_m the partial safety factor and z the lever arm which is to be taken as follows:

$$\begin{aligned} z&=0.2(l+2h) && \text{for } 1<(l/h)<2 \\ z&=0.6l && \text{for } (l/h)<1 \end{aligned} \tag{1.15}$$

The two expressions show that in deep beams the lever arm varies at a lower rate with the depth h. When the depth exceeds the span, the lever arm becomes independent of the beam depth. The main longitudinal reinforcement so calculated should extend without curtailment from one support to the other and be adequately anchored at the ends. According to the CEB-FIP Model Code, vertical hooks cause the development of cracks in the anchorage zone and should be avoided. The required steel should be distributed uniformly over a depth of $(0.25h–0.05l)$ from the soffit of the beam. The CEB-FIP Model Code recommends the use of small diameter bars which are more efficient in limiting the width and development of cracks under service loads and facilitate the anchorage at the supports.

1.5.2 *Flexural strength: continuous deep beams*

For continuous deep beams, the lever arm z is taken as:

$$\begin{aligned} z&=0.2(l+1.5h) && \text{for } 1<l/h<2.5 \\ z&=0.5l && \text{for } l/h<1 \end{aligned} \tag{1.16}$$

The main longitudinal steel in the span should be detailed as for simply supported beams. Over the support, half the steel should extend across the full length of the adjacent span; the remaining half is stopped at $0.4l$ or $0.4h$, whichever is smaller, from the face of the support.

1.5.3 *Shear strength and web reinforcement*

The design shear strength should not exceed the lesser of

$$0.10\,bh\,(f'_c/\gamma_m) \quad \text{and} \quad 0.10\,bl\,(f'_c/\gamma_m) \tag{1.17}$$

where b is the width, h is the beam depth, f'_c is the characteristic cylinder strength of concrete and γ_m is a partial safety factor for material.

The web reinforcement is provided in the form of a light mesh of orthogonal reinforcement consisting of vertical stirrups and horizontal bars placed near each face and surrounding the extreme vertical bars. The web steel ratio should be about 0.20% in each direction near each face for smooth round bars and 0.20% for high bond bars. Additional bars should be provided near the supports, particularly in the horizontal direction.

The aim of the web reinforcement is mainly to limit the crack widths which may be caused by the principal tensile stresses. For beams loaded at the bottom edge, vertical stirrups are required to transmit the load into the

upper portion of the beam; this is in addition to the orthogonal web reinforcement.

1.6 ACI Building Code 318–83 (revised 1986)

1.6.1 *Flexural strength*

For flexural design, ACI Code 318–83 (revised 1986) defines a deep beam as a beam in which the ratio of the clear span l_o to the overall depth h is less than the limits in Eqn (1.18):

$$\text{simple spans: } l_o/h<1.25 \tag{1.18a}$$

$$\text{continuous spans: } l_o/h<2.5 \tag{1.18b}$$

1.6.1.1 Minimum tension reinforcement The main steel ratio ρ shall not be less than ρ_{min} of Eqn (1.19)

$$\rho_{min}=200/f_y \tag{1.19}$$

where $\rho_{min}=A_s/bd$, A_s is the main tension reinforcement, b is the beam width, d is the effective depth and f_y is the steel strength (lb/in^2). For f_y=460N/mm^2 (about 66500 (lb/in^2)), ρ_{min} is about 0.3%.

1.6.1.2 Web reinforcement An orthogonal mesh of web reinforcement is required. The minimum areas of the vertical and horizontal bars shall satisfy Eqn (1.20).

$$A_v/bs_v\geq 0.15\% \tag{1.20a}$$

$$A_h/bs_h\geq 0.25\% \tag{1.20b}$$

where A_v is the area of the vertical bars within the spacing s_v and A_h is the area of the horizontal bars within the spacing s_h.

1.6.1.3 Flexural design Apart from the above requirements, the ACI Code does not give further detailed guidelines. It merely states that account shall be taken of the nonlinear distribution of strain and lateral buckling.

1.6.2 *Shear strength*

The shear provisions of ACI Code 318–83 (revised 1986) apply to top-loaded simple or continuous beams having a (clear span)/(effective depth) ratio l_o/d less than 5.

1.6.2.1 Shear strength: simply supported deep beams Calculations are carried out for the *critical section* defined as follows. For uniformly

distributed loading, the critical section is taken as $0.15l_o$ from the face of the support; for a concentrated load, it is taken as half way between the load and the face of the support. The shear reinforcement required at the critical section shall be used throughout the span.

The design is based on:

$$V_u < \phi V_n \tag{1.21}$$

$$V_n = V_c + V_s \tag{1.22}$$

where V_u is the design shear force at the critical section (lb), V_n is the nominal shear strength (lb) (Eqn (1.22)) and ϕ is the capacity reduction factor for shear, taken as 0.85, V_c is the shear strength provided by concrete (lb) and V_s is the shear strength provided by steel (lb). The nominal shear strength V_n should not exceed the following:

$$V_n < 8\sqrt{f'_c}\, bd \qquad \text{for} \quad l_o/d < 2 \tag{1.23a}$$

$$V_n < (2/3)(10 + l_o/d)\sqrt{f'_c}\, bd \qquad \text{for} \quad 2 \le l_o/d < 5 \tag{1.23b}$$

where f'_c is the concrete cylinder compressive strength (lb/in^2), b is the beam width (in) and d is the effective depth (in).

The shear provided by concrete is calculated from:

$$V_c = (3.5 - 2.5M_u/V_u d)(1.9\sqrt{f'_c} + 2500\,\rho V_u d/M_u)bd \tag{1.24}$$

where M_u is the design bending moment (lb-in) which occurs simultaneously with V_u at the critical section and ρ is the ratio of the main steel area to the area of the concrete section ($\rho = A_s/bd$).

The second term on the right-hand side of Eqn (1.24) is the concrete shear strength for normal beams, given in ACI(318–83) (revised 1986). The first term on the right-hand side is a multiplier to allow for strength increase in deep beams, subject to the restrictions that follow:

$$[3.5\text{-}2.5(M_u/V_u d)] < 2.5 \tag{1.25}$$

$$V_c < 6\sqrt{f'_c}\, bd \tag{1.26}$$

In the case where V_u exceeds ϕV_c, a system of orthogonal shear reinforcement must be provided to carry the excess shear. The contribution V_s of shear reinforcement is given by:

$$\frac{V_s}{f_y d} = \frac{A_v}{s_v}\left[\frac{1 + l_o/d}{12}\right] + \frac{A_h}{s_h}\left[\frac{11 - l_o/d}{12}\right] \tag{1.27}$$

Combining between equations (1.21), (1.22) and (1.27) gives

$$\frac{A_v}{s_v}\left[\frac{1 + l_o/d}{12}\right] + \frac{A_h}{s_h}\left[\frac{11 - l_o/d}{12}\right] = \frac{(V_u/\phi) - V_c}{f_y d} \tag{1.28}$$

where A_v is the area (in^2) of vertical web reinforcement within a spacing s_v, A_h is the area (in^2) of horizontal web reinforcement within a spacing s_h, f_y is the strength of the web steel which should not be taken as more than 60 000 lb/in^2 (410N/mm^2), s_v is the spacing (in) of the vertical web bars—which must exceed neither $d/5$ nor 18 in—and s_h is the spacing (in) of the horizontal web bars—which must exceed neither $d/3$ nor 18 in.

The orthogonal mesh provided must satisfy not only Eqn (1.28) but also the minimum web reinforcement requirement of Section 1.6.1.1.

In (Eqn 1.28.) the quantities $(1+l_o/d)/12$ and $(11-l_o/d)/12$ represent weighting factors for the relative effectiveness of the vertical and horizontal web bars. ACI Code 318–83 (revised 1986) rightly considers that horizontal web reinforcement is more effective than vertical web reinforcement (Kong and Robins, 1971; Kong and Singh, 1972). At the limiting l_o/d ratio of 5, quoted in Section 1.6.2, the weighting factors $(1+l_o/d)/12$ and $(11-l_o/d)/12$ are equal. As the l_o/d ratio decreases, horizontal web bars become increasingly more effective compared with vertical web bars.

1.6.2.2 Shear strength: continuous deep beams Calculations for continuous deep beams, unlike those for simply supported ones, are not based on the design shear force at the critical section as defined in Section 1.6.2.1. Instead, the shear reinforcement at any section is calculated from the design shear force V_u at that section. The design is based on Eqn (1.29) and (1.30).

$$V_u < \phi V_n \tag{1.29}$$

$$V_n = V_c + V_s \tag{1.30}$$

where ϕ, V_n, V_c and V_s are as defined for Eqns (1.21) and (1.22). The nominal shear strength V_n is subject to the same limits as imposed by Eqn (1.23a, b). However, for continuous deep beams, the concrete nominal shear strength V_c is to be taken as the least value given by Eqns (1.31a–c):

$$V_c = 3.5\sqrt{f'_c}\,bd \tag{1.31a}$$

$$V_c = [1.9\sqrt{f'_c} + 2500\rho]bd \tag{1.31b}$$

$$V_c = [1.9\sqrt{f'_c} + 2500\rho(V_u d/M_u)]bd \tag{1.31c}$$

where M_u is the design moment occurring simultaneously with V_u at the section considered (lb-in); p is the main steel ratio A_s/bd; f'_c is the concrete cylinder strength (lb/in^2).

Where V_u exceeds $0.5\phi V_c$, vertical shear reinforcement should be provided to satisfy the condition:

$$(A_v/bs_v) > (50/f_y) \tag{1.32}$$

where A_v is the area (in^2) of the vertical shear reinforcement within the spacing s_v and f_y is the strength of the shear reinforcement which should not be taken as exceeding 60 000 lb/in^2 (410 N/mm^2).

Where the design shear force V_u exceeds ϕV_c vertical shear reinforcement shall be provided to carry the excess shear. The contribution V_s of this shear reinforcement is given by:

$$V_s=(A_v f_y d/s_v) \tag{1.33}$$

where the symbols are as defined for Eqns (1.32) and (1.31).

Combining Eqns (1.29), (1.30) and (1.33),

$$(A_v/bs_v) > ((V_u/\phi)-V_c)/bdf_y \tag{1.34}$$

Irrespective of the values obtained from Eqns (1.34) or (1.33), A_v/bs_v shall not be taken as less than 0.0015; the spacing s_v shall not exceed $d/5$ nor 18 in (450 mm). In addition, nominal horizontal web reinforcement must also be provided, such that A_h/bs_h is not less than 0.0025 and the spacing s_h of this horizontal reinforcement shall not exceed $d/3$ nor 18 in (450 mm).

1.7 Canadian Code CAN3-A23.3-M84

1.7.1 *Flexural strength*

For flexural design the Canadian Code CAN3-A23.3-M84 (1984) defines a deep beam as a beam in which the ratio of the clear span l_o to the overall depth h is less than the limits in Eqn (1.35):

simple spans : $l_o/h < 1.25$ (1.35a)

continuous spans : $l_o/h < 2.5$ (1.35b)

1.7.1.1 Minimum tension reinforcement The main steel ratio ρ shall not be less than ρ_{min} of Eqn (1.36)

$$\rho_{min}=1.4/f_y \tag{1.36}$$

where $\rho_{min}=A_s/db$, A_s is the area of the main tension reinforcement, b is the beam width, d is the effective depth and f_y is the steel strength. (Note: unlike the ACI Code, the Canadian Code is in SI units)

1.7.1.2 Web reinforcement A system of orthogonal web reinforcement is required, with bars in each face. The minimum areas of the vertical and horizontal reinforcement shall satisfy Eqn (1.37)

$$A_v/bs_v \geq 0.2\% \tag{1.37a}$$

$$A_h/bs_h \geq 0.2\% \tag{1.37b}$$

where A_v is the area of the vertical web reinforcement within the spacing s_v which shall exceed neither $d/5$ nor 300 mm and A_h is the area of the horizontal web reinforcement within the spacing $s_{h,}$ which shall exceed neither $d/3$ nor 300 mm.

1.7.1.3 Flexural design Apart from the above requirements, the Canadian Code does not give further detailed guidelines. It merely states that account shall be taken of the nonlinear distribution of strain, lateral buckling and the increased anchorage requirements.

1.7.2 *Shear strength*

The Canadian code uses the concept of the shear-span/depth ratio (Kong and Singh, 1972) rather than the span/depth ratio. The shear provisions of the Canadian code apply to those parts of the structural member in which:

i) the distance from the point of zero shear to the face of the support is less than 2*d;* or
ii) a load causing more than 50% of the shear at a support is located at less than 2d from the face of the support.

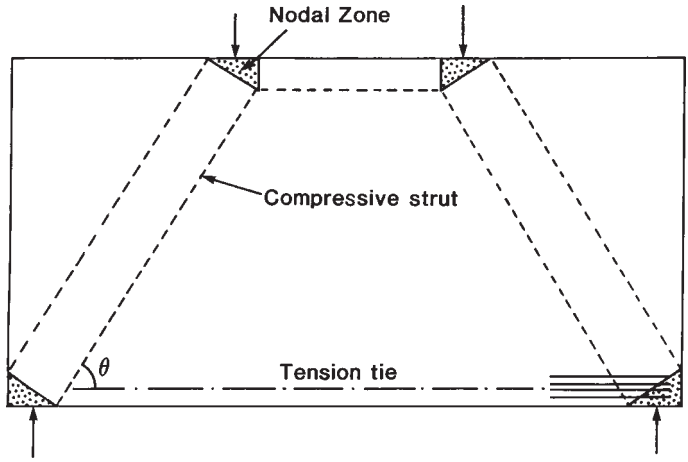

Figure 1.4 Canadian Code's truss model for deep beams

The calculations are based on truss model consisting of compression struts and tension tie as in Figure 1.4.

Unless special confining reinforcement is provided, the concrete compressive stresses in the nodal zones, defined as the regions where the strut and tie meet (Figure 1.4), should not exceed: $0.85\phi_c f'_c$ in nodal zones bounded by compressive struts and bearing areas, $0.75\,\phi_c f'_c$ in nodal zones

anchoring one tension tie, or $0.60\phi_c f'_c$ in nodal zones anchoring tension ties in more than one direction, where ϕ_c is a material resistance factor=0.6 for concrete and f'_c is the cylinder compressive strength of concrete.

The nodal zone stress limit conditions together with the equilibrium condi-tion determine the geometry of the truss such as the depth of the nodal zones and the forces acting on the struts and tie. The main tension tie reinforcement is determined from the tensile tie force. These reinforcing bars should be effectively anchored to transfer the required tension to the lower nodal zones of the truss to ensure equilibrium. The code, then, requires the checking of the compressive struts against possible crushing of concrete as follows:

$$f_2 \leq f_{2max} \tag{1.38}$$

where f_2 is the maximum stress in the concrete strut, and f_{2max} is the diagonal crushing strength of the concrete, given by:

$$f_{2max} = \lambda \phi_c f'_c / (0.8 + 170\,\varepsilon_1) \tag{1.39}$$

where λ is a modification factor to take account of the type of concrete, (λ=1.0 for normal weight concrete) and e1 is the principal tensile strain, crossing the strut.

Eqn (1.39) takes account of the fact that the existence of a large principal tensile strain reduces considerably the ability of concrete to resist compressive stresses.

For the design purpose ε_1 may be computed from:

$$\varepsilon_1 = \varepsilon_x + (\varepsilon_x + 0.002)/\tan^2 \theta \tag{1.40}$$

where ε_x is the longitudinal strain and θ is the angle of inclination of the diagonal compressive stresses to the longitudinal axis of the member (Figure 1.4). An orthogonal system of web reinforcement must be provided. This shall meet the requirements of Section 1.7.1.1.

References

Albritton, G.E. (1965) *Review of literature pertaining to the analysis of deep beams.* Technical Report 1–701. US Army Engineer Waterways Experiment Station, Vicksburg, Miss.

American Concrete Institute (revised 1986) *Building Code Requirements for Reinforced Concrete.* ACI 318–83, American Concrete Institute, Detroit.

Barry, J.E. and Ainso, H. (1983) Single-span deep beams. *J.Strut. Engng, Am.Soc.Civ.Engrs.* 109, ST3: 646–663.

Braestrup, M.W. and Nielsen, M.P. (1983) Plastic methods of analysis and design. In *Handbook of Structural Concrete,* eds Kong, F.K., Evans, R.H., Cohen, E. and Roll, F. Ch.20, Pitman, London, 20/1–20/54.

British Standards Institution. (1985) *The Structural Use of Concrete,* BS 8110, British Standard Institution, London, Parts 1, and 2.

British Standards Institution. (1972) The Structural Use of Concrete. CP 110. BSI, London, Part 1.

Canadian Standards Association. (1984) *Design of Concrete Structures for Buildings*. CAN3A23.3-M84, Canadian Standards Association, Toronto, Canada.

Cement and Concrete Association. (1969) *Bibliography on deep beams.* Library Bibliography No. Ch. 71(3/69). Cement and Concrete Association, London.
Chemrouk, M. (1988) *Slender concrete deep beams: behaviour, serviceability and strength.* Ph.D thesis, University of Newcastle upon Tyne.
Coates, R.C., Coutie, M.G. and Kong, F.K. (1988) *Structural Analysis.* Van Nostrand Reinhold (UK) London, 3rd edn.
Comité Européen de Béton. (1964) *Recommendations for an International Code of Practice for Reinforced Concrete.* English Edition, Cement and Concrete Association, London.
Comité Européen de Béton-Fédération Internationale de la Précontrainte. (1978). *Model Code for Concrete Structures.* English Edition, Cement and Concrete Association, London.
Commission of the European Communities. (Draft, 1984). *Common Unified Rules for Concrete Structures,* Eurocode 2, CEC, Brussels.
Construction Industry Research and Information Association. (1977) *The Design of Deep Beams in Reinforced Concrete.* CIRIA Guide 2. Ove Arup & Partners and CIRIA, London.
Cusens, A.R. and Besser, I. (1985) Shear strength of concrete wall beams under combined top and bottom loads. *Struct. Eng.* **63B,** 3: 50.
de Paiva, H.A.R. and Siess, C.P. (1965) Strength and behaviour of deep beams in shear. *J.Struct. Engng, Am. Soc. Civ. Engrs.* **91,** ST 5: 19.
Garcia, R.C. (1982) *Strength and stability of concrete deep beams.* Ph.D thesis. University of Cambridge.
Kong, F.K. (1985) Design of reinforced concrete deep beams—British, European and American practices. Chairman's Address delivered at the Northern Counties Branch of the Institution of Structural Engineers, 15 October.
Kong, F.K. (1986a) Reinforced concrete deep beams. Lecture delivered at Ove Arup and Partners, London, 3 October.
Kong, F.K. (1986b) Reinforced concrete deep beams. In *Concrete Framed Structures—Stability and Strength,* ed. Narayanan, R. Ch. 6. Elsevier Applied Science, London: 169.
Kong, F.K. and Charlton, T.M. (1983) The fundamental theorems of the plastic theory of structures. *Proc. M.R.Horne Conf. on Instability and Plastic Collapse of Steel Structures, Manchester,* ed. Morris, J.L. Granada Publishing, London:
Kong, F.K. and Evans, R.H. (1987) *Reinforced and Prestressed Concrete.* 3rd edn, Van Nostrand Reinhold (UK), London 200–202 and 218–220.
Kong, F.K. and Kubik, L.A. (1977) Discussion of 'Collapse load of deep reinforced concrete beams by P.Kumar', *Mag. Concr. Res.* **29,** 98: 42.
Kong, F.K. and Kubik, L.A. (1991) Large scale tests on reinforced concrete deep beams with web openings. (Paper in preparation).
Kong, F.K. and Robins, P.J. (1971) Web reinforcement effects on lightweight concrete deep beams. *Proc. Am. Concs. Inst.* **68,** 7: 514.
Kong, F.K. and Sharp, G.R. (1973) Shear strength of lightweight reinforced concrete deep beams with web openings. *Struct. Engr.* **51:** 267.
Kong, F.K. and Sharp, G.R. (1977) Structural idealization for deep beams with web openings. *Mag. Concr. Res.* **29,** 99: 81.
Kong, F.K. and Singh, A. (1972) Diagonal cracking and ultimate loads of lightweight concrete deep beams. *Proc. Am. Concr. Inst.* **69,** *8: 513.*
Kong, F.K. and Singh, A. (1974) Shear strength of lightweight concrete deep beams subjected to repeated loads. In *Shear in Reinforced Concrete.* ACI Publication SP42, American Concrete Institute, Detroit: 461.
Kong, F.K., Robins, P.J., Kirby, D.P. and Short, D.R. (1972a) Deep beams with inclined web reinforcement. *Proc. Am. Concr. Inst.* **69,** 3
Kong, F.K., Robins, P.J. Singh, A. and Sharp. G.R. (1972b) Shear analysis and design of reinforced concrete deep beams. *Struct. Engr.* **50,** 10: 405.
Kong, F.K., Robins, P.J. and Sharp, G.R. (1975) The design of reinforced concrete deep beams in current practice. *Struct. Engr.* **53,** 4: 173.
Kong, F.K., Sharp, G.R., Appleton, S.C., Beaumont, C.J. and Kubik, L.A. (1978) Structural idealization of deep beams with web openings: further evidence. *Mag. Concr. Res.* **30,** 103: 89.
Kong, F.K., Evans, R.H., Cohen, E. and Roll, F. (1983a) *Handbook of Structural Concrete.* Pitman, London.
Kong, F.K., Prentis, J.M. and Charlton, T.M. (1983b) Principle of virtual work for a general deformable body—a simple proof. *Struct. Engr* **61 A,** 6: 173.

Kong, F.K., Garcia, R.C., Paine, J.M., Wong, H.H.A., Tang, C.W.J. and Chemrouk, M. (1986) Instability and buckling of reinforced concrete deep beams. *Struct. Engr.* **64B,** 3: 49.
Kotsovos, M.D. (1988). Design of reinforced concrete deep beams. *Struct. Engr.* **66,** 2: 28.
Kubik, L.A. (1980) Predicting the strength of reinforced concrete deep beams with web openings. *Proc. Inst. Civ. Engr.* Part 2, **69**: 939.
Kumar, P. (1976) Collapse load of deep reinforced concrete beams. *Mag. Concr. Res.* **28,** 94: 30.
Leonhardt, F. and Walther, R. (1966) *Deep beams.* Bulletin 178, Deutscher Ausschuss fur Stahlbeton, Berlin. (Enlgish translation: CIRIA, London, 1970).
Mansur, M.A. and Alwis, W.A.M. (1984) Reinforced fibre concrete deep beams with web openings. *Int. J. Cement Composites Lightwt. Concr.* **6,** 4: 263.
Mau, S.T. and Hsu, T.T.C. (1987) Shear strength prediction for deep beams with web reinforcement. *Am. Concr. Inst. Struct. J.* **84,** 6: 513.
Nielsen, M.P. (1971) *On the strength of reinforced concrete discs.* Civil Engineering and Building Construction Series, No. 70, Acta Polytechnica Scandinavica, Copenhagen.
Rasheeduzzafar, M.H. and Al-Tayyib, A.H.J. (1986) Stress distribution in deep beams with web openings. *J. Struct. Engrg, Am. Soc. Civ. Engrs.* **112,** ST 5: 1147
Ray, S.P. (1980) Behaviour and Ultimate Shear Strength of Reinforced Concrete Deep Beams With and Without Opening in Web. Ph. D. thesis, Indian Institute of Technology, Kharagpur, India.
Regan, P.E. and Hamadi, Y.D. (1981) *Concrete in the Oceans. Part 1: Reinforced Concrete Deep Beams with Thin Webs.* Cement and Concrete Association, London.
Reynolds, C.E. and Steedman. J.C. (1981) *Reinforced Concrete Designer's Handbook.* 9th edn Cement and Concrete Association, London. 402 and Table 151.
Reynolds, C.E. and Steedman, J.C. (1988). *Reinforced Concrete Designer's Handbook.* 10th edn, E. and F.N. Spon, London. 59, 61, 338, and Table 148.
Roberts, T.M. and Ho, N.L. (1982) Shear failure of deep fibre reinforced concrete beams. *Int. J. Cement Composites and Lightwt. Concr.* **4,** 3: 145.
Robins, P.J. and Kong, F.K. (1973) Modified finite element method applied to reinforced concrete deep beams. *Civ. Engng. Publ. Works Review.* **68,** 808: 963.
Rogowsky, D.M., MacGregor, J.G. and Ong, S.Y. (1986) Tests of reinforced concrete deep beams. *Proc. Am. Concr. Inst.* **83,** 4: 614.
Shanmugan, N.E. and Swaddiwudhipong, S. (1988) Strength of fibre reinforced deep beams containing openings. *Int. J. Cement Composites and Lightwt. Concr.* **10,** 1: 53.
Singh, R., Ray, S.P. and Reddy, C.S. (1980) Some tests on reinforced concrete deep beams with and without opening in the web. *Indian Concr. J.* **54,** 7: 189.
Smith, K.N. and Vantsiotis, A.S. (1982) Shear strength of deep beams. *Proc. ACI 79, 3: 201.*
Subedi, N.K. (1988) Reinforced concrete deep beams: a method of analysis. *Proc. Inst. Civ. Engrs,* Part 2 **85**: 1.
Swaddiwudhipong, S. and Shanmugan, N.E. (1985) Fibre-reinforced concrete deep beams with openings. *J.Struct. Engng, Am. Soc. Civ. Engrs.* **111**, ST 8: 1679.
Taner, N., Fazio, P.P. and Zielinski, Z.A. (1977) Strength and behaviour of beam-panels—tests and analysis. *Proc. Am. Concr. Inst.* **74,** 10: 511.
Tang, C.W.J. (1987). *Reinforced concrete deep beams: behaviour, analysis and design.* PhD thesis, University of Newcastle upon Tyne.
Wong, H.H.A. (1987). *Buckling and stability of slender reinforced concrete deep beams.* Ph.D thesis, University of Newcastle upon Tyne.
Zienkiewicz, O.C. and Taylor, R.L. (1989) *The Finite Element Method,* 4th edn, McGraw Hill, Maidenhead.

2 Strength and behaviour of deep beams

M.D.KOTSOVOS, Imperial College, London

Notation

f_c	cylinder compressive strength of concrete
a	shear span
L	effective length of beam
d	distance of centroid of tension reinforcement from extreme compressive fibre
M_f	section flexural capacity
M_c	maximum moment sustained by cross-section through tip of inclined crack

2.1 Introduction

While current design concepts are based on uniaxial stress-strain characteristics, recent work has shown quite conclusively that the ultimate limit-state behaviour of reinforced concrete (RC) elements such as, for example, beams in flexure (or combined flexure and shear), can only be explained in terms of multiaxial effects which are always present in a structure. It is the consideration of the multiaxial effects that has led to the introduction of the concept of the compressive-force path which has been shown not only to provide a realistic description of the causes of failure of structural concrete, but also to form a suitable basis for the development of design models capable of providing safe and efficient design solutions. In the following, the work is summarised and the concept of the compressive-force path is used as the basis for the description of the behaviour of RC deep beams of their ultimate limit state. The implications of the application of the concept in RC deep beam design are also discussed and a simple design method is proposed.

2.2 Current concepts for beam design

It is a common design practice first to design an RC beam for flexural capacity and then to ensure that any type of failure, other than flexural (that would occur when the flexural capacity is attained), is prevented. The

flexural capacity is assessed on the basis of the plane sections theory which not only is generally considered to describe realistically the deformational response of the beams, but is also formulated so that it provides a design tool noted for both its effectiveness and simplicity.

However, an RC beam may exhibit a number of different types of failure that may occur before flexural capacity is attained. The most common of such failures are those which may collectively be referred to as shear types of failure and may be prevented by complementing the initial (flexural) design so that the shear capacity of the beam is not exhausted before the flexural capacity is attained, while other types of failure such as, for example, an anchorage failure or a bearing failure (occurring in regions acted upon by concentrated loads), are usually prevented by proper detailing.

Although a generally accepted theory describing the causes of shear failure is currently lacking, there are a number of concepts which not only are widely considered as an essential part of such a theory, but also form the basis of current design methods for shear design. These concepts are the following:

i) shear failure occurs when the shear capacity of a critical cross-section is exceeded
ii) the main contributor to shear resistance is the portion of the cross-section below the neutral axis, with strength, in the absence of shear reinforcement, being provided by "aggregate interlock" and "dowel action", whereas for a beam with shear reinforcement the shear forces are sustained as described in iii) below
iii) once inclined cracking occurs, an RC beam with shear reinforcement behaves as a truss with concrete between two consecutive inclined cracks and shear reinforcement acting as the struts and ties of the truss, respectively, and the compressive zone and tension reinforcement representing the horizontal members.

A common feature of both the above concepts and the plane section theory that form the basis of flexural design is that they rely entirely on uniaxial stress-strain characteristics for the description of the behaviour of concrete. This view may be justified by the fact that beams are designed to carry stresses mainly in the longitudinal direction, with the stresses developing in at least one of the transverse directions being small enough to be assumed negligible for any practical purpose. As will be seen, however, such a reasoning underestimates the considerable effect that small stresses have on the load-carrying capacity and deformational response of concrete. Ignoring the small stresses in design does not necessarily mean that their effect on structural behaviour is also ignored. It usually means that their effect is attributed to other causes that are expressed in the form of various design assumptions.

Therefore before an attempt is made to use current design concepts as the basis for the description of the behaviour of RC deep beams, it is essential to investigate the effect of the small transverse stresses on structural concrete behaviour.

2.3 Effect of transverse stresses

2.3.1 *Flexural capacity*

Flexural capacity is assessed on the basis of the plane sections theory. The theory describes analytically the relationship between flexural capacity and geometric characteristics by considering the equilibrium conditions at critical cross-sections. Compatibility of deformation is satisfied by the 'plane cross-section remain plane' assumption and the longitudinal concrete and steel stresses are evaluated by the material stress-strain characteristics. Transverse stresses are not considered to affect flexural capacity and are therefore ignored.

It is well known, however, that concrete is weak in tension and strong in compression. Therefore, its primary purpose in an RC structural member is to sustain compressive forces, while steel reinforcement is used to sustain tensile forces with concrete providing protection to it. As concrete is used to sustain compressive forces, it is essential that its strength and deformational response under such conditions are known.

The stress-strain characteristics of concrete in compression are considered to be described adequately by the deformational response of concrete specimens such as prisms or cylinders under uniaxial compression. Typical stress-strain

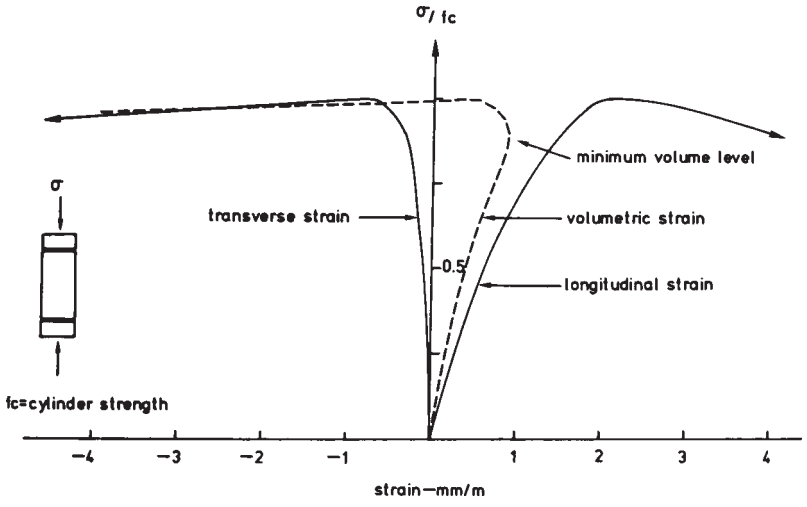

Figure 2.1 Typical stress-strain curves obtained from tests on concrete cylinders under uniaxial compression.

curves providing a full description of the behaviour of such specimens are given in Figure 2.1 which indicates that a characteristic feature of the curves is that they comprise an ascending and a gradually descending branch. (It will be seen later, however, that perhaps the most significant feature of concrete behaviour is the abrupt increase of the rate of lateral expansion that the specimen undergoes when the load exceeds a level close to, but not beyond, the peak level. This level is the minimum volume level that marks the beginning of a dramatic volume dilation which follows the continuous reduction of the volume of the specimen that occurs to this load level. The variation of the volume of the specimen under increasing uniaxial compressive stress is also shown in Figure 2.1). Although the curves shown in Figure 2.1 describe the deformational response of concrete in both the direction of loading and at right angles with this direction, it is only the former which is considered essential by the plane sections theory for the description of the longitudinal stress distribution within the compressive zone of the beam cross-section.

The axial stress-axial strain and the axial stress-lateral strain curves of Figure 2.1 may be combined to form the axial strain-lateral strain curve shown in Figure 2.2. The curve of Figure 2.2 also comprises two portions, which correspond respectively to the ascending and descending branches of the stress-strain curves of Figure 2.1. The transition between these portions corresponds to the portions of the stress-strain curves between the minimum volume and peak stress levels. If uniaxial stress-strain data do indeed describe the deformational behaviour of the compressive zone of the beam, an axial strain-lateral strain relationship (such as that shown in Figure 2.2) should provide a realistic description of the deformational behaviour of an element of concrete in this zone throughout the loading history of the beam.

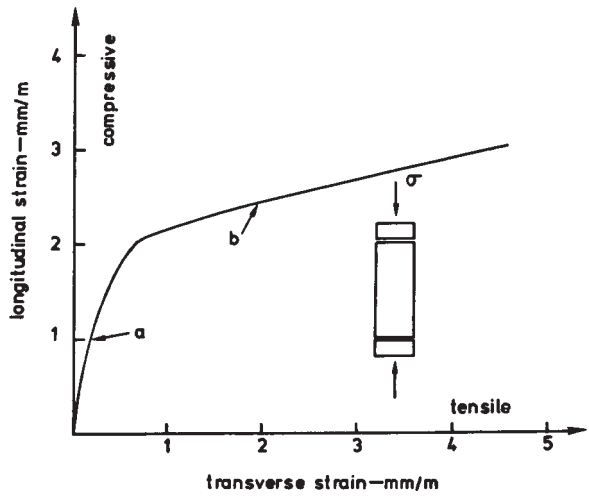

Figure 2.2 Typical axial strain-lateral strain curve constructed from the stress-strain curves in Figure 2.1 (branches a and b correspond to ascending and descending branches, respectively).

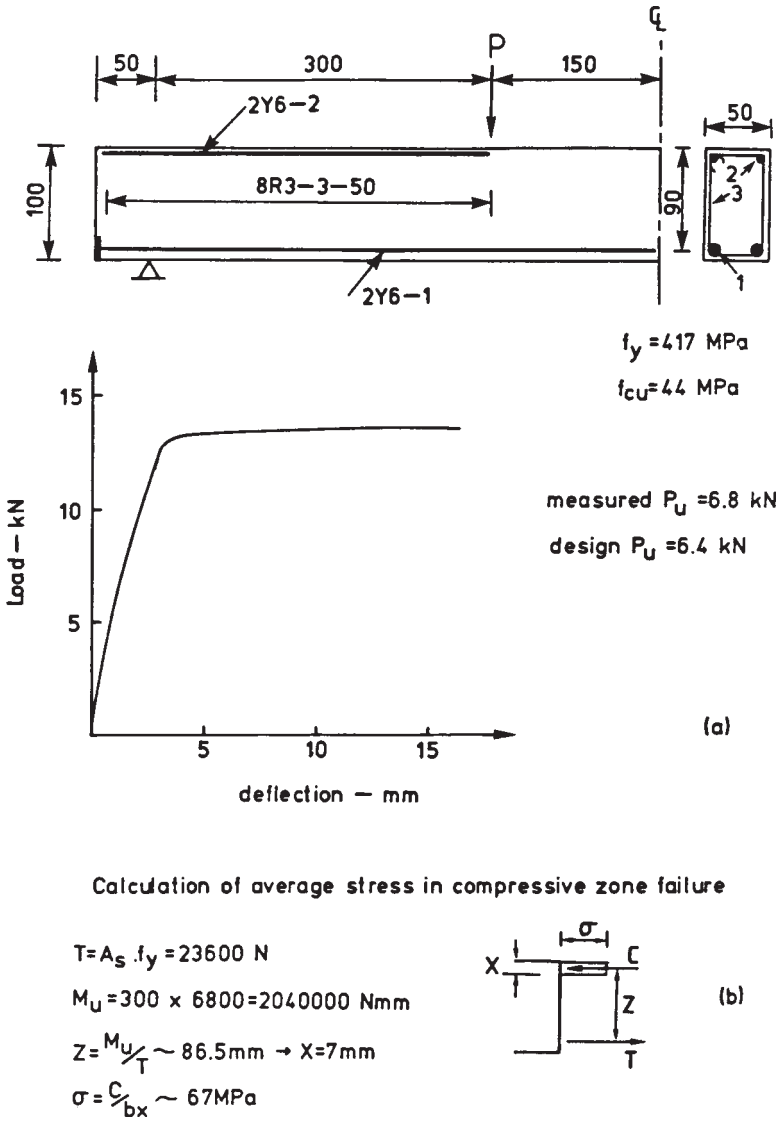

Figure 2.3 (a) Design details and mesured response of a typical RC beam, (b) Assessment of average stress in compressive zone based on measured values.

The deformational response of the compressive zone can established by testing an RC beam (such as that shown Figure 2.3) under two-point loading and measuring longitudinal and transverse strains at the top face of the beam within the middle zone. Such tests have already been carried out (Kotsovos, 1982) and those of the strains measured in the region of the deepest flexural cracks have been used to plot the longitudinal strain-transverse strain curve shown in Figure 2.4. The Figure also includes the corresponding curve

established from tests on cylinders under uniaxial compression and it is apparent that only the portion of the latter to the minimum volume level can provide a realistic description of the beam behaviour; beyond this level, there is a dramatic deviation of the cylinder from the beam curve.

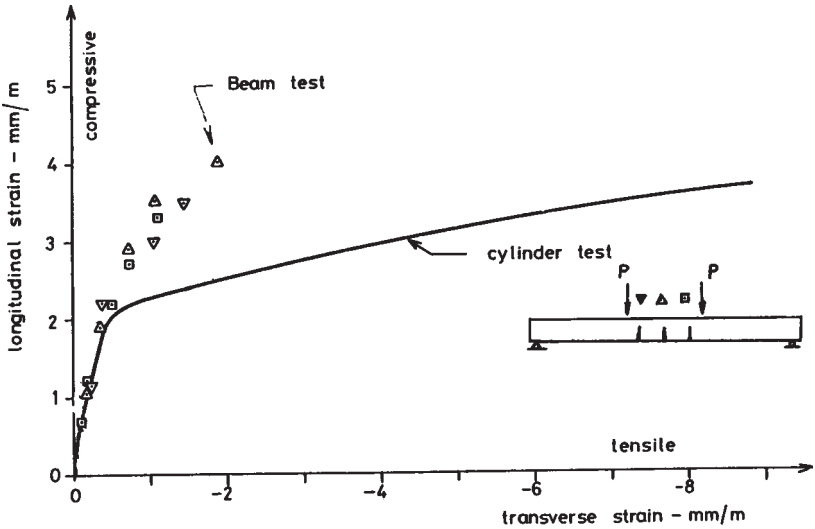

Figure 2.4 Typical relationships between longitudinal and transverse strains measured on the top face of RC beams at critical sections.

Such results demonstrate that, in spite of the prominence given to them in flexural design, the post-ultimate uniaxial stress-strain characteristics *cannot* describe the behaviour of an element of concrete in the compressive zone of an RC beam in flexure. Such a conclusion should come as no surprise because it has been found by experiment that, unlike the ascending branch, the descending branch does not represent material behaviour; it merely describes secondary testing procedure effects caused by the interaction between testing machine and specimen (Kotsovos, 1983a). However, the ascending branch can only partially describe the deformational response of a concrete element in the compressive zone and this can only lead to the conclusion that uniaxial stress-strain data are insufficient to describe fully the behaviour of the compressive zone.

Additional evidence in support of these arguments can be obtained easily by assessing the average longitudinal stress in the compressive zone of the RC beam shown in Figure 2.3. The Figure also provides design details of the beam together with its experimentally obtained load-deflection relationship. Using the measured values of the load-carrying capacity of the beam and the strength of the tensile reinforcement, the average stress in the compressive zone at failure can be calculated as indicated in the Figure. The calculated

average stress in the compressive zone is found to be 67 MPa which is 75% higher than the uniaxial compressive strength of concrete (f_c) and about 150% higher than the design stress, assuming a safety factor equal to 1. Such a large stress can only be sustained if the stress conditions in the compressive zone are *triaxial* compressive.

It has been argued that, in the absence of stirrups, a triaxial compressive state of stress can be developed due to the occurrence of volume dilation in localised regions within the compressive zone (Kotsovos, 1982). This view is supported by the experimentally established shape of the transverse deformation profile of the top face of the beam shown in Figure 2.5. The characteristic feature of this profile is the large transverse expansion (indicative of volume dilation) that occurs in the region of cross-sections that coincide with a deep flexural crack when the load-carrying capacity of the beam is approached. This localised transverse expansion is restrained by concrete in the adjacent regions and such a restraint may be considered to be equivalent to the application of a confining pressure that has been assessed to be at least 10% f_c. An indication of the effect that such a small confining stress has on the load-carrying capacity of concrete in the longitudinal direction is given in Figure 2.6a which describes the variation of the peak axial compressive stress sustained by cylinders with increasing confining pressure. The Figure indicates that a confining pressure of 10% f_c is sufficient to increase the load-carrying capacity of the specimen by more than 50% and this should be the cause of the large compressive stresses developing in the compressive zone.

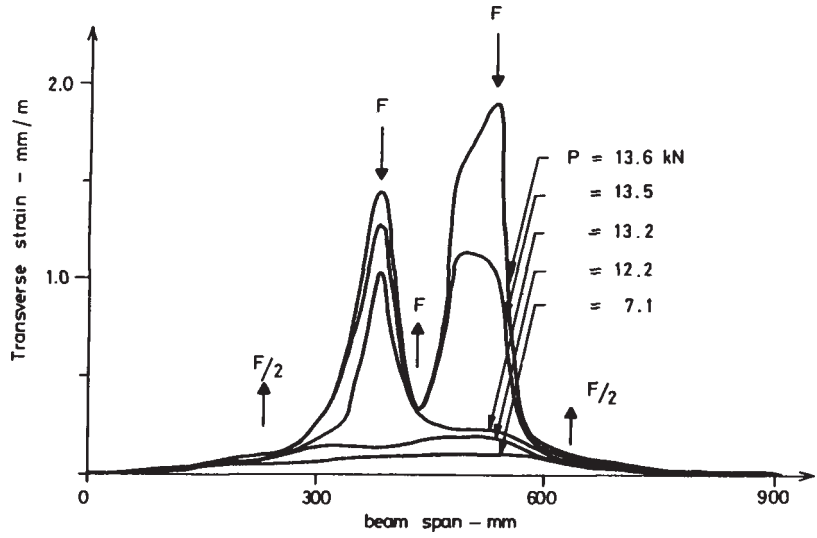

Figure 2.5 Typical variation of transverse deformation profile of compressive top face of the RC beam in Figure 2.3, with increasing load, indicating the development of internal actions (F) for compatibility purposes.

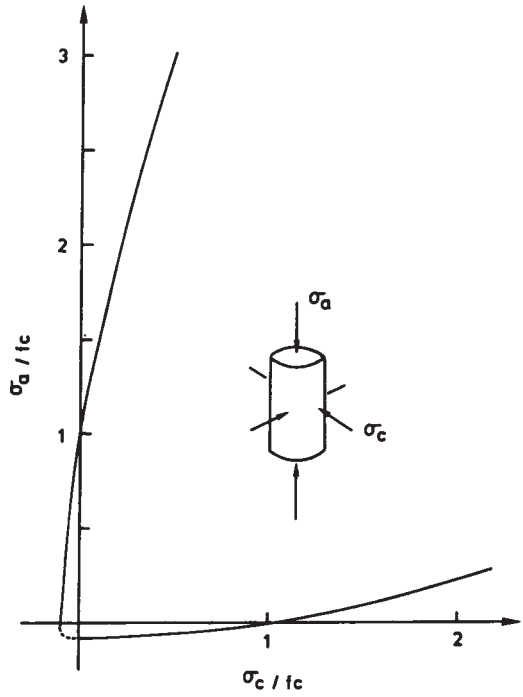

Figure 2.6a Typical failure envelope of concrete under axisymmetric triaxial stress.

Concurrently, the expanding concrete induces tensile stresses in adjacent regions and this gives rise to a compression-tension-tension state of stress. Such a state of stress reduces the strength of concrete in the longitudinal direction (Figure 2.6a indicates that a tensile stress of about 5% f_c is sufficient to reduce the cylinder strength by about 50%) and it has been shown (Kotsovos, 1984) that collapse occurs due to horizontal splitting of the compressive zone in regions between deep flexural cracks (Figure 2.7). Concrete crushing, which is widely considered to be the cause of flexural failure, appears to be a post-failure phenomenon that occurs in the compressive zone of cross-sections which coincides with a deep flexural crack resulting from the loss of restraint provided by the adjacent concrete.

It is important to emphasise that the development of triaxial stress conditions is a key feature of structural behaviour only at the late stages of the loading history of the beam. This becomes apparent from the experimental data shown in Figure 2.5 which indicate that the localised transverse tensile strains become significant only when the load increases to a level nearly 90% of the beam's maximum load-carrying capacity. Figure 2.6b indicates that under such triaxial stress conditions the corresponding strains can be comparable to those measured at the top face of the beam.

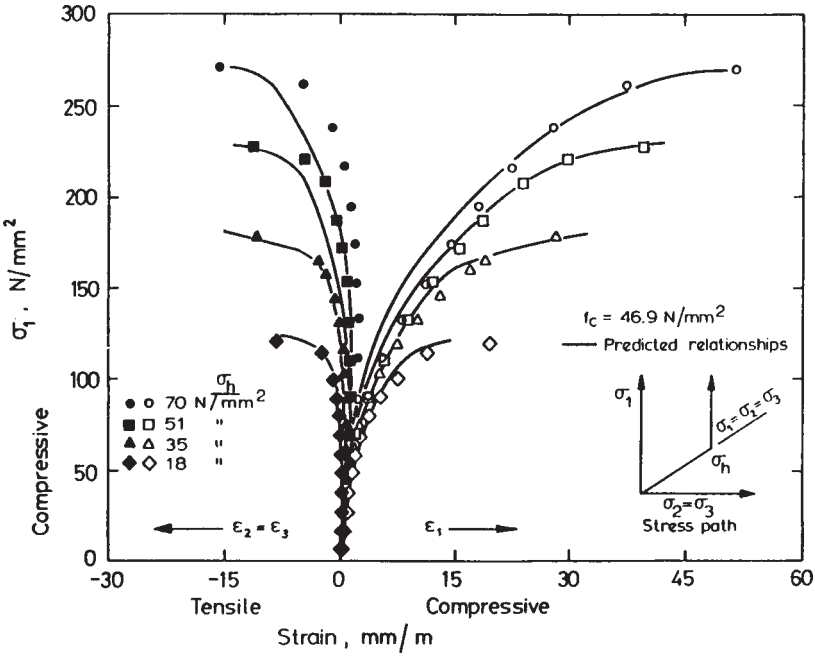

Figure 2.6b Typical stress-strain curves obtained from tests on concrete cylinders under various states of axisymmetric stress.

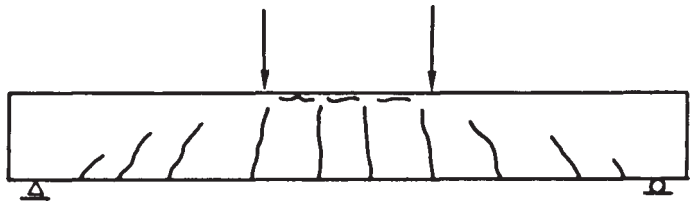

Figure 2.7 Typical failure mode of RC beams in flexure.

2.3.2 *Shear capacity*

As discussed in Section 2.2, shear capacity of an RC beam is defined as the maximum shear force that can be sustained by a critical-section. When deemed necessary, shear reinforcement is provided in order to carry that portion of the shear force that cannot be sustained by concrete alone. The amount of reinforcement required for this purpose is assessed by using one of a number of available methods invariably developed on the basis of the truss analogy concept (Ritter, 1899: Morsch, 1909) which stipulates that an RC beam with shear reinforcement may be considered to behave as a truss once inclined cracking occurs.

A prerequisite for the application of the concept of "shear capacity of critical sections" in design appears to be (by implication) the widely accepted

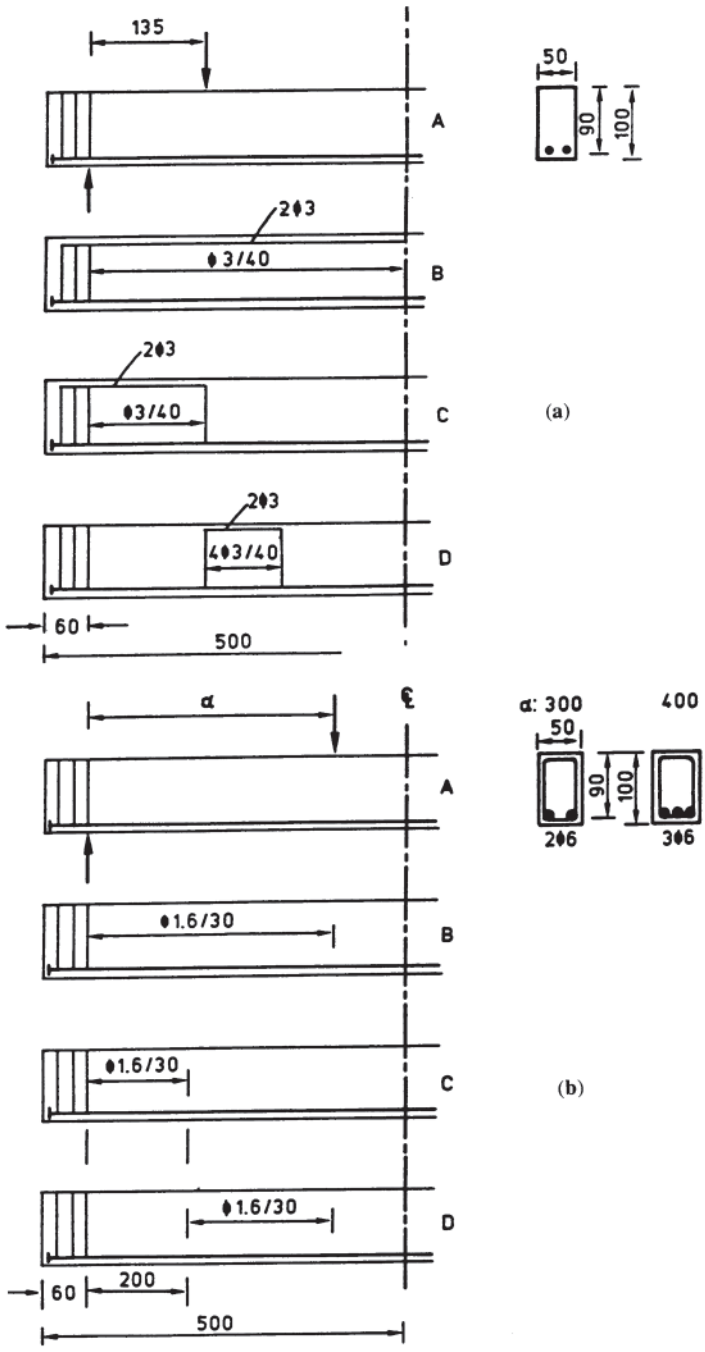

Figure 2.8 Design details of beams with (a) a/d=1.5. (b) a/d>2.5

view that the main contributor to shear resistance is aggregate interlock (Fenwick and Paulay, 1968; Taylor, 1968; Regan, 1969). This is because only through aggregate interlock can the cracked web be the sole contributor to the shear resistance of an RC T-beam, as specified by current code provisions e.g. BS 8110 (British Standards Institution, 1985). The concept of the shear capacity of critical sections is itself a prerequisite for the application of the truss analogy because it is the loss of the shear capacity below the neutral axis that the shear reinforcement is considered to offset.

It appears therefore, that the aggregate interlock concept, although not explicitly referred to, forms the backbone of current concepts that describe the causes of shear failure. And yet this concept is incompatible with fundamental concrete properties; a crack propagates in the direction of the maximum principal compressive stress and opens in the orthogonal direction (Kotsovos, 1979; Kotsovos and Newman, 1981a). If there was a significant shearing movement of the crack faces, which is essential for the mobilisation of aggregate interlock, this movement should cause crack branching in all localised regions where aggregate interlock is effected. The occurrence of such crack branching has not been reported to date.

The inadequacy of the concepts currently used to describe the causes of shear failure has been demonstrated in an experimental programme (Kotsovos, 1987a, b). The programme was based on an investigation of the behaviour of RC beams, with various arrangements of shear reinforcement (Figure 2.8), subjected to two-point loading with various shear span to depth ratios *(a/d)*. The main results of this programme are given in Figure 2.9 which shows the load-deflection curves of the beams tested.

On the basis of the concept of shear capacity of critical sections, all beams that lack shear reinforcement, over either their entire shear span or a large portion of its length, should have a similar load-carrying capacity. However, beams C and D were found to have a load-carrying capacity significantly higher than that of beams A which had no shear reinforcement throughout their span. Beams D, in all cases, exhibited a ductile behaviour, which is indicative of a flexural mode of failure, and their load-carrying capacity was higher than that of beams A by an amount varying from 40 to 100% depending on *a/d*. These results indicate that such behaviour *cannot* be explained in terms of the concept of shear capacity of critical sections and the failure of the beams cannot be described as a shear failure as defined by this concept.

The evidence presented in Figure 2.9 also counters the view that aggregate interlock makes a significant contribution to shear resistance. This is because the large deflections exhibited by beams D, in all cases, and beams C, in most cases, led to a large increase of the inclined crack width and thus considerably reduced, if not eliminated, aggregate interlock. In fact, near the peak load, the inclined crack of beams D had a width in excess of 2 mm which is an order of magnitude larger than that found by Fenwick and Paulay (1968) to reduce aggregate interlock by more than half. It can only be

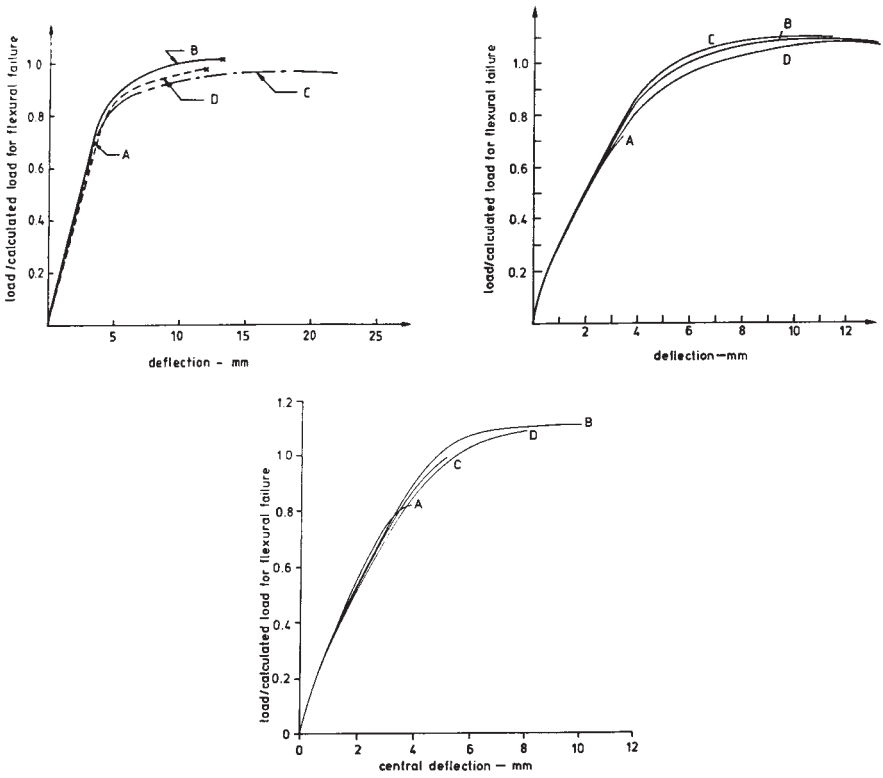

Figure 2.9 Load-deflection curves of beams with (a) *a/d*=1.5 (b) *a/d*=3.3 (c) *a/d*=4.4

concluded, therefore, that, in the absence of shear reinforcement, the main contributor to shear resistance of an RC beam at its ultimate limit state is the *compressive zone,* with the region of the beam below the neutral axis making an insignificant contribution, if any.

As with the concepts discussed so far, the test results are in conflict with the truss analogy concept. The shear span of beam D with *a/d*=1.5 and a large portion of the shear span of beams C and D with *a/d* 2.0 *cannot* behave as trusses because the absence of shear reinforcement does not allow the formation of ties; but the beams sustained loads significantly larger than those widely expected. Such behaviour indicates that, in contrast with widely held views, truss behaviour is *not* a necessary condition for the beams to attain their flexural capacity once their shear capacity is exceeded.

In view of the negligible contribution of aggregate interlock to the shear resistance of an RC beam without shear reinforcement, shear resistance should be associated with the strength of concrete within the region of the beam *above* the neutral axis. The validity of this view has been verified by

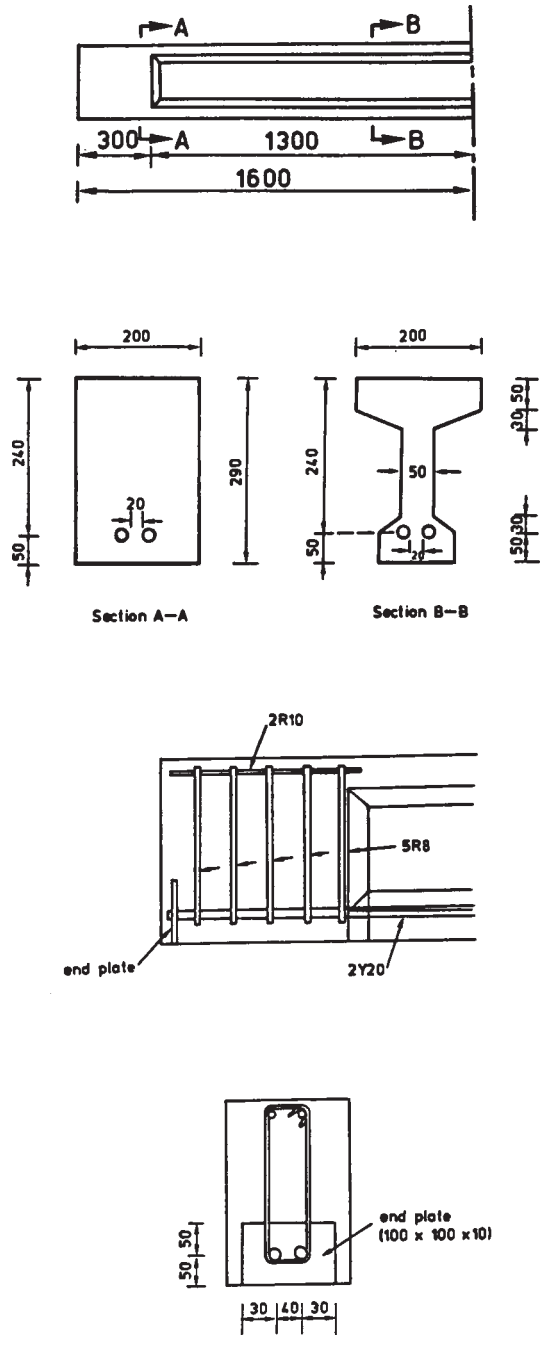

Figure 2.10 Design details of a typical RC T-beam tested under six-point loading.

testing RC T-beams with a web width significantly smaller than that generally considered to provide adequate shear resistance (Kotsovos *et al.,* 1987). Design details of a typical beam, with 2.6 m span, tested under six-point loading are shown in Figure 2.10. Figure 2.11 shows a typical mode of failure.

The tests indicated that the load-carrying capacity of the beams was up to 3 times higher than that predicted on the basis of the currently accepted concepts. It was also found that failure usually occurred in regions not

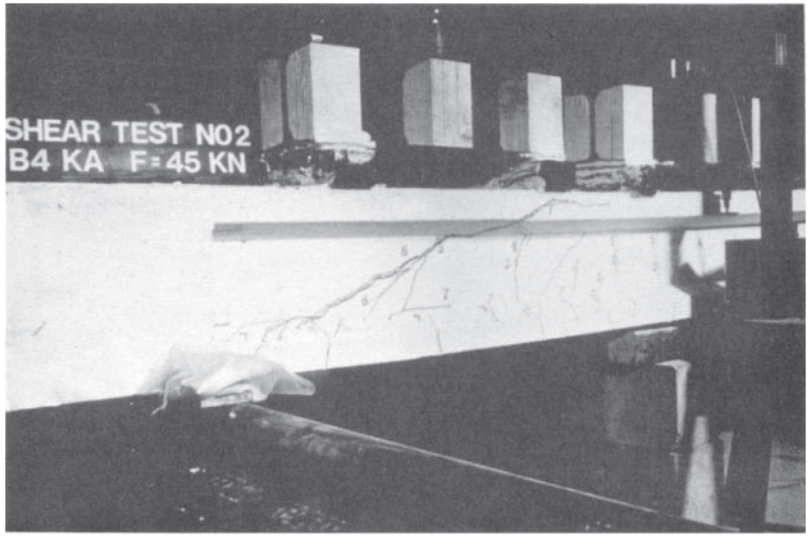

Figure 2.11 Typical mode of failure of an RCT-beam under six-point loading.

regarded, by current Code provisions, as the most critical. As the web width of these beams was inadequate to provide shear resistance, the results support the view that the region of the beam above the neutral axis (the flange in the present case) is the main, if not the sole, contributor to shear resistance.

Figure 2.11 shows that the inclined crack, which eventually caused failure, penetrated very deeply into the compressive zone. Locally it reduced the depth of the neutral axis to less than 5% of the beam depth. In view of such a small depth of the compressive zone, it may be argued that concrete is unlikely to be able to sustain the high tensile stresses caused by the presence of the shear force. Such an argument is usually based on the erroneous assumption that concrete behaviour within the compressive zone of a beam at its ultimate limit state is realistically described by using

uniaxial stress-strain characteristics. This assumption is in conflict with the failure mechanism discussed in the preceding section for the case of flexural capacity.

As in the case of the compressive zone in the region of a section that coincides with a flexural crack, concrete in the region of a section through the tip of a deep inclined crack is also subjected to a wholly compressive state of stress. This is because concrete (due to the small neutral axis depth) will reach its minimum volume level before this level is reached anywhere else within the compressive zone. The compressive state of stress mentioned represents the restraining effect of the surrounding concrete.) A part of the vertical component of this compressive state of stress conteracts the tensile stresses that develop in the presence of shear force. Hence, in spite of the presence of such a force, the state of stress remains compressive and this causes a significant enhancement of the local strength. The mechanism that provides shear resistance is represented in Figure 2.12.

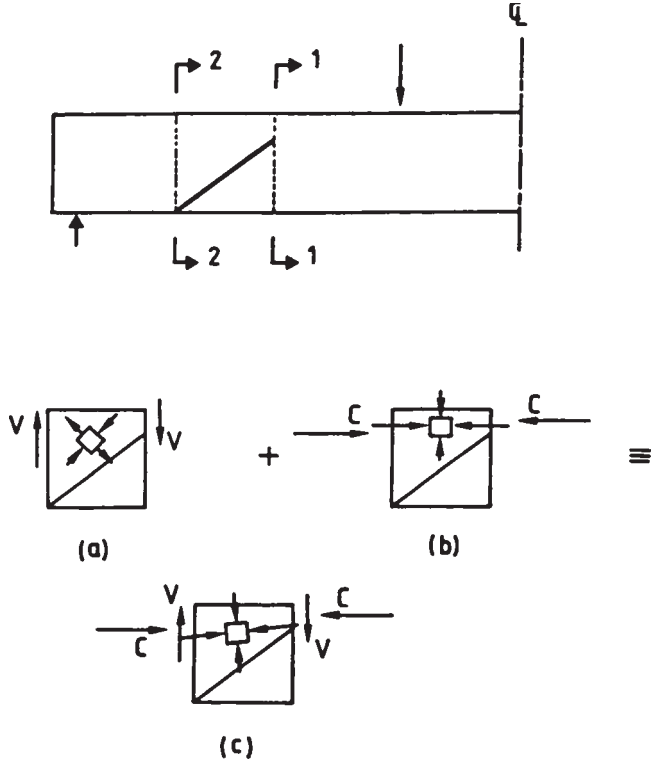

Figure 2.12 Mechanism for shear resistance.

2.4 Compressive force path concept

An attempt to summarise the experimental information discussed in the preceding sections and present it in a unified and rational form has led to the concept of the 'compressive force path' (Kotsovos, 1988a). On the basis of this concept, the load-carrying capacity of an RC structural member is associated with the strength of concrete in the region of the paths along which compressive forces are transmitted to the supports. The path of a compressive force may be visualised as a flow of compressive stresses with varying sections perpendicular to the path direction and with the compressive force, representing the stress resultant at each section (Figure 2.13). Failure is considered to be related to the development of tensile stresses in the region of the path that may develop due to a number of causes, the main ones being as follows.

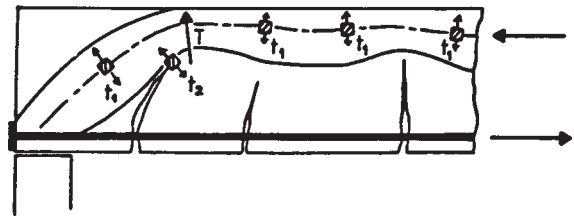

Figure 2.13 Compressive force path.

i) *Changes in the path direction.* A tensile stress resultant (*T* in Figure 2.13) develops for equilibrium purposes at locations where the path changes direction.

ii) *Varying intensity of compressive stress field along path.* The compressive stress will reach a critical level at the smallest cross-section of the path where stress intensity is the highest before that level is reached in adjacent cross-sections. As indicated in Section 2.3, this level marks the start of an abrupt, large material dilation which will induce tensile stresses (*t*1 in Figure 2.13) in the surrounding concrete.

iii) *Tip of inclined cracks.* It is well known from fracture mechanics that large tensile stresses (*t*2 in Figure 2.13) develop perpendicular to the direction of the maximum principal compressive stress in the region of the crack tip (Kotsovos, 1979; Kotsovos and Newman, 1981a).

iv) *Bond failure* (Kotsovos, 1986). Bond failure at the level of the tension reinforcement between two consecutive flexural cracks changes the stress conditions in the compressive zone of the beam element between these cracks, as indicated in Figure 2.14. From the Figure, it can be seen that the loss of the bond force results in an extension of the right-hand side flexural crack sufficient to cause an increase *dz* of the lever arm *z,* such that *Cdz=Va*. Extension of the flexural crack reduces the depth of the neutral axis and thus increases locally the intensity of the compressive stress block. This change in the stress intensity should give rise to tensile stresses as described in ii).

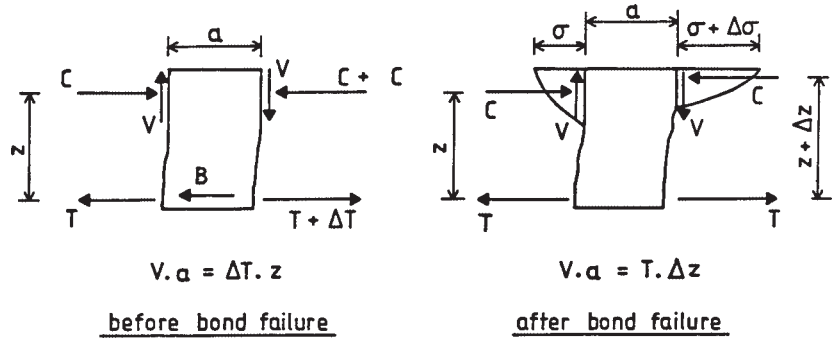

Figure 2.14 Effect of bond failure on stress conditons in compressive zone.

In order to use the concept as the basis for description of the causes of failure of structural concrete members it is essential to visualise the shape of the path along which a compressive force is transmitted to the support. This is not

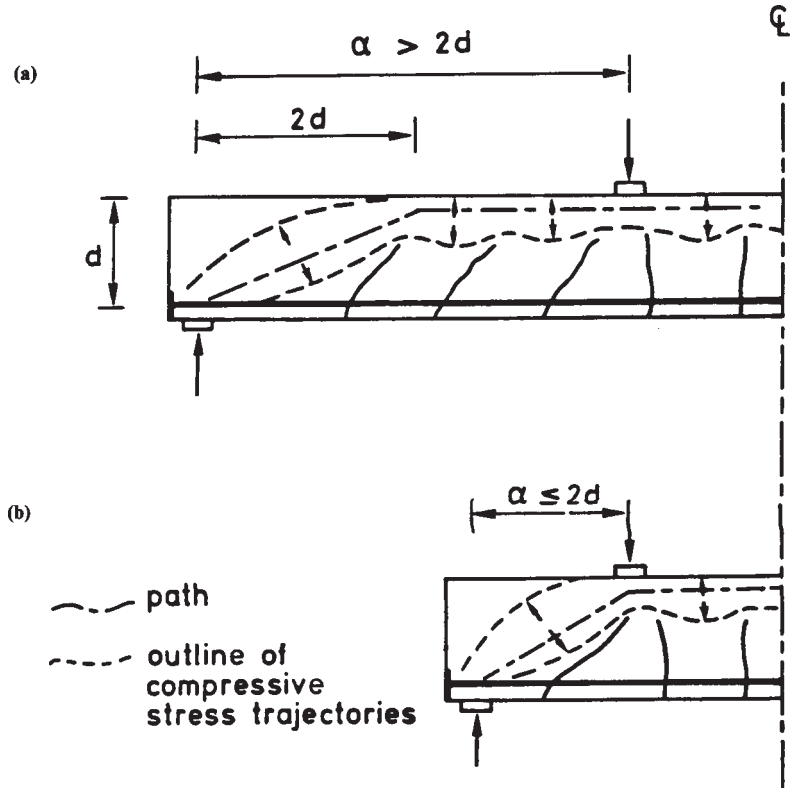

Figure 2.15 Path of compressive force and corresponding outline of compressive stress trajectories for RC beams with various *a/d* ratios.

necessarily a difficult task and it has been shown that, for a simply supported RC beam at its ultimate limit state, the compressive force at the mid cross-section is transmitted to the support by following a path which, for any practical purpose, may be considered to be bi-linear (Kotsovos, 1983b; 1988a). The change in path direction appears to occur at a distance of approximately twice the beam depth *d* for the cases of *(a)* two-point loading with a shear span-to-depth *(a/d)* ratio greater than a value of approximately 2.0 and *(b)* uniformly distributed loading (UDL) with a span-to-depth *(L/d)* ratio greater than a value of approximately 6.0 (Figure 2.15a); for smaller ratios it is considered to occur at the cross-section coinciding with the load point, assuming that UDL can be replaced by an equivalent two-point loading at the third points (Figure 2.15b). Although a deep beam is usually considered to be, by definition, a beam with $L/d<2.0$, investigations of deep beam behaviour often include beams with values of L/d as large as 3.0. It would appear, therefore, that, in all cases, an RC deep beam should be characterised by a compressive force path similar to that of a beam with $a/d<2.0$ or $L/d<6.0$ (Figure 2.16).

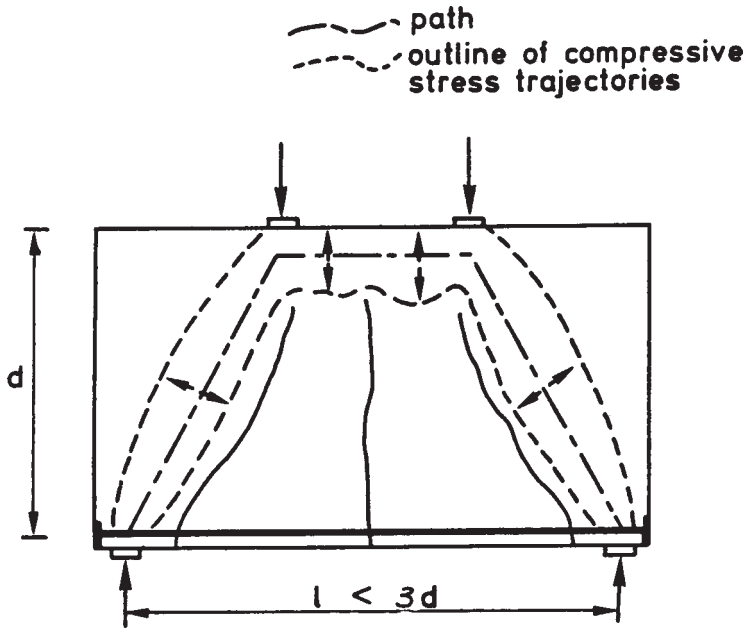

Figure 2.16 Path of compressive force and corresponding outline of compressive stress trajectories for a typical deep beam.

2.5 Deep beam behaviour at ultimate limit state

It is well known that the behaviour of an RC beam with a rectangular cross-section and without shear reinforcement may be divided into four types of behaviour depending on either *a/d,* for beams subjected to two-point

loading, or *L/d,* for beams under UDL (Kani, 1964). Figure 2.17 indicates the variation of bending moment, corresponding to the maximum load sustained by such beams, with varying *a/d,* for the case of two-point loading, and *L/d,* for the case of UDL. The Figure includes a representation of the failure mode that characterises each type of behaviour. It has been shown that the concept of the compressive force path can provide a realistic description of the causes of failure in all four types of behaviour (Kotsovos,

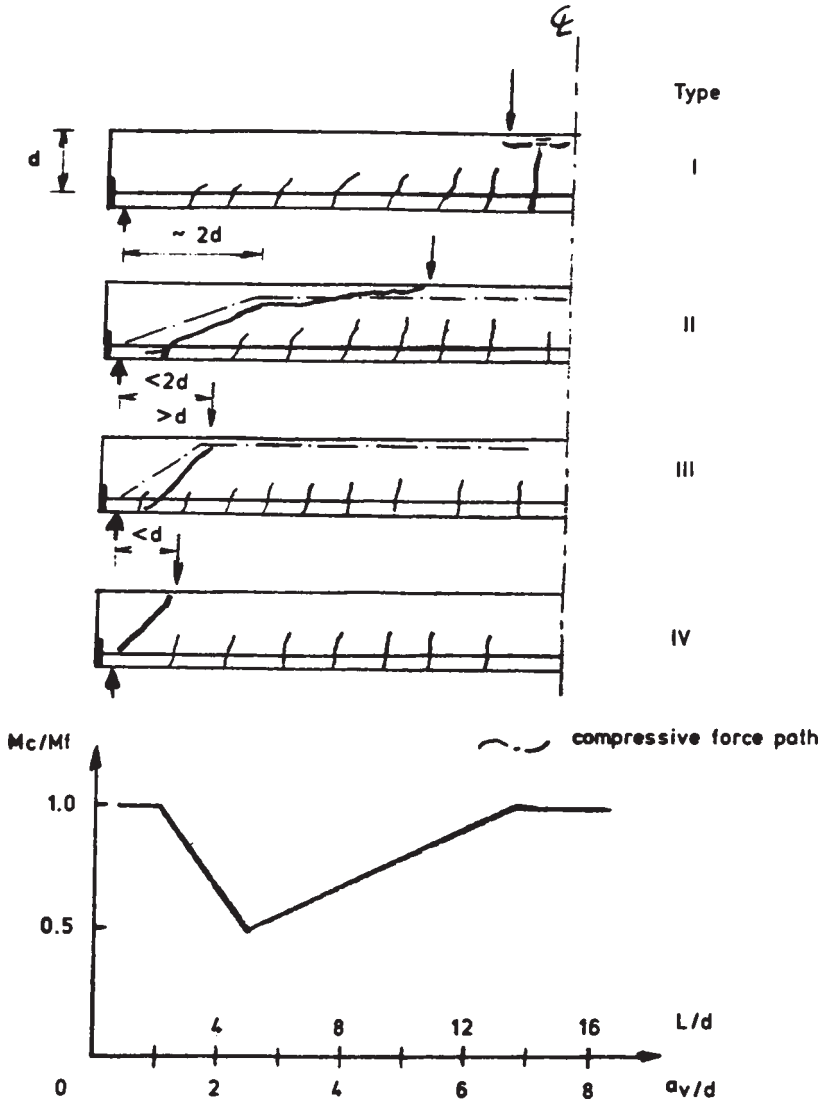

Figure 2.17 Types of behaviour exhibited by RC beams without shear reinforcement subjected to two-point loading.

1983b; 1988a). In the following, however, attention will be focused on types of behaviour III and IV as only these are generally considered to represent deep beam behaviour.

2.5.1 *Causes of failure*

2.5.1.1 Type III behaviour Figure 2.18a is a representation of the typical mode of failure for the case of a deep beam, without web reinforcement, subjected to two-point loading with a/d=1.5 (Leonhardt and Walther, 1962). The Figure indicates that the mode of failure is characterised by a deep inclined crack which appears to have formed within the shear span independently of the flexural cracks. The inclined crack initiated at the bottom face of the beam close to the support, extended towards the top face of the beam in the region of the load point and eventually caused failure of the compressive zone in the middle zone of the beam.

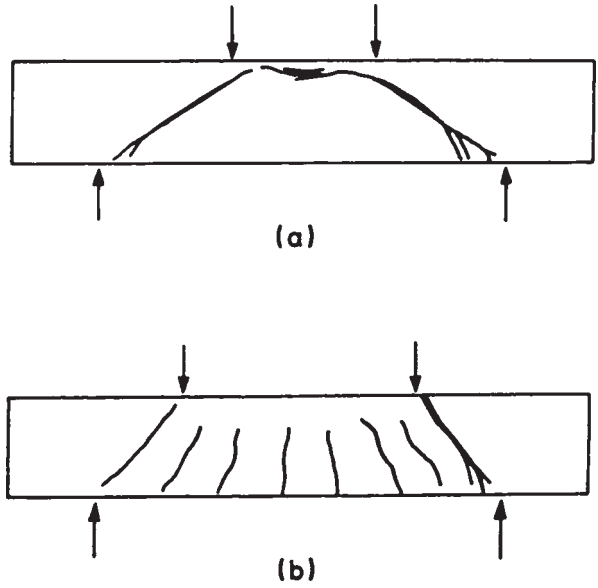

Figure 2.18 Typical modes of failure of deep beams exhibiting (a) type III, (b) type IV behaviour.

Although such a mode of failure does not indicate clearly the underlying causes of failure, the possibility that these are associated with the 'shear capacity of a critical section' within the shear span appears to be remote. As discussed in Section 2.3.2 for the case of an RC beam under similar loading conditions (beam D in Figure 2.8a), reinforcement with stirrups of only the region adjacent to the load-point within the middle portion delays the extension of the inclined crack into the middle portion and allows the beam not only to sustain the design load, but also to respond in a ductile manner

(beam D in Figure 2.9a). The causes of failure should therefore be sought within the middle, rather than the shear, span of such beams.

Figure 2.18a indicates that the inclined crack penetrates the compressive zone of the middle span significantly deeper than any of the flexural cracks that develop within this region of the beam. As the area of the compressive zone of the cross-section coinciding with the tip of the inclined crack is the smallest, it will be there that concrete will first reach its minimum volume level. It should be expected, therefore, that, as discussed in Section 2.3.1, a further increase in load will cause volume dilation that will induce transverse tensile stresses in the adjacent regions. It is the failure of concrete in such regions under the combined action of compressive and tensile stresses that will eventually lead to collapse of the beam. Collapse, therefore, occurs under a load that can be significantly smaller than that which corresponds to flexural capacity and this is indicated in the variation of the maximum moment sustained by the beams with *a/d,* shown in Figure 2.17.

This description of the causes of failure is based entirely on the concept of the compressive force path and it should be emphasised that such a description would be impossible without consideration of the triaxial stress conditions which *always* develop within an RC structural member at its ultimate limit state in the region of the compressive force path. Although such triaxial stress conditions may develop in both the horizontal and the inclined portions of the path (Figure 2.16), it appears that for type III behaviour the most critical conditions develop within the horizontal portion of the path.

2.5.1.2 *Type IV behaviour* Figure 2.18b is a representation of a typical mode of failure for a case of a deep beam, without shear reinforcement, under two-point loading with a/d=1.0 (Leonhardt and Walther, 1962). As for the case of type III behaviour, the above mode of failure is characterised by a deep inclined crack which appears to have formed within the shear span independently of the flexural cracks. However, in contrast with type III behaviour, the inclined crack that characterises type IV behaviour almost coincides with the line joining the load point and the support. It usually starts within the beam web, almost half way between the loading and support points, at a load level significantly lower than the beam load-carrying capacity, and propagates simultaneously towards these points with increasing load. Eventually, collapse of the beam occurs owing to a sudden extension of the inclined crack towards the top and bottom face of the beam in the regions of the load point and support, respectively, within the shear span.

Such a mode of failure is usually referred to as ‘diagonal- splitting’ and its causes are considered to be associated with the shape of the compressive stress trajectories within the shear span of the beam. The shape of these trajectories is given in Figure 2.16 which indicates that they form a barrel-shaped region with its larger cross-section situated roughly half-way between load-point and the support. The curved shape of the stress trajectories should

give rise, for purpose of equilibrium, to tensile stresses at right angles to the direction of the trajectories with the tensile stress resultant acting in the region of the largest cross-section as indicated in Figure 2.16. However, the inclined crack, which starts in this region when the local strength of the material is exceeded, is insufficient to cause collapse of the beam. The inclined crack starts at a load level often several times lower than the collapse load (Kong and Evans, 1987). With increasing load the inclined crack extends simultaneously towards the loading and support points and such an extension should inevitably result in a continuous stress redistribution in the region of the crack tips. The stage is reached, however, when such redistributions cannot maintain the stress levels below critical values and therefore crack extension continues in an unstable fashion simultaneously towards the top and bottom faces and leads to collapse.

The cracking process of structural concrete under increasing load has been investigated analytically by means of nonlinear finite element analysis (Kotsovos and Newman, 1981b; Kotsovos, 1981; Bedard and Kotsovos, 1985; 1986). The results obtained from such investigations for the case of deep beams under two-point loading are shown in Figure 2.19 which shows the crack pattern of a typical beam at various load levels up to ultimate. Cracking not only always starts in regions subjected to a critical combination of compressive and tensile stresses, but also propagates into regions subjected to similar states of stress. The Figure also indicates that the region of the loading point, which is subjected to a wholly compressive state of stress, reduces in size as the applied load increases above the level which causes crack initiation. This is due to stress redistribution which transforms the state of stress at the periphery of this region from a wholly compressive state of stress to a state of stress with at least one of the principal stress components being tensile. When the strength of concrete under this latter state of stress is exceeded cracking occurs and the size of the compressive region further reduces. In all cases investigated collapse occurs before the strength of concrete in the compressive region is exceeded. Such behaviour is in compliance with the conclusions of the experimental information discussed in Section 2.3.

The mode of failure shown in Figure 2.18b is also characterised by a number of flexural and inclined cracks. However, although the inclined cracks extend towards the compressive zone within the middle span as do the inclined cracks that characterise type III behaviour, they differ from the latter in that their depth is similar to that of the flexural cracks. For type IV behaviour, the presence of such cracks may lead to an alternative mode of failure which is characterised by failure of the compressive zone of the middle span of the beam. The causes underlying this mode of failure should be similar to those described earlier in the section for type III behaviour: volume dilation of the concrete in the region of the section that coincides with the tip of the deepest flexural or inclined crack will induce tensile stresses in adjacent regions. It is failure of these regions under the combined

action of the compressive and tensile stresses that will cause collapse of the beam. However, in contrast with type III behaviour, failure of the compressive zone for type IV behaviour occurs when flexural capacity is attained.

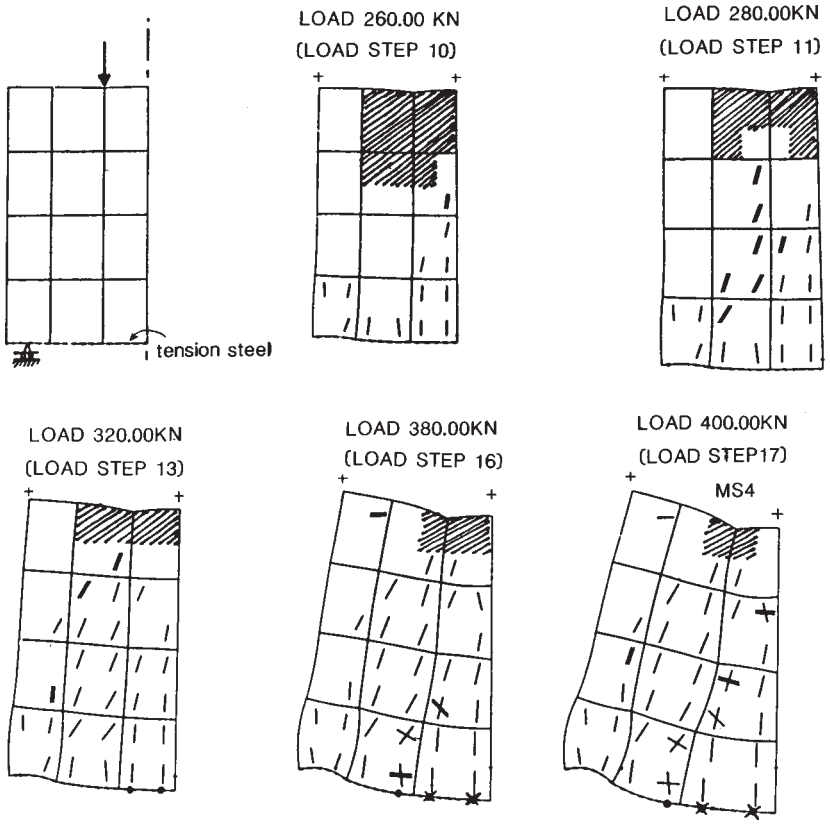

Figure 2.19 Typical stages of crack pattern of deep beams predicted by finite element analysis. (Shaded regions represent regions subjected to a wholly compressive state of stress; single and double short lines inside elements represent cracks occurring at previous and current, respectively, load stages)

As with type III behaviour, the foregoing description of the causes of failure characteristic of type IV behaviour complies with the concept of the compressive force path. Consideration of the triaxial stress conditions has been essential, not only to explain the development of tensile stresses within the horizontal portions of the compressive force path, but also to identify the source of strength of the inclined portion of the path after the occurrence of diagonal-splitting. The existence of a triaxial wholly compressive state of stress in the region of the loading point delays the extension of cracking into

such regions; additional load is, therefore, required for cracking to overcome this local resistance and lead to structural collapse. Unlike type III behaviour, critical conditions may develop within both the inclined and the horizontal portions of the compressive force path.

2.5.2 *Arch and tie action*

The causes of failure of the horizontal portion of the compressive force path (Section 2.5.1) are similar to those which characterise the flexural mode of failure discussed in section 2.3.1. However, unlike the flexural mode of failure, that mode of failure is not associated with beam action. The variation in bending moment along the beam span, essential for a beam to carry shear forces, is mainly effected by a change of the lever arm rather

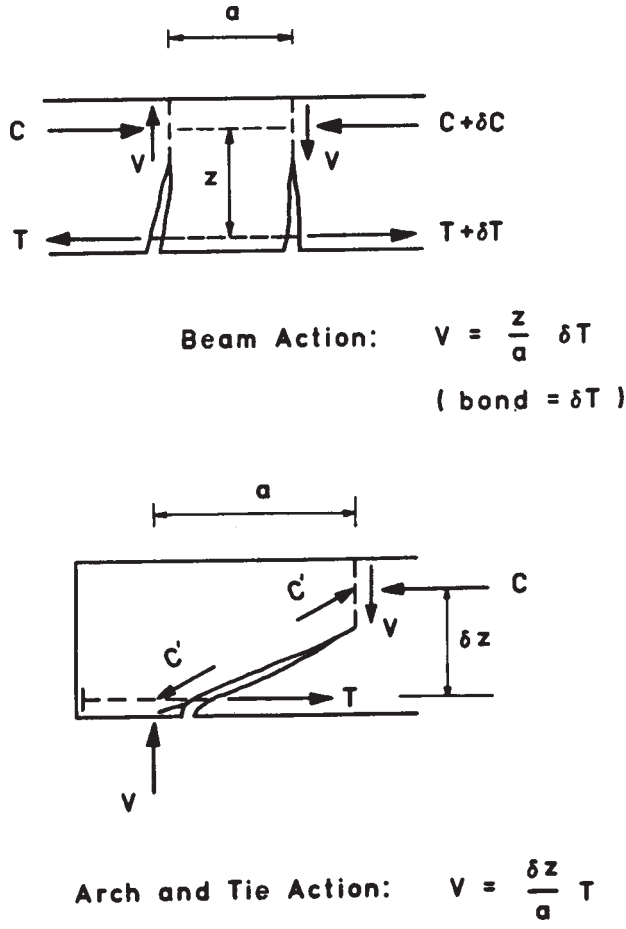

Figure 2.20 Beam, arch and tie actions.

than the size of the internal horizontal actions (Figure 2.20). Such behaviour has been found to result from the fact that the force sustained by the tension reinforcement of a deep beam at its ultimate limit state is constant throughout the beam span (Rawdon de Paiva and Siess, 1965).

It may be deduced therefore that if an RC deep beam at its ultimate limit state cannot rely on beam action to sustain the shear forces, it would have to behave as a tied arch. However, the word 'arch' is used in a broad context; it is considered to describe any type of frame-like structure that would have a shape similar to that of the compressive force path shown in Figure 2.16. It appears, therefore, that the concepts of tied arch action and compressive force path are compatible in the sense that while the former identifies the internal actions providing ultimate resistance to the structure, the latter provides a qualitative description of the causes of structural failure.

2.5.3 *Effect of transverse reinforcement*

2.5.3.1 Type III behaviour As discussed in Section 2.5.1.1, for type III behaviour failure is associated with a large reduction of the size of the compressive zone of the cross-section coinciding with the tip of the main inclined crack. Such a reduction in size will lead to the development of tensile stresses within the compressive zone for the reasons described in item ii) of Section 2.4. Failure, therefore, will occur when the strength of concrete under the combined action of compressive and tensile stresses is exceeded. This type of failure may be prevented either by providing transverse reinforcement that would sustain the tensile stresses that cannot be sustained by concrete alone, or by reducing the compressive stresses.

The effectiveness of transverse reinforcement in sustaining the tensile stresses that develop within the compressive zone is indicated by the fact that such reinforcement prevented the extension of the inclined crack into the compressive zone of beam D in Figure 2.8a and allowed the beam to attain its flexural capacity (Figure 2.9a). However, the amount of reinforcement required to sustain the tensile stresses is difficult to assess, because the tensile stresses are difficult to calculate. Figure 2.9a also indicates that provision of transverse reinforcement only within the shear span can be equally effective (beam C in Figure 2.8a). Such reinforcement reduces the compressive stresses that develop in the cross-section which coincides with the tip of the inclined crack, as it sustains a portion of the bending moment developing in that section (Figure 2.21). A method for designing such reinforcement is discussed in Section 2.6.2.

However, the presence of transverse reinforcement beyond the critical section is essential, as it has been shown experimentally that reinforcing with stirrups only to the critical section does not safeguard against brittle failure (Kotsovos, 1987a). This is because the inclined crack is likely to extend deeply into the compressive zone and, although the presence of such reinforcement within this region inhibits crack opening (and therefore may

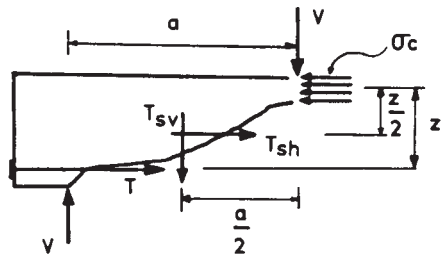

T_{sv} , T_{sh} resultants of tensile forces sustained by uniformly distributed vertical and horizontal, respectively, web reinforcement

σ_c average compressive stress

A_c area of compressive zone

without web reinforcement : $$\sigma_c = \frac{V * a}{A_c * z}$$

with web reinforcement : $$\sigma_c = \frac{V * a - T_{sv} * \frac{a}{2} - T_{sh} * \frac{z}{2}}{A_c * z}$$

If flexural capacity is $M_f = V * a$ and ultimate moment of resistance of critical section is M_c then,

$$T_{sv} * a + T_{sh} * z = 2 (M_f - M_c)$$

Thus,

$$A_{sv} = \frac{T_{sv}}{f_{yv}} \qquad A_{sh} = \frac{T_{sh}}{f_{yh}}$$

Figure 2.21 Effect of transverse reinforcement on compressive stresses at critical cross-section for type III behaviour and method of design of such reinforcement.

prevent further crack extension), the section through the tip of the inclined crack has the smallest compressive zone and it will be there that concrete will reach its minimum volume level. The volumetric expansion that follows will, induce tensile stresses in adjacent sections and these may lead to splitting of the compressive zone and collapse before the flexural capacity is attained. This type of failure may be prevented by extending the transverse reinforcement beyond the critical section to a distance approximately equal to the depth of the compressive zone.

2.5.3.2 Type IV behaviour In contrast, due to the large compressive forces carried by deep beams, it is unlikely that, for type IV behaviour, the presence of conventional web reinforcement in the form of vertical stirrups and/or horizontal (in the longitudinal direction) bars considerably improves load-carrying capacity. Such reinforcement may delay the cracking process but may give only a small increase in load-carrying capacity. This view is supported by most experimental evidence published to date which indicates that the presence of the web reinforcement has little (Rawdon de Paiva and Siess, 1965; Smith and Vatsiotis, 1982), if any (Kong *et al,* 1970), effect on the load-carrying capacity of deep beams. However, the use of nominal web reinforcement is considered essential not only for crack control purposes but also because it reduces the likelihood of instability failures due to out plane actions related to the heterogeneous nature of concrete.

For type IV behaviour, web reinforcement is provided in order to prevent splitting of the inclined portion of the compressive force path (diagonal-splitting). Although the crack faces due to such splitting can, in theory, coincide with any plane including the direction of the inclined portion of the path, conventional web reinforcement can only be effective in sustaining tensile stresses that cannot be sustained by concrete alone *on* the plane of the beam; web reinforcement designed to sustain tensile stresses developing at right angles to this plane is not normally provided. It should come as no surprise, therefore, that conventional web reinforcement does not appear to have any significant effect on load-carrying capacity. Furthermore, for the cases where it was reported that there was some improvement in load-carrying capacity due to the provision of web reinforcement, the improvement may have been due to the simultaneous provision of transverse reinforcement used to form the cage of the web reinforcement.

2.6 Design implications

2.6.1 *Modelling*

As discussed in Section 2.4, the path of the compressive force may be visualised as a flow of compressive stresses with varying sections perpendicular to the path direction and with the compressive force representing the stress resultant at each section (Figure 2.15 and 2.16).

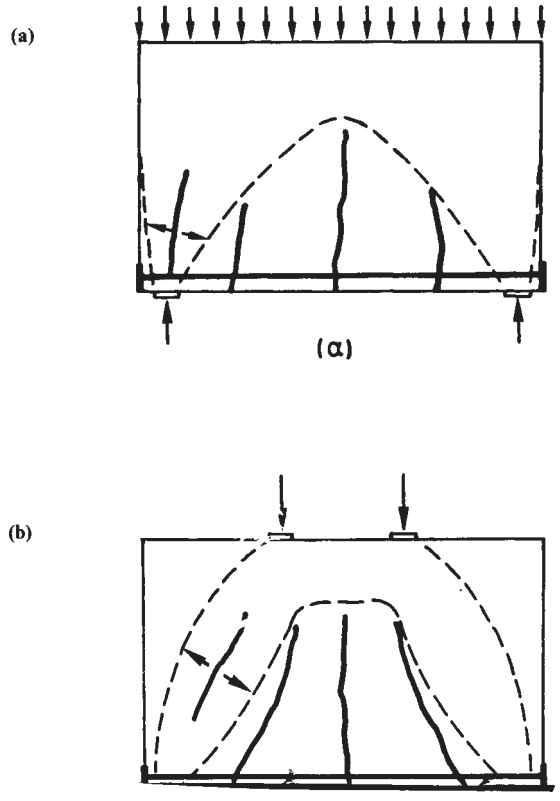

Figure 2.22 Typical inclined compression failures of deep beams under (a) uniform (b) two-point loading.

Although the compressive force carried along the path at a particular location may be easily assessed, such as to satisfy the static equilibrium conditions, the shape of the stress flow and the intensity of the stresses are difficult to establish without resorting to sophisticated methods of analysis (such as, for example, finite element analysis). The use of such methods in design is, however, prohibitive not only because of their high cost but also because they are not widely available and their use depends on expert advice. A simple method is required, as such information regarding the stress field in the region of the compressive force path is essential for assessing the maximum force that can be carried along the path.

The shape of the stress flow and the intensity of the stress field are very much dependent on the beam boundary conditions. For a simply supported deep beam subjected to a load uniformly distributed on its top face, the stress flow may have a shape similar to that indicated in Figure 2.22a. It has been suggested (Kotsovos, 1988a) that it is realistic to consider that the difference in shape between such a flow and that caused by an equivalent

load concentrated at the two third points affects only the location of failure initiation within a particular portion (inclined or horizontal) of the path and not the magnitude of the force that can be carried along this portion (Figure 2.22). Based on this reasoning, it is considered realistic for design purposes to replace the actual stress flow with a uniform stress flow of intensity equal to the uniaxial cylinder compressive strength (f_c). The cross-section of the flow should be chosen such that the actual maximum compressive force carried along the path remains unchanged.

Figure 2.23 shows two such simplified compressive force paths for the case of a deep beam subjected to single-and two-point loading, respectively. The compressive force path for a two-point loading may also be valid for the case of a uniform load if the equivalent two-point load is applied at the third

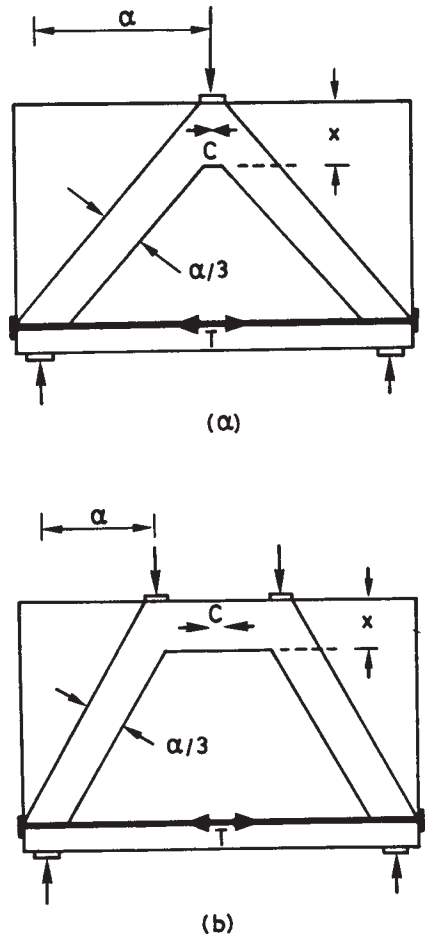

Figure 2.23 Proposed models for deep beams under (**a**) single-point (**b**) two-point and/or uniform loading.

points. The stress flow is considered to have a rectangular cross-section with a width equal to the beam width. The depth of the *horizontal* portion of the stress flow of the path may be assessed such that the compressive force equals the force sustained by the tensile reinforcement. As indicated in Figure 2.23, the inclined stress flow of the path is symmetrical with respect to the line connecting the intersection of the directions of the applied load and the horizontal path of the compressive force, with the intersection of the directions of the reaction and the tensile reinforcement. A suitable depth for the *inclined* stress flow is considered to be $a/3$, where a is the shear span. If $a/3$ is smaller than the effective width of the bearing, $a/3$ should be substituted with the width of the bearing, as recommended by the Joint Committee of the Institution of Structural Engineers and the Concrete Society (1979).

A precise description of the shape of the idealised path of the compressive force in the region where it changes direction is not deemed essential. This is because as discussed in Section 2.5.1, the causes of failure appear to be associated with the stress conditions in regions away from the location where the path changes direction. Furthermore, implicit is the assumption that failure in localised regions resulting from anchorage problems, concentrated loads, and so on are prevented by proper detailing.

2.6.2 *Design method*

The concepts described in the preceding section indicate that a deep beam will withstand the action of an applied load if the resulting internal actions can be safely sustained by the members of the proposed model. The objective of a design procedure, therefore, should be the sizing of these members such as to sustain these actions. A typical procedure for the case of two-point loading (Figure 2.23b) may be formulated as follows (Figure 2.24):

i) Assuming the beam depth d and width b, are given, assess the depth of the horizontal portions of the stress flow by satisfying the moment equilibrium condition with respect to the intersection of the directions of the reaction and the tension reinforcement. If that condition cannot be satisfied with the given values of d and b, adjust d and b accordingly.
ii) Considering that the tension reinforcement yields before the load-carrying capacity of the horizontal portion of the stress flow is attained, assess the amount of tension reinforcement required to satisfy the equilibrium condition of the horizontal internal actions,
iii) Check whether the vertical component of the compressive force carried by the inclined portion of the stress flow is greater than, or equal to, the external load carried by the flow to the support. If not, adjust the beam width b and repeat the process.

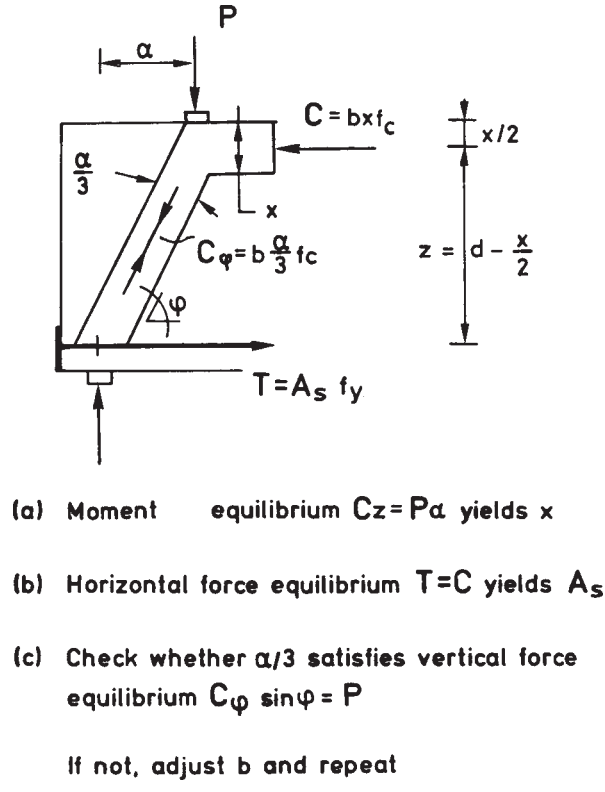

Figure 2.24 Proposed method for designing an RC deep beam.

For type IV behaviour, this design procedure needs only to be complemented by good detailing which can be achieved by following the recommendations of current Code provisions for deep beam design. For type III behaviour, the proposed procedure does not safeguard against failure of the horizontal compression member of the model due to the deep penetration of the inclined crack (see Section 2.5.1). The maximum moment M_c that can be sustained by the section through the tip of the inclined crack can be assessed as described by Kotsovos (a) (Figure 2.25) by using the empirical formula proposed by Bobrowski and Bardham-Roy (1969) and recommended by the joint committee of the Institution of the Structural Engineers and the Concrete Society (1979). If M_f is the flexural capacity of the beam, then web reinforcement is provided such that its contribution to the flexural capacity of the critical section is M_f-M_c (see Figure 2.21). Such reinforcement is uniformly distributed in both the horizontal and vertical directions.

The proposed design method may be easily extended to apply for deep beams subjected to loading applied to their bottom face. This load can be easily transferred to the top face of the beam by using stirrups designed so

Maximum moment Mc at critical cross—section, at a distance $a \begin{matrix} < 2d \\ > d \end{matrix}$ from support, may be assessed as follows:

1. Assess flexural capacity $M_f = A_s * f_y * z$ (see Fig.24)
2. Use eqn (1) below to assess M_c' for $s=2d$
3. $M_c = M_f - (M_f - M_c')(a-d)/d$

$$M_c = 0.875\, s\, d\, (0.342 b_1 + 0.3\, \frac{M_f}{d^2} \sqrt{\frac{z}{s}}\,) \sqrt[4]{\frac{16.66}{p_w f_y}} \qquad ...(1)$$

where s is the distance of cross—section from support (mm)

$$s = \begin{cases} \text{shear span for two—point loading} \\ \text{2d for uniformly distributed loading} \\ \text{all parameters refer to cross—section s} \end{cases}$$

M_c is the moment corresponding to "shear" failure (Nmm)

M_f is the flexural capacity (Nmm)

d is the effective depth (mm)

z is the lever arm of horizontal internal actions (mm)

p_w is the ratio $\dfrac{\text{area of tension steel}}{\text{web area of concrete to effective depth}}$

f_y is the characteristic strength of the tension steel (N/mm^2)

b_1 is the effective width (mm) given by the lesser of $b_o + 2b_s$, $b_o + 2d_s$; b_o , b_s , d_s , are as shown in the Figure below

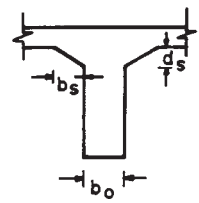

Figure 2.25 Assessment of ultimate moment of resistance of an RC beam cross-section under combined flexure and shear (type III behaviour).

as to withstand the loading as indicated in Figure 2.26 (Leonhardt and Walther, 1966).

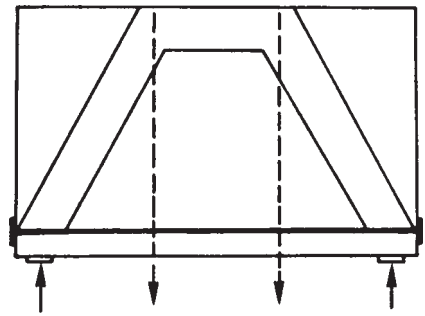

Figure 2.26 Schematic representation of method of transfer of load from bottom to top face of deep beam.

2.6.3 *Verification of design method*

The design procedure described has been used to assess the load-carrying capacity of a large number of deep beams whose behaviour has already been established by experiment elsewhere (Rawdon de Paiva and Siess 1965, Ramakrishnan and Ananthanarayana, 1968; Kong *et al.,* 1970; Smith and Vantsiotis, 1982; Rogowski *et al.,* 1986; Subedi, 1988). The correlations between prediction and measured values are shown in Figures 2.27 – 2.29. The investigation covers a wide range of loading conditions including uniform, single-point, and two-point loading. In most cases, the beams considered are simply supported (Rawdon de Paiva and Siess, 1965; Ramakrishnan and Ananthanarayana, 1968; Kong *et al.,* 1970; Smith and Vantsiotis, 1982; Subedi, 1988); however, the results obtained from work on continuous deep beams (Rogowski *et al.,* 1986) have also been included.

No distinction has been drawn between beams with and without web reinforcement as all beams had L/d=2.0 (type IV behaviour) and, as discussed in section 2.5.3, the effect of such reinforcement on load- carrying capacity appears to be insignificant. However, the values measured for beams without web reinforcement exhibit a significantly larger variability.

As indicated in the Figures, the predicted modes of failure are classified into two types: i) those characterised by failure of the inclined concrete member of the model (inclined compression failure) and ii) those characterised by failure of the horizontal concrete member of the model (flexural failure). For the latter type yielding of the tension steel is assumed always to have preceded collapse for the cases considered. In general, the observed modes of failure appear to be in agreement with the predictions, although those of the observed modes of failure characterised by inclined cracking are usually reported in the literature as shear or diagonal splitting failures.

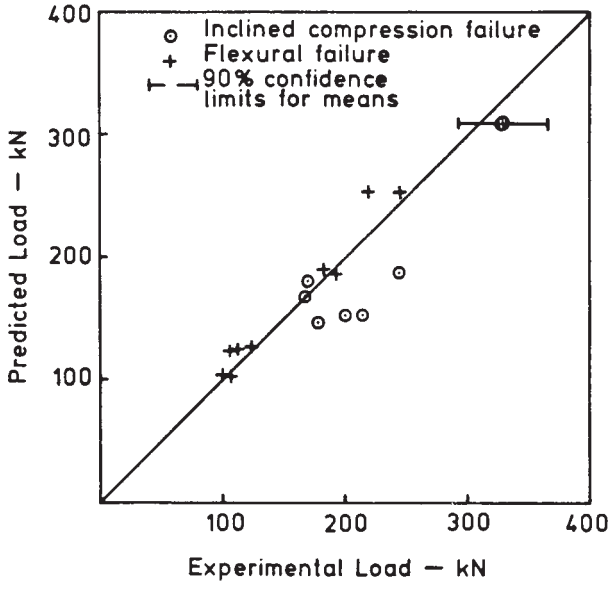

(a)

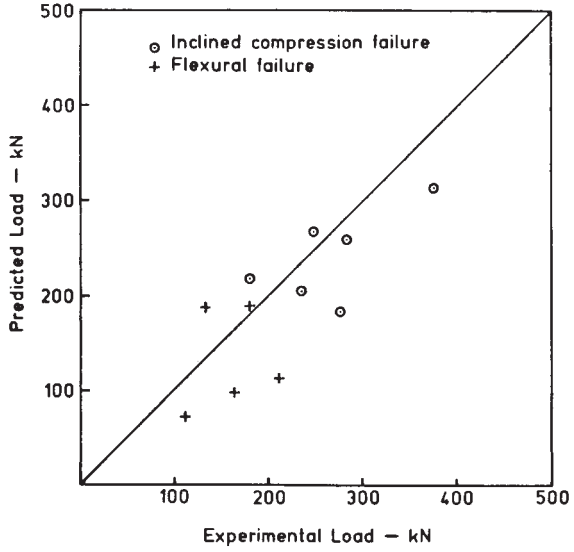

(b)

Figure 2.27

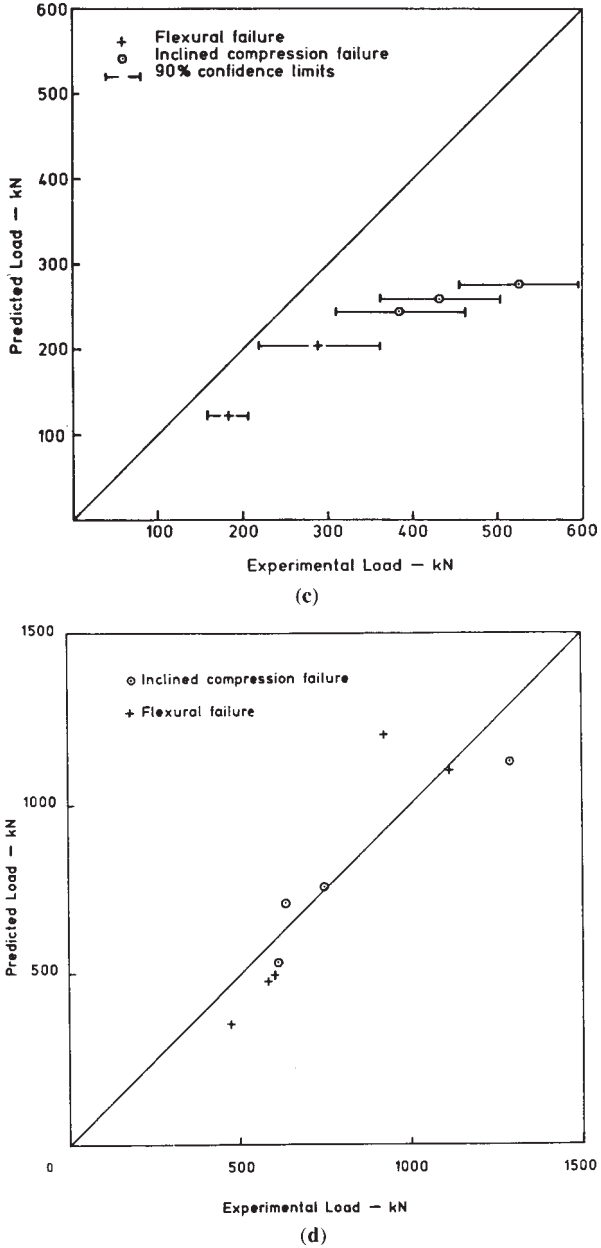

Figure 2.27 Correlation of predicted load-carrying capacity of RC deep beams under two-point loading with experimental values reported by (a) Rawdon de Paive and Siess (1965) and Smith and Vantsiotis (1982), (b) Ramakrishnan and Ananthanarayana (1968), (c) Kong *et al* (1970), (d) Subedi (1988).

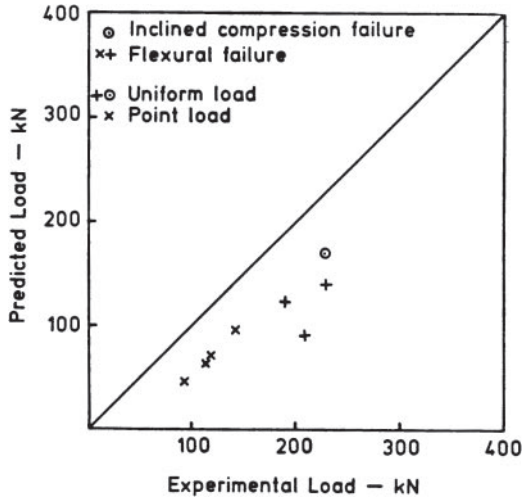

Figure 2.28 Correlation of predicted load-carrying capacity of RC deep beams under single-point loading and uniformly distributed loading with experimental values reported by Ramakrishnan and Ananthanarayana (1968).

2.6.3.1 Simply supported deep beams Figure 2.27 indicates a sufficiently close correlation for practical purposes between predicted and experimental values for the case of deep beams subjected to two-point loading. The slight overestimate of load-carrying capacity in certain cases is due to the larger variability of the results obtained for the beams without web reinforcement. Placing nominal web reinforcement considerably reduces the variability and

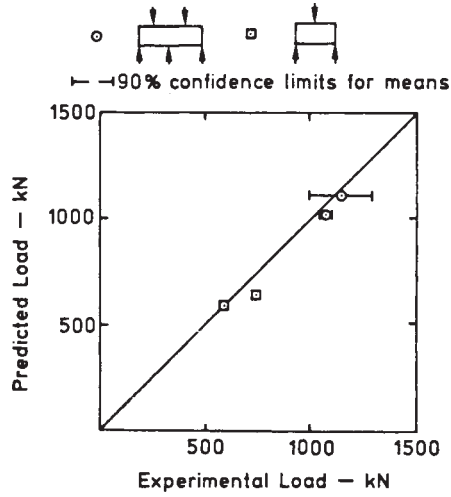

Figure 2.29 Correlation of predicted load-carrying capacity of continuous and simply-supported RC deep beams under single-point loading with experimental values reported by Rogowski *et al.* (1986).

the predicted values appear always to be on the safe side. Figure 2.28 indicates an equally good correlation between predicted and experimental values for the case of deep beams subjected to uniform and single-point loading, with the predicted values always being on the safe side.

2.6.3.2 Continuous deep beams The load-carrying capacity of the continuous RC deep beams may be calculated by assuming that the indeterminate bending moment of the internal support is equal to that obtained by elastic analysis. For a continuous beam with a uniform flexural capacity throughout its length, the above moment will be the first to reach its ultimate value. When this occurs, an under-reinforced beam should behave in a ductile manner in the region of the support. Such behaviour allows load redistribution and the ultimate limit state is reached when the flexural capacity at another section away from the supports is attained.

On the basis of the above, the model proposed for simply supported deep beams can easily be extended to describe the ultimate limit state of a continuous deep beams as indicated in Figure 2.30. Using this model to predict the load-carrying capacity of continuous deep beams tested by Rogowski *et al.,* (1986), the close correlation between predicted and experimental values shown in Figure 2.29 is obtained.

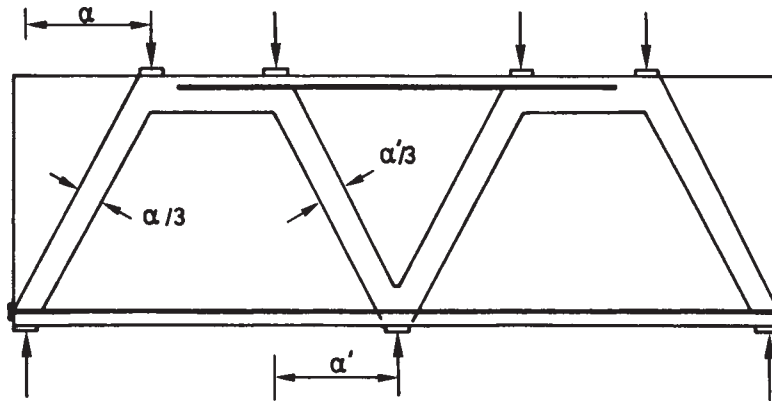

Figure 2.30 Proposed model for continuous RC deep beams.

References

Bedard, C, and Kotsovos, M.D. (1985) Application of non-linear finite element analysis to concrete structures. *J.Struct. Engng. Am. Soc. Civ. Engrs.* **111:** 2691.

Bedard, C. and Kotsovos, M.D. (1986) Fracture processes of concrete suitable for non-linear finite element analysis. *J. Struct. Engng, Am. Soc. Civ. Engrs.* **112:** *573.*

Bobrowski, J. and Bardham-Roy, B.K. (1969) A method of calculating the ultimate strength of reinforced and prestressed concrete beams in combined flexure and shear. *Struct. Engr.* **47**: 197.

British Standards Institution. (1985) *Code of Practice for Design and Construction,* BS8110, **1.**

Fenwick, R.C and Paulay, T. (1968) Mechanisms of shear resistance of concrete beams. *J.Struct. Div. Am. Soc. Civ. Engrs.* **94:** 2325.
Joint Committee of the Institute of Structural Engineers and The Concrete Society. (1978) *Design and Detailing of Concrete Structure for Fire Resistance.* Institution of Structural Engineers, London.
Kani, G.N.J. (1964) The riddle of shear and its solution. *Am. Concr. Inst*. **61:** 441.
Kong, F.K. and Evans, R.H. (1987) *Reinforced and Prestressed Concrete*. 3rd edn, Van Nostrand Reinhold (UK), London: 200.
Kong, F.K., Robins, P.J. and Cole, D.F. (1970) Web reinforcement effects on deep beams. *Am. Concr. last. J.* **67:** 1010.
Kotsovos, M.D. (1979) Fracture processes of concrete under generalised stress states. *Maters, and Structures* **12:** 431.
Kotsovos, M.D. (1982) A fundamental explanation of the behaviour of reinforced concrete beams in flexure based on the properties of concrete under multiaxial stress. *Mater, and Structures* **15:** 529.
Kotsovos, M.D. (1983a) Effect of testing techniques on the post-ultimate behaviour of concrete in compression. *Mater, and Structures* **16:** 3.
Kotsovos, M.D. (1983b) Mechanisms of shear failure. *Magazine Conr. Res.* **35:** 99.
Kotsovos, M.D. (1984) Deformation and failure of concrete in a structure. *Proc. Internat. Conf. on Concrete Under Multiaxial Conditions, Toulouse.*
Kotsovos, M.D. (1984c) Behaviour of reinforced concrete beams with a span to depth ratio between 1.0 and 2.5 *Am. Concr. Inst.* **81:** 279.
Kotsovos, M.D. (1986) Behaviour of reinforced concrete beams with a shear span to depth ratio greater than 2.5. *Am. Concr. Inst.* **83,** 1026–1034.
Kotsovos, M.D. (1987a) Shear failure of reinforced concrete beams. *Engng. Structures* **9:** 32.
Kotsovos, M.D. (1987b) Shear failure of RC beams: a reappraisal of current concepts. *CEB Bull. 178/179:* 103.
Kotsovos, M.D. (1988a) Compressive force path concept: basis for ultimate limit state reinforced concrete design. *Am. Concr. Inst.* Jo. **85:** 68.
Kotsovos, M.D. (1988b) Design of reinforced concrete deep beams. *Struct. Engr.* **66:** 28.
Kotsovos, M.D. (a) Designing RC beams in compliance with the concept of the compressive force path (in preparation).
Kotsovos, M.D. (b) Behaviour of RC beams designed in compliance with the compressive force path (in preparation).
Kotsovos, M.D, Bobrowski, J. and Eibl, J. (1987) Behaviour of RC T-beams in shear. *Struct. Engr.* **65B:** 1.
Kotsovos, M.D. and Newman, J.B. (1981a) Fracture mechanics and concrete behaviour. *Magazine Concr. Res.* **33:** 103.
Kotsovos, M.D. and Newman, J.B. (1981b) Effect of boundary conditions on the behaviour of concrete under concentrations of load. *Magazine Concr. Res.* **33:** 161.
Kotsovos, M.D. and Pavlovic, M.N. (1986) Non-linear finite element modelling of concrete structures: basic analysis, phenomenological insight, and design implications, *Engng. Computations* **3:** 243.
Kotsovos, M.D., Pavlovic, M.N. and Arnaout, S. (1985) Non-linear finite element analysis of concrete structures: a model based on fundamental material properties. *Proc. NUMETA 85, Numerical Methods in Engineering: Theory and Applications, Conf. Swansea,* eds J.Middleton and G.N.Pande, 2 Vols, A.A.Balkema, Rotterdam **2:** 733.
Leonhardt, F. and Walter, R. (1961–2) *The Stuttgart shear tests, 1961. Cement and Concrete Association Library, London,* (translation of articles that appeared in *Beton and Stahlbetonbau,* **56,** No. 12, 1961; **57,** Nos. 2,3,6,7 and 9, 1962. Translated by C.V.Amerongen).
Morsch, E. (1909) *Concrete Steel Construction.* English Translation E.P.Goodrich, McGraw-Hill, New York, from 3rd edn of *Der Eisenbetonbau* (1st edition 1902).
Ramakrishna, V. and Ananthanarayana, Y. (1968) Ultimate strength of deep beams in shear. *Am. Concr. J.* **65:** 87.
Rawdon de Paiva, H.A. and Siess, C.P. (1965) Strength and behaviour of deep beams in shear. *J. Struct. Div. Am. Soc. Civ. Engrs.* **91:** 19.
Regan, P.E. (1969) Shear in reinforced concrete beams. *Magazine Concr. Res.* **21:** 31.

Ritter, W. (1899) Die Bauweise Hennebique. *Schweizerische Bauzeitung* **33:** 59.
Rogowski, D.M., MacGregor, J.G. and Ong, S.Y. (1986) Tests of reinforced concrete deep beams. *Am. Concr. Inst.* **83:** 614.
Smith, K.N. and Vantsiotis, A.S. (1982) Shear strength of deep beams. *Am. Concr. Inst.* **79:** 201.
Subedi, N.K. (1988) Reinforced concrete deep beams: a method for analysis. *Proc. Instn Civ.* Engrs, Part 2, **85:** 1.
Taylor, H.P.J. (1968) *Shear Stresses in Reinforced Concrete Beams without Shear Reinforcement*. Technical Report TRA 407, Cement and Concrete Association, London.

3 Deep beams with web openings

S.P.RAY, Regional Institute of Technology, Bihar, India

Notation

A_s sectional area of tensile steel

A_w sectional area of individual inclined web steel

A_{wt} sectional area of individual inclined web steel below NA

a_1, a_2 coefficients defining the dimensions of web opening

b breadth (thickness) of beam

C total compressive force

C_e coefficient for concrete

c cohesion of concrete

D overall depth of beam

d effective depth of beam

e_x, e_y eccentricities of web opening centre

F_s total force in tensile steel

F_w total force in inclined web steel

F_{ct} total force of concrete in the tension region

F_{wt} total force in inclined web steel below NA

f'_c cylinder (150 mm dia.×300 mm height) compressive strength of concrete ($= 0.8f'_{cu}$)
cylinder (150 mm dia.×300 mm height) splitting tensile strength of concrete.

f_r modulus of rupture strength of concrete ($= 1.8f'_t$)

f'_{cu} cube (150 mm) compressive strength of concrete.

f_{sy} yield point stress of tensile steel

f_{wy} yield point stress of web steel intercepted by the critical diagonal crack.

J_s lever arm coefficient for tensile steel

J_{wt} lever arm coefficient for inclined web steel in the tension region

K coefficient as defined in figure 3.14

K_w empirical coefficient, equal to 0.85 for horizontal, cot ß for vertical and 1.15 for inclined web bars.

K_{ct} centroidal distance of F_{ct} from bottom of the compression stress block $= \frac{2}{3}(1 - K)d$.

K_{wt} centroidal distance of the web bars under the NA from bottom of the compression stress block ($= \frac{1}{n}\sum_{n} k_{wt}$)

K_1, K_2 coefficients defining position of web opening

L effective span of beam (i.e. distance from centre to centre of supports)

M_{FL} flexural moment capacity of beam due to concrete, tensile steel and web steel,

m ratio of path length intercepted to total path length along the

	natural load path (or critical diagonal crack)
N	normal force on the inclined plane
n	number of bars intercepted by the critical diagonal crack.
P_c, P_s, P_w	first, second and third terms respectively of Eqn (3.16)
P_u, $P_{u(test)}$	measured ultimate load of beam
$P_{u(calc)}$	computed ultimate load of beam
p_s	A_s/bD (expressed in percentage)
p'_s	A_s/bD (expressed in ratio)
p_{wt}	$\sum_n A_{wt}/bd$ (expressed in ratio)
Q_u	ultimate shear strength of beam (=$P_u/2$ for two-point loading; =$P_u/2$ and $P_u/4$ in cases of path I and path II, respectively, for four-point loading)
r_w	$\sum_n A_w/bD$ (expressed in percentage)
S	spacing of inclined web steel
T	tangential force along the inclined plane
T_c	cohesive force of concrete along the inclined plane
W	total load on beam
X	effective shear-span of beam
X_N	nominal shear-span of beam
X_{net}	$(X_N\text{-}a_1X)$
Y_{net}	$(0.6D\text{-}a_2D)$
Z	lever arm.
α	angle of inclination of the inclined web bar with the horizontal
ß	angle of inclination of the natural load path with the horizontal
γ_c, γ_f, γ_m	partial safety factors for loads and materials
η	ratio of the tensile strength to the compressive strength of concrete ($=f'_t/f'_c$)
λ_1, λ_2, λ_3	empirical coefficients as defined in Eqns (3.17)–(3.20)
μ, μ'	empirical coefficient as defined in Eqn (3.33)
ξ_1, ξ_2	performance factor or safety factors as defined in Eqns (3.45) and (3.46)
$\bar{\sigma}$	average normal stress on the plane of rupture,
σ_x, σ_y	normal stresses at a point in the directions of X and Y respectively
σ_1, σ_3	principal stresses in decreasing order of magnitude
$\bar{\tau}$	average shearing stress along the plane of rupture
τ_{xy}	shearing stress at a point (x, y)
φ	angle of internal friction of concrete as defined by Eqn (3.15)
ψ_s, ψ_w	empirical co-efficients, as defined in Eqn (3.21)

3.1 Introduction

In various forms of constructions, openings in the web region of deep beams are sometimes provided for essential services and accessibility. Figure 3.1 shows a deep beam with web opening in a building. In such situations, it is highly important to know the behaviour and ultimate

strength of these beams. It is well known that the so-called classical elastic theory of bending is not applicable to problems involving deep beams. As such, the stress pattern is non-linear and deviates considerably from those derived by Bernaulli and Navier. Based on ultimate load theory a number of investigators studied the problem of deep beams with solid webs and put forward certain empirical and semi-empirical equations for predicting their ultimate load capacity. Some national codes (CEB-FIP, 1970; BSCP 110, 1972; ACI318, 1971; 1978) eventually incorporated some provisions regarding design of such beams. However, studies on deep beams with web openings are very limited and no national code even provides any guidance for design of deep beams with web openings.

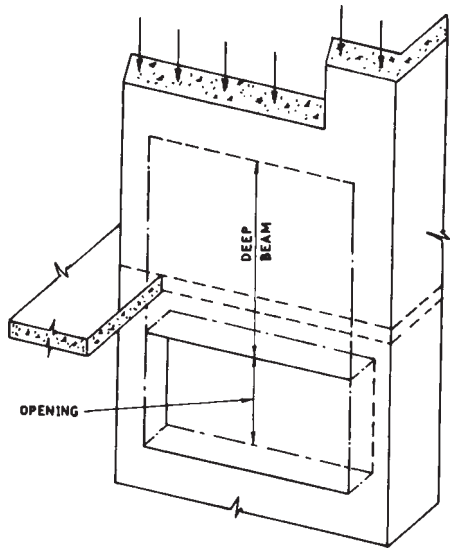

Figure 3.1 Deep beam with web opening.

In the recent past Kong and his associates (1973) at the Universities of Nottingham Cambridge and Newcastle upon Tyne studied at length the problems of deep beams and presented semi- empirical formulae for predicting the ultimate strengths of both solid beams and beams with web openings.

The CIRIA deep-beam design guide (Ove Arup and Partners, 1984) dealing with the design and detailing of web openings was mainly based on published literature, intuitive feel for the forces and constructional experiences. These approaches tended to be cautious in the absence of adequate test data.

Therefore, there is a definite need for understanding of in particular the behaviour and strength of deep beams with openings in the web.

3.2 Factors influencing behaviour

The main factors affecting the behaviour and performance of deep beams with web openings are

i) span to depth ratio;
ii) cross-sectional properties (i.e. rectangular section, Tee-section, etc.);
iii) amount and location of main longitudinal reinforcement;
iv) amount, type and location of web reinforcement;
v) properties of concrete and reinforcements;
vi) shear span to depth ratio;
vii) type and position of loading;
viii) size, shape and location of web opening etc.

3.3 General behaviour in shear failure (under two-point loading)

Concrete strain variation at mid-span section indicates that before first cracking, the beam behaves elastically, shows non-linear distribution of strain and more than one neutral axes (Figure 3.2). The number of neutral axes decreases with incremental loads and at ultimate stage only one neutral axis is present. Concrete strain variation at the plane of rupture shows the deep beam behaviour also before cracking and persistance of diagonal tension till failure. However, the extent of crack width and the deflection pose no problem at the service loads. If, however, the crack width is limited to 0.3 mm, the corresponding load will be in the range of 60–70% of the ultimate load (Ray and Reddy, 1979; Ray, 1980, 1982).

3.3.1 *Beam with rectangular web openings*

The first visible inclined cracks normally appear in the support bearing regions and from the opening corners at load varying levels of about 36–55% of the ultimate loads (Figure 3.3). With incremental loads, these initial cracks of short lengths tend to propagate in their forward diagonal direction slowly. Some similar types of crack parallel to and alongside the initial ones also form for short lengths and these are not much active in the formation of critical diagonal crack. For the loading range of about 50–97% of the ultimate, typical diagonal cracks longer than the initial ones (resembling the phenomenon of a critical diagonal crack in a solid web deep beam) suddenly emerge with a harsh noise in the upper and lower shear zones above and below the openings but appreciably away from the openings and bearing points. These critical diagonal cracks instantaneously propagate both ways towards the bearing regions and opening corners, widen and announce the failure of the structure.

3.3.2 *Beam with circular web openings*

The first visible cracks normally appear at almost the same range of percentages of ultimate loads as in the case of rectangular openings (Figure 3.4) There are two main distinctive features.

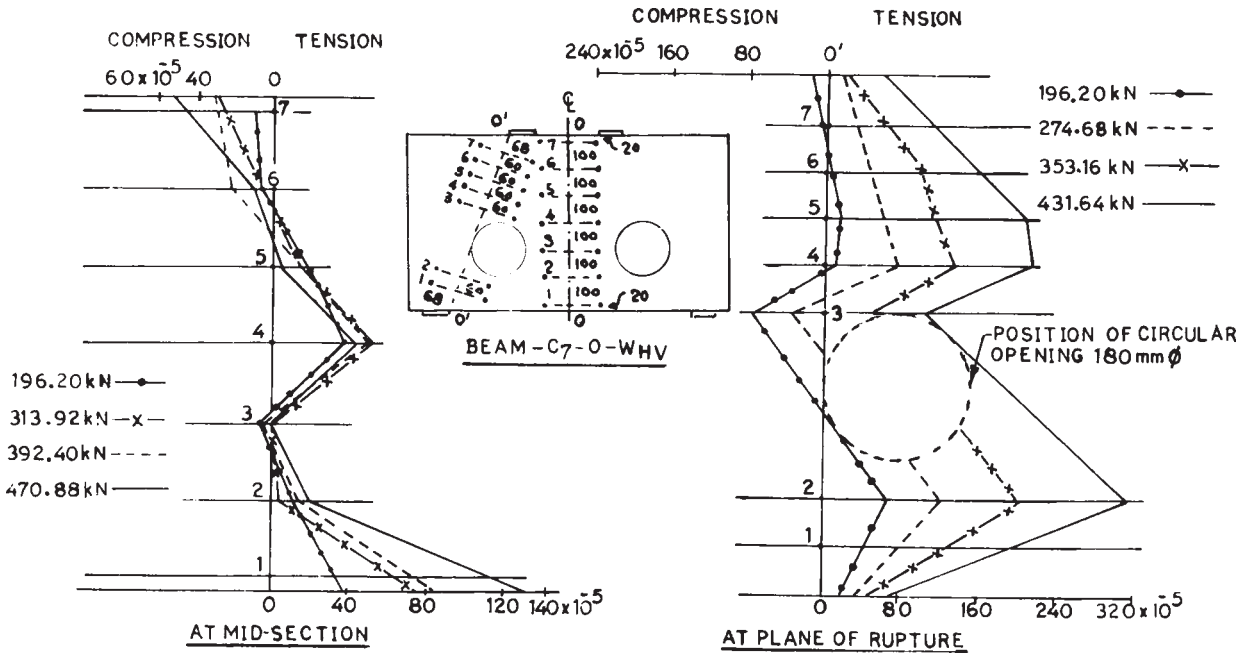

Figure 3.2 Concrete strain variation at the mid-section and plane of rupture of a typical deep beam with web openings (Ray 1980, 1982.)

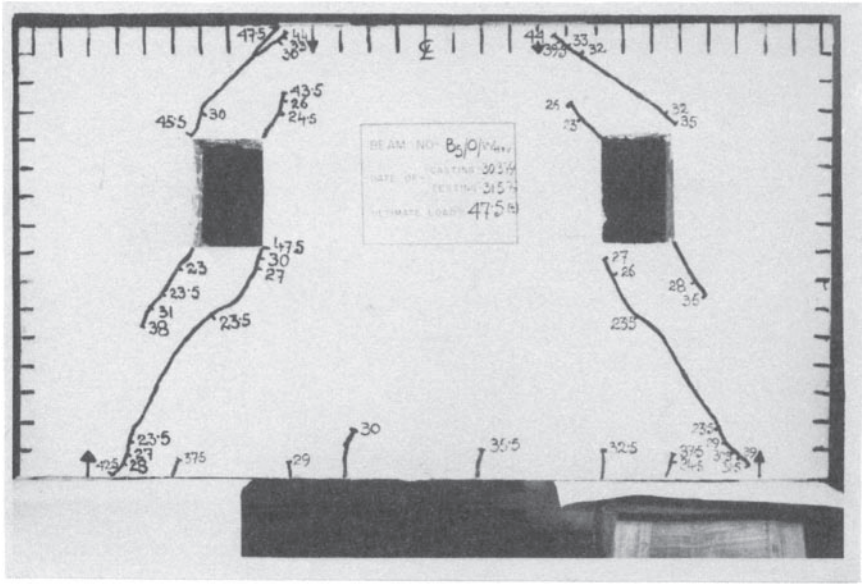

Figure 3.3 Crack patterns at failure of a typical deep beam with rectangular web openings (under two-point loading)

i) The cracks that start at about the bottom-most diametrical position of openings in the shear zones propagate towards the support bearing regions and become established as the critical diagonal cracks in the course of the load increments. Some of these initial cracks may completely stop propogating towards the support bearing regions after a small length of advancement at a few incremental load stages and prove to be harmless, as in the case of rectangular openings.
ii) The cracks initiated at the mid-shear zones (but away from the regions of openings and bearings) progress both ways diagonally and tangentially to the curved contour of the openings on further incremental loading. Similar cracks suddenly arise at positions about diametrically opposite on the opening surface towards the bearings.

Either of these crack patterns can be responsible for final failure of the beam.

3.3.3 *Flexural cracks*

In both cases of opening—rectangular and circular—flexural cracks are very few and generally occur in the range of ultimate loads of about 60–95%. These cracks propagate hardly beyond a height of about 0.3D from the beam soffit and close up on load release.

From the crack patterns shown in Figure 3.3 and 3.4 in general, it is obvious that failure occurs by a diagonal cracking mode of shear failure—mainly by sliding—and that the beams carry considerable loads after establishment of the

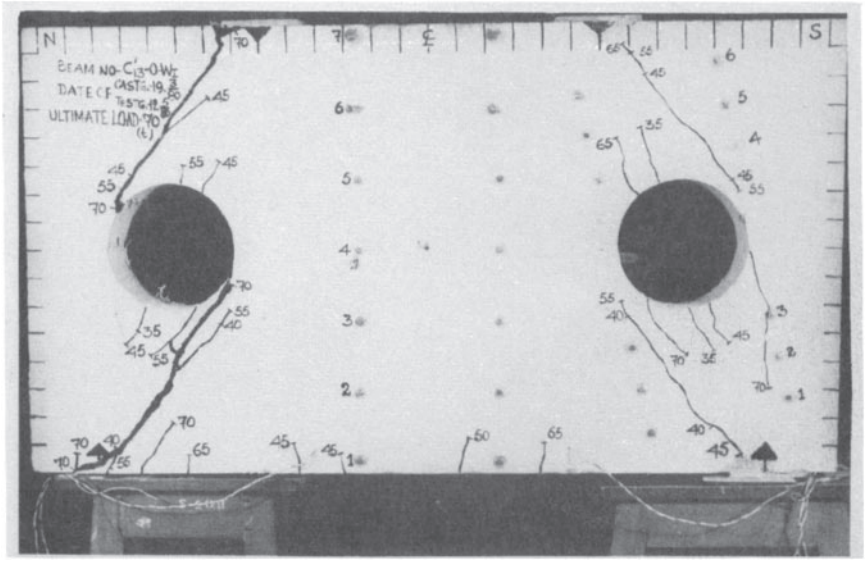

Figure 3.4 Crack patterns at failure of a typical deep beam with circular web openings (under two-point loading).

diagonal crack in the region of shear between opening and support. The principle stress trajectories (CIRIA guide, 1977) for the uncracked state amply support this phenomenon.

3.4 General behaviour in shear failure (under four-point loading)

In earlier stages of loading, up to 30% of the ultimate load, the beam behaves in a truly elastic manner and the load-deflection relation is linear. Normally, the diagonal cracks appear first in the vicinity of the opening at about 30–45% of the ultimate load and extend both ways towards the support and load bearing points (Figure 3.5). A diagonal crack may also appear first in the lower part of the beam and extend up to the mid-depth or join the opening.

The load deflection is in no way appreciably affected at this stage. Further increase in load may cause the existing cracks to widen and to extend; simultaneously, new diagonal cracks develop more or less parallel to the existing ones.

Flexural cracks appear only after the appearance of the diagonal cracks at loads about 42–90% of the ultimate. The flexural cracks hardly reach the mid-depth of the beam nor their widths exceed 0.1 mm. The formation of the diagonal and flexural cracks affects the load-deflection relation. At this stage, i.e. at 80–90% of the ultimate load, one of the diagonal cracks widens and extends conspicuously and the final failure of the beam is caused.

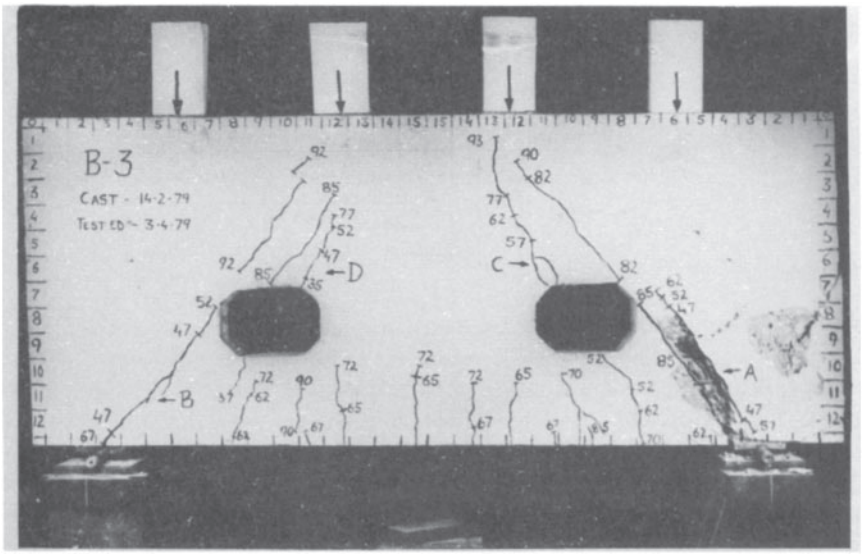

Figure 3.5 Crack patterns at failure of a typical deep beam with web openings (under four-point loading).

The maximum width of diagonal crack does not pose any problem. If, however, the crack width is limited to 0.3 mm, the corresponding load level will be about 60% (Singh, Ray and Reddy, 1980; Ray, 1982).

3.5 Effect of web opening

Of the two shapes of web opening, the circular type is found to be more effective in transmitting the load and the diagonal cracking is well-defined. This type therefore may be recommended for provision in the design.

Maximum crack width at failure will be greater when the opening centre is located at the centre of the shear zone than at any other position. So location of the opening centre at this point is undoubtedly the maximum damaging situation in the web region. The opening should not be brought too close to the vertical edge and inner and outer soffits of the beam either, because at higher loads secondary cracks might appear and cause failure of the beam. The strength of the beam increases when the opening is located away from what can be called the loaded quadrant to the unloaded quadrant and vice-versa (Ray and Reddy, 1979; Ray, 1980; 1982) (see Section 3.8). Again, for openings located completely outside the shear region, the beam with a web opening may be assumed to be a solid web beam. The location of the web opening is therefore a major factor influencing the strength of the beam. It is interesting from the load-deflection characteristics that the flexibility of the beam decreases as the location of the opening is moved

away from the support to the interior of the beam. This is contrary to the usual expectation. However, it should be remembered that the deflection in deep beams are substantially influenced by shear and, as such, location of the opening in the region of high shear and intercepting the critical path is understandable. The openings should invariably be provided with some loop reinforcement in their periphery to avoid possible stress concentration.

3.6 Effects of main and web reinforcements

It was probably for the first time that Kong and his associates, in 1970–72, considered the main reinforcement as an integral part of the shear reinforcement for calculation purposes. The main steel not only acts as tension reinforcement in flexure, but contributes substantially to the shear strength of beams. Further, web reinforcement controls crack widths and deflection. However, first cracking is generally not influenced by its provision. Of all types of web reinforcement, the inclined type placed perpendicular to the plane of rupture (critical diagonal crack) has been found to be the most effective arrangement to offer resistance to sliding (Ray, 1980; 1982a, b 1983; 1984). The next practical and effective type is the horizontal web steel which with nominal vertical web steel may further increase the effectiveness of the beam and so its strength. It was observed (Ray, 1980; 1982a, b; 1983; 1984) that in beams with web openings, horizontal web reinforcement distributed equally on either side of the opening location showed better results. In beams with unusually high web reinforcement, special attention should be paid to the detailing of anchorage and bearings at the load and support points. Otherwise, web steel must be limited to a certain amount.

Failure will be gradual and slow in beams with web reinforcement, while it is sudden in beams without web reinforcement. A vertical web reinforcement placed near the vertical edge of a beam with web opening located in its neighbourhood, guards against any premature failure due to rotation of the corner of the beam. From electrical strain measurements on main steel it was observed (Ray, 1980; 1982) that the general trend of the stress-strain characteristics under different load levels resembled stress-strain behaviour of steel but shear failure occurred at steel strains below the yield-point values normally expected in shear failures. It was further seen (Ray, 1980; 1982) that after cracking of the beams the steel strain rapidly increased at the location near the supports and the steel strain in the flexural zone remained almost constant (i.e. tension was uniform). The inclined cracks began to develop at higher loads.

3.7 Diagonal mode of shear failure load

The failure of reinforced concrete deep beams occurs under a state of biaxial stress. It is assumed that the diagonal mode of failure, more commonly

encountered in problems involving deep beams, is a state of failure which is akin to the rupture phenomenon in the Mohr-Coulomb failure criterion with straight line envelopes. Equilibrium equations involving c and tan ϕ of the Mohr diagram have been developed with the normal and tangential forces acting on the ruptured inclined plane at failure of the beam. These equations have been modified to account for the shear span depth ratio and web opening parameters (Ray and Reddy, 1979; Ray, 1980; 1982). For a clear understanding, a few definitions related to the analysis of the beam are given in section 3.8.

3.8 Definitions

a) Failure: A test specimen is said to have reached the state of failure when it has attained the ultimate load carrying capacity.

b) Shear span:

(i) Nominal shear span X_N: The distance from centre of the support bearing block to the centre of the load bearing block measured longitudinally is known as the nominal shear span.

(ii) Effective shear span *X:* The distance measured longitudinally from the inner edge of the support bearing block to the outer edge of the load bearing block is the effective shear span.

c) Diagonal tension crack: The first diagonal crack that forms at about the mid-depth of the beam (solid web) and extends both ways towards the support and load bearing blocks is the diagonal tension crack. Sometimes, this crack might form at the tension steel level and extend towards the mid-depth of the beam (solid web).

In beams with web openings, normally the diagonal cracks develop from levels of the openings and extend both ways towards the load and support bearing blocks. Sometimes the diagonal cracks may develop from the tension steel level and extend towards the opening.

d) Critical diagonal crack: The diagonal crack which extends from the support bearing block to the load bearing block (for solid web beam) is the critical diagonal crack. In the case of beams with openings, the crack may be intercepted by the opening. Establishment of this type of crack warns of impending failure.

e) Rupture plane: A diagonal surface in the cross-section of the beam on which the two parts of the beam slide before failure is known as the rupture plane. The critical diagonal crack follows this rupture plane.

f) Failure by sliding: The diagonal mode of failure by sliding along the critical diagonal crack is known as failure by sliding. The other modes of failure reported here, such as shear-compression, shear-flexure and shear-proper, are considered to be manifestations of the diagonal mode of failure by sliding influenced by the beam parameters.

g) Local and anchorage failure: Failure due to crushing of concrete over supports or under concentrated load points due to insufficient resistance is

called the local failure. Anchorage failure results from insufficient anchorage length or splitting of concrete above the upright bend of the tensile steel.

h) Shear zone or practical region for web opening: The zone or region bounded by the verticals from the centre of support point and centre of load point and the horizontals at 0.2*D* and 0.8*D* from top of the beam. The region marked EFGH in Figure 3.6 represents the practical region. This region is divided into four equal quadrants 1–4 by the axes XX' and YY' passing through the centre of the plane of rupture (natural load path). It is not advisable to position any opening within the 0.2*D* width regions at the top and bottom soffits of the beam.

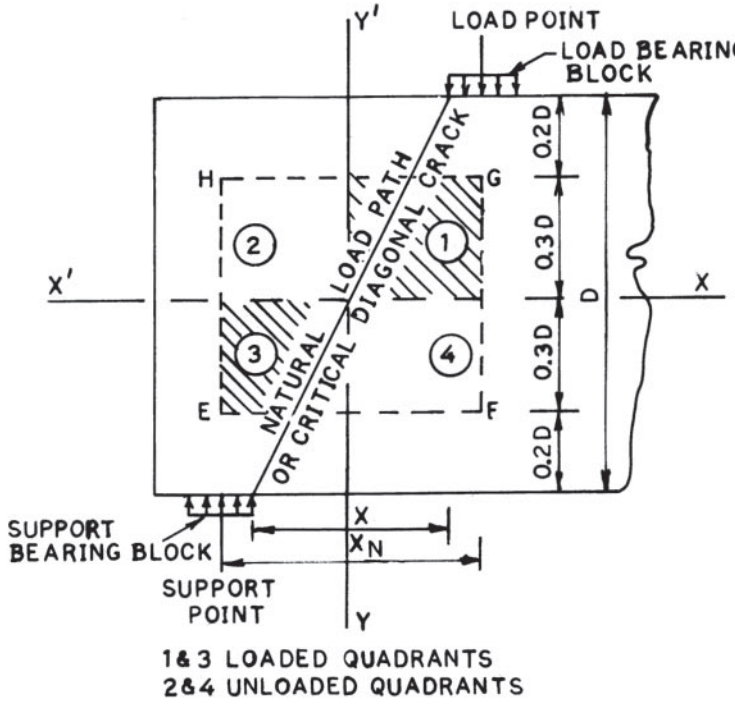

Figure 3.6 Practical region for web opening (Ray and Reddy, 1979; Ray, 1980; 1982).

i) Loaded and unloaded quadrants: In Figure 3.6 the quadrants marked 1 and 3 are known as the loaded quadrants (shown hatched), whereas the quadrants marked 2 and 4 are taken to be the unloaded quadrants. Loaded quadrants are the regions located nearer to the load and support bearing blocks. An opening in any loaded quadrant is naturally more harmful than one in the unloaded quadrant.

j) Maximum size of web opening: For practical applicability, rectangular web opening of a maximum size $X_N/2 \times 0.6D/2$ has been considered to be admissible. For circular or other types of opening geometrically not much

different from the rectangular types, an equivalent square or rectangle that encompasses the opening may be considered for defining prescribed limits.

k) Eccentricity of web opening: The eccentricity of the centre of the opening with respect to the centre point of the critical diagonal crack (plane of rupture) is expressed by the co-ordinates e_x and e_y as shown Figure 3.7. The limits of eccentricity come from the maximum admissible size of web opening and are given by

$$e_x \leq X_N/4 \text{ and } e_y \leq 0.6D/4 \tag{3.1}$$

For eccentricities e_x and e_y greater than $X_N/4$ and 0.6 D/4 respectively, the limiting values are to be taken as $X_N/4$ and 0.6 D/4.

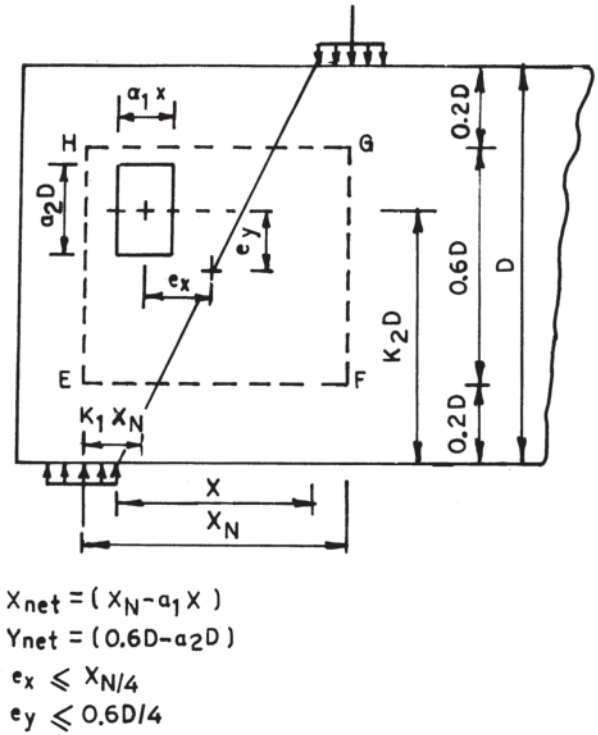

Figure 3.7 Typical opening in the web and other dimensions (Ray and Reddy, 1979; Ray, 1980; 1982).

l) X_{net} and $Y_{net:}$ These are dimensions of solid shear zone in the X and Y directions, obtained after deducting the dimensions of the web opening in the respective directions, that is

$$X_{net} = (X_N - a_1 x)$$

and $$Y_{net}=(0.6D-a_2D) \quad (3.2)$$

In the case of a circular opening these measurements are made with reference to the equivalent square opening, the side of which is equal to the diameter of the circular opening.

3.9 Criterion of failure and strength theory

From the mode of failure shown in Figures 3.2, 3.3 and 3.5 for beams with web openings and in Figure 3.8 for a beam without web opening, it is clear that the failure along the critical diagonal path is by sliding. This particular mode of failure can be interpreted in terms of Coulomb's internal friction theory and Mohr's generalised failure criterion with straight line envelopes, combined as used by Guralnick (1959) in the case of an ordinary reinforced concrete beam, Figure 3.9. By this, two independent physical properties of concrete, namely cylinder compressive strength f'_C and cylinder splitting tensile strength f'_t are accounted for. The ratio f'_t/f'_C varies widely (from about 1/8 to 1/16) with the quality of concrete. In absence of any practical test data, adoption of a suitable ratio for f'_t/f'_C may be erratic. Therefore, it is advisable that the parameters f'_C and f'_t to be used for deep beams be determined by independent tests.

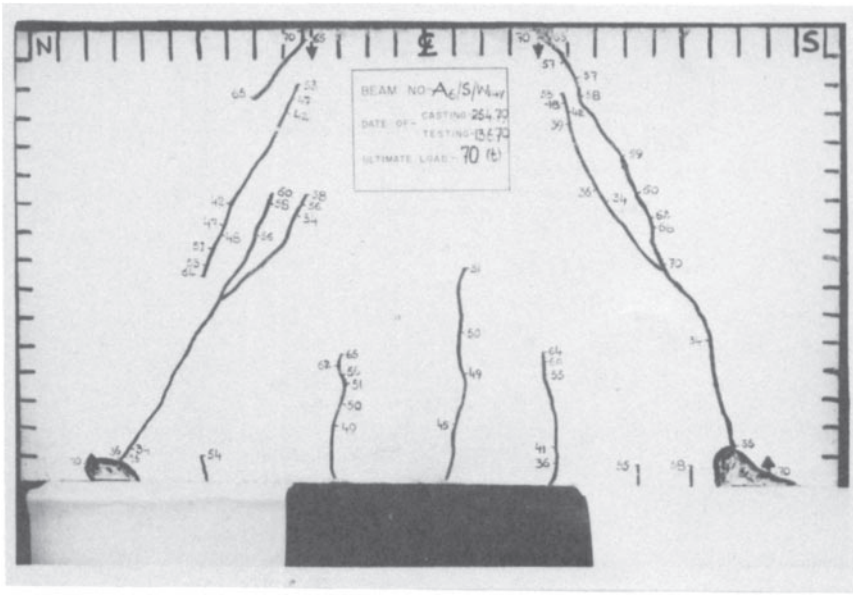

Figure 3.8 Crack patterns at failure of a typical deep beam with solid web (under two-point loading).

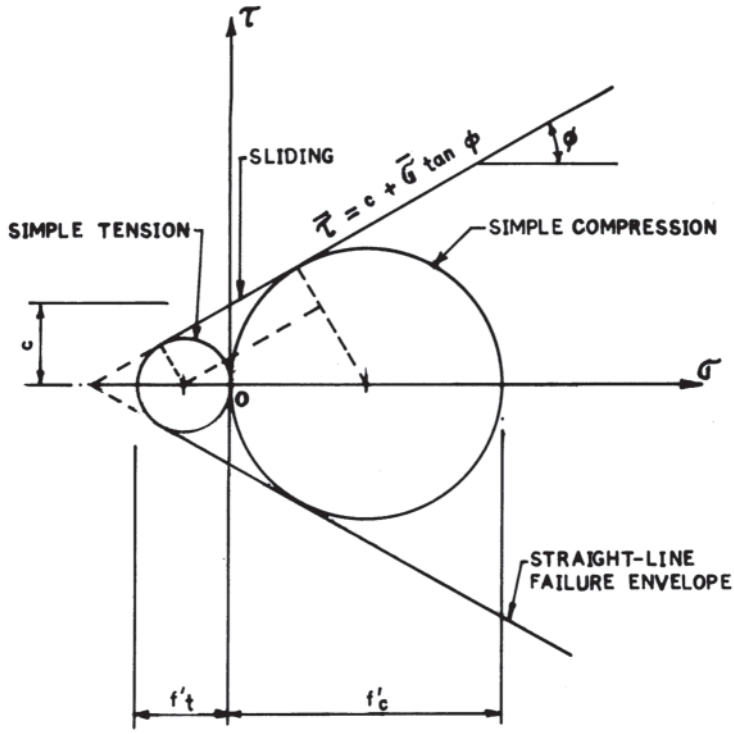

Figure 3.9 Proposed simplified Morh-Coulomb failure criterion (Ray and Reddy, 1979; Ray, 1980; 1982; 1984).

In deep beams under applied loading, an average shearing stress ($\bar{\tau}$) and an average normal stress ($\bar{\sigma}$) acting on the rupture plane of sliding may be given by the Mohr-Coulomb internal friction theory as

$$\tau = c + \sigma \tan\phi \tag{3.3}$$

where *c* is the internal cohesion of concrete and $\tan\phi$ is the coefficient of internal friction. This apparent internal cohesion of concrete is due to the cement paste and the sliding friction (i.e. internal frictional resistance is due to the presence of aggregates in concrete.)

Under the biaxial stress condition, if the normal stresses σ_x and σ_y and shearing stress τ_{xy} at some point on the plane of rupture, before failure, are known, the expression for the principal stresses (maximum normal stress denoted by σ_1 and minimum normal stress denoted by σ_3) is given by

$$(\sigma_n)_{\substack{\max \\ \min}} = \sigma_{1 \text{ or } 3} = \sigma_x + \sigma_y/2 \pm \sqrt{(\sigma_x - \sigma_y/2)^2 + (\tau_{xy})^2} \tag{3.4}$$

The Mohr-Coulomb theory of failure (Figure 3.9) gives the relationship between the stresses σ_1, σ_3, f'_c and f'_t in the form

$$(\sigma_1/f'_c) - (\sigma_3/f'_t) = 1 \tag{3.5}$$

Eqn (3.5) (Timoshenko, 1956) is an alternative presentation to Eqn (3.3) and is an interaction type of equation for failure criterion. Just prior to failure, classical elastic stress analysis does not hold good, because of redistribution of stresses at higher loads in concrete, resulting from the post-cracking behaviour of concrete. As a result, evaluation of σ_1 and σ_3 will be a difficult problem in as much as these principal stresses are dependent on σ_x, σ_y and τ_{ry} which, in turn, could not be precisely measured just before failure. Herein lies the difficulty in using the Eqn (3.5). Therefore, for calculation of the sliding strength of reinforced concrete deep beams, Eqn (3.3) is invariably preferred.

From Figure 3.9 the characteristic constants c and ϕ and other relationships are evaluated, using geometry only, and Eqn (3.3) for the Mohr-Coulomb failure criterion assumes the form

$$\bar{\tau} = (f_c'\sqrt{\eta})/2 \; ; + \bar{\sigma}(1-\eta)/2\sqrt{\eta} \tag{3.6}$$

where $c = \sqrt{f_c' f_t'}/2 \; ; \quad \tan\phi = (f_c' - f_t')/2\sqrt{f_c' f_t'}$

and $$\eta = f_t'/f_c' \tag{3.7}$$

Eqn (3.6) represents the failure criterion which will be utilised in developing the ultimate strength of deep beams.

3.10 Ultimate shear strength

A typical solid deep beam with main and web reinforcement and a plane of rupture is shown in Figure 3.10a. A part of the beam separated by the potential diagonal crack is shown as the free body diagram in Figure 3.10b. The penetration of the crack is considered to extend to the full depth although usually this crack stops at one-fifteenth to one-tenth of the depth of the beam from the top and acts in a manner similar to the compression zone of a tied arch.

Considering the plane of rupture:

$$N \text{ (=Normal force)} = bD \text{ cosec } ß \times \bar{\sigma} \tag{3.8}$$

$$T \text{ (=Tangential force)} = bD \text{ cosec } ß \times \bar{\tau} \tag{3.9}$$

From Eqns (3.3, 3.8 and 3.9), it may be stated that:

$$T = (cbD/\sin ß) + N \tan\phi$$

or $$T = T_c + N \tan\phi \tag{3.10}$$

T_c is the cohesive force of concrete along the inclined plane

$$= cbD/\sin ß \tag{3.11}$$

Since N is taken as a tensile normal force, Eqn (3.10) may be written as

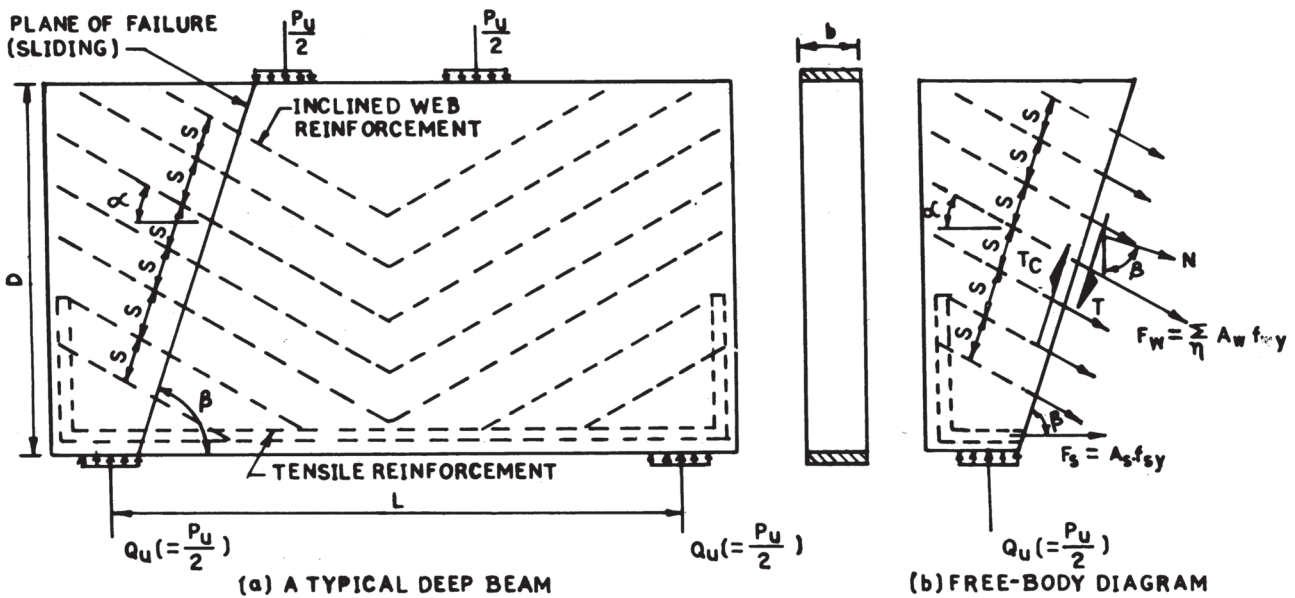

Figure 3.10 Ultimate strength of RC deep beams with solid webs under two-point loading. (a) typical deep beam; (b) free-body diagram. (Ray and Reddy. 1979; Ray, 1980, 1982, 1984)

$$T=T_c\text{-}N\tan\phi \tag{3.12}$$

Referring to the free-body diagram, the statical equilibrium equations at failure of the beam may be written as:

$$N\sin ß+F_s+F_w\cos a = T\cos ß \tag{3.13}$$

$$N\cos ß+T\sin ß+F_w\sin a = Q_u\ (=P_u/2) \tag{3.14}$$

From Eqns (3.12)–(3.14), on simplification, the ultimate strength equation may be written as:

$$Q_u\ (=P_u/2)=\frac{cbD}{\sin\beta\cos\beta\,(\tan\beta+\tan\phi)}+F_s\left[\frac{\tan\beta\tan\phi-1}{\tan\beta+\tan\phi}\right]$$
$$+F_w\left[\frac{\sin\alpha\cos\beta+\cos\alpha}{\left(\frac{\tan\beta+\tan\phi}{\tan\beta\tan\phi}\right)}-\frac{\cos\alpha}{\left(\frac{\tan\beta+\tan\phi}{1-\tan\alpha\tan\beta}\right)}\right] \tag{3.15}$$

where $F_s=A_sf_{sy}$; $F_w=\sum_{\eta}A_wf_{wy}$; F_{sy} is yield point stress of tensile steel, F_{wy} is yield point stress of inclined web steel intercepted by the potential diagonal crack at failure, β is the angle of inclination of the rupture plane with the horizontal, α is the angle of inclination of the inclined web bar with the horizontal and η is the number of web bars intercepted by the potential diagonal crack.

Eqn (3.15) which is the general equation for the ultimate strength of a deep beam without web opening, consists of the contributions due to concrete, tensile steel and web steel and may be written in the short form as:

$$Q_u\ (=P_u/2)=P_c+P_s+P_w \tag{3.16}$$

In the comprehensive test programme (Ray and Reddy, 1979; Ray 1980; 1982), the strength of a deep beam with web openings was found to be affected mainly by:

i) the shear span/depth ratio X/D;
ii) the amount of interception of the diagonal crack by the openings;
iii) the location of the centre of the openings in the web region;
iv) the dimensions of the openings.

It may be emphasised that the exact analysis of the problem, involving a large number of parameters, presents a formidable task. However, the problem is made amenable to an analytical solution by proposing the following simplifying assumptions:-

(i) the effect of the opening lying within the region EFGH (practical region) in the web of the deep beam is considered (Figure 3.6);
(ii) the size of the opening is limited to $a_1x\leq x_N/2$ and $a_2\ D\leq 0.6\ D/2$, as shown in Figures 3.6 and 3.7.

(iii) the eccentricities e_x and e_y of the opening are limited to the maximum of $X_N/4$ and 0.6 $D/4$ in the X- and Y- directions respectively (Figure 3.7)

Based on these assumptions, the parameters relating to the web opening will be evaluated for the restrictions laid down here. Incorporation of these simplified measurements of the opening parameters in the strength equation for the solid deep beam—Eqn (3.16) —, will give the ultimate strength equation for the deep beam with web openings.

3.10.1 Evaluation of web opening parameters

Openings in web are considered in the following manner:

(i) As well as the typical diagonal mode of failure, slightly different but similar types of failure—generally termed shear-proper, shear-flexure and shear-compression—are observed. This variation in the mode of failure is seen to be related mainly to the shear span depth ratio which is accounted for by proposing a constant λ_1 in P_c (Figures 3.6 and 3.7):

$$\lambda_1 = \left[1 - \frac{1}{3}\left(\frac{K_1 X_N}{K_2 D}\right)\right] \quad \text{for} \quad \frac{K_1 X_N}{K_2 D} \leq 1 \tag{3.17}$$

$$= \frac{2}{3} \quad \text{for} \quad \frac{K_1 X_N}{K_2 D} \geq 1 \tag{3.18}$$

(ii) If the opening is so placed that it intercepts the natural load path,

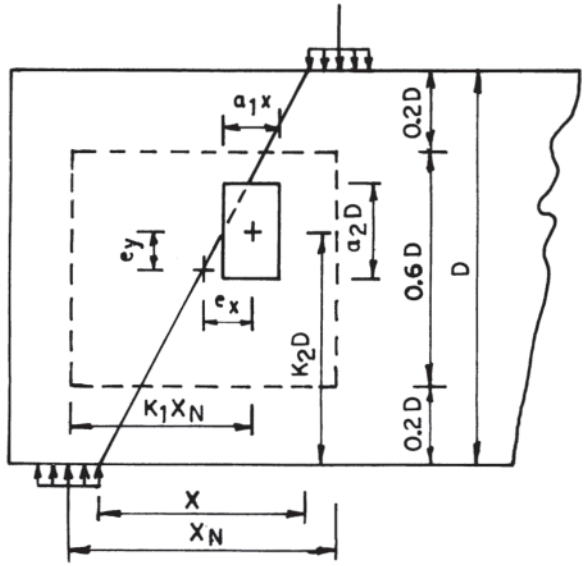

Figure 3.11 Typical position of an opening intercepting natural load path (Ray and Reddy, 1979; Ray, 1980, 1982).

(Figure 3.11), then the effect of this discrete load path is taken into account by incorporating a constant λ_2 in evaluating P_c, such that

$$\lambda_2=(1-m) \tag{3.19}$$

where, m is the ratio of path length intercepted to total path length along the natural load path=0 for non-interception, (Figure 3.7)

(iii) The combined effect of the size of the opening as well as location of the opening is accounted for by incorporating a constant λ_3 in assessing P_c. Hence, with reference to Figure 3.7.

$$\lambda_3 = \left[0.85 \pm 0.3\left(\frac{e_s}{X_{net}}\right)\right]\left[0.85 \pm 0.3\left(\frac{e_e}{Y_{net}}\right)\right] \tag{3.20}$$

where

$$e_x \le X_N/4; \quad e_y \le 0.6D/4 \tag{3.1}$$

and

$$X_{net} = (X_N - a_1 x); \quad Y_{net} = (0.6D - a_2 D) \tag{3.2}$$

Notes: a) The coefficient λ_3 may take any value between 0.50 and 1, depending on the location of the opening in the most unfavourable loaded quadrant and the favourable unloaded quadrant.

b) In Eqn (3.20) the negative sign is to be used when the opening centre is in the loaded quadrant or on one of the axes X-X' and Y-Y', the positive sign when the opening centre is in the unloaded quadrant.

c) For openings located partially outside the shear zone, parameters e_x, e_y, K_1X_N and K_2D may be measured as indicated in Figure 3.12. That is, for

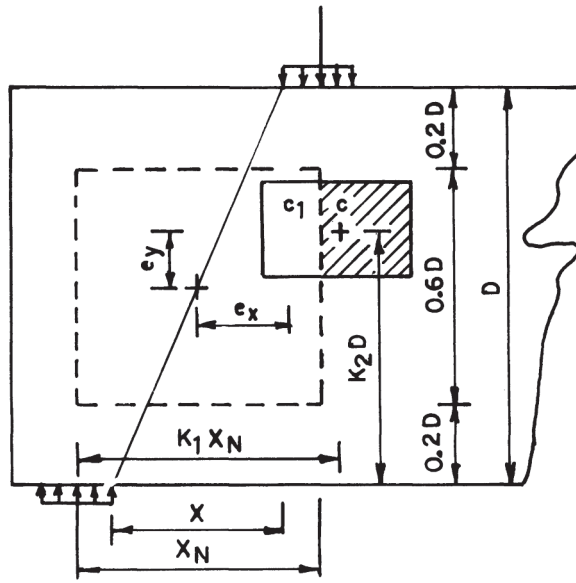

Figure 3.12 Typical position of an opening partially outside the shear zone (Ray and Reddy, 1979; Ray, 1980; 1982).

calculating λ_1, the measurements of K_1X_N and K_2D are to be made as usual; but for calculating λ_3, the part of the opening that lies outside the shear zone (shown hatched) is to be ignored. Consequently, the centre C_1 of the opening is to be determined for the remaining part which lies within the domain of the shear zone (Figure 3.12).

d) For openings located completely outside the shear zone, the beam may be assumed to be one with solid web.

e) For larger dimensions of openings beyond the prescribed limits (i.e. for $a_1x>X_N/2$ and $a_2D>0.6D/2$, when values of X_{net} and Y_{net} will be found less than half the width of the load bearing block) the minimum values for X_{net} and Y_{net} are to be taken as half the width of the load bearing block. In such cases, the values for λ_1 and λ_3 are to be further reduced by the ratio of the side (or sides) of the limited (admissible) dimensions to the exceeded side (or sides) of the actual dimensions of the opening, as the case may be.

f) For marginal extensions of openings into the top and bottom $0.2D$ cover regions (normally not advised), a procedure similar to that for an opening partially outside the shear zone might be adopted for computing λ_1 and λ_3.

3.10.2 *Ultimate shear strength*

Therefore, after knowing the values of λ_1, λ_2 and λ_3 from Eqns (3.17)–(3.20), the general equation for the ultimate shear strength of deep beams with web openings can be written from Eqn (3.16) as:

$$Q_u\ (=P_u/2)=P_c\ (\lambda_1).(\lambda_2).(\lambda_3)+\psi_s\ P_s+\psi_w\ P_w \tag{3.21}$$

where, y_s is an empirical coefficient=0.65 and y_w is an empirical coefficient =0.50.

The coefficient ψ_s reflects the levels of stress in the main steel, the value of which was observed (Ray and Reddy, 1979; Ray 1980; 1982) to be about 60–70% of the corresponding stress in the case of the companion solid web beams just prior to failure. Further, ultimate strengths of beams with web openings were found to vary (Ray and Reddy, 1979; Ray, 1980; 1982) within the range 40–90% of those of identical solid web beams.

Again, the coefficient ψ_w reflects the location of placement of web reinforcement. In beams where the web steel is distributed over the full depth, the value of ψ_w=0.50 is a reasonable factor. Moreover, from electrical strain measurements in some typical beams (Ray, 1980, 1982) it was seen that the steel strains in the neighbourhood of the openings were found to be maximum. The strain variation of web steel can thus be approximated as varying linearly from maximum near the opening to a minimum at the top or bottom faces. This further justifies the stipulated value of ψ_w.

Thus, knowing the geometric dimensions of the beam and the openings, the loading arrangement and the material properties of concrete and steel, Q_u ($=P_u/2$) can be calculated easily from Eqn (3.21).

However, the last expression does not consider any secondary failures at anchorage and bearing regions—which can be taken care of by providing suitable extra reinforcements. If suitable reinforcement is provided around the opening, there will be no problem from this side either. For beams with unusually high web reinforcement the anchorage and bearing regions should receive special attention.

Eqn (3.21) has been derived for the beam with web openings and provided with main and web reinforcements. It can be adopted for beams that have web openings and are provided with only main reinforcement by deleting the term containing P_w and may be written as:

$$Q_u\ (=P_u/2)=P_c\ (\lambda_1).(\lambda_2).(\lambda_3)+\psi_s\ P_s \tag{3.22}$$

Even for a beam with plain concrete only, the strength of the beam with web openings can be obtained by deleting also the term containing P_s which corresponds to main reinforcement of Eqn (3.22) and may be written as:

$$Q_u\ (=P_u/2)=P_c\ (\lambda_1).(\lambda_2).(\lambda_3) \tag{3.23}$$

This analysis has been developed on the basis of the maximum size of opening admissible in the region of the shear zone. However, it can be utilised for other exceptional cases of marginal extensions of openings into the 0.2D cover regions and for larger openings as discussed previously.

The validity of the method has been verified by comparing the available test results, involving about 86 beams with web openings (Kong *et al.,* 1973; 1977; 1978; Singh, 1978; Ray, 1980; 1982), presenting them in a plot of Pu(test) versus Pu(calc) (Figure 3.13). These comparisons indicate that the predicted strengths are in close agreement with the tested values and that the variations beyond ±20% are limited to only a few beams.

3.11 Simplified design expression

ACI (1971, 1978) put forward some design guidance of solid web beams based on ultimate strength but that was only an extension design for the shallow beam problems involving large calculations. PCA's (1946) design guidance on solid web beams is very old and that of CEB-FIP (1970) is conservative. However, none of the national codes (CEB-FIP, 1970; BS CP110, 1972; ACI-318, 1971, 1978) have incorporated any guidelines for design of beams with web openings.

The expressions developed for the ultimate strength of beams with web openings in Section 3.10 are generally rigorous and time-consuming and are, therefore, important in the academic aspects of the problem. Deep beams generally fail in shear following splitting or sliding. So in the kind of complex problem that they present it is highly important to consider shear in so far as the ultimate limit state and serviceability limit state of cracking are concerned. For a controlled concrete mix, the parameter f'_t varies in a

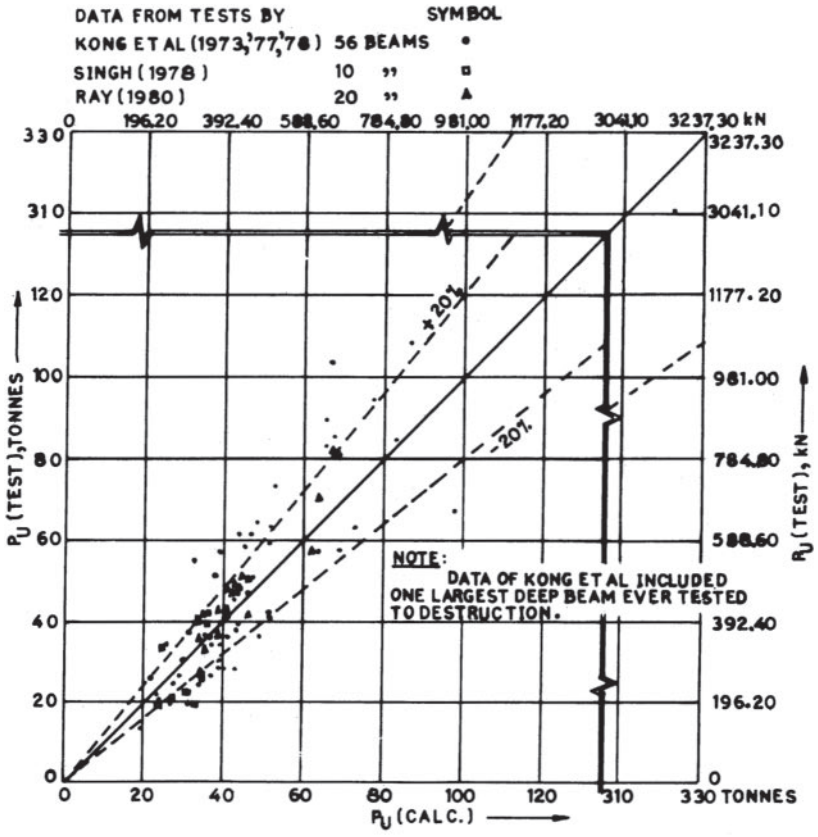

Figure 3.13 Comparison of tested and computed ultimate shear strengths of beams with opening in web under two-point loading (Ray, 1980; 1982).

definite relation to the parameter f'_c. Therefore the nominal shearing stress at ultimate load (Q_u/bD) should be expressed in terms of f'_c, $p_s f_{sy}$ and $K_w r_w f_{wy}$ which was emphasised by ASCE-ACI practice.

With suitable use, therefore, of the average values of the dimensional and non-dimensional parameters in Eqn (3.15) the simplified design expression for the strength of the beam with web openings can be written as

$$Q_u/bD\ (=P_u/2bD) = 0.1 f'_c(\lambda_1)(\lambda_2)(\lambda_3) + 0.0085\ \psi_s p_s f_{sy} + 0.01 \psi_w K_w r_w f_{wy} \tag{3.24}$$

where

$$p_s = A_s/bD \times 100\ (\%);\quad r_w = \sum_n A_w/bD \times 100\ (\%) \tag{3.25}$$

and K_w=0.85 (for a horizontal web bar); cot ß (for a vertical web bar); and 1.15 (for inclined web bar). The meanings of the coefficients $\lambda_1, \lambda_2, \lambda_3, \psi_s$ and ψ_w are as assigned earlier for a beam with web openings.

Eqn (3.24) is the general one and can even be used for plain beams as well as beams with and without web reinforcements by deleting the terms which are not involved. Ray (1980; 1982) observed that this simplified strength predicted strength very close to that computed by the rigorous Eqn (3.15). It is, therefore, hoped that Eqn (3.24) will find favour with practising engineers for their day-to-day design work.

3.12 Ultimate strength in flexure

Knowledge of strengths of beams in both shear and flexure would enable the designer to fix the dimensions and detailing of the beams. Normally, flexural failure of beams is affected if the percentage of main reinforcement is kept below the balance percentage. It has further been observed (Ray, 1980; 1982; 1985) that shear failure in deep beams could be prevented and flexural failure might be expected if excessive web reinforcements are provided perpendicular to the plane of rupture. In this particular case, the support and load bearing regions must be properly strengthened to guard against any local or anchorage failures.

Determination of the lever arm is highly important in fixing up the amount of balance reinforcement at initial design. Even the national codes (CEB-FIP, 1970; BS CP110, 1972; ACI318, 1971, 1978; IS456, 1978) do not provide any design guidance for beams failing in flexure. Recommendations put forward by CEB-FIP (1970) are rather conservative and limited to the case of solid web beams.

Consider simplified stress block, which is in many respects similar to the one adopted for shallow beams but which accounts for the stress distribution of concrete on the tension side as well as presence of the web reinforcement. Its geometry and the associated forces are shown in Figure 3.14. The assumptions made in the derivations are as follows:

i) Only one neutral axis prior to failure (see also Section 3.3).
ii) A rectangular stress block (after Whitney, 1940) as used in shallow beams, for the compression zone,
iii) A triangular stress distribution for the concrete portion in the tension zone (in shallow beams, this effect is neglected),
iv) The effect of web steel in compression zone is neglected,
v) The tension steel and the web steel below the neutral axis yield at failure. The contribution of the vertical web steel is also neglected.

Referring to Figure 3.14, the following relations of forces are obtained:

$$F_s = A_s f_{sy};\ F_{wt} = \sum_n A_{wt} f_{wy} \cos\alpha$$

$$F_{ct} = \frac{1}{2} bd\,(1-K) f_r;\quad C = 0.85 f'_c\, Kbd \qquad (3.26)$$

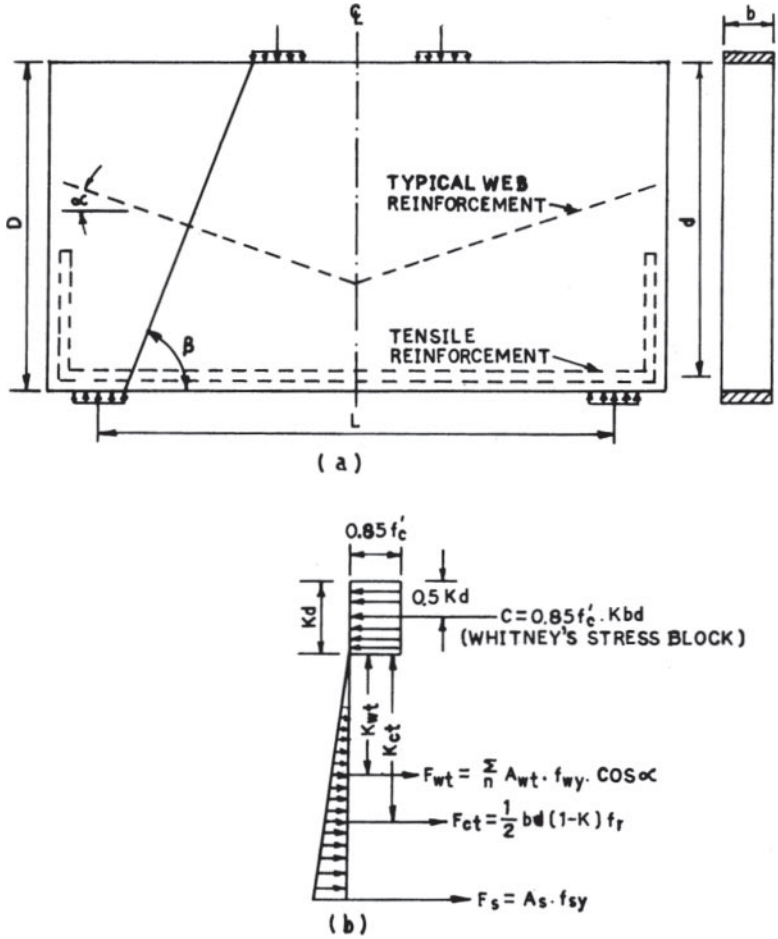

Figure 3.14 Stress-block for flexure strength of deep beams (mid-section) (Ray, 1980; 1982; 1985).

where F_s is total force in tensile steel, F_{wt} is total force in web steel below NA, A_{wt} is sectional area of individual web steel below NA, F_{ct} is total force of concrete in the tensile region, f_r is modulus of rupture strength of concrete, C is total compressive force and K parameter as defined in Figure 3.14. From statical equilibrium of forces, we obtain

$$C=F_{ct}+F_s+F_{wt} \tag{3.27}$$

on substitution of the values of equations in 3.26 into Eqn 3.27 and solving for K we obtain

$$K=\frac{p'_s f_{sy}+p_{wt}\cdot f_{wy}\cdot\cos\alpha+f_r/2}{0.85f'_c+f_r/2} \tag{3.28}$$

where $$p'_s = A_s / b\,d;\ \text{and}\ p_{wt} = \sum_n A_{wt}/bd \tag{3.29}$$

Based on test observations (Ray, 1980; 1985), it is assumed suitably that

$$f_r = 1.8 f'_t \text{ and } f_t = 1.25\sqrt{f'_c} \tag{3.30}$$

giving the relation

$$f_r = 2.25\sqrt{f'_c} \tag{3.31}$$

On simplification of Eqns (3.28) and (3.31) the value of K comes to:

$$K=(\mu+1)/(\mu'+1) \tag{3.32}$$

where $$\mu = (p'_s f_{sy} + p_{wt} \cdot f_{wy} \cos\alpha)/(1.125\sqrt{f'_c})$$

$$\mu' = 0.7555\sqrt{f'_c} \tag{3.33}$$

Considering moments about the centre of gravity of the stress block and substituting the values given in Eqns (3.26)–(3.30), we get:

$$\frac{M_{FL}}{bd^2 f'_c} = \frac{p'_s f_{sy}}{f'_c}\left(1-\frac{K}{2}\right) + \frac{p_{wt}\cdot f_{wy}\cdot\cos\alpha}{f'_c}\left(\frac{K}{2}+\frac{K_{wt}}{d}\right)$$

$$+\frac{2.25\sqrt{f'_c}}{3}\left(1-1.25K+0.25K^2\right) \tag{3.34}$$

where M_{FL}=flexural moment capacity of beam due to concrete, tensile and web steels.

From the values given in Eqns (3.32) and (3.33), Eqn (3.34) can be rewritten as:

$$\frac{M_{FL}}{bd^2 f'_c} = \frac{p'_s f_{sy}}{f'_c}(J_s) + \frac{p_{wt}\cdot f_{wy}\cdot\cos\alpha}{f'_c}(J_{wt}) + C_c \tag{3.35}$$

where $$J_s = 1 - 0.5\left(\frac{\mu+1}{\mu'+1}\right) \tag{3.36}$$

$$J_{wt} = \left[0.5\left(\frac{\mu+1}{\mu'+1}\right)+\frac{K_{wt}}{d}\right] \tag{3.37}$$

$$C_c = \frac{1}{\sqrt{f'_c}}\left[0.75 - 0.9375\left(\frac{\mu+1}{\mu'+1}\right)+0.1875\left(\frac{\mu+1}{\mu'+1}\right)^2\right] \tag{3.38}$$

K_{wt} = Centroidal distance of web bars under NA from bottom of compression stress block.

$$= \frac{1}{n}\sum_n K_{wt} \tag{3.39}$$

Thus the flexural capacity of the beam given by Eqn (3.35) is a function of $p'_s f_{sy}/f'_c$ $p_{wt} \cdot f_{wy}/f'_c$ and C_c (a coefficient for concrete contributing towards the flexural strength).

3.13 Simplified expression for flexural strength

Based on the average values (Ray, 1980; 1985) for $J_{s,}$ J_{wt} and C_c the ultimate load capacity of beams failing in flexure is given by the following simple form which is very close to the rigorous Eqn (3.35).

$$\frac{M_{FL}}{bd^2 f'_c} = \frac{p'_s f_{sy}}{f'_c}(0.86) + \frac{p_{wt} \cdot f_{wy} \cdot \cos\alpha}{f'_c}(0.52) + 0.033 \qquad (3.40)$$

where, the meanings of p'_s and p_{wt} are as discussed in Section 3.12.

The mode of failure of beams—either in shear or flexural—may be known from the comparative values of the ultimate load capacities computed from Eqns (3.24) and (3.40).

3.14 Extension of theory of ultimate shear strength of beams to four-point loading

Uniformly distributed loading has been stimulated by replacing it with four equally-spaced concentrated loads.

It is contended in Section 3.9 that the failure of a deep beam eventually follows a critical diagonal crack path (or critical path) and the strength of the beams depends upon the resistance of concrete and steel met with along that path. The resistance of the beam along this critical path can be predicted satisfactorily on the basis of the simplified Mohr-Coulomb internal friction theory with straight line envelopes as given in Figure 3.9 for the two-point loading system.

Based on observations and developments of diagonal cracks and their progress up to the stage of failure (Singh, Ray and Reddy, 1980), the critical path in the case of the four-point loading system may be approximated to follow one of the following two planes of rupture:

i) a plane of rupture given by joining a line from the inner edge of the support bearing block to the near edge of the exterior load bearing block (henceforth termed critical path I),
ii) a plane of rupture given by joining a line from the inner edge of the support bearing block to the near edge of the next interior load bearing block (henceforth termed critical path II)

Depending on the stipulated mode of failure as envisaged in the two-point loading case, final failure of the beam is considered to occur always along

one of the two critical paths according to the resistance of the beam along those paths as shown in Figure 3.15.

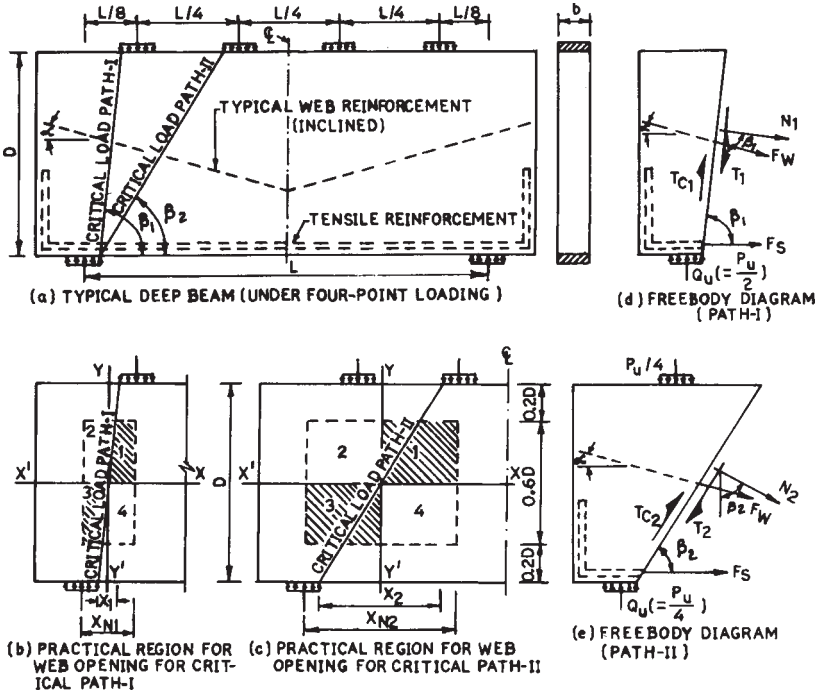

Figure 3.15 Ultimate strength of RC deep beams with solid web and practical regions for web openings (under four-point loading) (Ray, 1980)

The Figure shows a typical deep beam under four-point loading and includes the practical regions for web openings and the free-body diagrams for critical load paths I and II. Critical path I lies wholly in a region of external shear, $Q_{u=}P_u/2$, whereas critical path II traverses partly through a region having shear $Q_u=P_u/2$ and partly through region of shear $Q_u=P_u/4$. However, it was observed (Singh, Ray and Reddy, 1980) that after formation of initial diagonal cracks which usually entered into the region of shear, $Q_y=P_u/4$, the beam carried a substantial load before failing along the second path. As such it is reasonable to assume that the shear causing failure along path II is $Q_u=P_u/4$.

The ultimate strength equations for beam with web openings can be written directly from Eqn (3.21) for critical path I:

$$Q_{u_1}\,(=P_u/2)_1 = P_{c_1}\,(\lambda_1)_1\,(\lambda_2)_1\,(\lambda_3)_1 + \psi_s \cdot P_{s_1} + \psi_w \cdot P_{w_1} \qquad (3.41)$$

for critical path II:

$$Q_{u_2}\,(=P_u/4)_2 = P_{c_2}\,(\lambda_1)_2\,(\lambda_2)_2\,(\lambda_3)_2 + \psi_s\,P_{s_2} + \psi_w\,P_{w_2} \qquad (3.42)$$

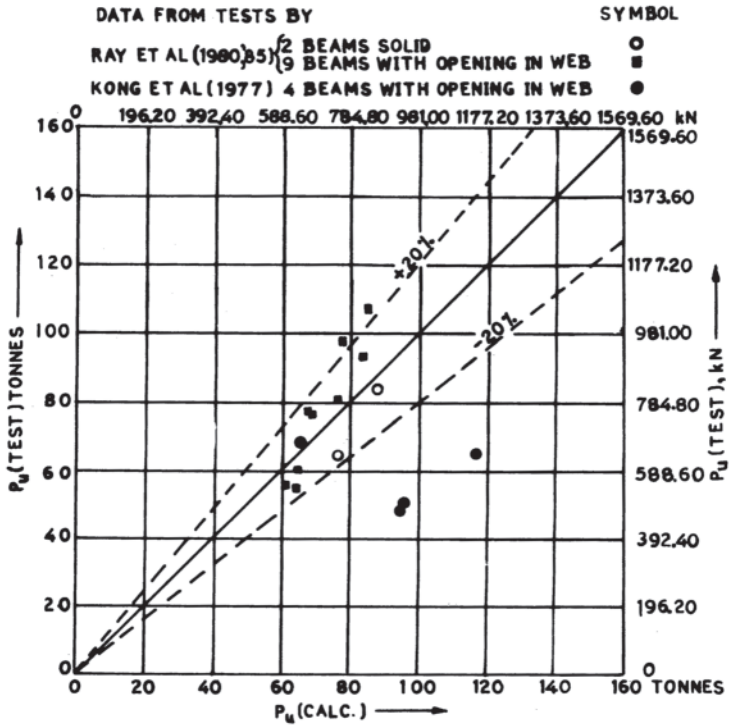

Figure 3.16 Comparison of tested and computed ultimate shear strengths of beams with and without opening in web under four-point loading (Ray, 1980; 1985).

where, the subscripts 1 and 2 refer to the values with respect to critical paths I and II respectively.

Eqns (3.41) and (3.42) can be utilised in predicting the ultimate strength of beams with web openings. Moreover, the failure load path can be predicted in advance and with greater certainty by computing the resistance of the two critical paths, unless the difference is only marginal. Eqns (3.4.1) and (3.42) developed for a general case of reinforced concrete deep beams with web openings and provided with main and web steel, however, can be utilised for finding out the ultimate strengths of reinforced concrete beams with main steel only and of plain concrete beams by deleting the terms not involving.

However, in the four-point loading, unlike the two-point system, the admissible size of the opening will be fixed on the basis of the larger shear span (Figure 3.15) and the restrictions stipulated for the opening parameters will apply in this case also.

The validity of the Eqns (3.41) and (3.42) has been verified for a few beams available (Kong *et al.,* 1977; Ray, 1980; 1985) and found satisfactory. Variations beyond ±20% are limited to only few beams and within a variation of ±30%, 80% of the beams under four-point loading can be covered (Figure 3.16).

3.15 Extension for uniformly distributed loading

For a truly uniformly distributed load the failure path described by angle ß may be obtained by minimising the resistance of the concrete as given in the first part of Eqn (3.15). That is,

$$\frac{\delta(Q_U)}{\delta\beta} = \frac{\delta}{\delta\beta}\left[\frac{cbD}{\sin\beta \cdot \cos\beta\,(\tan\beta + \tan\phi)}\right] = 0 \qquad (3.43)$$

This yields a relation between ß and ϕ in the form:

$$\tan 2ß = -\tan\phi \qquad (3.44)$$

Once the value of ß is established, evaluation of the ultimate strength of beam under uniformly distributed load, will follow the usual procedure (Ray, 1980; 1982).

3.16 Recommendations for design of beams for shear and flexure

It is now well known that elastic theory characterises the action and behaviour of deep beams before cracking in its true perspective, but cannot highlight the behavioural performance and strength capacity of the beams up to the stage of collapse, which ultimate load theory can do. Limited crack width, controlled deformation and deflection are the essential prerequisites for the satisfactory performance of any structural element. The simplified formulae put forward in the preceding sections, for *L*/*D* ratio up to 1.5 and shear span/depth ratio varying from 0.22 to 0.47, can predict the strength of beams with web openings at failure condition either in shear or flexure. For a safe design, the ultimate limit state as well as the serviceability limit states should be considered. The important codes like CEB-FIP (1970) ACI (1971; 1978) and UNESCO international code (1971) have recommended the use of limit state design for the concrete structures. These recommendations are based on a semi-probabilistic approach in fixing the accepted values of probability of reaching the limiting states in any structure. This involves the use of characteristic values and partial safety factors for the various actions and mechanical properties of the materials. The CEB-FIP (1970), BS CP110 (1972) and IS456 (1978) have stipulated these factors. Such factors have been used conveniently in the present formulations for simplified design guide.

Thus, in order to keep the predicted ultimate load capacity of beams under safe design, a general performance factor (or safety factor) for the ultimate limit state (UNESCO, 1971; Winter School etc., 1978) is chosen as 0.75 for shear and 0.85 for flexure in order to get reasonable lower bounds on these failures. In addition, the following partial safety factors (UNESCO, 1971; Winter School etc., 1978) for loading and materials so as to cover their inherent deficiencies have been used:

γ_f (=partial safety factor for loading)=1.40
γ_m (=partial safety factor for steel)=1.15
γ_c (=partial safety factor for concrete)=1.50

The lower bound values of the expressions for simplified design of beams failing either in shear or flexure may be written as follows: Beams with web openings failing in shear: from Eqn (3.24)

$$\frac{Q_u}{bD}\left(=\frac{P_u}{2bD}\right)=\xi_1\,[0.1\,f'_c(\lambda_1)(\lambda_2)(\lambda_3)+0.0085\,\psi_s\,p_s f_{sy} + 0.01\psi_w K_w r_w f_{wy}\,] \tag{3.45}$$

where ξ_1=performance factor or safety factor for beams failing in shear= 0.75.
Beams failing in flexure: from Eqn (3.40)

$$\frac{M_{FL}}{bd^2 f'_c}=\xi_2\left[\frac{p'_s f'_{sy}}{f'_c}(0.86)+\frac{p_{wt} f_{wy}\cos\alpha}{f'_c}(0.52)+0.033\right] \tag{3.46}$$

where ξ_2 is the performance factor or safety factor for beams failing in flexure =0.85.

As well as the performance factor (or safety factor), the partial safety factors for loading and materials as suggested in this section will have to be used.

3.17 Recommendations for lever arm (Z)

Beams with solid webs
For a preliminary design, an approximate value of Z is necessary which cannot be obtained from the Eqn (3.46) without full knowledge of details of the beams in advance. So, for the preliminary design of beams a value of Z=0.7D is recommended.

The value of Z suggested by Kong *et al.* (1975) was 0.6D and that by CEB-FIP (1970) was 0.2 (L + 2D) for 1≤L/D≤2, which comes to 0.7D also for L/D ratio 1.5 (Ray, 1980; 1983). So, the design bending moment should not exceed:

$$0.7\,A_s\,(f_{sy}/\gamma_m)D \tag{3.47}$$

Beams with openings in webs
Eqn (3.47) is applicable for beams with web openings also, but a capacity reduction factor of 0.65 is recommended (Ray, 1980; 1982) —i.e. the design bending moment should not exceed the limit:

$$0.65\,[0.7\,A_s\,(f_{sy}/\overline{\gamma}_m)D] = 0.45\,A_s\,(f_{sy}/\overline{\gamma}_m)D \tag{3.48}$$

3.18 Design example

For comparison the data assumed for the design example are the same as those used by Kong and his associates (1975). In working out the example,

the simplified design equations along with the partial safety factors suggested in sections 3.16 and 3.17 have been utilised (Ray, 1980; 1983).

Example: Beam with web opening

Data: symmetrical two-point loading;
L=750 mm, D=750 mm; X_N=250 mm;
Bearing width=75 mm; W=330 kN; f'_c=22.5 N/mm^2;
f'_{cu}=30 N/mm^2; f'_t=3 N/mm^2; f_{sy}=250 N/mm^2.
Opening size: a_1x=100mm; a_2D=150mm;
Co-ordinates of opening centre: K_1X_N=137.50 mm, K_2D=475 mm.

Design procedure

i) Main steel A_s:

Design moment M=5775×10^4 Nmm (3.49)

The design moment should not exceed

$$0.455 A_s (f_{sy}/\bar{\gamma}_m).D = \frac{0.455 \times A_s \times 250 \times 750}{1.15}$$

$$= 74.1848 \times 10^3 . A_s \text{ Nmm} \quad (3.50)$$

From Eqns (3.49) and (3.50) on simplification, A_s=778.4614mm^2. Provide 2 –25 mm diameter bars (981 mm^2) as main steel.

ii) Beam width: The web opening parameters are shown evaluated in Table 3.1. The shear resistance of concrete alone given by the first part of Eqn (3.45) is:

$$0.75\left(0.1 \times 0.371 \times \frac{22.5}{1.5}\right) \times b \times 750 = 313.0313\, b\text{N} \quad (3.51)$$

Table 3.1 Web opening parameters

K_1X_N (mm)	K_2D (mm)	e_x (mm)	X_{net} (mm)	e_y (mm)	Y_{net} (mm)	λ_1	λ_2	λ_3	$\lambda_1\lambda_2\lambda_3$
137.50	475.00	12.50	150	100	300	0.91	0.75	0.543	0.371

It is assumed that the contribution of concrete for resisting shear is about (0.65×50%) of that of the solid web. That is,

$$0.65 \times 115.50 \times 10^2 = 75.075 \times 10^3 \text{ N} \quad (3.52)$$

Simplifying Eqns (3.51) and (3.52)

$$b=239.8322\text{mm}; \; b=200 \text{ mm (say)} \quad (3.53)$$

iii) Shear strength of beam with tensile steel only. Using the first two terms of Eqn (3.45):

$$0.75\left[0.1 \times 0.371 \times \frac{22.50}{1.5} + 0.0085 \times 0.65 \times \frac{981 \times 100}{200 \times 750} \times \frac{250}{1.15}\right] \times \frac{200 \times 750}{1000}$$

$$= 150.9762 \text{ kN} \quad (3.54)$$

iv) Web steel A_w:

Design shear force=231 kN (3.55)

Hence, shear strength due to web steel=231-150.9762=

$$=80.0238 \text{ kN} \tag{3.56}$$

Considering horizontal web steel to be provided for, the last part of Eqn 3.45 gives:

$$0.75\left[0.01\times 0.5\times 0.85\times \frac{A_{wh}\times 100}{200\times 750}\times \frac{250}{1.15}\right]\times \frac{200\times 750}{1000}$$

$$=0.0693\, A_{wh} \text{ kN} \tag{3.57}$$

Simplifying Eqns (3.56) and (3.57)

$$A_{wh}=1154.7446 \text{ mm}^2 \tag{3.58}$$

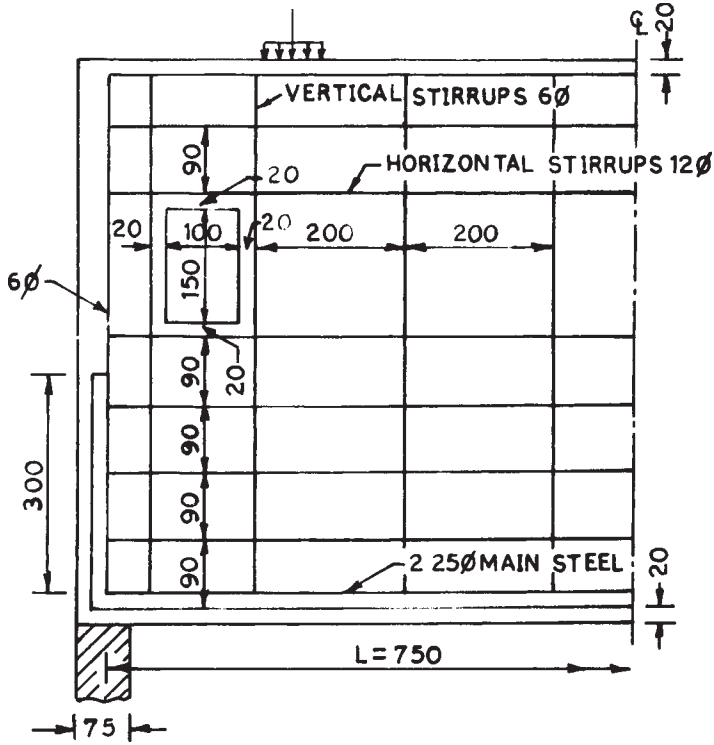

Figure 3.17 Details of beam with web openings (Kong *et al.,* 1975) and provided with horizontal and vertical web reinforcement (Ray, 1980; 1983). Beam thickness=200: all dimensions in mm.

Provide 6–12 mm diameter two-legged horizontal stirrups (1356 mm^2) such that 4 bars at 90 mm centres below the opening and 2 bars at 90 mm centres above the opening are provided. In addition, nominal vertical two-legged stirrups of 6 mm diameter may be provided. The detailing is shown in Figure 3.17.

v) Alternatively, inclined web reinforcement can be provided using the last part of Eqn (3.45)

$$0.75\left[0.01\times 0.5\times 1.15\times \frac{A_{w1}\times 100}{200\times 750}\times \frac{250}{1.15}\right]\times \frac{200\times 750}{1000}$$

$$=0.0938\,A_{w1}\ \text{kN} \tag{3.59}$$

From Eqns (3.56) and (3.59) on simplification,

$$A_{w1}=853.1322\ \text{mm}^2 \tag{3.60}$$

Provide 5–12 mm diameter two-legged stirrups (1130 mm^2) such that 3 bars below the opening and 2 bars above the opening and arranged perpendicular to the plane of rupture are provided. The detailing is shown in Figure 3.18.

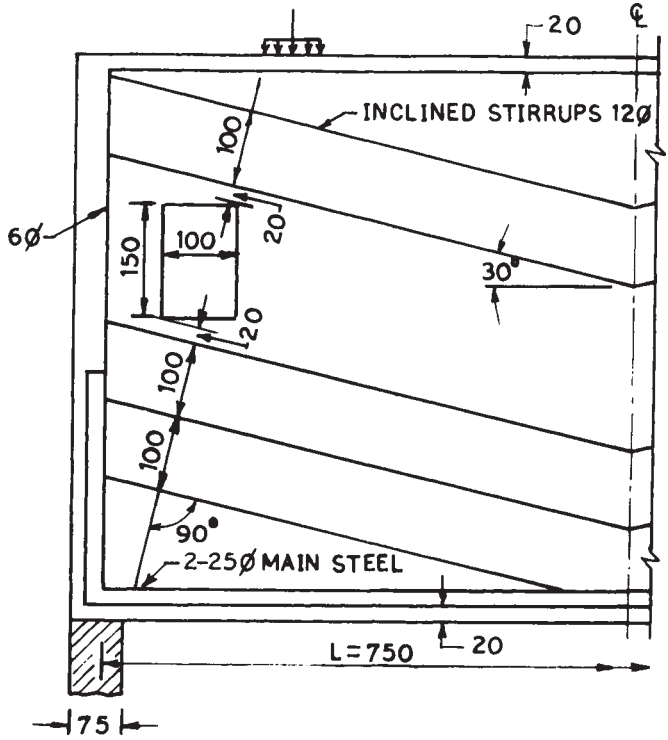

Figure 3.18 Details of beam with web openings (Kong *et al.,* 1975) and provided with inclined web reinforcement (Ray, 1980; 1983). Beam thickness=200; all dimension in mm.

vi) Shear strength of beam with tensile and web steels:

(a) With horizontal and vertical stirrups, Figure 3.18:

$$Q_u = 150.9762 + 0.75\left[0.01 \times 0.5 \times 0.85 \times 1356 \times 100 \times \frac{250}{1.15}\right] \times \frac{1}{1000} + 0.75\left[0.01 \times 0.5 \times 0.233 \times 112 \times 100 \times \frac{250}{1.15}\right] \times \frac{1}{1000}$$

$$= 247.0655 \text{ kN} > 231 \text{ kN} \tag{3.61}$$

(b) With inclined stirrups only, Figure 3.18:

$$Q_u = 150.9762 + 0.75\left[0.01 \times 0.5 \times 1.15 \times 1130 \times 100 \times \frac{250}{1.15}\right] \times \frac{1}{1000}$$

$$= 256.9137 \text{kN} > 231 \text{kN} \tag{3.62}$$

vii) In addition to providing an anchorage length of about 300 mm as per BS CP110, part I (1972) with 90° upright bends on either end of the main steel, the load and support bearing points should be properly strengthened, each with a 40 mm diameter spiral made of 6 mm diameter mild steel (MS) bars 150 mm long with (e.g.) 30 mm pitch and a mesh reinforcement (e.g. one layer of 6 mm diameter MS mesh of size 120mm×175mm) to avoid any premature failure by crushing of concrete.

Further, to guard against any possible stress concentration, the openings should be suitably strengthened by providing a loop of 140 mm×190mm around the opening with 6 mm diameter bars in the inclined web steel case, whilst in the case of horizontal and vertical web steel, such a loop may get formed by such arrangement of web steel, (Figures 3.17 and 3.18).

References

American Concrete Institute. (1971) *Standard Building Code Requirements For Reinforced Concrete,* ACI318–71, ACI, Detroit.

American Concrete Institute. (1978) *Manual of Concrete Practice.* Parts 1 And 2, ACI, Detroit.

Comite Européen du Béton-Fédération Internationale de la Précontrainte. (1970) *International Recommendations for the Design and Construction of Concrete Structures.* Cement And Concrete Association, Appendix-3, London: 17.

Guralnick, S.A. (1959) Shear strength of reinforced concrete beams. *J. Struct. Div. Am. Soc. Civ. Engrs.* **85**, ST1 : 1.

Indian Standards Institution, (1978): IS. 456–1978 (Revised), *Code of Practice for Plain and Reinforced Concrete for General Building Construction,* India.

Kong, F.K. (1986) Reinforced concrete deep beams. In Concrete Framed Structures-Stability and Strength, ed. Narayanan, R. Ch.6. Elsevier Applied Science, London: 169.

Kong, F.K. and Robins, P.J. (1971) Web reinforcement effects on lightweight concrete deep beams. *J. Am. Concr. Inst.* July: 514.

Kong, F.K., Robins, P.J. and Cole, D.F. (1970) Web reinforcement effects on deep beams. *J. Am. Concr. Inst.* 67, Dec.: 1010.

Kong, F.K., Robins, P.J., Kirby, D.P. and Short, D.R. (1972) Deep beams with inclined web reinforcement, *J. Am. Concr. Inst.* **69,** No.3, March: 172.

Kong, F.K., Robins, P.J. and Sharp, G.R. (1975) The design of reinforced concrete deep beams in current practice. *Struct. Engr.* **53,** No.4, Apr. p: 173.
Kong, F.K., Robins, P.J., Singh, A. and Sharp, G.R. (1972) Shear analysis and design of reinforced concrete deep beams. *Struct. Engr.* **50,** No.10 Oct.: 405.
Kong, F.K., and Sharp, G.R. (1973) Shear strength of lightweight reinforced concrete deep beams with web openings. *Struct. Engr.* **51,** Aug.: 267.
Kong, F.K. and Sharp, G.R. (1977) Structural idealization for deep beams with web openings. *Mag. Concr. Res.* **29,** No.99, June: 81.
Kong, F.K., Sharp, G.R., Appleton, S.C. Beaumont, C.J. and Kubik, L.A. (1978) Structural idealization for deep beams with web openings: further evidence. *Mag. Concr. Res.* **30,** No. 103, June: 89.
Kong, F.K. and Singh, A. (1972) Diagonal cracking and the ultimate loads of light-weight concrete deep beams. J. *Am. Concr. Inst.* **69,** Aug.: 513.
Ove Arup and Partners. (1977) *The Design of Deep Beams in Reinforced Concrete.* CIRIA Guide 2, Ove Arup, London.
Portland Cement Association. (1946) *Concrete Information ST66, Design of Deep Girders,* PCA, Chicago.
Portland Cement Association. (1978) *Notes on ACI-318–77 Building Code Requirements For Reinforced Concrete With Design Applications,* 2nd edn revised, Portland Cement Association, Chicago.
Ray, S.P. (1980) *Behaviour and Ultimate Shear Strength of Reinforced Concrete Deep Beams With And Without Opening in Web.* PhD thesis, Indian Institute of Technology, Kharagpur, India.
Ray, S.P. (1982a) Behaviour and strength of deep beams with web openings: further evidence, *Bridge and Struct. Engr. (IABSE), India* 12, No.1 March: 1.
Ray, S.P. (1982b) A short review of literature on reinforced concrete deep beams with and without opening in web. *J. Struct. Eng.,* India **9,** No.1, Apr.: 5.
Ray, S.P. (1983) Present design practice on reinforced concrete deep beams with and without opening in web. *Bridge and Struct. Engr. (IABSE), India 13,* No.2, June: 15.
Ray, S.P. (1984) Shear strength of reinforced concrete deep beams without web opening: further evidence. *Bridge and Struct. Engr. (IABSE), India* **14,** No.2, June: 37.
Ray, S.P. (1985) Flexural strength of reinforced concrete deep beams with and without opening in web. *J. Struct. Engg., India,* 12, No.3, Oct: 75.
Ray, S.P. and Reddy, C.S. (1979) Strength of reinforced concrete deep beams with and without opening in web. *Indian Concr. J.* **53,** No.9, Sept.: 242.
Singh, J.P. (1978) *An investigation into the behaviour and strength of reinforced concrete deep beams with web openings.* M.Tech. thesis, Indian Institute of Technology, Kharagpur, India.
Singh, R., Ray, S.P. and Reddy, C.S. (1980) Some tests on reinforced concrete deep beams with and without opening in web. *Indian Concr. J.* **54,** No.7, July: 189.
British Standard Institution. (1972) *The Structural Use of Concrete,* CP110–72, BSI, London.
Timoshenko, S. (1956) *Strength of Materials,* Vol.2, D.Van Nostrand, New York.
UNESCO. (1971) *Reinforced Concrete, an International Manual.* Translated by C.Von Amerougen, Butterworths, London.
Whitney, C.S: (1940) Plastic theory of reinforced concrete design. *Trans. Am. Soc. Civ. Engrs.* **107** (1942) : 251.
Winter School Short Term Course on Limit State Design. (1978) Sponsored by Q.I.P., Government of India, Dept. of Civil Engineering, Indian Institute of Technology, Kharagpur, India.

4 Continuous deep beams

D.ROGOWSKY, Underwood McLellan Ltd., Canada

4.1 Introduction

This chapter will address design issues unique to continuous deep beams. Continuous deep beams are fairly common structural elements which occur as transfer girders, pile caps and foundation walls. Figure 4.1 illustrates some typical examples. The areas immediately over openings in load bearing walls also act as deep beams.

As a practical matter, extreme accuracy in predicting the strength of a continuous deep beam is not warranted and often not possible (due to, among other things, the inability to predict accurately differential support settlements). Fortunately, simple rational models are available to permit designs which are both economical of material and design time and of an accuracy consistent with other design inputs. Concrete member sizes are often fixed by considerations other than the purely structural. In practice, designers are often presented members with proportions which cause them to behave as deep beams. While it is rare to have the dimensions of a deep beam governed by strength and serviceability, appropriate reinforcement detailing is essential for adequate performance.

Continuous deep beams behave differently from either simply supported deep beams or continuous shallow beams. By ignoring these differences during design, one gives up potential available strength and may get significant unexpected cracking. Continuous deep beams develop a distinct ‘tied arch’ or ‘truss’ behaviour not found in shallow continuous beams. The net result of this is that conventional reinforcement detailing rules, based on shallow beams or simply span deep beams, are not necessarily appropriate for continuous deep beams.

Continuous deep beams exhibit the same general trend of increased shear strength with a decrease in shear-span/depth ratio as found in simply supported deep beams. In continuous beams, the locations of maximum negative moment and shear coincide, and the point of inflection may be very near the critical section for shear. Both of these conditions render most empirical strength prediction equations for simply supported deep beams useless for continuous deep beams. The existing empirical equations which are based almost exclusively on simple span beam tests should not be blindly applied to continuous beams. There are too many parameters and currently too few tests to develop empirical strength prediction equations specifically for continuous deep beams.

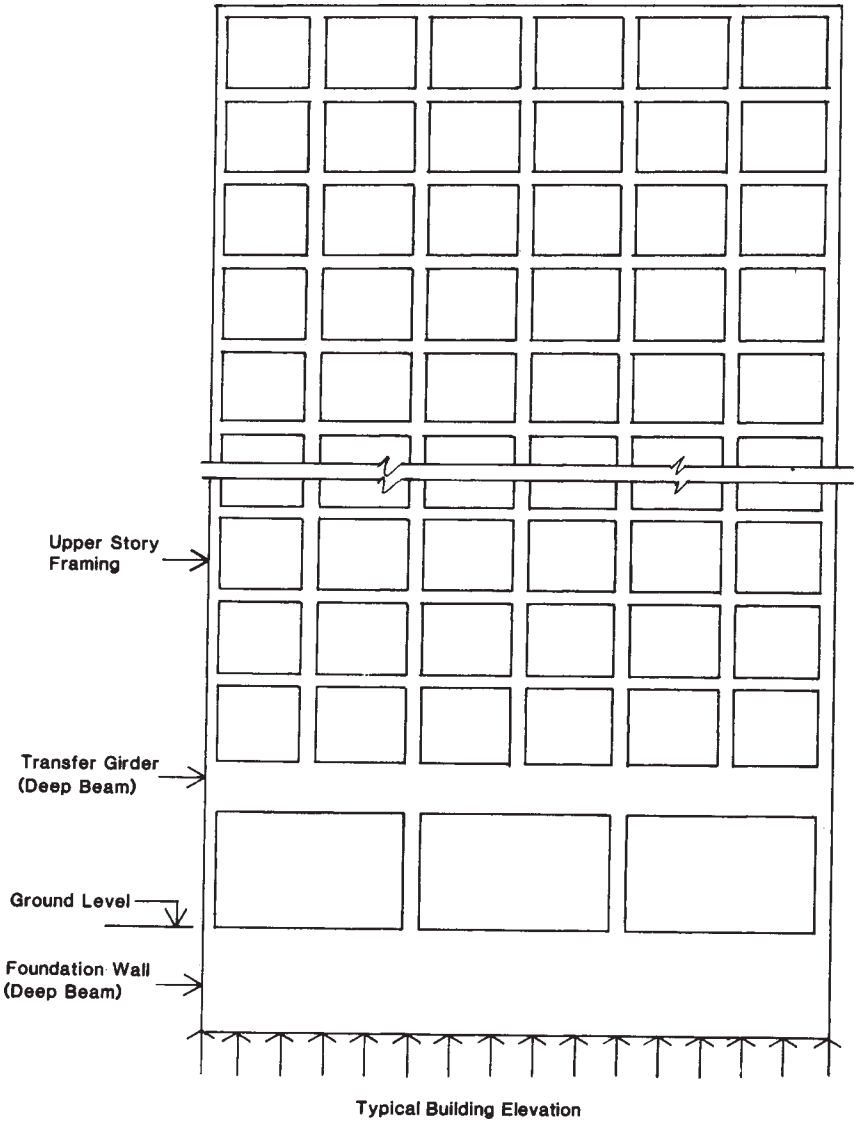

Figure 4.1 Examples of continuous deep beams

There is no universally accepted definition of deep beam. In general, European deep beams are approximately twice as deep as North American deep beams. For example, CEB-FIP (1970) suggests that simply supported beams of span/depth ratio L/D (where L is the beam span in m, the smaller of the centre to centre span, or 1.15 times the clear span; D is overall beam depth in m) less than 2 and continuous beams of L/D ratio less than 2.5 be designed as deep beams. ACI (1986) suggests that beams with clear with

clear span to effective depth ratios greater than 5 (and loaded at the top or compression face) be treated as deep beams. The ACI deep beam definition is based on shear behaviour while CEB definition is based on flexural behaviour. It is important to recognise the different definitions when reviewing design recommendations. In reality the deep beam problem is a coupled problem. This chapter will provide a review of the literature and attempt to present a coupled or integrated solution which addresses both shear and flexure with one consistent model.

4.2 Distinguishing behaviour of continuous deep beams

4.2.1 *Previous tests*

There are very few tests of continuous deep beams available in the literature. Nylander and Holst (1946) reported perhaps the first test. They reported the results of a test for a two span specimen with an elaborate arrangement of truss bars. The specimen was part of a general investigation of reinforced concrete beams, hence no general conclusions could be drawn.

Leonhardt and Walther (1966) conducted a well known and extensive series of tests on deep beams. The tests included different loading conditions, different reinforcement arrangements and different support conditions including some two span beams. These tests formed the basis for the CEB-FIP (1970) recommendations.

Rogowsky, MacGregor and Ong (1986) conducted a series of tests on 17 large-scale two span deep beams. Both spans were brought to failure, providing a total of 34 test results. The tests covered span to depth ratios ranging from approximately 5 to 2 and had various amounts of horizontal and vertical web reinforcement (none; minimum ACI vertical stirrups for deep beams; four times minimum stirrups; about half ACI minimum horizontal shear reinforcement for deep beams; and 1.5 times minimum horizontal reinforcement). All beams were loaded by and supported by monolithic concrete columns. For comparison purposes, six additional companion simple span deep were also tested. Both ends of the simple spans were brought to failure, providing a total of 12 large-scale simple shear span test results. These tests formed the basis for some of the deep beam recommendations in the current Canadian concrete code (CSA A23.3 M84) and proposed revisions to the American concrete code (ACI 318–86).

A brief description of the behaviour of a typical deep beam test specimen is now presented. Figure 4.2 illustrates the key events in the life of a continuous deep beam. In general, deep beams develop little initial flexural cracking. For the beams tested by Rogowsky *et al.* (1986), midspan flexural cracks tended to form before negative cracks over the interior support. The first significant event during loading of a deep beam is the development of diagonal, inclined or shear cracks which occur

suddenly and are accompanied by a loud bang. The cracks tend to delineate a truss or tied arch mode of behaviour. In the tests by Rogowksy *et al.* (1986) the inclined cracking occurred at about 50% of the ultimate load. This stage, illustrated in Figure 4.2b, is the key stage in terms of understanding deep beam behaviour. (The transparency of behaviour is subsequently obscured by secondary flexural cracking as the reinforcement is brought to yield.) As the load is increased, additional flexural cracks form. Yield of the main flexural reinforcement brings about significant deflections. These deflections are accompanied by joint rotations of the so called truss which eventually cause the concrete compression struts to fail. The strength of the member is governed by the

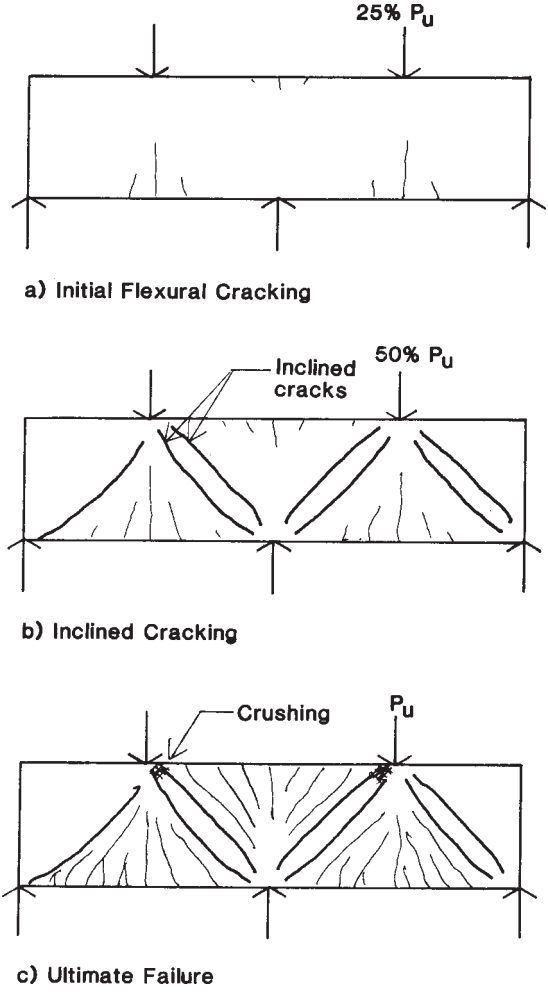

Figure 4.2 Typical continuous deep beam cracking behaviour

yield of the main flexural reinforcement while ductility is governed by failure of the concrete.

For the tests which have been conducted, the main reinforcement ratios (typical of these found in practice) were low enough for the main reinforcement to yield. It is theoretically possible to increase the amount of reinforcement to the point where it does not reach yield before the concrete crushes. As in the case of normal or shallow beams, such over-reinforced members are to be avoided in practice.

4.2.2 *Continuous deep beams vs continuous shallow beams*

The two test series noted in section 4.2.1. revealed the following major behavioural differences between deep and shallow continuous deep beams,

i) Deep beams develop a marked truss or tied arch action while shallow beams do not. Figure 4.3 presents a comparison of deep beam and a shallow beam. In the shallow beam the shear is transferred through a fairly uniform diagonal compression field with compression fans under the point load and over supports. In the deep beam most of the force is transferred to the supports through distinct direct compression struts (zones of predominately uniaxial compression).

ii) After cracking, stresses in deep beams deviate significantly from those predicted by an elastic analysis. Figure 4.4 presents the stresses in the main flexural reinforcement of a deep beam immediately before and after diagonal cracking.

iii) The initial diagonal cracks in a deep beam do not cross the major compression strut. In some instances they outline the strut. After diagonal cracking, the concrete contribution to shear strength increases for a deep beam because a stable truss is formed. In a shallow beam there is little if any increase in shear capacity.

iv) The bending moments over supports are smaller and the midspan bending moments are correspondingly larger than predicted by elastic theory for shallow beams. The crack patterns, support reactions, and strain measurements all indicated that the negative moment over the interior support was smaller than the positive moment at midspan. The ratio between experimental and elastic interior support moment was typically 60–70% prior to yielding of the bottom flexural reinforcement. For several of the beams without heavy stirrup reinforcement, the top flexural reinforcement did not reach yield before the specimen failed.

v) The deep beams were found to be very sensitive to differential support settlements. Even small differences in support settlements lead to large redistribution of moments for deep beams which must be considered in design. In the laboratory under ideal conditions, differential support settlements (elastic shortening of load cells and so on were hard to control. The laboratory differential settlements ranged from about $L/2000$ to $L/10\,000$. In real structures, differential support settlements can be an order of

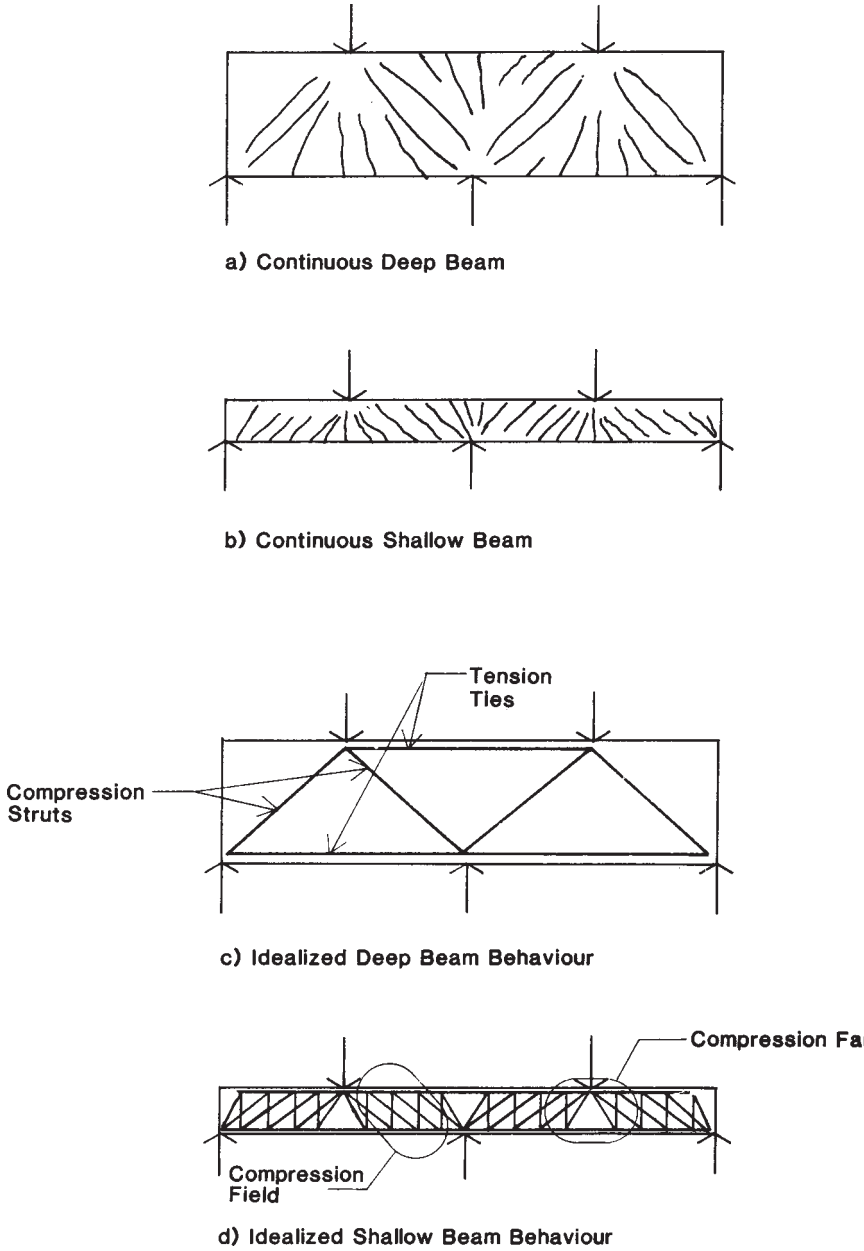

Figure 4.3 Comparison of deep and shallow continuous beam behaviour.

magnitude larger and must be accounted for in the design of continuous deep beams. One must either make the beams strong enough or ductile enough to accomodate all possible combinations of support movement.

vi) As a result of the truss or tied arch action, the main flexural reinforcement carries significant tension along its full length. At a given section both the top and bottom reinforcement can carry significant tension. Figure 4.4 gives an example. As a result, in deep beams, the development and anchorage of the main reinforcement is critical.

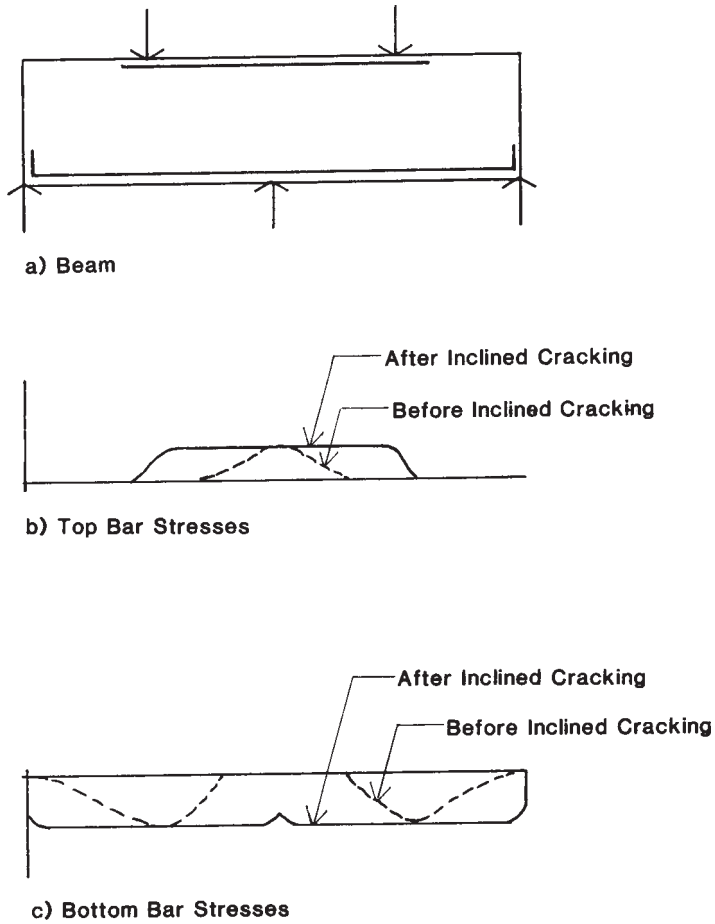

Figure 4.4 Steel stress redistribution after inclined cracking

vii) Vertical web reinforcement did not significantly increase the shear strength of the deep beams. (As will be demonstrated later, the strength does not increase until there is sufficient vertical web reinforcement to eliminate the direct compression strut.) Heavy vertical web reinforcement did significantly reduce the variability in strength and increase the ductility,
viii) The addition of minimum amounts of horizontal and/or vertical web reinforcement often reduced the failure load to below that of a comparable

beam without web reinforcement. The reductions were generally minor and were believed to be due to the direct compression strut being pulled apart by the web reinforcement as the steel strained. This pulling apart reduces the effective concrete strut capacity.

4.2.3 *Continuous deep beams vs simple span deep beams*

There are some distinguishing features of continuous deep beams which render empirical equations based on simple span tests less than useful,

i) In a continuous deep beam, the point of contraflexure often occurs near the critical section for shear. This situation causes difficulty with some empirical equations. In the ACI procedures the ratio of moment to shear at the critical section is a main parameter in the shear strength prediction equation. Unfortunately, this ratio changes drastically when the point of contraflexure is near the critical section for shear which produces wildly varying strength predictions. If the point of contraflexure coincided with the critical section (moment equals zero), the ACI equations would require division by zero!

ii) At an interior support in a continuous beam, the region of high shear and high negative bending moment coincide. In simple span beams the region of high shear coincides with a region of low bending moment. These differences cast further doubt on the usefulness of empirical equations based on simple span test data.

iii) In the tests by Rogowsky *et al.* (1986) horizontal web reinforcement was found to have little influence on the ultimate strength of the continuous beams. The amounts of horizontal web reinforcement used were relatively light (typical of minimum reinforcement used in practice). Had greater amounts of horizontal web reinforcement been used it is possible that an observable strength increase might have resulted. It will be shown later that for beams with proportions similar to those tested, the addition of horizontal web reinforcement is not a particularly efficient method of increasing shear strength.

4.3 Capacity predictions by various methods

Several of the methods available for analysing deep beams are discussed. They were used to predict the ultimate shear strength for the continuous deep beams tested by Rogowsky *et al*. (1986). The comparisons of prediction accuracy are not intended as a criticism of the various methods. The comparisons are intended to illustrate the difficulty of extrapolating methods developed from or for simple span deep beams to continuous deep beams.

4.3.1 *Elastic analysis*

The discussion in this section pertains primarily to the classic elastic flexural problem associated with deep beams. It has long been recognised that in

deep beams sections that are plane before bending do not remain so after bending. The stresses on the beam cross section therefore do not vary linearly with depth. Generally, the nonlinearity is of more interest when reinforcement is designed by the working stress method than when reinforcement is designed by the strength method. Much of the early work on deep beams emphasised elastic analysis and many elastic solutions can be found in the literature. The Portland Cement Association (1980) still provides information on the elastic stress distribution in deep beams. It covers simple span and continuous beams.

Leonhardt and Walther (1966) found that until cracking develops, the stresses approximate those predicted by elastic theory. After cracking, the stresses deviate significantly from the elastic distribution. Beam capacity cannot be predicted by elastic analysis.

If reinforcement is proportioned solely in accordance with an elastic analysis, main reinforcement would for example be curtailed in regions of low bending moment. In real beams that demonstrate marked strut and tie action the curtailed reinforcement is ineffective as a tie and much of the potential post-cracking strength is lost.

One useful insight which can be drawn from the elastic solutions is the estimation of the depth of the tension zones. The main flexural reinforcement should be distributed over most of the tension zone to control cracks. The CEB and CIRIA recommendations recognise this in their reinforcement detailing requirements. The amount of reinforcement is determined by a strength design, but the reinforcement is distributed in general accordance with elastic analysis. Shear strength analysis was largely ignored because the beams of interest at the time (i.e. deep enough to have non-linear but elastic behaviour) were generally deep enough for shear strength not to be critical.

4.3.2 *Finite element analysis*

Finite element analysis is the subject of Chapter 9 so the comments here will be brief and pertain to continuous deep beams. Finite element programs are now available which can with reasonable accuracy predict the capacity of reinforced concrete beams. The literature now contains the results of such an analysis for continuous deep beams.

Cook and Mitchell (1988) report a non-linear finite element analysis of two of Rogowsky *et al.*'s test specimens. The beams had shear span to depth ratios of 1.5 and 2.0 respectively, and contained heavy vertical stirrups. The analysis predicted deformations, principal stresses, principal strains and ultimate loads. All four (two failures per beam) test results were within 4% of the predicted values. The failure resulted from yielding of the transverse reinforcement followed by crushing of the concrete. The high negative moment near the central support produced large tensile strains in the adjoining shear spans thus softening the concrete and reducing its compressive strength. The softening was gradual as demonstrated by the ductile experimental load deflection curve.

All finite element programs are different. It is, however, essential that the model incorporate non-linear constitutive relationships for the steel and concrete. In the case of the concrete, the model should account for strain softening. The accuracy will be best for under-reinforced members with at least modest web reinforcement (to ensure some ductility).

Currently non-linear finite element analysis is still not used for routine design, but for special critical problems it offers an alternative to physical testing.

4.3.3 *ACI 318*

The recommendations of ACI 318 (1977) were used to assess the strength of Rogowsky *et al.*'s test specimens. For the continuous beams, the ratios of test to calculated strengths ranged from 1.38 to 0.48. Over half of the tests had measured strengths less than the strength predicted by the ACI code. The discrepancy arises because the empirical design method given in ACI is based on simple span test data. Had ACI chosen to use the ratio of shear span to depth ratio as the prime parameter rather than the ratio of shear to moment at the critical section, better agreement may have been achieved. The ACI code is not based on a clear mechanical model of behaviour and is not recommended.

4.3.4 *Kong, Robins and Sharp*

The method of Kong, Robins and Sharp (1975) was used to analyse the data of Rogowsky *et al.* The ratio of test to calculated strength ranged from 0.53 to 1.31. Their method was found to be safe for beams with heavy stirrup reinforcement (vertical web reinforcement ratio approximately 0.006) where the average test to predicted ratio was 1.17. For the remainder of the tests, the ratio of test to predicted values was highly variable and generally quite unsafe. The method was originally developed for simple span deep beams deeper than those analysed.

4.3.5 *Truss models*

In a truss model analysis one idealises the beam as a truss consisting of concrete compression struts and steel tension ties. These models are based on the theory of plasticity and in various forms have been proposed by a number of authors including Grob and Thurlimann (1976), Nielsen *et al.* (1978), Marti (1985a, b) and Schliach (1987). Truss models specifically for deep beams have been presented by Rogowsky and MacGregor (1986). Truss models have gained increasing acceptance as they have grown less rigorous. The Canadian concrete design code (CSA A23.3-M84) contains rules for use of truss models in design.

Truss models were used to analyse the two span data of Rogowsky *et al.* Some of the predictions were excellent. For the beams with heavy stirrups (assuming the effective concrete strength equal to the specified strength) the

ratio of test to calculated strength ranged from 0.94 to 1.02 (mean 1.00 and standard deviation 0.03). For the other beams, the prediction accuracy depended upon the truss model used because the beams were not always ductile enough fully to redistribute forces in accordance with the truss model. If the model assumed full yield of the top reinforcement over the support when in fact it did not yield, unconservative predictions resulted.

4.4 Truss models for continuous deep beams

This section reviews truss models in detail and describes specific models suitable for continuous deep beams. These are discussed at some length because the selection of truss model has a significant impact on capacity predictions.

Truss models are based on the lower-bound theorem of plasticity which states that:

> If an equilibrium distribution of stresses can be found which balances the applied load and is everywhere below yield or at yield, the structure will not collapse. Since the structure can carry at least this applied load, it is a lower bound to the load carrying capacity of the structure.

While the theorem has a rigorous mathematical basis, it is obvious to most designers that if one can find a safe load path through the structure, it will be a conservative lower bound to the true capacity. The structure will undoubtedly find other more complex load paths with greater capacity. With truss models, one produces a simple load path in the form of a truss and checks or designs the components of the truss for the required load.

Truss models assume or require that:

i) equilibrium is satisfied
ii) concrete resists compression stresses only and has an effective strength less than the specified design strength
iii) steel is required to resist all tensile forces
iv) the centroids of each truss member and the lines of actions of all externally applied loads must coincide (this ensures that local equilibrium is satisfied)
v) failure of the truss model occurs when a concrete compression member crushes or when a sufficient number of steel tension members reach yield to produce a mechanism.

Truss models are composed of three elements

i) steel tension members which are permitted to reach and sustain yield stresses; collapse of the beam does not necessarily occur with yielding of a single tension member; collapse occurs when sufficient tension members yield to convert the truss into a mechanism

ii) concrete compression members which carry a uniaxial compressive stress; the struts have finite width and thickness which depend on the imposed member force and permissible stress; the ends of the strut are principal stress faces and therefore must be perpendicular to the longitudinal axis of the strut.

iii) joints which transfer the stresses from loads and from truss member to truss member; the joints consist of concrete in biaxial compression (sometimes refered to as "hydrostatic stress"), their dimensions are finite and depend on the imposed joint forces and permissible concrete stress; all forces at a joint must be concurrent, making the assumption of a pinned joint reasonable.

Additional truss elements can be built up from these three basic building blocks. Compression fans occur when a number of small compression struts fan out from a single joint to spread out or collect a load, such as under a point load or over a support. Compression fans can be seen in Figure 4.3d. Compression fields occur when a number of small parallel compression struts transfer forces from one stirrup to another. Compression fields can be seen in Figure 4.3d. Marti (1980) provides additional elements or building blocks which may also be used.

Before demonstrating the application of truss models to continuous deep beams, further discussion of the permissible compression stress is warranted. In the development of truss models by the various investigators, the permissible or effective concrete strength has received much but perhaps unwarranted attention. Since the capacity of a well designed beam should be governed by steel yielding, the permissible concrete strength has little influence. Reasonable but approximate values of permissible stress may be used. The stress level chosen will determine the dimensions of the joints and compression struts. This will in turn have a minor impact on the overall truss geometry and the load which can be carried when a mechanism is developed. In the Canadian Code (CSA A23.3-M84), the permissible concrete stress for compression struts may be taken as 85% of the specified concrete strength. In general, the inclination of the struts should be limited to between 25 and 65° from the horizontal. The inclination limitation is required to prevent the selection of a model with unrealistically steep or flat struts. Steeper struts may be justified when point loads occur very close to a support.

For truss joints, a further reduction is warranted to account for the incompatibility of strains and the oversimplification of stress conditions. The Canadian Code (CSA A23.3-M84) indicates that for joints bounded by compression struts and bearing areas, the permissible stress may be taken as 85% of the specified strength. For joints which anchor one tension tie the permissible stress may be taken as 75% of the specified strength, and for joints which anchor tension ties in more than one direction the permissible stress may be taken as 60% of the specified strength. The Canadian code uses live and dead load factors of 1.5 and 1.25 respectively. It also uses

material performance factors of 0.85 for steel, and 0.6 for concrete. (The permissible concrete stresses should be adjusted to suit other load and resistance factors.) The net result is that the final effective concrete stresses under factored loads are limited to 51%, 45% and 36% of the specified strength for 0, 1 and more than 1 tension tie anchored at a joint.

Tension ties are shown in the diagrams with anchor plates. This convenient shorthand emphasises the importance of positive bar anchorage and encourages the distribution of the bar forces over the entire joint. In practice bars will usually be developed with hooks and adequate development length. The truss model clearly shows what bar forces need to be developed at a joint.

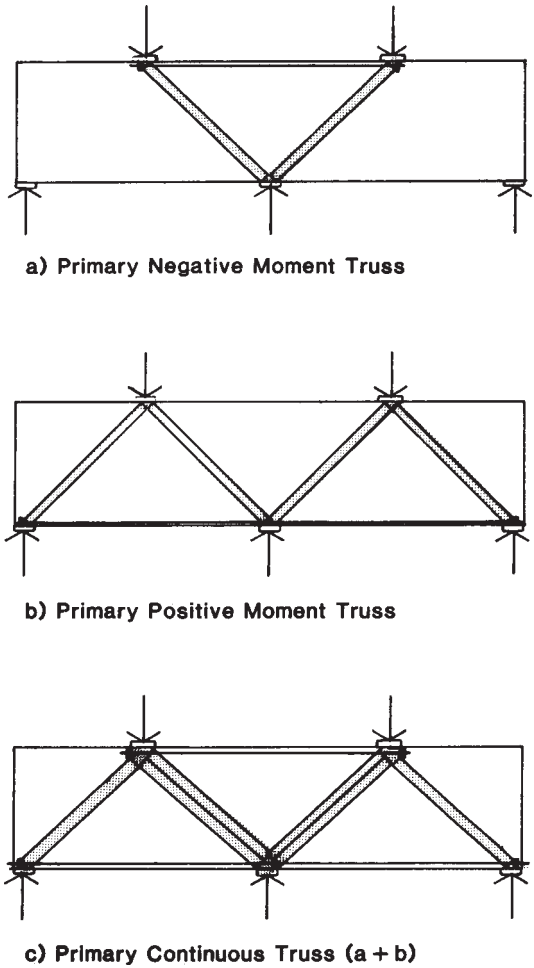

Figure 4.5 Primary continuous truss models

Loads are also shown acting through bearing plates. Again, this is convenient shorthand which emphasises the need for reasonable force transfer into the beam. In practice loads will be transfered to and from the beam through concrete columns.

Typical truss models for continuous beams are presented in Figures 4.5 and 4.6. Their detailed use will be illustrated in the design examples. Conceptually, they are statically indeterminate trusses. Assuming yield of the reinforcement, the truss is rendered determinate and the compression member forces can be solved by the method of joints provided it is done in an appropriate order.

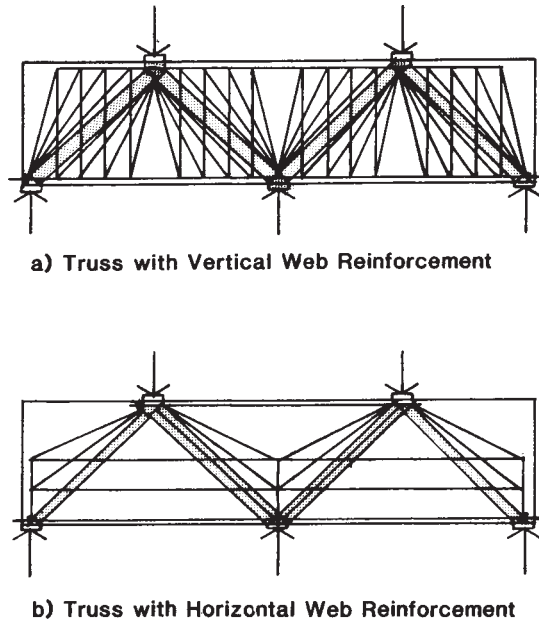

Figure 4.6 Continuous truss models with web reinforcement

The solution procedure is as follows:

i) For simplicity use a final effective concrete strength of 45% of the specified strength. (For the models shown, no more than one tie will be anchored at a joint.)
ii) Draw the truss to scale (including strut widths).
iii) Measure the strut slopes from the diagram.
iv) Calculate the vertical and horizontal components for each strut reacting against a stirrup assuming that, if it can, the stirrup will yield, thus defining the vertical strut force. (Stirrups connected to struts with inclinations steeper than 65° are not likely to yield. These occur close to supports and point loads.)

v) Calculate the top and bottom chord forces assuming that the bars are at yield at points of maximum moment and reduce the chord force by the horizontal component of each strut at each stirrup,
vi) Use any chord tension force remaining to equilibrate a direct concrete compression strut.
vii) Check that the truss as drawn in step 2 is still appropriate and revise if necessary. Occasionally two or three iterations may be required,
viii) The shear capacity is the sum of the vertical components of each strut which comes down at the support in question.

This detailed procedure is illustrated in Figure 4.8. In steps v) and vi), the addition of stirrups reduces the load which can be supported by the direct compression strut. With sufficient stirrups, the direct compression strut will not form. In deep beams, most of the load is supported by the direct compression strut hence additional stirrups are not entirely effective in supporting additional load until the direct compression strut is eliminated.

4.5 Design of continuous deep beams

Loading and support conditions are perhaps the most important considerations in the design of continuous deep beams. Continuous deep beams are very sensitive to support movements and without heavy stirrup reinforcement, they may not be ductile enough to permit a design for one set of moments and support reactions. The designer should select reinforcement which can accommodate all reasonable distributions of moments and support reactions. The distributions will depend on the specific application, but consideration should be given to foundation settlement, column shortening, and so on. For ideal support conditions at least the following two distributions should be considered:

i) A distribution based on an elastic analysis that includes support settlements but ignores shear deformation effects (e.g. moment distribution)
ii) A distribution in which the negative moments from the first distribution are reduced by 40% and the remaining positive moments adjusted accordingly (this comes from experimental observations).

To ensure some ductility and reduce variability in behaviour, a well distributed minimum reinforcement should be provided. This minimum reinforcement should be at least twice as great as current minimum horizontal and vertical web reinforcement. Reinforcement ratios of at least 0.003 in the horizontal and vertical directions would be appropriate. In the case of stirrups, they should be increased if required to support at least 30% of the direct compression strut capacity.

Truss models should be used to determine the principal reinforcement requirements. The reinforcement should be distributed and detailed (anchored) in accordance with the model analysis.

Crack control under service loads is expected to be satisfied by the use of greater than normal minimum reinforcement. For large long numbers subjected to significant shrinkage, temperature variations and restraint, one may wish to increase the horizontal and vertical web reinforcement ratios to 0.006. This represents three to four times normal minimum reinforcement. As a practical matter, this additional reinforcement has little impact on total project cost as it permits much longer concrete placements (in excess of 30 m) with fewer construction and control joints.

Service load deflection predictions may be based on an elastic analysis of the truss model duly adjusted for creep and shrinkage. The deflections due to deformation of the web members of the truss correspond to shear deformations, while the chord deformations account for the flexural deformations. Appendix E of CIRIA Guide 2 (1977) should be consulted for further details.

4.6 Design example

Consider the design of the transfer girder shown in Figure 4.7. It is continuous at one end and supports a uniformly distributed load as well as a major point load. The specified concrete strength is 35 MPa and the specified steel yield strength is 400 MPa.

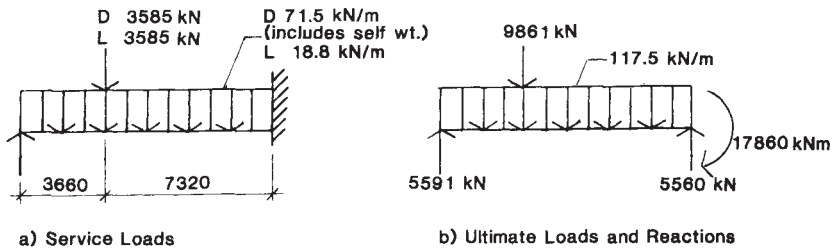

Figure 4.7 Loads and spans for design example

Use dead and live load factors of 1.25 and 1.5 respectively. Use an effective concrete strength equal to 75% of the specified strength times a concrete performance factor of 0.6. This produces a final effective permissible concrete stress equal to 45% of the specified compression strength. Limit strut angles to between 25 and 65° from the horizontal. Select the overall size of the beam to give an ultimate shear between 0.5 and 0.67 times the square root of the specified concrete strength.

Normally, one would consider a series of loading cases and a series of support settlement cases. For simplicity, only one load case will be considered.

For this design, the uniformly distributed load will be idealised as a series of concentrated loads spaced at 600 mm centres along the length of the beam. Similarly, the initial design will consider stirrups at a hypothetical spacing of 600 mm coinciding with the concentrated loads. When the area of stirrups required per 600 mm segment has been calculated, it will be provided by stirrups appropriately spaced throughout the segment.

After two or three iterations, the truss shown in Figure 4.8 was developed. Through the iterations, the slopes and widths of the struts, and the size and location of nodal zones were adjusted to ensure that equilibrium is maintained without overstressing the concrete.

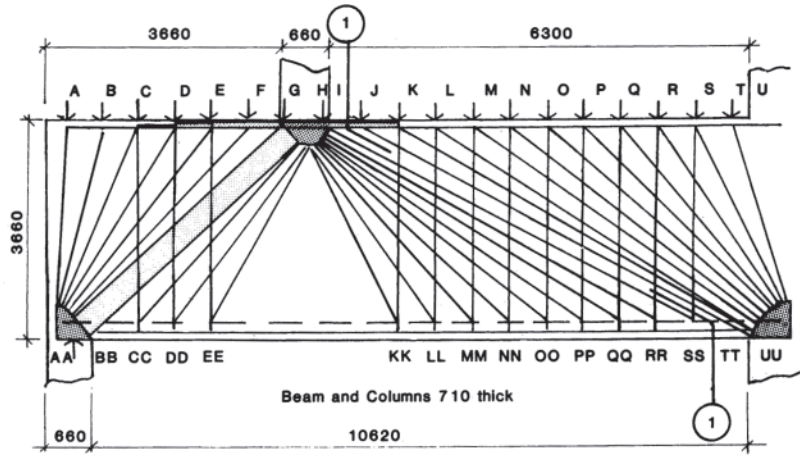

Figure 4.8 Truss selected in design example

There is no unique 'correct' final design. Any one of several trusses will prove satisfactory provided that the detailing of the structure allows the truss to carry the loads in the manner assumed. For example, the left shear span designs could have varied from having all of the shear carried by concrete strut, through to having all of the shear carried by stirrups. The stirrup reinforcement for the left shear span was selected on the basis of having 30–35% of the shear carried by stirrups. This reduces the size of the direct compression strut and improves ductility. The stirrups in the right shear span were selected so that all of the shear across section 1–1 is carried by stirrups. Stirrups loaded by struts steeper than 65° were ignored as these stirrups are not likely to reach yield before beam failure.

Longitudinal flexural reinforcement requirements at mid span and at the right support were determined from the moments at these locations assuming that the steel yields at both locations. Figure 4.9 illustrates the calculation of force in the top chord. At support U, the bar force is 6565 kN. At joint T, the vertical applied load is equilibrated by a steep inclined strut T-UV (Figure 4.8) Horizontal equilibrium at the joint shows that the top chord force drops to

6539 kN. At joint S, the inclined strut equilibrates the vertical force applied at S plus the force in stirrup S-SV which is assumed to have yielded. Joint equilibrium shows that the top chord force drops to 6209 kN and so on.

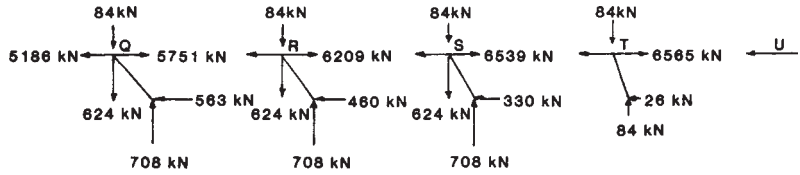

Figure 4.9 Forces on upper chord joints Q, R, S, T and U

The stepped envelope shown in Figure 4.10a shows the top chord force calculated in this way. The capacity of the steel provided is shown in the outer sloped envelope. The sloping portions of this outer envelope were drawn assuming that the force in the bar varies linearly from zero to yield over the development length. The steel chosen is shown in Figure 4.10b. Figure 4.10c is similar for the bottom chord.

The bottom chord is in tension from support to support. At the left support, the bottom chord still has significant tension forces which must be properly anchored.

The detailing and distribution of the bars must be such that the resultants of all the compression forces coincide with the tension force and loads or reactions at points such as AA.

4.7 Summary

This chapter has presented an overview of the design of continuous deep beams. The writer's personal bias as a practising engineer is towards the use of equilibrium truss models which have been shown to give good agreement with tests for beams, particularly for beams with heavy stirrups.

For the design of deep beams, it is recommended that the equilibrium truss model be use. There are three key elements to producing a successful design:

i) Proportion and detail the reinforcement in accordance with an equilibrium truss model. The consequent and consistent detailing of the reinforcement is essential.
ii) Consider the effects of support settlements (and the experimentally observed shift of moment from support to midspan regions) and included them in the resulting design envelopes for shear and moment.
iii) Use enough web reinforcement to ensure ductile behaviour. In shear spans where a major strut exists, the stirrups crossing the diagonal of the span should have a shear capacity not less than 30% of the applied shear force.

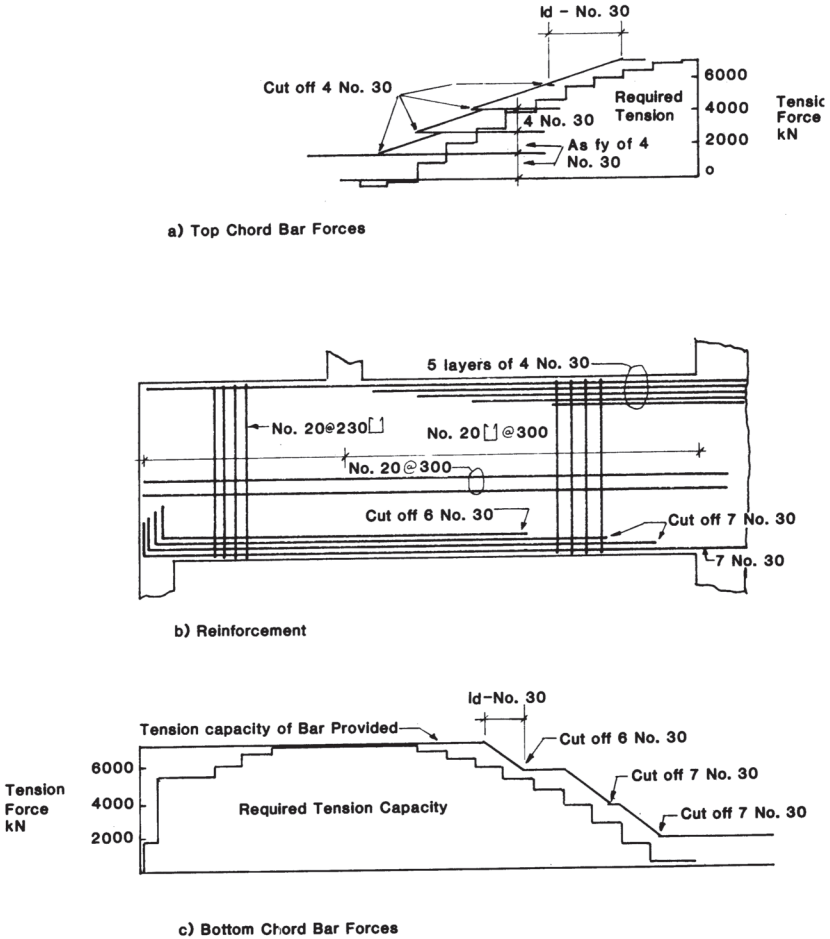

Figure 4.10 Forces in top and bottom chords and reinforcement selected in design example

References

American Concrete Institute. (1986) *Building Code Requirements for Reinforced Concrete.* (ACI 318–86), Committee 318, American Concrete Institute, Detroit (Michigan).

Canadian Standards Association. (1984) *Design of Concrete Structures for Buildings,* CAN3-A23.3-M84, Committee A23.3, Canadian Standards Association, Rexdale.

Comité Euro-International du Béton/Fédération Internationale de la Précontrainte. (1978) *Model Code for Concrete Structures,* CEB-FIP, Paris.

Construction Industry Research and Information Association. (1977) *The Design of Deep Beams in Reinforced Concrete.* Guide 2, CIRIA, London.

Cook, W.D. and Mitchell, D. (1988) Studies of disturbed regions near discontinuities in reinforced concrete members. *Am. Conc. Inst. Struct.* **85,** No.2: 206.

Grob, J. and Thurlimann, B. (1976) Ultimate strength and design of reinforced concrete beams under bending and shear. *Memo. Internat. Assoc. Bridge and Struct. Engng.,* Zurich, **36,** 11: 105.

Kong, F.K., Robins, P.J., and Sharp, G.R. (1975) Design of reinforced concrete deep beams in current practice. *Struct. Engr.* **53,** No.4.
Leonhardt, F. and Walther, R. (1966) Wandartige Trager. *Deutscher Ausschuss für Stahlbeton,* **178,** Wilhelm Ernst und Sohn, Berlin, West Germany.
Marti, P. (1985a) Basic tools of reinforced concrete beam design. *J. Amer. Concr. Inst.* 82, No. 1: 46. Discussion. **82,** No. 6: 933.
Marti, P. (1985b) Truss models in detailing. *Concr. Internat.: Design and Construction 7, No. 12: 66. Discussion.* ***8,*** *No. 10: 66.*
Neilsen, M.P., Braestrup, M.W., Jensen, B.C. and Bach, F. (1978) *Concrete plasticity, beam shear — shear in joints—punching shear.* Special publication, Danish Society for Structural Science and Engineering, Technical University of Denmark, Lyngby.
Nylander, H. and Holst, H. (1946) *Some investigations relating to reinforced concrete beams,* Transactions-Royal Technical University Stockholm No.2, (Unpublished translation made by Ove Arup & Partners Library, London).
Portland Cement Association (1980) *Design of Deep Girders,* Publication ISO79.01D, PCA, Skokie, Illinois.
Rogowsky, D.M., MacGregor, J.G. and Ong, S.Y. (1986) Tests of reinforced concrete deep beams, *Am. Conc. Inst.* **83,** No. 4: 614.
Rogowsky, D.M. and MacGregor, J.G. (1986) The design of reinforced concrete deep beams, *Concr. Internat.: Design & Construction* **8,** No. 8: 49.
Schlaich, J., Schaefer, K. and Jennewein, M., (1987) Toward a consistent design of structural concrete. *J. Prestressed Concr. Inst.* **32,** No. 3: 74.

5 Flanged deep beams

H.SOLANKI and A.GOGATE, Smally Wellford and Nalven Inc., and Gogate Engineers, USA

Notation

a	shear span
A_s	area of tension reinforcement
A_v	area of shear reinforcement within a spacing s_v
A_{vh}	area of horizontal shear reinforcement within a spacing s_h
b	width of beam
b_w	width of beam web
c	clear shear span
d	effective depth
f_{cu}	concrete characteristic cube strength
f_y	reinforcement yield strength or characteristic strength
f'_c	concrete cylinder compressive strength
h	height of beam
h_f	thickness of flange
l	span length
l_n	clear span length, measured face to face of supports
M_u	factored moment
s_h	spacing of horizontal shear reinforcement
s_v	spacing of vertical shear reinforcement
V_c	nominal shear strength provided by concrete; vertical shear force
V_s	nominal shear strength provided by shear reinforcement
V_u	factored shear force
z	lever-arm distance
ρ_w	steel ratio; web steel ratio
ϕ	strength reduction factor

5.1 Introduction

A beam having a span to depth ratio less than about 5 may be classified as a deep beam. Deep beams occur as transfer girders at the lower levels in tall buildings, offshore gravity type structures, foundations and so on (Figures 5.1 and 5.2). The main design recommendations for deep beams have been summarised in Chapter 1. This chapter covers the behaviour of reinforced concrete flanged deep beams. Flanged beams are usually deep and consist of a thin web (Figure 5.3). The application of flanged deep beams normally may not be apparent in ordinary reinforced concrete structures but they are for instance a major structural component in the foundation of offshore gravity type structures and in the horizontal and vertical diaphragms used to transmit wind forces in tall buildings. Little published information is available on the behaviour of reinforced concrete flanged deep beams.

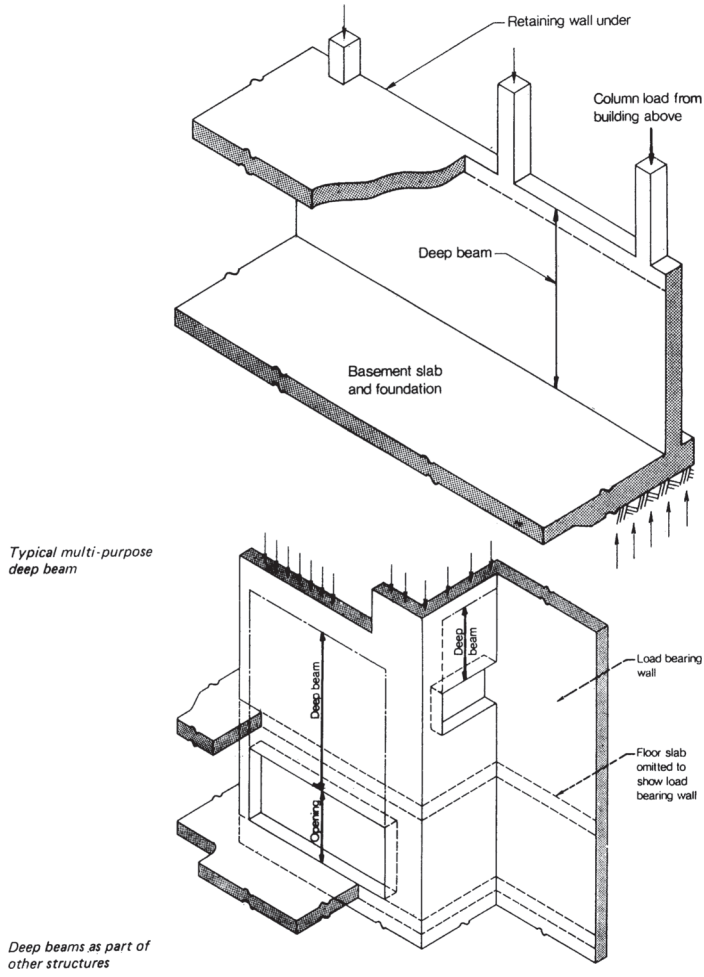

Figure 5.1 Tall buildings after CIRIA Guide 2, 1977

5.2 Review of current knowledge

Considerable literature is available on the elastic behaviour of ordinary (not flanged) deep beams (Albritton, 1965: Cement and Concrete Association (C & CA), 1969). Dischinger (1932) used trignonometric series to determine the stresses in continuous deep girders. Uhlmann (1952) and Chow *et al.* (1953) used finite-difference equations to solve simple-span deep beams. Cheng and Pei (1954) contributed much to the theory of deep beams by solving the case in which no displacement was permitted at the supports. Kaar (1957) reported on tests made on models of simply supported deep beams. Förster and Stegbauer (1974) and Robins and Kong (1973) have applied the finite element

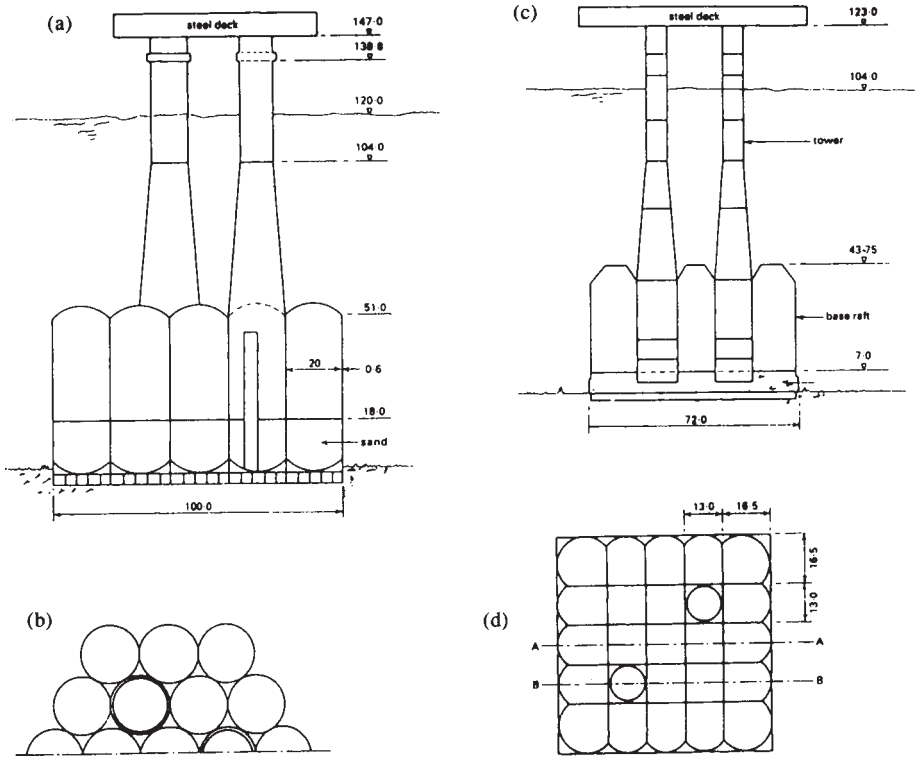

Figure 5.2 Offshore structures after Subedi, 1983: (a) circular form of base raft-Condeep type; (b) section; (c) square form of base raft-TP1 type; (d) section.

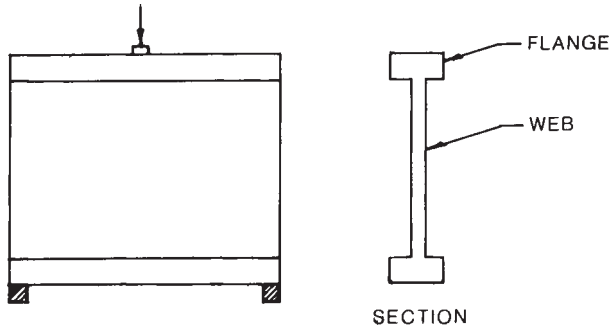

Figure 5.3 Flanged deep beam.

method to produce solutions for deep beam problems. Leonhardt and Walther (1966) undertook extensive investigation of deep beams under all loading and support conditions and presented comprehensive findings for directly and indirectly loaded beams. Gogate (1977) developed a finite element approach for deep beams with progressive cracking.

Around 1965 an extensive long-term programme was initiated in the UK which is still continuing at the University of Newcastle upon Tyne under Kong and his coworkers. Their published work does not include investigations of different loading conditions of deep beams. El-Behairy (1968) included these types of loading condition in the study.

Before discussing flanged deep beams, it is necessary to consider the research work of Robinson and Demorieux (1976). They examined 15 beams having a double T-section. They analysed the cracking of the web and observed that the stresses of the concrete theoretical stressed directions of the cracked web can be estimated by reference to a stress-strain diagram observed in simple compression. They also introduced the concrete strain softening concept.

Nylander (1967) undertook an extensive investigation of deep beams under various loadings and support conditions. He also studied 28 flanged deep beams. He observed that the variation in the amount of transverse reinforcement designed to prevent bursting did not produce any significant effect on the strength of the beam. He also observed that provision of heavy flexural reinforcement at the inner edge of flange increased the strength substantially.

Taner *et al.* (1977) studied six beam-panels with variable tensile reinforcement, simply-supported and subjected to mid-span or third point loading. They found that the formulas based on cylinder splitting analogy underestimate the ultimate capacity for over-reinforced and/or asymmetrically loaded beam-panels.

Paul (1978) studied 18 wall-panels with variable tensile and web reinforcement and different loading patterns. He concluded that the panels loaded below the compression zone (i.e. indirectly loaded,) are weaker than the panels which were directly loaded at the compression face under similar conditions. He also concluded that adequate suspension or hanger reinforcement at the location of the load and good anchoring in the compression zone increased the load-carrying capacity of indirectly loaded beams.

Regan and Hamadi (1981) studied six beams using a simple point load from the top. They concluded that web strength is limited by crushing of the concrete in the diagonal strut that joins the loading point and the reaction point. The web strength does not appear to be influenced by instability for height/thickness ratios up to 50.

Subedi (1983) studied two micro-concrete models. He concluded that the diagonal splitting force depends upon the limiting tensile strength of concrete in a biaxial-compression-tension state of stress. He also concluded that the dowel resistance of main reinforcement is significant in the resistance of the applied load.

5.3 Modes of failure

The structural behaviour of flanged deep beams could be analysed with those of the conventional deep or panel beams of rectangular cross-sections. The methods of design for conventional deep beams are available in several documents. The main differences between a conventional deep beam and a flanged deep beam can be categorised as follows:

i) *Overall depth/web thickness ratio h/t*
Conventional deep beams are designed to have an *h/t* of about 10 or less. This ratio for flanged deep beams is generally much larger and

Table 5.1 Beam geometry

Investigation	Beam number	Overall Depth h (mm)	Web thickness t_w (mm)	h/t_w	$t_c = t_t$	h_w (mm)
Subedi (1983)	1	500	16	31	20	460
	2	500	16	31	20	460
CIRIA beams (1981)	1	2000	75	27	150	1700
	2	2000	75	27	150	1700
	3	1200	20	60	70	1060
	4	1200	20	60	70	1060
	6	1200	20	60	70	1060
Paul (1978)	211					
	212					
	213					
	221					
	222					
	223					
	231	1120	38	30	70	980
	232					
	233					
	311					
	312					
	313					
	321					
	322					
	323					
	331					
	332					
	333					
Taner *et al.* (1977)	p111					
	p121					
	p211	1120	38	30	70	980
	p221					
	p311					
	p321					

may be as high as 60, so flanged beams are considerably more slender than conventional deep beams. Table 5.1 lists the *h/t* ratio of the beams used by the different investigators.

ii) *Accommodation of main tensile reinforcement*
In conventional deep beams, the main reinforcement is accommodated within the plane of the web. Flanged deep beams have wider flanges to accommodate them.

The usual mode of failure of slender reinforced concrete flanged beams involves the diagonal splitting of the web between the edge of the loading plate and the support. A segment of the web between the load and the support is subjected to a stress field equivalent to pure shear, as shown in Figure 5.4. This produces diagonal tension and compression in the web. When the principal tensile stress due to shear reaches the limiting tensile strength of the concrete, rupture occurs in the web. The limiting tensile strength of concrete could be defined as the maximum tensile in a biaxial compression-tension field. The total splitting force in the web consists of a contribution from the web concrete and the web reinforcement at compatible strain. Four parameters affect the modes of failure of flanged deep beams: the strength of concrete f'_c the amount of tensile and compressive reinforcement, the amount of web reinforcements, and the geometry of beam. Based on the relative values and amounts of various parameters, the modes of failure could be classified into four types.

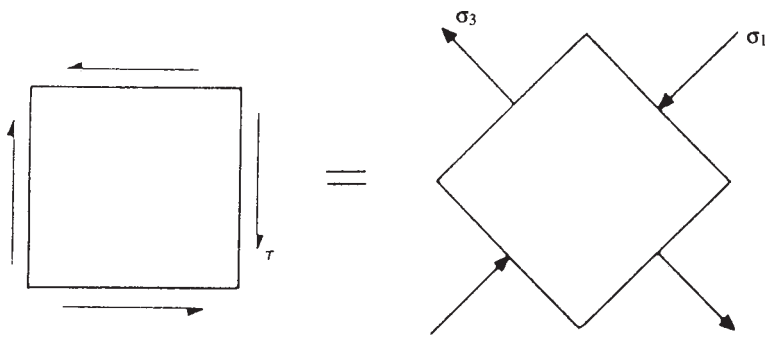

Figure 5.4 Biaxial state of stress due to a pure shear

5.3.1 *Mode of failure 1: flexural-shear failure*

The first mode, flexural-shear failure, occurs in a beam with a very small amount of main tensile reinforcement. At first, flexural cracks develop on the bottom flange at or near the midspan of the beam. (Figure 5.5a) As load is increased, more flexural cracks follow accompanied by diagonal web cracking. Finally failure occurs due to the diagonal cracks in the web and the flexural cracks in the bottom flange near the support. The main

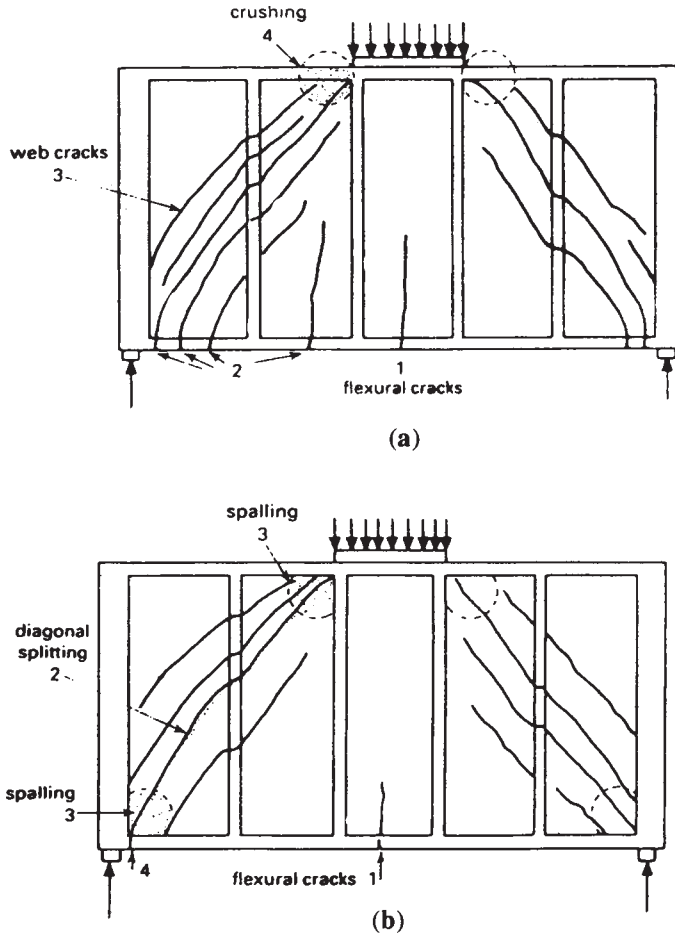

Figure 5.5 Modes of failure (numbers indicate order of events) (a) flexural shear mode 1; (b) diagonal splitting mode 3 (after Subedi (1983))

reinforcement (tension steel) will yield and large cracks will develop along the web diagonal. If the load is further increased, the excessive strain in the main reinforcement and the large deflections will cause the crushing of the concrete near the top compressive flange. This type of failure occurs when: the horizontal component of the diagonal tension force that causes the web crack is: i) greater than the capacity of the reinforcement in the web traversing the diagonal crack, ii) greater than the compression capacity of the web between diagonal cracks that force diagonal compression strut; iii) greater than the capacity of the flexural reinforcement.

5.3.2 *Mode of failure 2: flexural-shear-compression failure*

The second mode, flexural-shear-compression failure is similar to mode 1 failure except that crushing of the compression flange will occur before the full tensile capacity is realised. This will happen when the compression capacity is less than the tension capacity (i.e. the beam is over-reinforced flexually). This type of failure occurs when: i) the horizontal component of the diagonal splitting force is (a) greater than the capacity of the tensile reinforcement (b) greater than the compression capacity; ii) the capacity of tensile reinforcement is greater than the compression capacity.

5.3.3 *Mode of failure 3: diagonal splitting failure*

Diagonal splitting failure, the third mode of failure, occurs by diagonal splitting and excessive cracks in web in beams with thin webs and a moderate amount of reinforcement in the top and bottom flanges.

When these beams are loaded cracking may develop on the bottom flange at or near the mid span of the beam. These flexure cracks do not substantially grow during the subsequent increment of loading. Additional increments will increase the shear in the web until the limiting tensile strength is reached. When this happens, the diagonal splitting will occur.

The splitting is generally located at mid-depth of the beam as shown in Figure 5.5b. Additional increments of load result in more cracks of this type. Failure occurs when the first crack at the centre of the web grows sufficiently large. The beam may be termed ‘unserviceable’ in this state. At the last stages of web splitting, concrete in the web near the load or the support may spall and crush if further load is applied. The crack will penetrate into either the tension flange near the support or the compression flange near the edge of load and lead to the crushing of the compression zone.

This type of failure mode will occur when: the horizontal component of the diagonal splitting force is; i) less than the capacity of the tensile reinforcement; ii) less than the compression capacity. If the compression capacity is greater than the capacity of tensile reinforcement, the diagonal crack may penetrate into the tensile flange.

5.3.4 *Mode of failure 4: splitting with compression failure*

The fourth mode of failure splitting with compression is similar to mode 3 except that the diagonal crack may eventually penetrate into the compression flange. In other words, crushing of the compression flange will occur.

This type of failure will occur when: i) the horizontal component of diagonal splitting force is; a) less than the capacity of tensile reinforcement, b) less than the compression capacity; ii) the capacity of tensile reinforcement is greater than the compression capacity.

The modes of failure are also summarised in Table 5.2. In the Table it is assumed that the amount of horizontal web reinforcement is small and that:

$f_{tc}\ t_w\ h_w > A_h\ f_{sy}$. It is possible that the amount of web reinforcement could be high and that $A_h\ f_{sy} > f_{tc}\ t_w\ h_w$. In such a case, the horizontal component of diagonal splitting force would be $A_h f_{sy}$.

Table 5.2 Modes of failure (after Subedi; 1983)

Mode of failure	Criteria*	Contribution of main reinforcement
1. Flexural–shear	$f_{tc}\ t_w\ h_w + A_h f_s > A_{st} f_y$ $< A_{sc} f_y + (A_c - A_{sc}) f'_c$	$A_{st} f_y$
2. Flexural–shear–compression	$f_{tc}\ t_w\ h_w + A_h f_s > A_{st} f_y$ $> A_{sc} f_y + (A_c + A_{sc}) f'_c$ and $A_{st} f_y > A_{sc} f_y + (A_c - A_{sc}) f'_c$	$A_{sc} f_y + (A_c - A_{sc}) f'_c$
3. Diagonal splitting	$f_{tc}\ t_w\ h_w + A_h f_s < A_{st} f_y$ $< A_{sc} f_y + (A_c - A_{sc}) f'_c$ and $A_{st} f_y < A_{sc} f_y + (A_c - A_{sc}) f'_c$	$f_{tc}\ t_w\ h_w + A_h f_s$
4. Diagonal splitting with compression	$f_{tc}\ t_w\ h_w + A_h f_s < A_{st} f_y$ $< A_{sc} f_y + (A_c - A_{sc}) f'_c$ and $A_{st} f_y > A_{sc} f_y + (A_c - A_{sc}) f'_c$	$f_{tc}\ t_w\ h_w + A_h f_s$

* When $f_{tc}\ t_w\ h_w < A_h f_{sy}$, then $f_{tc}\ t_w\ h_w + A_h f_s$ should be replaced by $A_h f_{sy}$.

5.4 Analysis

As mentioned earlier the conventional deep beams method can be conservatively used for the design and detailing of flanged deep beams. A number of commonly used methods are available for the designing of reinforced concrete deep beams. Most of the methods are developed for directly loaded deep beams, but these also can be applied to indirectly loaded deep beams provided properly designed suspension or hanger reinforcements are provided and well anchored in the top compression zone. Paul (1978) showed that indirectly loaded deep beams with hanger reinforcement attained strength equivalent to those of directly loaded beams if well anchored hanger reinforcement was provided. The commonly used procedures for deep beam analysis are:
i) ACI Building Code; ii) CEB-FIP Model Code (See Chapter 1, Section 1.5 for an account); iii) CIRIA Guide 2; iv) the method proposed by Taner *et al.;* v) the method proposed by Regan and Hamadi; vi) the method proposed by Subedi.

5.4.1 *ACI Building Code*

Section 11.8 of the 1983 ACI Building Code stipulates special provision for deep beams with l_n/d less than 5 and loaded at top or compression face. The critical section for calculating the factored shear force V_u is taken at distance $0.15\ l_n$ for uniformly loaded beams and $0.50l_n$ for a beam with a concentrated load but no more than d from the face of the support.

The factored shear force V_u has to satisfy the following conditions:

$$V_u \le \phi(8\sqrt{f'_c}b_w\, d) \qquad \text{for} \quad l_n/d < 2.0 \tag{5.1a}$$

or

$$V_u \le \phi\left[\frac{2}{3}\left(10 + \frac{l_n}{d}\right)\sqrt{f'_c}\, b_w\, d\right] \qquad \text{for} \qquad 2 \le l_n/d \le 5 \tag{5.1b}$$

Gogate *et. at.* (1980) have shown that this equation is irrational but on the conservative side. The nominal shear strength V_u of the plain concrete can be taken as:

$$V_c = \left(3.5 - 2.5\,\frac{M_u}{V_u\, d}\right)\left(1.9\,\sqrt{f'_c} + 2500\,\rho_w\,\frac{V_u\, d}{M_u}\right)b_w\, d \le 6\sqrt{f'_c}\, b_w\, d \tag{5.2a}$$

where $\qquad 1.0<3.5\text{-}2.5(M_u/V_u d) \le 2.5$

Eqn (5.2a) takes into account the effect of the tensile reinforcement and $M_u/V_u d$ at a critical section. Otherwise V_c can be determined from the simple equation:

$$V_c = 2\sqrt{f'_c}\, b_w\, d \tag{5.2b}$$

Eqn (5.2a) is illustrated in Figure 5.6. When the factored shear V_u exceeds ϕV_c, shear reinforcement is required such that:

$$V_u \le \phi\,(V_c + V_s) \tag{5.3}$$

where V_s is the force resisted by the shear reinforcement:

$$V_s = \left(\frac{A_v}{S_v}\,\frac{1 + l_n/d}{12} + \frac{A_{vh}}{S_h}\,\frac{11 - l_n/d}{12}\right) f_y d \tag{5.4}$$

where A_v is the area of shear reinforcement perpendicular to flexural tension reinforcement, spaced at S_v and A_{vh} is the area of shear reinforcement parallel to flexural reinforcement spaced at S_h.

Maximum $S_v \le d/5$ or 18 in
Maximum $S_h \le d/3$ or 18 in } which ever is smaller (5.5a)

Minimum $A_v = 0.0015\ bS_v$
Minimum $A_{vh} = 0.0025\ bS_h$ (5.5b)

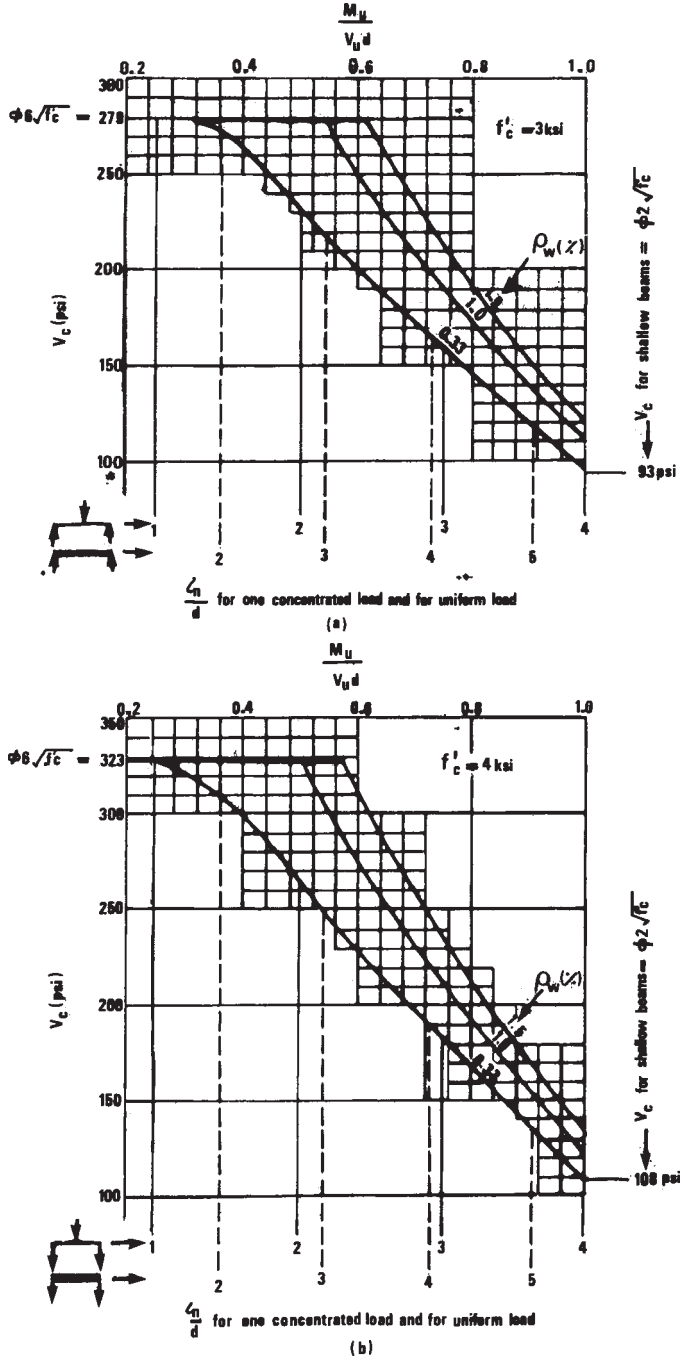

Figure 5.6 Concrete shear capacity in deep beams as a function of the span-to-depth ratio (ACI Code Eqn 11–30).

The shear reinforcement required at the critical section must be provided throughout the deep beams. Extensive shear revision to the ACI provisions are under way at the present time (1989) based on the diagonal compression field theory and the use of truss models based on the work of Vecchio *et al.* (1986).

5.4.2 *CIRIA Guide 2*

The CIRIA Guide (CIRIA, 1977) applies to deep beams with an effective span/depth ratio of less than 2 for single span beams and less than 2.5 for multi-span beams. The following equation is suggested in the guide for the evaluation of the ultimate load capacity of a deep beam loaded from the top.

$$V_u = C_1\left(1 - 0.35\frac{x}{h}\right) f_u bh + C_2 \sum A_s \frac{y}{h} \sin^2 \alpha \qquad (5.6)$$

where f_u is the cylinder-splitting tensile strength of concrete or $f_u = 0.5\sqrt{f_{cu}}$; A_s is the area of a typical web bar; C_1 is a coefficient equal to 1.4 for normal-

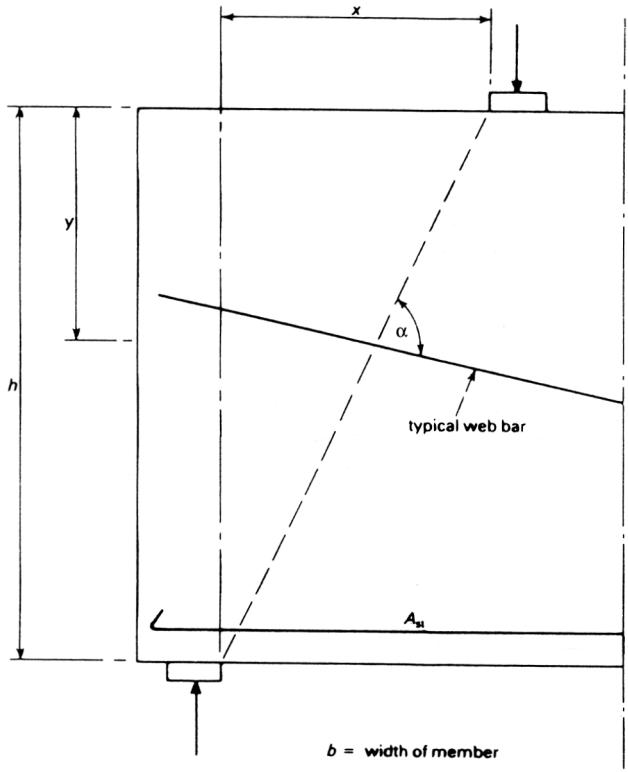

Figure 5.7 CIRIA Guide 2 deep beams—symbols

weight concrete; C_2 is a coefficient equal to 130N/mm² for plain round bars and 300N/mm² for deformed bars and *b, h, y, x* and a are as shown in Figure 5.7. Eqn (5.6) was based on the large number of tests carried out at Nottingham and Cambridge Universities under the leadership of Professor Kong, on simple span deep beams with low *a/d* ratios and with various web reinforcement configurations.

The first term on the right hand side of the equation is the load carrying capacity of the concrete compression strut on the variables. The compression diagonal is a component of the truss model intended to explain the beam resisting system. It is assumed that the concrete strut fails in splitting mode when this capacity is reached.

The second term on the right hand side is the contribution of steel reinforcement. The contribution varies as *y,* the depth of individual web bar, measured from top of the beam.

5.4.3 *Method of Taner et al.*

Based on the diagonal splitting strength of concrete Taner *et al.* have suggested that the ultimate capacity of beam panels can be obtained from the following equation

$$V_u = f_{tc}\, ab + \sum f_s\, A_s \cos\theta \qquad (5.7a)$$

where f_{tc} is the limiting tensile strength at which diagonal splitting will occur; As is the area of individual web bar located along the diagonal (main

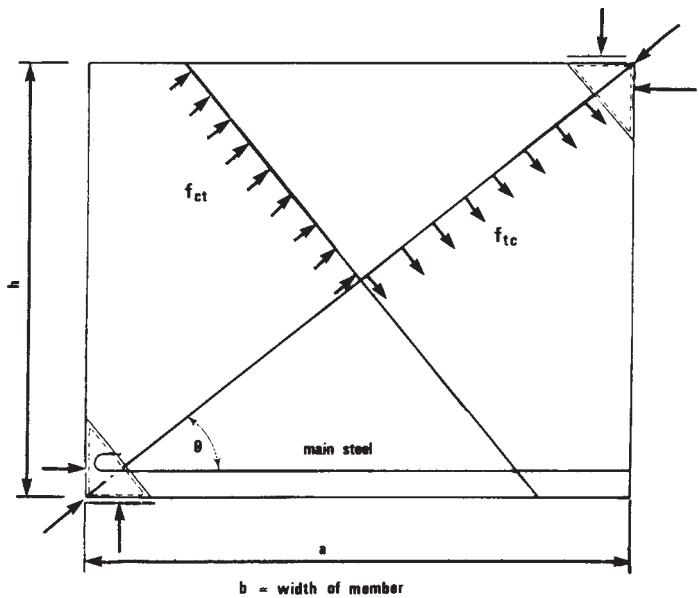

Figure 5.8 Taner *et al.* panel beam—symbols

flexural tensile steel included); f_s is the stress in steel which should be established in such a way that the width of the splitting crack will be limited (proposed strain 0.002); and θ is the angle between the web bar and the principal tension direction (Figure 5.8).

In this method the incidence of diagonal splitting cracks does not lead to the assumed failure of flexural member provided that there is sufficient web reinforcement to take over the splitting force. It also assumes that the biaxialcompression-tension field of stress exists in the web and therefore biaxial stress depends on the geometry of the support segment.

If the web reinforcement can take over the splitting force, then at the load corresponding to the yielding of the reinforcement V_u is given by:

$$V_u = \sum A_s\, 0.9 f_y \cos\theta \tag{5.7b}$$

The contribution of the concrete to the ultimate strength is considered negligible or unreliable at this stage of the loading.

5.4.4 *Method of Regan and Hamadi*

Regan and Hamadi have suggested that the ultimate capacity of deep webs surrounded by frames (flanges and stiffening ribs) can be obtained from:

$$V_u = \rho_w f_{yw}\, b_w\, z\cot\theta + \left(1 - \frac{\rho_w f_{yw}}{0.4 f_{cu} \sin^2\theta}\right) f_{cu}\, b_w\, l^* \sin^2\theta \tag{5.8}$$

where ρ_w is the ratio of web reinforcement, assumed equal in vertical and horizontal directions, f_{yw} is the yield stress of web reinforcement, b_w is the web breadth of beam, f_{cu} is the cube compressive strength of concrete and a, l_b, l^*, h_f, h_r, z and θ are shown in Figure 5.9

In this method two simple models of inclined web compression actions are considered. The first terms relates to actions associated with web reinforcement action similar to the CEB-FIP Code. The second term relates to the single strut which can be formed in the absence of web steel joining the reaction point to the compression zone and forming an angle θ with the beam axis.

5.4.5 *Method of Subedi for flanged beams with web stiffeners*

The method of Subedi is based on force equilibrium conditions with the observed behaviour from the model tests. The ultimate capacity of the beam can be obtained (Figure 5.10)

$$= \frac{1}{a}\left(f_{tc}\, t_{tw}\, A_1 + P_{st}\, A_2 + A_v f_s c + A_h f_s A_3 + 2F_d c\right) \tag{5.9}$$

where $A_1 = h_w t_c + c^2 + h_w^2$, $A_2 = 2h_w + t_t + t_c$, $A_3 = h_w + t_c$ and $P_{st} = A_{st} f$

In this method the ultimate strength of flanged beam is a sum of the contribution from: the web concrete f_{tc}, the main reinforcement, the orthogonal reinforcement in the web, A_h and A_v and the dowel force in the reinforcement

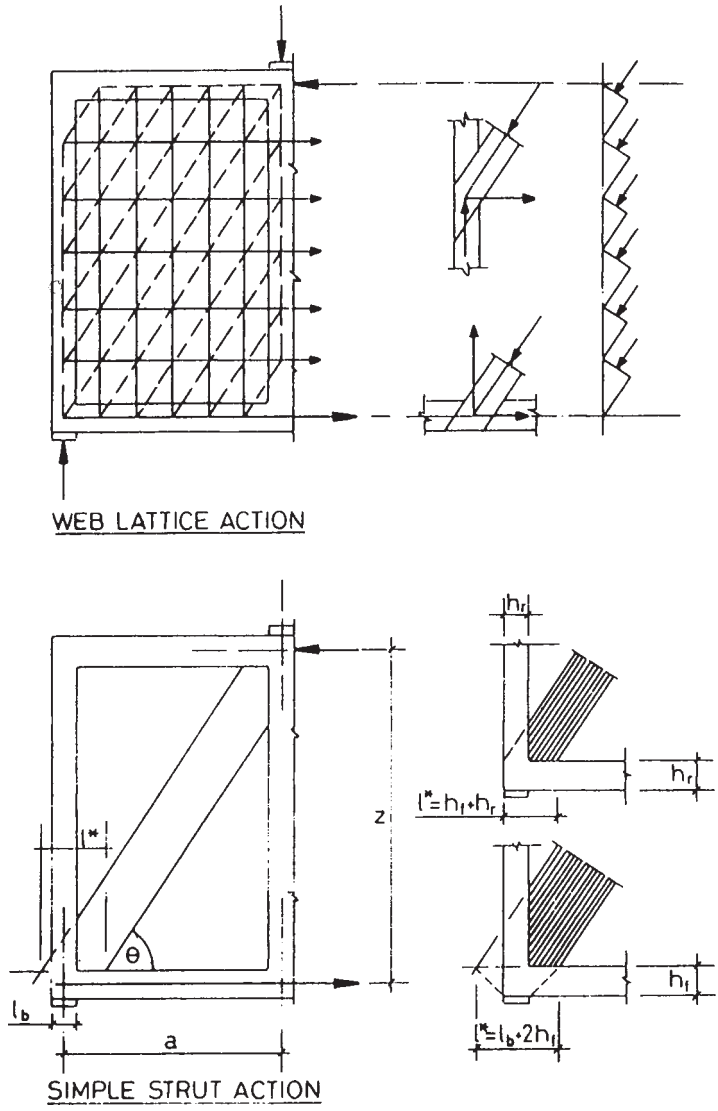

Figure 5.9 Regan and Hamadi frame-symbols

F_d. The contribution of the main reinforcement is based on the magnitude of the diagonal splitting force. It is taken as the smallest value obtained from: i) the horizontal component of the diagonal splitting force; ii) the strength of the main reinforcement; iii) the ultimate strength of the compression flange.

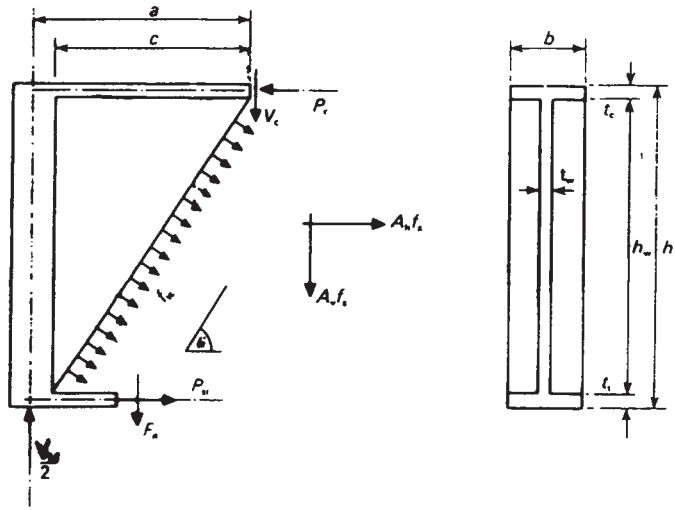

Figure 5.10 Subedi flanged beam-symbols

Taner *et al.* (1977), Regan and Hamadi (1981) and Subedi (1983) have suggested a simplified method for calculating the ultimate load capacity at deep beams based on the flanged section. Taner *et al.* (1977) and Regan and Hamadi (1981) have proposed a simple expression as compared with the Subedi (1983) expression. However the Subedi's expression is more comprehensive and correlates better with test data.

The ACI Code, the CEB-FIP recommendations and the CIRIA Guide 2 do not provide a design guide for flanged deep beams. In the following section a design example is included to provide some information for the design of flanged deep beams. In this example, Section 11.8 of the 1983 ACI Code has been used with cutoff limits on the shear force. The result from this modified ACI procedure is compared with the test result of Taner *et al.* beam-panels.

5.5 Design example 1: Beam-panel P311 (Taner *et al,* 1977)

f'_c=5277psi (36.4 N/mm^2), f_y=78400 psi (541N/mm^2) for Gauge 6 wire mesh=50000psi (345N/mm^2) for No. 10 (32.0mm dia.) bar; l_n=89-2× 10=69 in (1750mm), h=44.0 in (1120mm) and b_w=1.5in (38mm). Self-weight of the beam is neglected.

Solution

Check l_n/d, evaluate factored shear force, V_u, d=h-cover-1/2 dia. of bar =44-0.5-0.625=42.875 in (1089 mm), l_n/d=69/42.875=1.609<5; hence treat as a deep beam.

Factored shear force V_u and resisting capacity V_c

$$V_u \le \phi\,(8\sqrt{f'_c}\,b_w d)$$

$$= 0.85\,(8\sqrt{5277}\,(1.5)\,(42.875)) = 31770\,lb\ (141.3\,\text{kN})$$

$$M_u = Wl_n/4 \quad [\text{Assume } W = V_u]$$

$$= 31\,770 \times 69/4 = 548\,000\ \text{in–lb}\ (61.9\ \text{kNm}).$$

$$M_u/V_u d = 548\,\text{p00}/(31770 \times 42.875) = 0.4023$$

$$3.5 - 2.5\,M_u/V_u d = 3.5 - 2.5 \times 0.4023 = 2.5$$

$$\rho_w = 2 \times 1.27/1.5 \times 42.875 = 0.0395;\ V_u d/M_u = 2.5$$

From Eqn 11.30 (ACI Code)

$$V_c = 2.5\,(1.9\sqrt{f'_c} + 2500\,\rho_w\,(V_u d/M_u))b_w d$$

$$= 2.5\,(1.9\sqrt{5277} + 2500 \times 0.0395 \times 2.5)1.5 \times 42.875$$

$$= 61\,880\ \text{lbs}\ (2653\ \text{kN})$$

$$6\sqrt{f'_c}\,b_w d = 28\,030\ 1b\ (124.7\ \text{kN})$$

Shear force due to shear reinforcement V_s: from Eq 11.31 (ACI Code)

$$V_s = \left[\frac{A_v}{S}\left(\frac{1 + l_n/d}{12}\right) + \frac{A_v h}{S_2}\left(\frac{11 - l_n/d}{12}\right)\right] f_y\, d$$

$$= \left[\frac{0.028}{6}\left(\frac{1 + 1.61}{12}\right) + \frac{0.028}{6}\left(\frac{11 - 1.61}{12}\right)\right] 78\,400 \times 42.875$$

$$= 15690\ \text{l}b\ (69.8\ \text{kN})$$

$s = d/5$ =42.875/5=8.6 in (218 mm)<18 in (457 mm)

$s_2 = d/3$ =42.875/3=14.3 in (363 mm)<18 in (457 mm)

Minimum A_v=0.00 15 bs

=0.0015 (1.5) (8.6)=0.019 in^2 (12.3 mm^2)

Provided A_v=0.04 in^2 (19.3 mm^2)

Minimum A_{vh}=0.0025 bs_2

=0.0025 (1.5) (14.3)=0.054 in^2 (34.6 mm^2)

Provided A_{vh}=0.067 in^2 (43.0 mm^2)

Total shear force: V_u=V_c+V_s=61 880+15 690=77 570 lb (345.0 kN)

Test, V_u=900001b (400.3 kN).

Revise

$$M_u = 7\,570 \times 69/4 = 1\,338\,080 \text{ in-lb}$$

$$M_u/V_u d = 0.4;\ V_u d/M_u = 2.5$$

From Eq 11.30: V_c=6l 880 lb (275.3 kN).
From Eq 11.3 1: V_s=15 690 lb (69.8 kN), V_u=77 570 lb (69.8 kN).
Check flexural reinforcement

$$M_u = 1\,338\,080 \text{ in-lb (151.2 kNm)}$$

$$l/h = 79/44 = 1.795 < 2$$

where l is the effective span measured centre to centre of support or 1.15 clear span l_n whichever is smaller.

$$l = 69 + 10 = 79 \text{ in (2007 mm)} \quad \text{control}$$

$$l = 1.15\,(69) = 79.35 \text{ (2015 mm)}$$

$$j_d = 0.2\,(1 + 2.0h) = 0.2\,(79 + 2.0 \times 44) = 33.4 \text{ in (848 mm)}.$$

$$A_s = M_u/j_d f_y$$

$$= \frac{1\,338\,080}{33.4 \times 50\,000} = 0.80 \text{ in}^2 \ (516 \text{ mm}^2)$$

Use 2.54 in^2 (1639 mm^2) $\therefore$ OK

$$\text{minimum reinforcement} = \frac{200\,bd}{f_y}$$

$$= \frac{200\,(1.5)\,(42.875)}{50\,000}$$

$$= 0.26 \text{ in}^2 \ (166 \text{ mm}^2) \therefore \text{OK}$$

Regan and Hamadi method (beam-panel P311)

$$V_u = \rho_w f_{yw} b_w z \cot\theta + \left(1 - \frac{\rho_w f_{yw}}{0.4 f_{cu} \sin^2\theta}\right) f_{cu} b_w l^* \sin^2\theta$$

$$z = h - \text{cover} - 1/2(\text{dia. of bars})$$

$$= 44 - 0.5 - 0.5 - 0.625 - 0.25 = 42.125 \text{ in.}$$

$$\tan\theta = l/2/h = 44.5/44 = 1.01$$

$$\therefore\ \theta = 45.32°$$

$$l^* = l_b + 2h_f = 10 + 2 \times 3 = 16 \text{ in}$$

$$f'_c = 0.8 f_{cu} = f_{cu} = 5277/0.8 = 6596 \text{ psi}$$

$$\rho_{wh} = \frac{0.028 \times 7}{44 \times 1.5} = 0.00297;\ \rho_{wv} = 0.00315$$

$$\rho_w \text{ (ave)} = 0.00306$$

$$V_u = 0.00306 \times 78\,400 \times 1.5 \times 42.125 \times 0.99 + \left(1 - \frac{0.00306 \times 78\,400}{0.4 \times 6596 \times 0.506}\right) 6596 \times 1.5 \times 16 \times 0.506$$

$$= 80\,710 \text{ lbs } (359.0 \text{ kN})$$

Taner et al. method (beam-panel P311)

Eqn (6b)

$$V = f_{tc}\, ab + f_s \sum A_s \cos\theta$$

From Eqn 5, f_{tc}=367 psi, f_s=26100psi (interpolated from the Authors' result), a=39.5 in (centre of support to centre of load), b=1.5 in, θ=tan^{-1}44/44.5=44.67°, V_u=367×39.5×1.5+26100 (2.95) 0.711
=21755+54 743=76 498 lb (340.3 kN)

Eqn 8

$V_u = f_s \sum A_s \cos\theta$, f_s=38100 (interpolated from the Authors' result),
V_u=38 100×2.95×0.711=79 930 lb (355.5 kN).

Subedi method (beam-panel P311)

$$V_u = \frac{1}{a}(f_{tc}\, t_w\, A_1 + P_{st}\, A_2 + A_v f + A_h f_s\, A_3 + 2 f_d C)$$

=(134.5+155+1.9+2.6+185.2)=479.2 kN (107 700 lbs).

5.6 Design example 2: ACI Code

12 k/ft (dead load)+100 k/ft (live load); f_c=4000 psi, f_y=60 000 psi.
Assume d=0.9/h=0.9 (15)=13.5 ft or 162 in.
l_n/d=25×12/13.5×12=1.85<2.0, hence treat as a deep beam.
beam self weight 15/12×15×0.150=2.8 k/ft
total factored load=1.4(12+2.8)+1.7 (50)=105.72 k/ft.
distance of the critical section=0.15 ln=0.15×25=3.75 ft.

Design of flexural reinforcement

$$M_u = W_u l_n^2/8 = 105.72 \times 25^2/8 = 8259.375 \text{ ft} - \text{k} = 99112.5 \text{ in} - \text{k}$$

$$l/h = 28/15 = 1.87 < 2$$

$$j_d = 0.2\,(1 + 2.0h)$$

$$= 0.2\,(28 + 2.0 \times 15)$$

$$= 11.6 \text{ ft.}$$

$$A_s = M_u/\phi\, j_d f_y = \frac{99112.5}{0.9\,(11.6 \times 12)} \times 60 = 13.18 \text{ in}^2$$

Provide 12# No. 10 bars A=15.24 in^2

$$\text{Min } A_s = \frac{200bd}{f_y} = \frac{200\,(15)(162)}{60000} = 8.1 \text{ in}^2 < 15.24 \text{ in}^2 \therefore \text{OK}$$

Calculate factored shear force—V_u

The factored shear force V_u at the critical section is

V_u=105.72×25/2-105.72×3.75=925.0 kips.

Nominal shear strength V_n and resisting capacity V_c

$$\phi_n = \phi\,(8\sqrt{f'_c})\,b_w d$$
$$= 0.85(8V\sqrt{4000} \times 15 \times (13.5 \times 12))$$
$$= 1045 \text{ kips} > 925.0 \text{ kips} \quad \text{OK}$$
$$M_u = (105.72 \times 25)/2 \times 3.75 - (105.72 \times (3.75)^2)/2$$
$$= 4214.28 \text{ ft} - \text{k} = 50\,547.4 \text{ in} - \text{k}$$
$$M_u/V_u d = 50\,547.4/(925 \times 162) = 0.337$$
$$3.25 - 2.5(M_u/V_u d) = 3.5 - 2.5 \times 0.337 = 2.66 > 2.5 \quad \text{use } 2.5$$
$$\rho_w = 15.24/(15 \times 162) = 0.00627$$
$$V_u d/M_u = 2.97$$
$$V_c = 2.5(1.9\sqrt{f'_c} + 2500\,\rho_w(V_u d/M_u)b_w d$$
$$= 2.5(1.9\sqrt{4000} + 2500 \times 0.00627 \times 2.97)15 \times 162$$
$$= 1\,012\,790 \text{ in–lb}$$
$$6\sqrt{f'_c}\,b_w d = 6\sqrt{4000} \times 15 \times 162 = 922\,120 \text{ lb} < 1\,012\,790 \text{ lb};$$

hence V_c=922120 lb controls

Shear reinforcement

Assume No. 4 bars placed both horizontally and vertically on both faces of the beam.

$A_v=A_{vh}$=2×0.20=0.40 in^2

$\phi V_s=V_u-\phi V_c$

$V_s=(V_u/\phi)-V_c$=(925 000/0.85)-922 120=166 115 lb

$$V_s = \left(\frac{A_v}{s}\,\frac{1+l_n/d}{12} + \frac{A_{vh}}{s_2}\,\frac{11 - l_n/d}{12}\right) f_y\, d$$

Assume that s=18 in in centre to centre and s_2=10.5 in centre to centre, hence

$$V_s = \left[\frac{0.40}{18} - \left(\frac{1+1.85}{12}\right) + \frac{0.40}{10.5}\left(\frac{11 - 1.85}{12}\right)\right] 60\,000 \times 162$$

=333642 lb>116 115 lb ? OK

The maximum permissible spacing of vertical bar: $s=d/5$ or 18.0 in which ever is smaller; s=162/5=32.4 in. Hence 18.0 in controls, use s=18.0 in.

The maximum permissible spacing of horizontal bar: $s_2=d/3$ or 18.0 in whichever is smaller; s_2=162/3=54.0in. Hence 10.5 in controls use s_2=10.5 in.

Check for minimum steel:

Minimum A_v=0.0015 bs=0.0015×15×18=0.40 in^2 ∴ OK

Minimum A_{vh}=0.0025 bs_2=0.0025×15×10.5=0.393 in^2 ∴ OK

Figure 5.11 shows the reinforcement details.

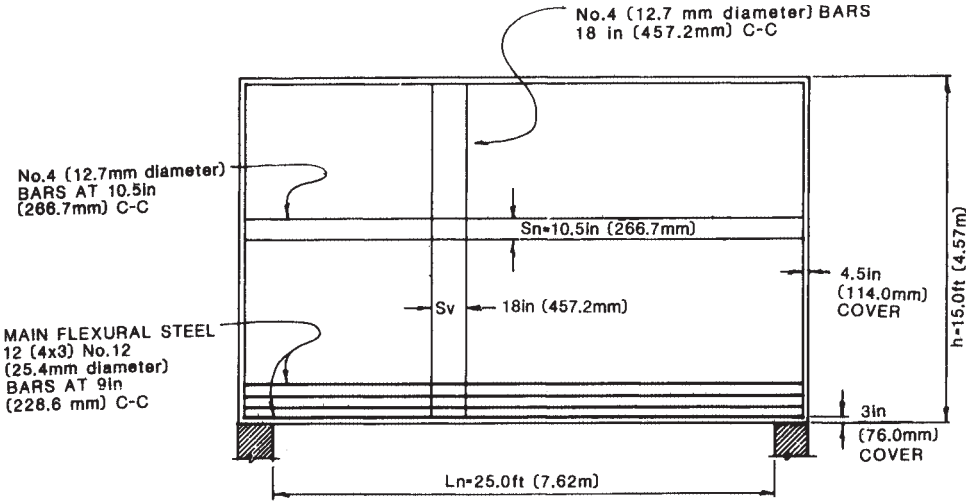

Figure 5.11 Reinforcement for a simply supported deep beam (Example2)

References

Albritton, G.E. (1965) *Review of Literature Pertaining to the Analysis of Deep Beams,* Technical Report 1–701, US Army Engineers Waterways Experiment Station, Vicksburg, Miss.

American Concrete Institute (1983), *Building Code Requirements for Reinforced Concrete* ACI 318–83 (1983), American Concrete Institute, Detroit, MI.

Cement and Concrete Association. (1969), *Bibliography on Deep Beams* Library Bibliography Ch. 71 (3169), Cement and Concrete Association, London.

Cheng, D.H. and Pei, M.L. (1954) Continuous deep beams *Proc. Am. Soc. Civ. Engrs* **80** Separate, No.450, June.

Chow, L., Conway, H.D. and Winter, G. (1953) Stresses in deep beams. *Trans. Am. Soc. Civ. Engrs* **118:** 686.

Comité Euro International du Béton/Fédération Internationale Dela Précontrainte, (1978), *Model Code for Concrete Structures* English Edition, Cement and Concrete Association, London.

Construction Industry Research and Information Association. (1977) *The Design of Deep Beams in Reinforced Concrete,* Guide 2 Ove Arup and Partners and Construction and Industry Research and Information Association, London.

Dischinger, F. (1932) Beitrag zur Theorie der Halbscheibe und des wandartigen Trägers". *Internat. Assoc. of Bridge and Struct. Engng,* **1:** 69.

El-Behairy, S. (1968) Spannungszustand wandartiger Träger mit im Inneren angreifenden Einzelkräften *Beton und Stahlbeton,* No. 10: 228.

Förster, W. and Stegbauer, A. (1974) *Wandartige Träger: Tafeln zur Ermittlung der Bewehrung.* Werner-Verlag, Dusseldorf.

Gogate, A.B. (1977) Finite element analysis of deep reinforced concrete beams with static, short term loading. Ph.D. dissertation Ohio State University.

Gogate, A.B. and Sabnis, G.M. (1980) Design of thick pile caps. *Am. Concr. Inst. J.* **77,** No.1, Jan-Feb.

Kaar, P.H. (1957) Stresses in centrally loaded deep beams *Proc. Soc. Experimental Stress Analysis* **15,** No.1.

Leonhardt, F. and Walther, R. (1966) *Wandartige Träger. Heft* 178, Deutscher Ausschuss für Stahlbeton, Berlin.
Nylander, H. (1967) Höga Balkar I, Inverkan av Klyvnings- förhindrahindrande Armering pa spanningsfördelningen under Koncentrerad last. *Nordisk Belong* No. 1: 53.
Nylander, H. (1967) Höga Balker III, Hällfasthet vid Upplag. *Nordisk Betong* No. 1: 79.
Nylander, J.O. (1967) Höga Balkar IV, Balkar belastade i underkant. *Nordisk Betong* No. 2: 173.
Nylander, H (1967) Höga Balkar V, Sammanfattande Synaspunkter för dimensionering. *Nordisk Betong* No. 2: 195.
Nylander, H., Nylander, J.O. (1967) Höga Balkar II, Moment-og Spänningsfördelning i Kontinuerling hög *balk. Nordisk Betong,* No. 1: 65.
Paul, I.S. (1978) *Behaviour of Indirectly Loaded Reinforced Concrete Thin- Wall Ribbed Panels Eng Thesis,* Department of Civil Engineering Concordia University Montreal.
Regan P.E. and Hamadi, Y.D. (1981) *Behaviour of Concrete Caisson and Tower Members Technical report 4,* Cement and Concrete Association for the Concrete in the Ocean Management Committee, Wexham Springs, Slough.
Robins, P.J. and Kong, F.K. (1973) Modified finite element method applied to reinforced concrete deep beams. *Civ. Engng Publ. Works Rev.* 69: 963.
Robinson, J.R. and Demorieux, J.M. (1976) Essais de poutres en double té en béton armée. *Annales I.T.B.T.P No. 335, Jan.:* 65.
Subedi, N.K. (1983) The behaviour of reinforced concrete flanged beams with stiffeners. *Mag. Concr. Res*. **35,** No. 122, March: 40.
Taner, No., Fazio, P.P. and Zielinski, Z.A. (1977) Strength and Behaviour of Beam-Panels-Tests and Analysis. *Am. Conc. Inst.* **74,** No. 10: 511.
Uhlmann, H.L.B., (1952) The theory of girder walls with special reference to reinforced concrete design. *Struct. Engr.* **30,** No. 8, Aug.: 172.
Vechhio, F and Collins M.P. (1986) The modified compression field theory for reinforced concrete elements subjected to shear *Am. Concr. Inst. J.* **83,** No. 2. March-April.

6 Deep beams under top and bottom loading

A.R.CUSENS, University of Leeds

Notation

A_i	area of reinforcement at distance y_i
A_s	area of main tension reinforcement
A_v	area of vertical shear reinforcement within a distance s
A_{vh}	area of horizontal shear reinforcement within a distance s2
b	width of deep beam
d	effective depth of deep beam (to centre of main tensile steel)
f_{cb}	modulus of rupture of concrete
f'_c	cylinder crushing strength of concrete
f_{cu}	characteristic cube strength of concrete
f_y	characteristic yield strength of reinforcement
h_a	effective height of deep beam
r_v	ratio A_v/bd
s	spacing of vertical shear reinforcement
s_2	spacing of horizontal shear reinforcement
v_u	maximum value of shear stress in concrete
w_b	uniform bottom loading on beam
w_t	uniform top loading on beam
x_e	clear shear span
y_i	distance from top of beam to reinforcing bar
L	effective span
L_1, L_2	combinations of top and botetc tom load
L_o	clear span
M_u	ultimate bending moment
V_{ab}	applied shear force from bottom loads
V_{at}	applied shear force from top loads
V_{cb}	shear capacity of beam assuming bottom loads only
V_{ct}	shear capacity of beam assuming top loads only
V_c	contribution of concrete to shear strength of beam
V_n	nominal shear strength of beam
V_r	contribution of steel to shear strength of beam
V_u	ultimate shear strength of beam
W1, W2 etc	wall types
θ_r	angle between reinforcement and diagonal crack
$\lambda_{1,2}$	constants (Eqn. 6.)
ρ_w	A_s/bd

6.1 Introduction

The nature of deep reinforced concrete beams has various implications in structural situations. In other chapters, attention has been drawn to the modifications needed to general flexural theory in order to predict the

structural behaviour of deep beams. In this chapter consideration is given to one specific implication of the depth of these elements, which is the additional action of vertical direct tensile forces arising from substantial loads applied at the soffit and lower levels of the beam. Research in this field has been limited and it is therefore reviewed within the scope of the chapter. It will be shown on the basis of comparison with laboratory tests that CIRIA design recommendations (1977) are safe and conservative in their recommendations for shear walls with combined top and bottom loadings. ACI procedures for deep beams 1983 are applicable only to top loading and these are also conservative.

6.2 Early tests on deep beams under top and bottom loading

Graf and colleagues (1943) appear to have been the first to test a deep beam under bottom loads. The beam had a height/span ratio of 2.2 and is shown in Figure 6.1. Load was applied through horizontal nibs built into the soffit and initial cracks were observed above the nibs. These cracks were horizontal but as the load was increased additional sloping cracks appeared at higher levels in the beam. Failure occurred due to yielding of the main reinforcement and deterioration of the section immediately above the line of the horizontal nibs.

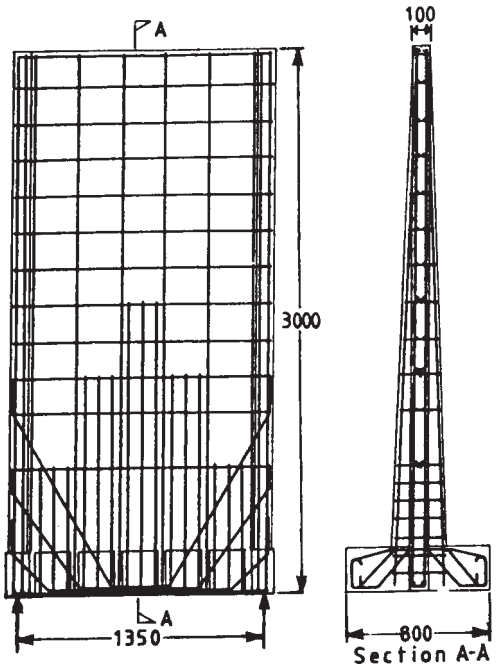

Figure 6.1 Details of specimens tested by Graf.

Schütt (1956) reported tests on a series of reinforced concrete walls under uniformly distributed load on the top or bottom edges. The specimens used for top loadings were as shown in Figure 6.2 and for bottom loading the specimens were identical to those used by Graf (Figure 6.1). All the specimens had vertical side nibs and shear reinforcement was present in only a few of the test specimens. As a result of his tests Schütt proposed some design rules which are summarised under Design approaches (Section 6.7)

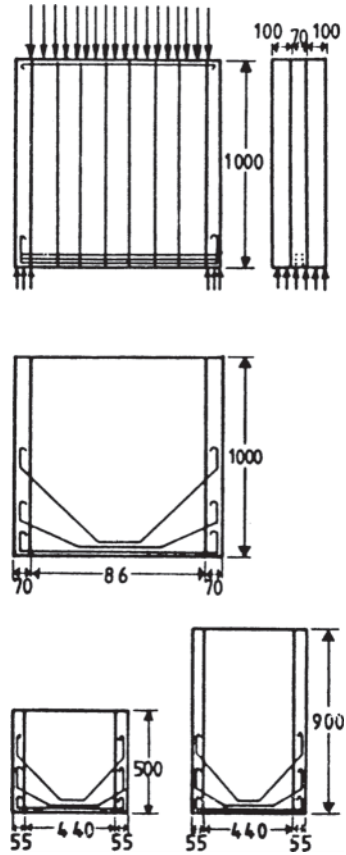

Figure 6.2 Details of specimens tested by Schütt.

Leonhardt and Walther (1966) have also reported tests on deep beams with top or bottom loading. They decided that the best means of providing main reinforcement was by means of well-anchored bars from support to support and that these should be distributed over the lower 20% of the height of the beam. It was suggested that inclined stirrups should be extended to a height equal to the span. Closely spaced (≤ 100 mm) stirrups were recommended to reduce crack widths, with vertical stirrups extending the full height of the beam.

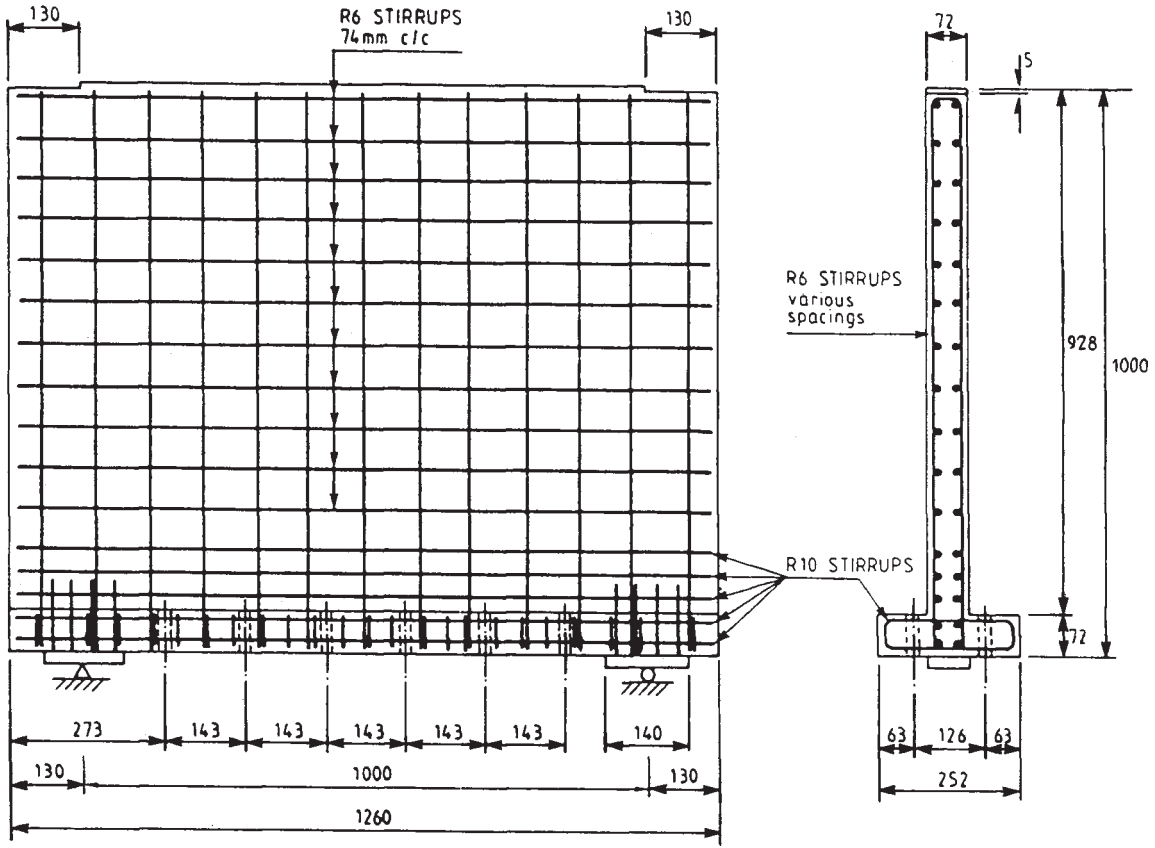

Figure 6.3 Dimesions and reinforcement details of Leeds test wall-beams (dimensions in mm).

6.3 Tests at Leeds University

A recent series of tests carried out by Besser (1983) and Cusens and Besser (1985) examined the effects of different combinations of top and bottom loads on the ultimate load of wall-beams (i.e. deep beams of small thickness). This work is the most comprehensive investigation reported on deep beams under combinations of top and bottom loading and it is used here as the basis of comparison with the principal design approaches.

6.4 Description of test specimens

The test specimens consisted of 17 model wall-beams 72 mm thick, 1000 mm deep and 1260 mm long (1000 mm clear span). At the soffit of each beam a 90×72 mm nib was formed on each side (Figure 6.3). Six vertical holes 25 mm in diameter were formed in each nib. On top of the wall, at each end, a step 5 mm deep and 130 mm long was formed leaving a central section of 1000 mm over which the uniformly distributed load was applied.

The main longitudinal reinforcement consisted of 10 plain bars of 10 mm nominal diameter (f_y=332N/mm^2). This reinforcement was placed in five layers, consisting of five closed stirrups. The web reinforcement was provided by an orthogonal arrangement of 6 mm diameter plain bars (f_y=367 N/mm^2) on both faces of the wall. The rib was reinforced with closed 10 mm diameter stirrups (f_y=332 N/mm^2). Additional diagonal bars were used in the nibs. These consisted of 6 mm diameter deformed bars (f_y=560 N/mm^2). Details of the reinforcement and dimensions are given in Figure 6.3.

All 17 wall-beam specimens tested had equal geometry and main reinforcement but different percentages of vertical reinforcement. A simple code was used to identify each wall. The numbering, W1 to W5, identified the percentage area of vertical reinforcement in the wall corresponding to the values given in Table 6.1.

Table 6.1 Percentage of vertical reinforcement in the walls

Notation	Spacing of vertical reinforcement (mm)	Vertical reinforcement r_v (%)
W1	74	1.06
W2	98	0.80
W3	56	1.40
W4	–	0.0
W5	39	2.0

The other two symbols (L1, L2, L3, L4 and L5) correspond to the loading. Five different combinations of top and bottom loads were used in the tests as follows:

L1 uniformly distributed load on top of the wall-beam
L2 uniformly distributed load applied at the soffit of the wall-beam
L3 combination of top and soffit loads in a ratio 1:1
L4 combination of top and soffit loads in a ratio 2:1
L5 combination of top and soffit loads in a ratio 1:2

Thus, W1-L4 refers to a wall-beam with 1.06% of vertical reinforcement and loaded under uniformly distributed load on top and soffit in the ratio 2:1.

A rig with two cross-heads and two independent hydraulic and mechanical systems was used to apply the loads (Figure 6.4). These loads were applied in constant increments up to failure; at each stage of loading the strains at both surfaces were measured and the widths of cracks were monitored with a hand microscope.

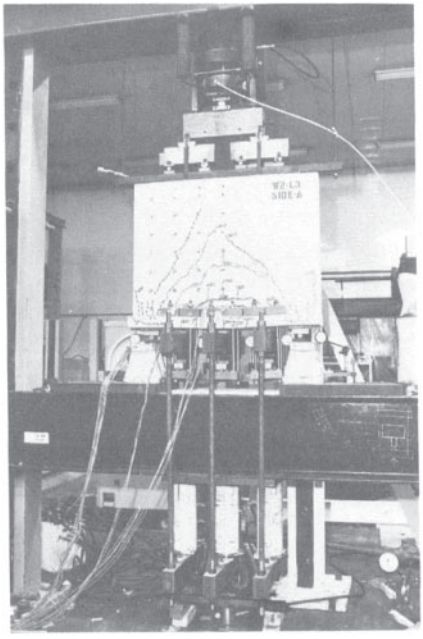

Figure 6.4 Test rig for Leeds tests on wall-beams.

6.5 Crack patterns

Despite differences in vertical reinforcement, crack patterns were similar for walls W1, W2 and W3 under top loading. In general, the first cracks to appear were small flexural cracks within the depth of the nib. The next

cracks to form were diagonal cracks, initiated near the supports and above the nib, spreading rapidly upwards and towards the middle of the wall. At higher loads, these cracks lengthened and new cracks were formed near the supports, propagating parallel with or at wider angles than previous cracks. The failure of the specimens was brought about by local crushing of the concrete at the support joints.

The development of cracks in walls W1, W2, W3, W4 and W5 under soffit loading, was influenced largely by the amount of vertical reinforcement. Different percentages of reinforcement were provided by varying the spacing of the 6 mm vertical bars in the members. In general, the first crack was observed at a depth of about 200 mm and extended horizontally along at least the middle third of the span. With increased load, new cracks were formed above the first, creating an arch-shaped pattern of cracks (Figure 6.6 b and c). The average spacing between cracks on the central vertical section of the walls varied with the spacing of vertical reinforcement. This is illustrated in Figure 6.5, which shows that for larger percentages of vertical reinforcement the average spacing between horizontal cracks reduced.

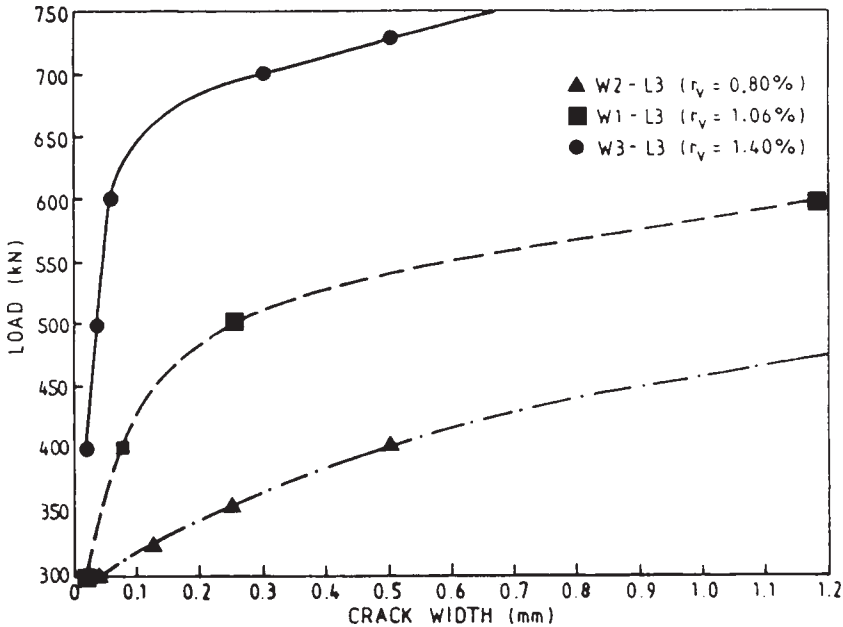

Figure 6.5 Effect upon average spacing of cracks of vertical reinforcement under bottom loading (L2).

Under combined top and bottom loads, the crack pattern was influenced by both the ratio of top loads to bottom loads and the percentage of vertical reinforcement. A selection of the final crack patterns exhibited in the tests is given in Figure 6.6. Fuller details are available in Besser's thesis (1983).

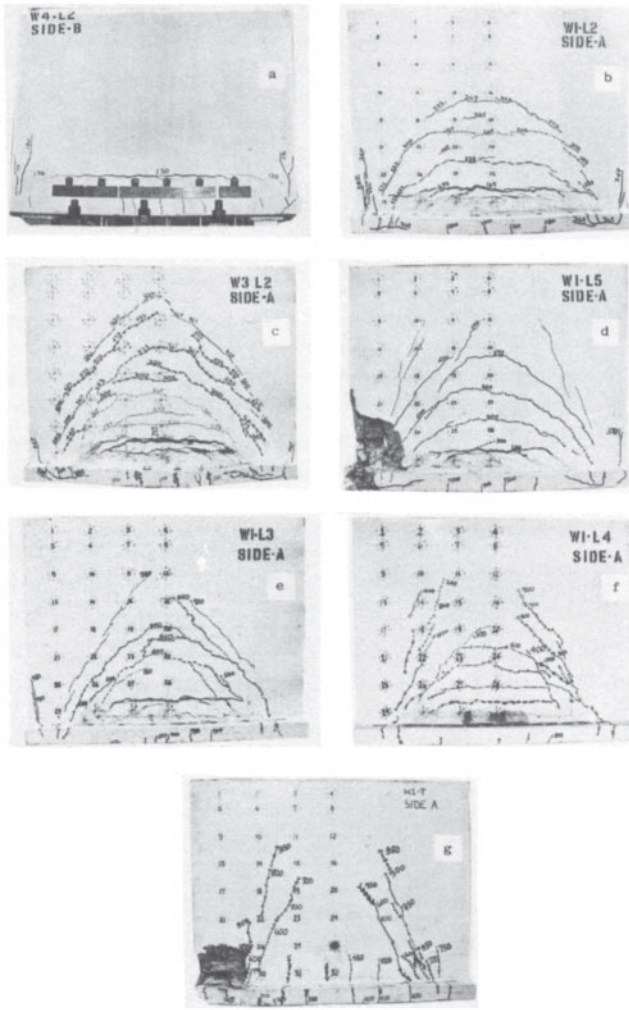

Figure 6.6 Final crack patterns a. W4-L2 (r_v=0) at 140 kN, soffit loading only; b. W1-L2 (r_v=1.06%), soffit loading only; c. W3-L2 (r_v=1.4%), soffit loading only; d. W1-L5 (r_v=1.06%), 1:2 top and soffit loading; e.W1-L3 (r_v=1.06%), 1:1 top and soffit loading; f. W1-L4 (r_v=1.06%), 2:1 top and soffit loading; g. W1-L1 (r_v=1.06%), top loading only.

6.6 Crack widths

Cracks are commonly regarded as a cause for concern by engineers because of the possibility of corrosion of the reinforcement. For serviceability purposes BS8110 limits the crack width to 0.3 mm for members exposed to an aggressive environment. The Comité Européen du Béton (CEB) (1970) has similar proposals, in which the crack width is restricted to 0.1 mm for aggressive environments, 0.2 mm for normal external conditions and 0.3 mm for normal

internal conditions. Table 6.2 shows the loads at which crack widths of 0.05, 0.1, 0.2 and 0.3 mm were observed for the specimens tested. For all wall-beams the general crack width limit of 0.3 mm recommended by the Construction Industry Research and Information Association (CIRIA) (1977) Guide is easily satisfied for all loads below design ultimate; even the crack width limit of 0.1 mm for aggressive environments demanded by CEB (1970) is satisfied.

Table 6.2: Loads at which crack widths of 0.05, 0.10, 0.2 and 0.3 mm were observed

Specimen	Ultimate load CIRIA (kN)	Cube splitting f_{cu} (N/mm^2)	Cylinder splitting strength f_{ct} (N/mm^2)	Crack width (mm) 0.05	0.1	0.2	0.3	Maximum test load (kN)	
W1-L1	527.8	38.8	2.47	600	700	–	–	1100	F
W1-L2	209.6	38.8	2.47	180	210	237	253	375	C
W1-L3	294.1	38.8	2.47	360	422	485	510	750	C
W1-L4	345.8	38.8	2.47	440	625	713	765	1000	C
W1-L5	262.1	38.8	2.47	250	325	400	427	570	C
W2-L1	543.4	43.9	2.63	575	700	1000	–	1100	F
W2-L2	158.2	43.9	2.63	167	190	217	227	300	C
W2-L3	240.5	43.9	2.63	305	318	343	365	600	C
W2-L4	289.6	43.9	2.63	470	565	635	662	900	C
W2-L5	206.7	43.9	2.63	200	250	305	325	400	C
W3-L1	564.9	43.9	2.63	650	800	1100	–	1300	F
W3-L2	276.8	43.9	2.63	255	315	358	375	500	C
W3-L3	365.2	43.9	2.63	575	645	685	700	940	F
W3-L4	416.8	43.9	2.63	860	1000	–	–	1200	F
W3-L5	332.8	43.9	2.63	450	510	550	570	800	F
W4-L2	–	43.9	2.63	130	130	130	130	150	C
W5-L2	395.4	43.9	2.63	275	–	–	–	375	C

F=failure in bearing at support.
C=test suspended due to large crack widths and extensive damage to concrete.
S=test suspended before failure.

In general, cracks were detected initially when their width was about 0.02 mm. For top-loaded specimens a diagonal crack provided the greatest crack width. For beams loaded at the soffit, a horizontal crack invariably gave the largest crack width. Figure 6.7 presents the maximum crack widths for top-loaded wall-beams (loading L1). For the three specimens, this measurement took place at a height of about 250 mm from the soffit. On examining Figure 6.7 the maximum crack width seems to have developed very similarly in specimens W1 and W2. For a given load, crack widths in specimen W3 were slightly narrower than those in the other two wall-beams, and this is attributed to the larger percentage of vertical reinforcement (1.4%) in specimen W3. In general, the results indicate that up to a load of 1000 kN the crack widths in the three specimens exhibited relatively linear behaviour.

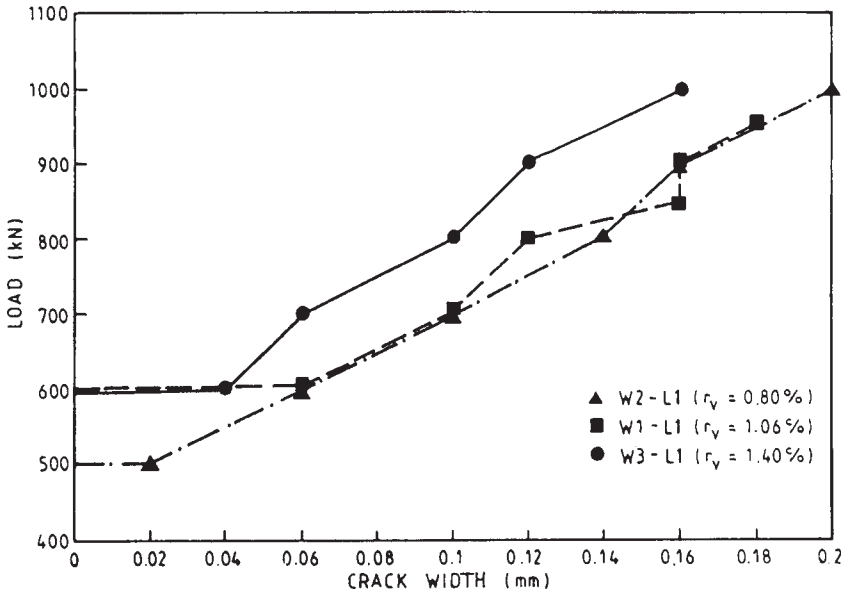

Figure 6.7 Crack width development for top-loaded walls.

The values of maximum crack width for bottom-loaded (L2) walls are summarised in Figure 6.8. This figure exhibits values of mid-span crack width up to 1.2 mm. In specimen W4, the first crack appeared at a load of 130 kN and measured 3.5 mm. This large instantaneous crack width was predictable because of the absence of vertical reinforcement in W4.

Under combined top and bottom loads, the maximum crack width was also recorded on horizontal cracks at mid-span. Figure 6.9 shows these values for crack widths up to 1.2 mm for the specimens loaded under equal top and bottom loading (L3). It is clearly shown in Figure 6.8 and 6.9 that when load was applied at the soffit, the crack width in the wall-beams was directly dependent upon the amount of vertical reinforcement.

6.7 Design approaches

6.7.1. *American Concrete Institute*

The ACI Building Code 318M-83 presents a series of rules applicable to flexural members with a clear span to effective depth ratio (L_o/d) less than 5 and loaded at the top face.

For members subject to shear and flexure the nominal shear strength V_n is found from the contributions of steel and concrete, i.e. $V_n=V_c+Vs$.

If $L_o/d < 2$, $V_n \leq \frac{2}{3}\sqrt{f_c'}\, bd$ (6.1a)

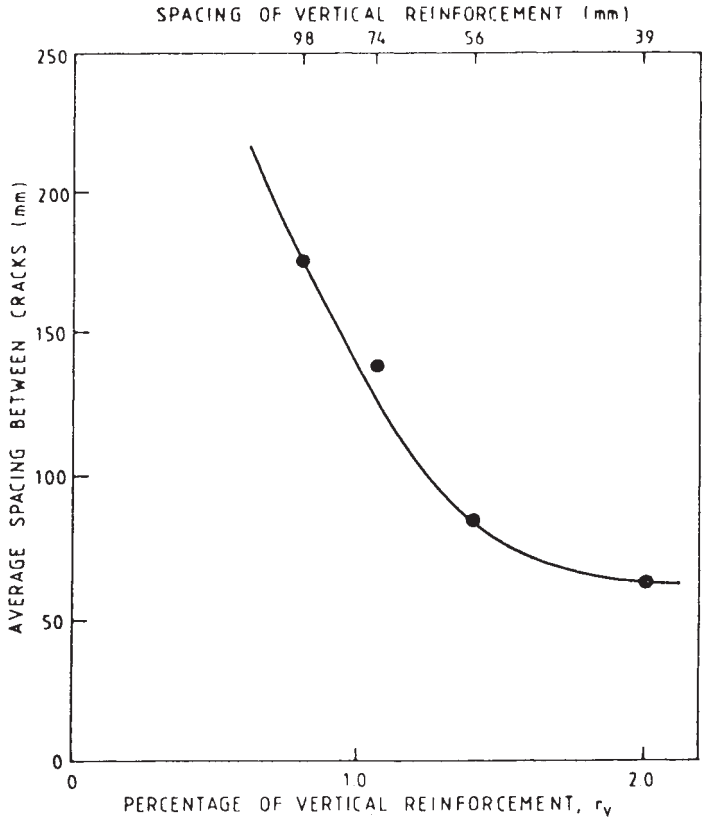

Figure 6.8 Crack width development for bottom loaded walls (Loading L2).

For

$$2 < L_o/d < 5 \qquad V_n \le 0.055\left(10 + \frac{L_o}{d}\right)\sqrt{f_c'}\, bd \tag{6.1b}$$

where f_c' is the cylinder crushing strength of concrete. These equations are expressed in SI units (note that Eqn (6.1b) is shown incorrectly in the June 1984 printing of the Code.)

Ultimate shear strength $V_u = 0.85 V_n$. For detailed calculations the shear strength provided by the concrete is

$$V_c = \left(\frac{3.5 - 2.5M_u}{V_u d}\right)\left(\sqrt{f_c'} + 120\,\rho_w \frac{V_d}{M_u}\right)\frac{bd}{7} \tag{6.2}$$

where M_u, V_u are the factored moment and shear force occurring simultaneously at the critical section for shear: $\rho_w = A_s/bd$ where A_s is the area of main tension reinforcement.

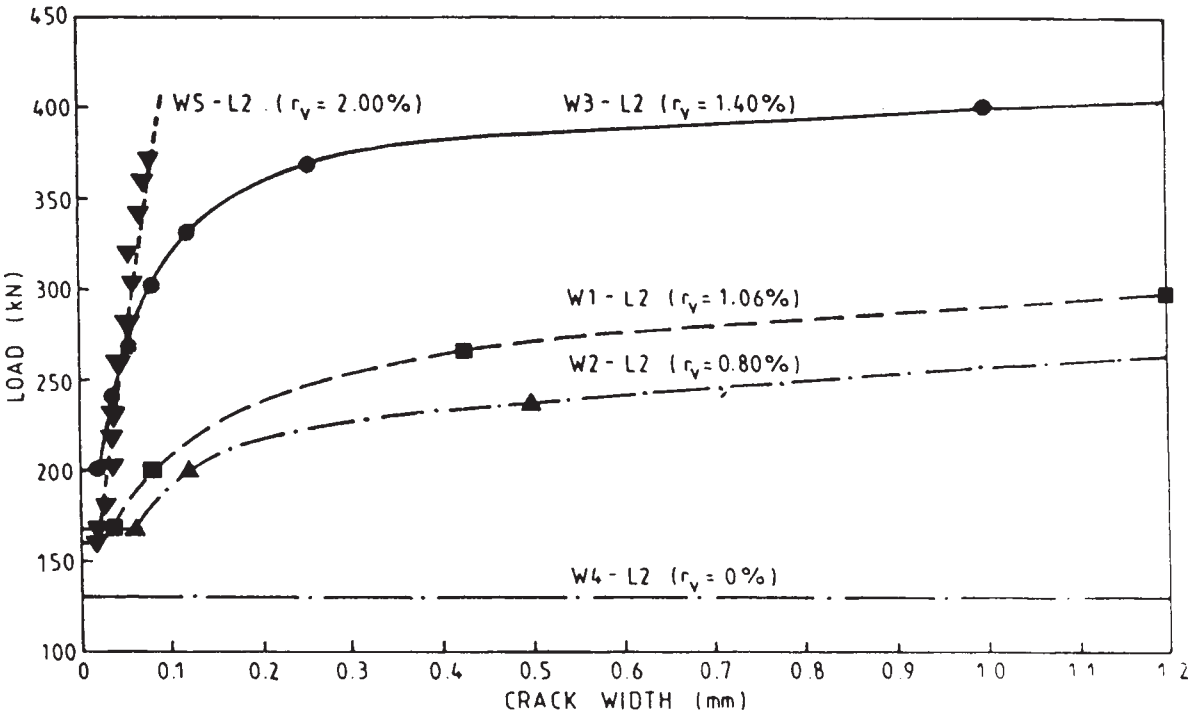

Figure 6.9 Crack width development for wall-beams under equal top bottom loading (Loads L3).

In Eqn (6.2)

$$3.5 - \frac{2.5\,M_u}{V_u d} \leq 2.5 \tag{6.2a}$$

$$V_c \leq \frac{1}{2}\sqrt{f_c'}\,bd \tag{6.2b}$$

$$V_u \leq 0.85\,V_c = \left[\frac{A_v}{s}\left(1 + \frac{L_o}{d}\right) + \frac{A_{vh}}{S_2}\left(11 - \frac{L_o}{d}\right)\right]\frac{f_y\,d}{12} \tag{6.3}$$

where A_v is the area of the vertical shear reinforcement within a distance s and A_{vh} is the horizontal shear reinforcement within a distance S_2.

6.7.2 *Schütt's equations*

Schütt (1956) evolved Eqn (6.3) on the assumptions that 1/3 to 2/3 of the main flexural reinforcement was bent up to provide shear reinforcement and that the area of main reinforcement was determined by the design bending moment on the beam. For uniform top and bottom loads w_t and w_b per unit length, his equations may be rearranged in the form:

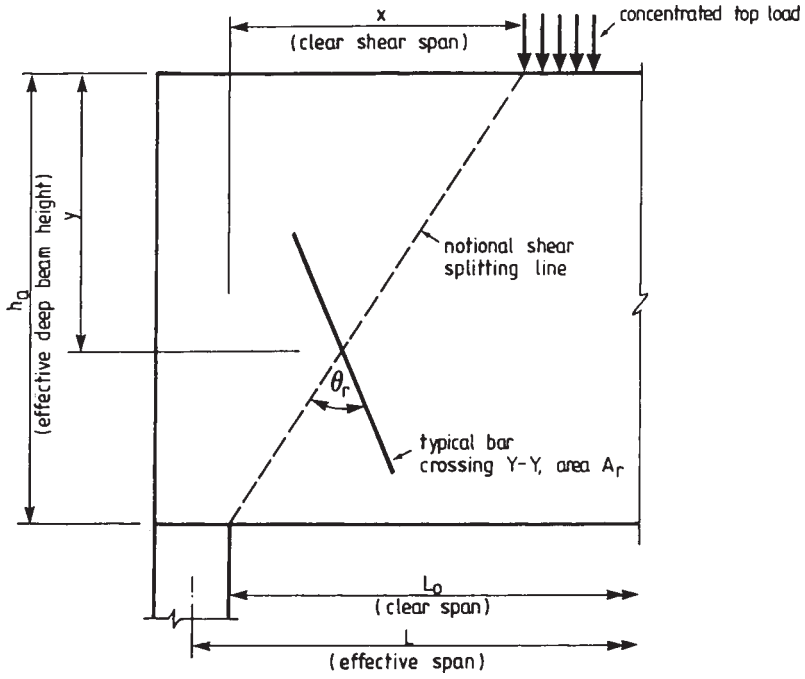

Figure 6.10 Clear shear span for top loads (CIRIA Guide 2).

ultimate shear force $$V_u = \frac{0.5w_t + 0.45w_b}{w_t + w_b} f_{cb} b^2 \frac{h_a}{b} \quad (6.4)$$

where f_{cb} is the modulus of rupture of the concrete. Eqn (6.4) takes no account of the volume of web shear reinforcement.

6.7.3 *CIRIA Guide*

In 1977, CIRIA published a Guide to the design of deep beams. This presents the most comprehensive set of design recommendations available and includes a condition to be satisfied when both top and bottom loading are present. The condition states

$$(V_{at}/V_{ct}) + (V_{ab}/V_{cb}) < 1 \quad (6.5)$$

where V_{at} and V_{ab} are the values of applied shear force from top and bottom loads respectively, V_{ct} and V_{cb} are the shear capacities assuming top loads only or bottom loads only. V_{cb} is defined as the lesser of $0.75\, bh_a v_u$ and the resultant force taken by the shear reinforcement, where v_u is the maximum value of shear stress in concrete from CP110 (Cusens and Besser, 1985) V_{ct} is based on Kong's work and is stated as:

$$\frac{V_{ct}}{b_d} < \lambda_1 \left(1 - 0.35 \frac{x_e}{h_a}\right) \left(\sqrt{f_{cu}} + \lambda_2 \sum \frac{100 A_i y_i \sin^2 \theta_r}{b h_a^2}\right) \quad (6.6)$$

where: λ_1, λ_2 are constants, dependent upon type of aggregate and type of reinforcement respectively; θ_r is the angle between reinforcement and diagonal crack (Figure 6.10); y_i is the distance from top of wall to position of bar; and x_e is the effective clear shear span (Figure 6.10). However, the ultimate shear capacity is subject to the condition:

$$V < 1.3\lambda_1 \sqrt{f_{cu}}\, bh_a \quad (6.7)$$

In all cases shear reinforcement must be provided to carry at least 20% of the ultimate shear force.

The CIRIA Guide recommends particular arrangements of shear reinforcement for bottom loads (which are also applicable to indirect loads). Figure 6.11 shows an arrangement where steel additional to the nominal web reinforcement is provided in the form of an orthogonal mesh. Figure 6.12 shows an alternative arrangement consisting of inclined bars.

6.8 Top-loaded wall-beams

The values of ultimate shear strength for the Cusens and Besser (1985) wall-beams W1-L1, W2-L1 and W3-L1, which were loaded on the top only, have been calculated using the three design approaches of ACI, Schütt and CIRIA.

Table 6.3 compares the ultimate load capacity of top-loaded wall-beams W1–3 as predicted by the respective equations. In the calculations for the ACI method Eqn (6.1a) governs for this group of wall-beams and the

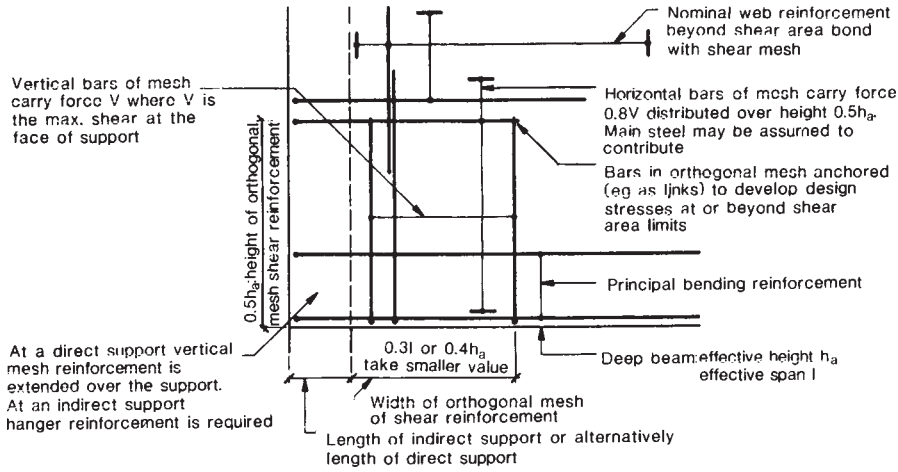

Table 6.3 Predicted ultimate loads and test values for top-loaded wall-beams

unmodified value of V_n has been used. In evaluating the Schütt Eqn (6.4) the value of the modulus of rupture of concrete has been assumed to be 2×splitting strength for each specimen. In the CIRIA Eqn (6.6) the recommended values λ_1=0.44 for normal concrete and λ_2=0.85 N/mm2 for plain bars have been used.

Figure 6.11 Shear reinforcement at support for bottom loads (CIRIA Guide 2).

Specimen	ACI (kN)	Schütt (kN)	CIRIA (kN)	Cracking load (kN)	Failure load (kN)
W1-L1	496	103	528*	600	1100
W2-L1	517	110	543	500	1100
W3-L1	545	110	565*	600	1300

* Value from Eqn (6.6). However, governing ultimate shear capacity values are W1-L2:513 kN and W3-L1:546 kN.

The load at which the first diagonal crack was detected in these specimens is also given in Table 6.3. It can be observed that Schütt's equation is grossly conservative and that the ACI figures are more conservative than the CIRIA values. Both CIRIA and ACI design values of ultimate loads are in the same range as the test values of load at first crack. However, the failure load for these three specimens is more than twice the shear strength calculated by Eqns (6.1a) and (6.6). Moreover Eqn (6.6) values for two of the wall-beams exceed the governing value of Eqn (6.7). In addition, failure of these specimens was

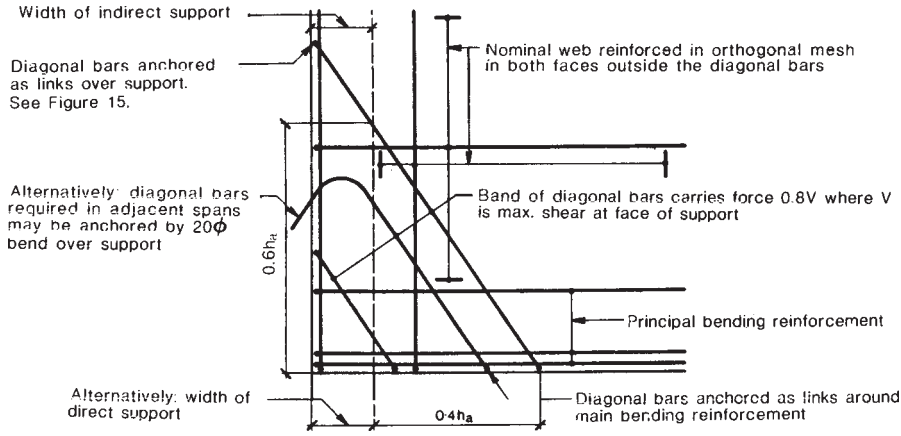

Figure 6.12 Alternative arrangement of shear reinforcement at end support for bottom loading (CIRIA Guide 2).

actually due to local crushing in bearing (Table 6.2), suggesting an even greater capacity of the section to resist shear.

Both the ACI and CIRIA equations refer to design ultimate loads with some in-built material factors and perhaps the conservatism of the calculated values is not surprising. It should be noted that concrete is the sole contributor to shear strength in the ACI code (Eqn (6.1a) which is the governing equation here) and that concrete strength is the major contributor in the CIRIA Eqn (6.6); in computing the values given in Table 6.3 the actual test results of concrete strength were used. A designer would use characteristic strength values which would lead to even lower estimates of ultimate load—i.e. effectively providing an additional material factor not considered here.

It may be concluded that for these wall-beams the CIRIA and ACI procedures predicted the approximate load at which the first diagonal cracks occurred, with the value of ultimate shear strength being more than twice the predicted figure. Schütt's equation does not appear to have any practical value.

6.9 Bottom-loaded wall-beams

Of recent documents dealing with recommendations for reinforced concrete design, only the CIRIA (1977) Guide has specific proposals for designing deep flexural members loaded at the soffit or under combined top and bottom loads. Schütt's equation considers top and bottom loads but does not consider the effect of the volume of shear reinforcement; moreover in view of the evidence of Table 6.3 it is unlikely to be of practical significance.

Table 6.4 presents data concerning five wall-beams tested under load at the soffit only (loading L2). This data is listed in relation to the ascending percentage of vertical reinforcement r_v in the specimens. Wall-beam W4,

without vertical reinforcement, sustained 130 kN before it cracked horizontally, forming a secondary beam at the lower level of the wall, whose flexural rigidity continued to carry load. A small increase in the cracking load can be observed in specimen W2 with 0.8% of vertical reinforcement. For the range of vertical reinforcement from 0.8 to 2.0%, the load at first horizontal crack was virtually constant. The cracking load noted for specimen W3 is inconsistent with other values and is thought to be due to a delay in detecting the initial crack.

Table 6.4 Effect of vertical reinforcement on cracking load and comparison with CIRIA ultimate load prediction for wall-beams loaded at the soffit only (loading L2)

Specimen	Vertical reinforcement r_v (%)	CIRIA (kN)	Schütt (kN)	Cracking load (kN)	Ultimate load
W4-L2	0	0	92	130	150
W2-L2	0.80	158	92	167	300
W1-L2	1.06	210	86	167	375
W3-L2	1.40	277	92	200	500
W5-L2	2.00	395	92	164	–

6.10 Combined top and bottom loading

When combined top and bottom loading is present the CIRIA Guide states that Eqn (6.4) should be applied. The equation controls the permissible amounts of top and bottom load for a given deep beam and clearly is of interest here. In Figure 6.13 the ultimate test loads are compared with the CIRIA values; with the exception of the bottom loaded wall-beams, all tests show an ultimate load of at least twice the design ultimate value. Bearing in mind that in tests the ultimate loads in shear of the stronger wall-beams were limited by local crushing failures (Table 6.2), the CIRIA values are obviously quite conservative for wall-beams with a high proportion of top loading.

Adopting the CEB criteria of a 0.1 mm crack width as a serviceability limit state, Figure 6.14 compares the corresponding loads in tests of wall-beams W1, W2 and W3 and the CIRIA ultimate load values calculated from Eqns (6.1) and (6.2). All test loads corresponding to a maximum crack width of 0.1 mm are in excess of the CIRIA predictions of ultimate load. The load factor is enhanced as the proportion of top-loading increases above 50% and also with the percentage of vertical reinforcement.

If Schütt's equation (Eqn (6.4)) is applied to these beams all of the results for ultimate load fall within the range 85–112 kN and although individual values are influenced by the ratio of top/bottom loading, the effects are small. Moreover the volume of shear reinforcement is not taken into account and, in comparison with test results, values are ultra-conservative. Use of this equation is not recommended.

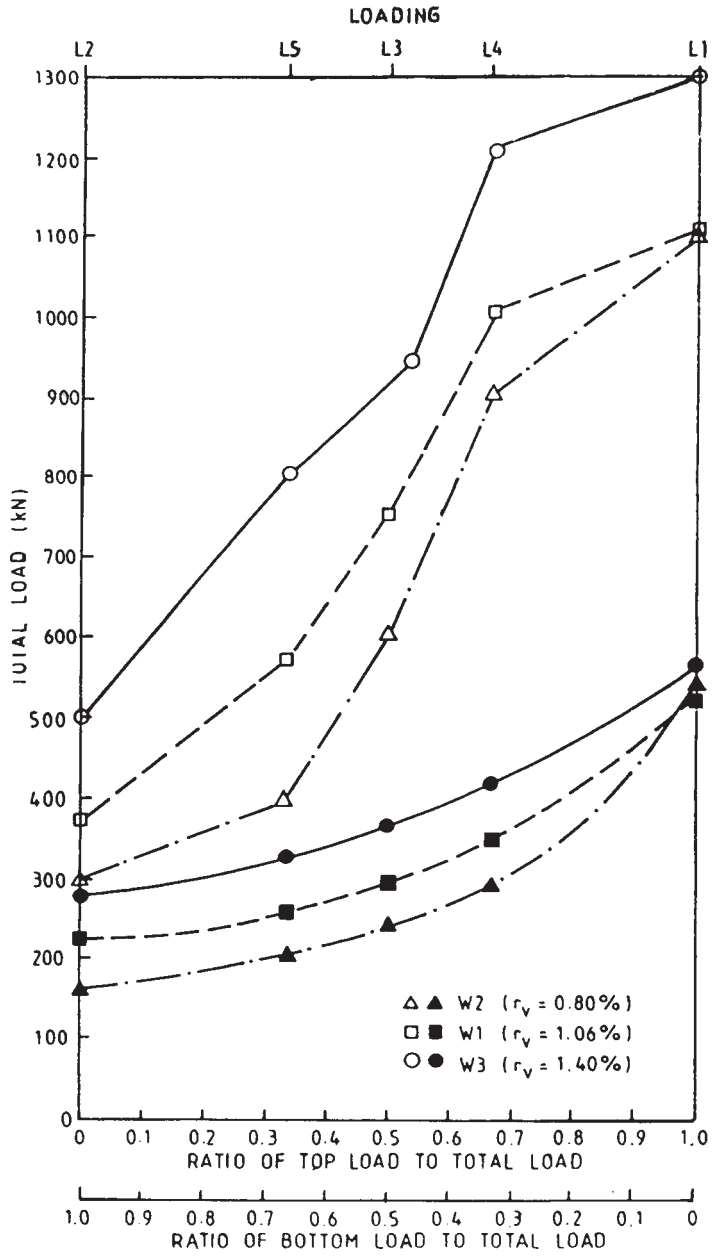

Figure 6.13 Comparison of CIRIA ultimate loads and ultimate test loads.

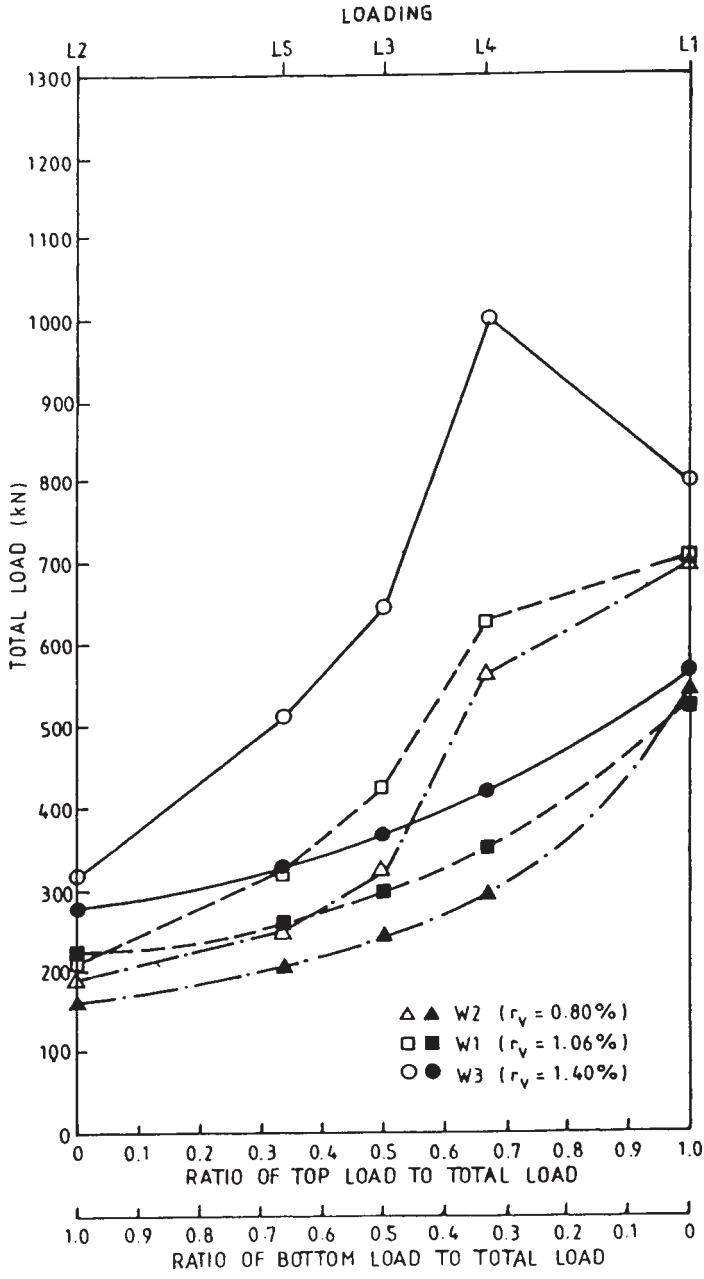

Figure 6.14 Comparison of CIRIA ultimate loads and loads at 0.1 mm crack width.

6.11 Summary and recommendations

The chapter has reviewed the principal research programmes and design approaches for deep beams under top and bottom loading. Of the three design approaches available, the *American Concrete Institute method* makes no special provision for bottom loading and is very conservative for top loaded beams. The *Schütt* equation (Eqn (6.4)) is dependent primarily upon the concrete tensile strength and dimensions of the deep beam. Although the ratio between top and bottom loading is taken into consideration in the equation the apparent effect is much smaller than obtained in tests. The equation also makes assumptions about the volumes of tensile and shear reinforcement which limit its use. All calculated results of ultimate load have been found to be grossly conservative and use of the equation by designers is not recommended.

The *CIRIA* Eqns (6.5) and (6.6) take into account the volume of shear steel and the ratio of top/bottom loading. The CIRIA estimates of ultimate load accord more accurately with test values of initial cracking (or serviceability) load than with values of ultimate load. Booth (1986) points out that the CIRIA recommendation (Eqn (6.6)) is based on a lower bound curve set at about 75% of Kong's experimental values. Moreover the λ_1 and λ_2 values in Eqn (6.6) include some allowance for variability of materials. Overall, the 1977 CIRIA recommendations provide a rational and safe approach to the design of deep beams under combinations of top and bottom loading, although, the design guide is long overdue for revision, to include the provisions of BS8110 (1985), rather than the obsolete CP110.

References

American Concrete Institute. (1983) *Building code requirements for reinforced concrete,* pp 318–83, ACI, Detroit.

Besser, I. (1983) *Strength of slender reinforced concrete walls.* PhD thesis, University of Leeds.

Booth, E. (1986) Discussion of shear strength of concrete wall-beams under combined top and bottom loads by Cusens, A.R. and Besser, I. (1985) *Struct. Engr* **64B**, 2, June: 48.

Comité Européen du Béton—FIP. (1970) International recommendations for the design and construction of concrete structures, Principles and recommendations. *Proc. 6th FIP Congress, Prague, Czechoslovakia.*

Construction Industry Research and Information Association (1977) *The design of deep beams in reinforced concrete.* CIRIA Guide 2, CIRIA, London.

Cusens, A.R. and Besser, I. (1985). Shear strength of concrete wall-beams under combined top and bottom loads. *Struct. Engr* 63B, 3, Sept.: 50.

Graf O., Brenner, E. and Bay, H. (1943) *Versuche mit einem wandartigen Trager aus Stahlbeton* Deutscher Ausschuss fur Stahlbeton, Heft 99, Berlin.

. Leonhardt, F. and Walther, R. (1966) *Wandartige Trager.* Deutscher Ausschuss fur Stahlbeton, Heft 178, Wilhelm Ernst and Sohn, Berlin.

Schütt, H. (1956) Uber das Tragvermogen wandartiger Stahlbetontrager. *Beton und Stahlbeton 51:* 220.

7 Shear strength prediction—softened truss model

S.T. MAU and T.T.C. HSU, University of Houston

Notation

a	shear span; measured centre-to-centre from load to support
a'	shear span measured from centre of loading to edge of support
A_{vl}	cross-section area of horizontal web steel
b	thickness of beam
C	stress ratio σ_r/f'_c
C_l	limiting constant for reinforcement index in 1-direction
C_s	limiting constant for strength ratio v_n/f'_c
C_t	limiting constant for reinforcement index in t-direction
d	effective depth of beam; measured from extreme compression fibre to centre of tension reinforcement
d'	distance from top surface of the beam to centre of flexural compression steel
d_v	effective depth of shear element, taken as d-d' when compression steel is present and 0.9d when compression steel is not present
E_c	initial modulus of elasticity of concrete taken to be $-2f'_c/\varepsilon_o$
E_s	modulus of elasticity of reinforcing bars
f'_c	cylinder compression strength of concrete
f_{cr}	cracking strength of concrete, assumed to be $4\sqrt{f'_c}$
f_l	steel stress in 1-direction
f_{ly}	yielding stress of longitudinal steel reinforcement
f_t	steel stress in the t-direction
f_{ty}	yielding stress of transverse steel reinforcement;
f_y	yield stress of steel reinforcement
h	total depth of beam
K	ratio of the effective compressive stress in transverse direction to the effective shear stress in the shear element
l	the longitudinal direction; usually horizontal for a beam;
L	clear span of the beam
p	effective transverse compression; acting on the shear element
R_F	ratio of calculated shear strength to test shear strength
R_T	ratio of theoretical shear strength from softened truss model to experimental shear strength
S	spacing of vertical reinforcement
S_2	spacing of horizontal web reinforcement
t	the transverse direction; usually vertical for a beam
v	effective shear stress in the shear element
v_n	shear strength taken as the maximum shear stress in the v-vs γlt curve
V	shear force in the shear span
V_n	ultimate shear force

x	clear span of the shear span, measured from edge of loading to edge of support
α	angle of inclination of the d-axis with respect to l-axis;
γ_{lt}	average shear strain in the l-t coordinate (positive as shown in Figure 7.1 for τ_{lt})
ε_{cr}	tensile strain at which concrete cracks, taken to be f_{cr}/E_c
ε_d	average principal strain in d-direction
ε_l	average normal strain in the l-direction (positive for tension)
ε_{ly}	yield strain of longitudinal steel reinforcement
ε_o	compression strain at maximum stress in a uniaxial stress-strain curve of concrete cylinder; taken as—0.002
ε_r	average normal strain in r-direction
ε_t	average normal strain in the t-direction (positive for tension)
ε_{ty}	yield strain of transverse steel reinforcement.
ζ	softening coefficient (reciprocal of λ) which is less than unity
λ	coefficient for softening effect, given by Vecchio and Collins
μ	Poisson's ratio
ρ_c	reinforcement ratio of flexural compression steel
ρ_l	reinforcement ratio in l-direction
ρ_t	reinforcement ratio in t-direction
ρ_{vl}	reinforcement ratio of horizontal web steel
ρ_w	reinforcement ratio of flexural tensile steel
σ_d	principal stress in concrete in the principal d-direction
σ_l	normal stresses in the combined reinforced concrete element in l-direction (positive for tension)
σ_r	principal stress in concrete in the principal r- direction
σ_t	normal stresses in the combined reinforced concrete element in t-direction (positive for tension)
σ_{lc}	normal stress in concrete in the l direction (positive for tension)
σ_{tc}	normal stress in concrete in the t direction (positive for tension)
τ_{lt}	shear stresses in combined reinforced concrete element in l-t coordinate (positive as shown in Figure 7.4)
τ_{ltc}	shear stress in concrete in the l-t co-ordinate (positive as shown in Figure 7.4)
ω_l	reinforcement index in l-direction
ω_t	sreinforcement index in t-direction

7.1 Introduction

In the past, there were two basic approaches used to analyse shear problems in reinforced concrete: namely, the mechanism method and the truss model method. The mechanism method is the basis of the current shear provisions in the ACI Code (ACI-318, 1989). By fitting the mechanism method to the test results, the ACI method becomes empirical or at best semi-empirical. From a theoretical point of view, this method cannot satisfy the compatibility condition, unless the materials (concrete and steel) are assumed to have infinite plasticity.

It is generally agreed by researchers in recent years that the truss model theory provides a more promising way to treat shear. First, it provides a clear

concept of how a reinforced concrete beam resists shear after cracking. Second, the effect of prestress can be included in a logical way. Consequently, the whole range of prestressing from nonprestressed structures to fully prestressed structures can be unified. Third, the interaction of bending and axial load with shear can be easily managed. The combination is quite consistent and comprehensible. Fourth, it can serve as a basis for the formulation of general design codes.

The original truss model concept was first proposed to treat shear problems by Ritter (1899) and Morsch (1909) at the turn of the twentieth century. It was extended to treat torsion problems by Rausch (1929) in 1929. In these theories, a concrete element reinforced with orthogonal steel bars and subjected to shear stresses will develop diagonal cracks at an angle inclined to the steel bars. These cracks will separate the concrete into a series of diagonal concrete struts, which is assumed to resist axial compression. Together with the steel bars, which are assume to take only axial tension, they form a truss action to resist the applied shear stresses. For simplicity, the concrete struts are assumed to be inclined at 45° to the steel bars. Consequently, these theories are known as the 45° truss model.

The rudimentary truss model of Ritter, Morsch and Rausch is very elegant and the equations derived from the equilibrium conditions are simple. Unfortunately, the predictions from these equations did not agree with the test results. For the case of pure torsion, the theory may overestimate the test values by 30%. For the case of low-rise shear walls, the overestimation may exceed 50%.

In order to improve the predictions of the truss model, the theory had undergone three major developments. The first important development was the generalisation of the angle of inclination of the concrete struts by Lampert and Thurlimann (1968). They assumed that the angle of inclination may deviate from 45°. On this basis, three basic equilibrium equations had been derived, which could explain why longitudinal and transverse steel with different percentages can both yield at failure. Their theory was known as the variable-angle truss model. The second development was the derivation of the compatibility equation by Collins (1973) to determine the angle of inclination of the concrete struts. Since this angle is assumed to coincide with the angle of inclination of the principal compression stress and strain, this theory is also known as the compression field theory. In this theory, the average strain condition should satisfy Mohr's strain circle and the stress in the concrete struts should satisfy Mohr's stress circle. The third development was the discovery of the softening of concrete struts by Robinson and Demorieux (1968) and the quantification of this phenomenon by Vecchio and Collins (1981). Vecchio and Collins proposed a softened stress-strain curve, in which the softening effect depends on the ratio of the two principal strains.

Combining the equilibrium, compatibility and softened stress-strain relationships, a theory was developed which can predict with good accuracy the test results of various types of reinforced concrete structures subjected to shear

or torsion. The theory can predict not only the shear and torsional strengths, but also the deformations of a structure throughout its post-cracking loading history. This thoery is called the softened truss model theory to emphasise the importance of the concrete softening phenomenon. It has been successfully used to predict the shear strength of low-rise shearwalls (Hsu and Mo, 1985d; Mau and Hsu, 1986), shear strength of framed wall panels (Mau and Hsu, 1987a), shear transfer strength across an initially uncracked shear plane (Hsu, Mau, and Chen, 1987), torsional strength of beams (Hsu and Mo, 1985a, b, c), and membrane strength of shell elements (Han and Mau, 1988).

The softening of concrete struts was also incorporated in the prediction of the shear strength of beams by Hagai (1983), For slender beams with shear-span to effective-depth ratio between 2.5 and 6, his truss model predictions agree well with experimental results. However, for beams with shear-span to effective-depth ratio below 2.5 (i.e. the range of deep beams), his predictions underestimate considerably the actual shear strength. For example, for shear-span to depth ratio equal to or less than 0.5, the underestimation may exceed 50%. In this study, it is shown that a correct model for deep beams in shear should include a component of transverse compression in the shear element. With the proper estimation of this transverse compression, the softened truss model theory predicts accurately the shear strength of deep beams.

In this chapter, the modelling of the deep beams is described first. The softened truss model theory is then introduced in detail and is applied to the deep beam model. A prediction of the shear strength is obtained by tracing the load-deformation history numerically and locating the peak shear stress. The accuracy of the theoretical prediction is established by a comparison with experimental data and a sensitivity study. From the theoretical equations, it is seen that the most important factors in the shear strength of deep beams are the shear-span to height ratio, the amount of longitudinal reinforcement, and the amount of transverse reinforcement. A parametric study is carried out to determine the influence of the three factors on the shear strength of deep beams.

Based on the results of the parametric study, an explicit shear strength formula is derived from the equilibrium equations and simplified to a form suitable for design purposes. The constants in the formula are calibrated with experimental data.

7.2 **Modelling of deep beams**

7.2.1 *Shear element*

Consider a typical deep beam of rectangular cross-section loaded on top and simply supported at bottom as shown in Figure 7.1. Within the shear span a, the beam can be separated into three elements—each with a different function to resist the applied load. The top element with a thickness of d', including the concrete and the longitudinal compression steel, is to resist the

longitudinal compression resulting from the sectional moment. The bottom element, including only the longitudinal tension steel, is to resist the longitudinal tension resulting from the sectional moment. The middle element, including the web reinforcement and both the top and bottom longitudinal steel, is to resist the sectional shear. This web shear element is indicated in Figure 7.1 by the dashed lines. The height of the web shear element is denoted by d_v and is equal to *d-d'*. The top and bottom longitudinal bars are used to carry the flexural stresses as well as the longitudinal stresses due to shear.

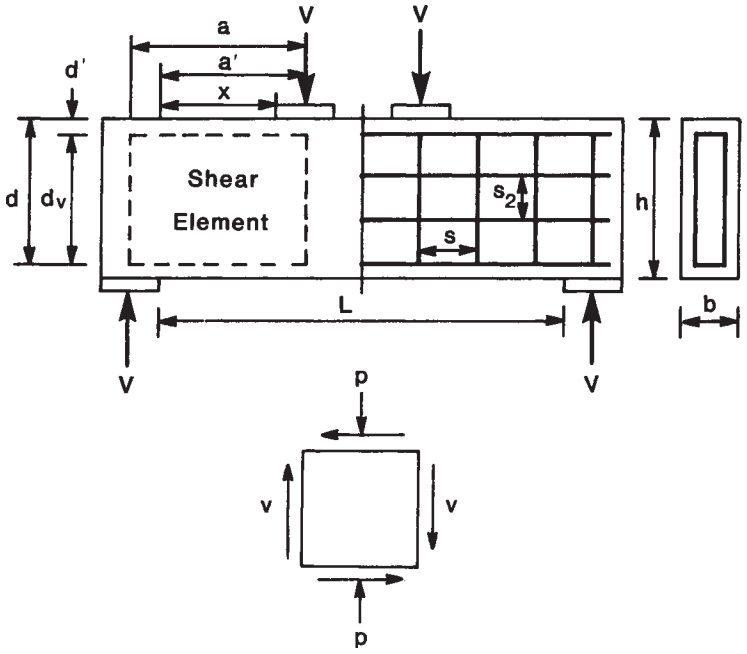

Figure 7.1 Definition of symbols and stress condition in shear element

If the shear element were assumed to carry only an average shear stress, then the model would be similar to that for a slender beam (Hagai, 1983). The model would lead to the underestimation of the shear strength when the softened truss model is applied. In order to reflect the special characteristic of a deep beam, the concept of an average compressive stress in the shear element is developed.

7.2.2 *Effective transverse compression*

For a simple deep beam with concentrated load on top, the top load and the bottom support reaction create large compressive stresses transverse to the horizontal beam axis. These transverse compression stresses interact with

the shear stresses to form a complicated stress field in the web. Because of the short horizontal distance between the top and bottom loading points (i.e. small *a/h* ratio), the effect of such a transverse compression stress on the shear strength of the web is quite significant and should not be ignored, as in the case of slender beams. In fact, such a transverse compression stress is the source of the arch action unique to deep beams.

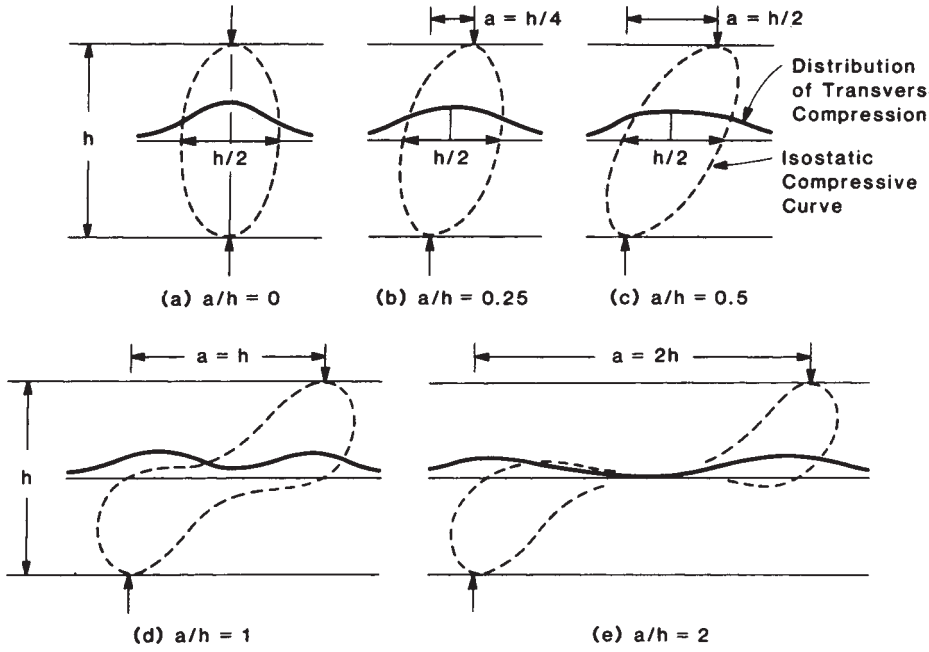

Figure 7.2 Distribution of transverse compressive stress for various shear span ratios

The distribution of the transverse compression stresses within the shear span is estimated as follows. In Figure 7.2, the distributions of transverse compression stresses at mid-height of the beam are sketched for various *a/h* ratio from 0 to 2. For *a/h*=0, transverse stress is maximum at the line of actions and gradually decreases when moving away from the line of action. This characteristic of stress distribution should remain the same for the two cases of *a/h* =0.25 and 0.5, except that the maximum stress is now located at the centre of the shear span. The magnitudes of the maximum stress also decrease slightly, and the stresses become more uniform when *a/h* increases from 0 to 0.5. For *a/h*=1, the maximum stress will occur at two locations near the two lines of action, and the distribution of stress shows the characteristics of two humps. For *a/h*=2, this two-humps characteristic becomes more distinct, meaning the stresses are approaching zero at the centre of the shear span.

Figure 7.2 also shows the isostatic compression curves (dotted) for the various cases. For the three cases a/h=0, 0.25 and 0.5, each isostatic curve can be approximated by an ellipse. In contrast, for the case of a/h=2, the isostatic curve concentrates near the two loading points. The curve for a/h=1 lies somewhere in between.

The effect of transverse compression can now be represented by an effective transverse compression of intensity p, acting uniformly throughout the shear element. The magnitude of the effective transverse compression p is related not only to the shear force V, but also to the shear span ratio. Obviously, the larger the shear span ratio, the smaller the effective transverse compression will be, given the same shear force V. Therefore, the effective transverse compression p can be developed as a function of shear force V and the shear span ratio a/h.

Consider the case of a/h=0.5 as shown in Figure 7.2(c). The dotted isostatic curve indicates the boundary of a possible stress path between the top and bottom loading points. The width of the load path at the mid-height can be estimated as $h/2$, which is the same as the shear span a. Thus, an estimate of the effective transverse compression is $p=V/ba$ or $2V/bh$, where b is the width of the beam. For larger a/h, p should decrease to zero at certain value of a/h. It is reasonable to assume that such a value is a/h=2. Beyond a/h=2, the shear behaviour would approach that of a slender beam. When a/h increases from 0.5 to 2, p will decrease not only with V/ba, but should incorporate a linear function $(4/3\text{-}2a/3h)$ so that p=0 when a/h=2. The resulting expression for p is

$$p = \frac{V}{ba}\left(\frac{4}{3} - \frac{2a}{3h}\right) \qquad 0.5 \le a/h \le 2$$

The right-hand side of this equation can be expressed in terms of the nominal shear across the whole section V/bh

$$p = \frac{V}{bh}\left[\frac{4}{3}\left(\frac{h}{a} - \frac{1}{2}\right)\right] \qquad 0.5 \le a/h \le 2 \tag{7.1}$$

This expression is plotted in Figure 7.3.

For $a/h<0.5$, the transverse compression is assumed to remain constant since the effective area remains essentially the same as shown in Figure 7.2(a) and (b). The expression of $p=2V/bh$ for $a/h<0.5$ is also shown in Figure 7.3.

An effective shear stress v in the shear element can be defined by the following formula

$$v=V/bdv \tag{7.2}$$

Thus the stress conditions for the shear element are completely defined by p and v. To find the shear strength of the beam is to find the maximum

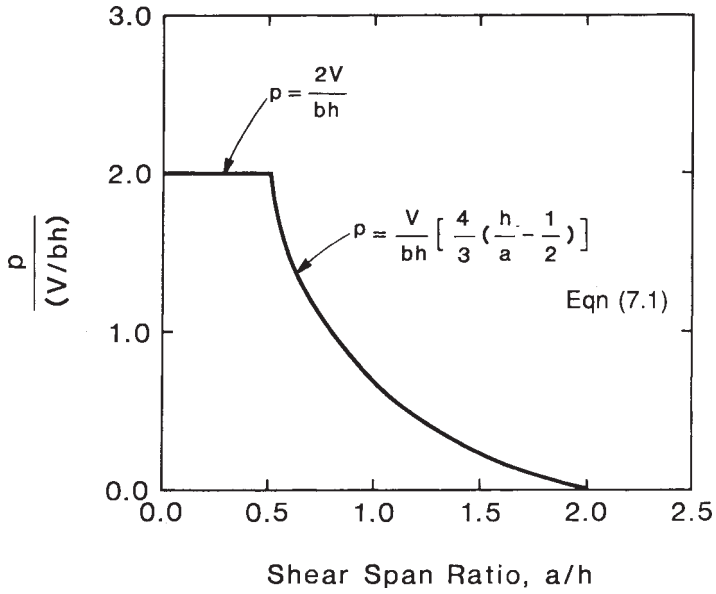

Figure 7.3 Estimation of effective transverse compression

shear stress v that the shear element can withstand. This calls for the solution of equations governing the equilibrium, compatibility and material behaviour of the shear element. These equations can be obtained from the equations of the softened truss model theory for a reinforced concrete element carrying general two-dimensional stresses.

7.3 Softened truss model

7.3.1 *Fundamental assumptions*

A reinforced concrete element is subjected to shear stresses and normal stresses as shown in Figure 7.4. The directions of the longitudinal and transverse steel bars are designated as the *l*-and t-axes, respectively, forming the *l*-t co-ordinate system. Accordingly, the normal stresses are denoted by σ_l and σ_t and the shear stresses are τ_{lt}.

After the development of diagonal cracks, the concrete struts are subjected mainly to compression and the steel bars act as tension links, thus forming a truss action. The compression struts are oriented in the d-axis, which is inclined at an angle α to the longitudinal steel bars. This direction is also assumed to be the direction of the principal compressive stress and strain of the concrete element. Taking the direction perpendicular to the d-axis as the r-axis, a d-r co-ordinate system in the direction of the principal stresses and strains is established. The normal principal stresses in the d- and

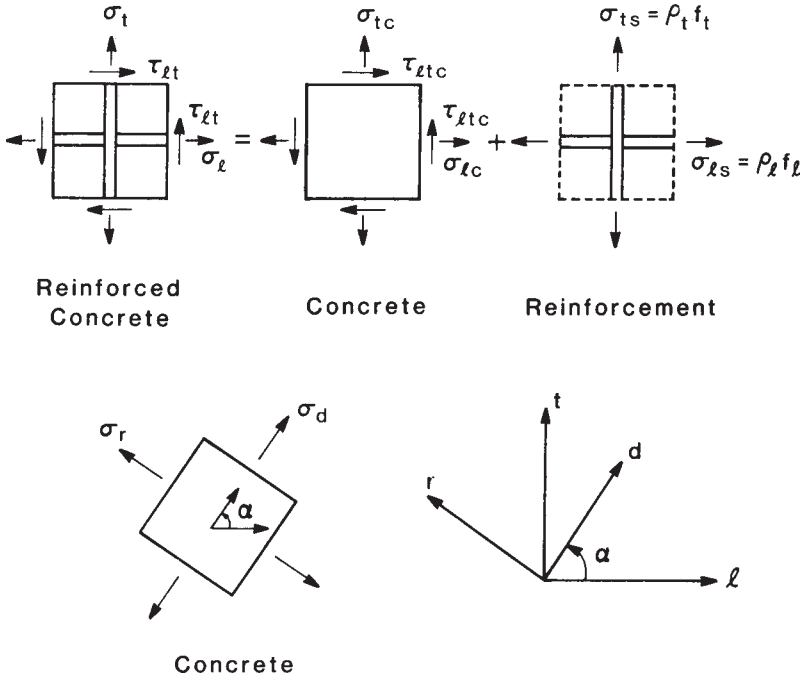

Figure 7.4 Stress condition in reinforced concrete element

r-directions are σ_d and σ_r respectively. The concrete strut is also assumed to carry a small tension in the r-direction, σ_r.

It is assumed that the behaviour of the cracked concrete element may be characterised by its overall average strain and stress. The assumption is based on the availability of an empirical material law linking the average strain to the average stress in the concrete. This material law will be described later. With this assumption, the difficulty encountered in the characterisation of the local behaviour between the cracks is bypassed. The average normal strains of concrete in the longitudinal and transverse directions are assumed to be identical to those in the longitudinal and transverse reinforcements.

7.3.2 *Stress transformation (equilibrium)*

From the three equilibrium conditions of the truss model, it can be shown (Hsu, 1984) that the stresses in the concrete satisfy Mohr's stress circle. Thus,

$$\sigma_c=\sigma_d\cos^2\alpha+\sigma_r\sin^2\alpha \quad (7.3a)$$

$$\sigma_{tc}=\sigma_d\sin^2\alpha+\sigma_r\cos^2\alpha \quad (7.3b)$$

$$\tau_{ltc}=(\sigma_d-\sigma_r)\sin\alpha\cos\alpha \quad (7.3c)$$

where σ_{lc}, σ_{tc} are normal stresses in concrete in *l* and t-directions, respectively (positive for tension); τ_{ltc} is shear stress in concrete in *l*-t co-

ordinate (positive as shown in Figure 7.4); σ_d, σ_r are principal stresses in concrete in d- and r-directions, respectively (positive for tension) and α is the angle of inclination of d-axis with respect to *l*-axis.

Assuming that the steel bars can resist only axial stresses, then the superposition of concrete stresses and steel stresses gives:

$$\sigma_l=\sigma_d\cos^2\alpha+\sigma_r\sin^2\alpha+\rho_l f_l \quad (7.4a)$$
$$\sigma_t=\sigma_d\sin^2\alpha+\sigma_r\cos^2\alpha+\rho_t f_t \quad (7.4b)$$
$$\tau_{lt}=(\sigma_d-\sigma_r)\sin\alpha\cos\alpha \quad (7.4c)$$

where σ_l, σ_t are normal stresses in the combined reinforced concrete element in *l* and t-directions, respectively (positive for tension); τ_{lt} is the shear stress in the combined reinforced concrete element in *l*-t co-ordinate (positive as shown in Figure 7.4); ρ_l, ρ_t are reinforcement ratios in *l*- and t-directions, respectively and f_l, f_t are steel stresses in *l*- and t-directions, respectively.

Comparison of the stress condition of a reinforced concrete element shown in Figure 7.4 with the stress condition of the shear element in a deep beam shown in Figure 7.1 leads to

$$\sigma_l=0 \quad (7.5a)$$
$$\sigma_t=-p \quad (7.5b)$$
$$\tau_{lt}=-v \quad (7.5c)$$

Combining Eqns (7.4) and (7.5), the following equilibrium equations are obtained for deep beams:

$$\sigma_r\sin^2\alpha+\sigma_d\cos^2\alpha+\rho_l f_l=0 \quad (7.6a)$$
$$\sigma_r\cos^2\alpha+\sigma_d\sin^2\alpha+\rho_t f_t=-p \quad (7.6b)$$
$$(\sigma_d-\sigma_r)\sin\alpha\cos\alpha=-v \quad (7.6c)$$

The above equilibrium equations are expressed in terms of s_r and sd because the concrete material law will be expressed in terms of these stresses.

7.3.3 *Strain transformation (compatibility)*

From the compatibility condition of the truss model, it can also be shown (Hsu, 1984) that the average strains (or smeared strains) satisfy Mohr's strain circle, giving:

$$\varepsilon_l=\varepsilon_d\cos^2\alpha+\varepsilon_r\sin^2\alpha \quad (7.7a)$$
$$\varepsilon_t=\varepsilon_d\sin^2\alpha+\varepsilon_r\cos^2\alpha \quad (7.7b)$$
$$\gamma_{lt}=2(\varepsilon_d-\varepsilon_r)\sin\alpha\cos\alpha \quad (7.7c)$$

where ε_l, ε_t are average normal strains in *l*- *a*nd t-directions, respectively (positive for tension), γ_{lt} denotes average shear strains in *l*-t co-ordinate (positive as shown in Figure 7.1 for τ_{lt}) and ε_d, ε_r are average principal strains in d- and r-directions, respectively (positive for tension). The normal strains in the d-r co-ordinate are needed in the concrete material law,

whereas the normal strains in the *l-t* co-ordinate are needed in the material law of the reinforcing bars.

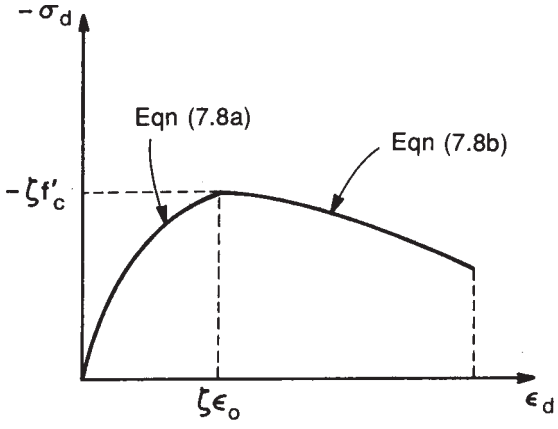

(a) Compression Stress–Strain Relationship

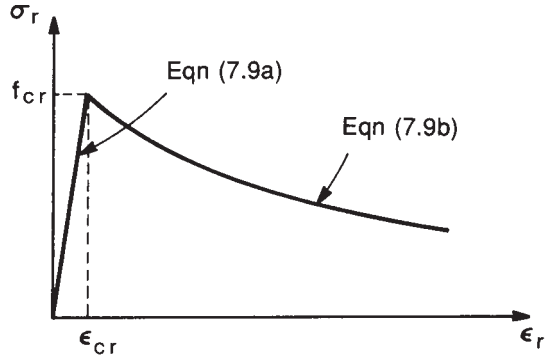

(b) Tension Stress–Strain Relationship

Figure 7.5 Stress-strain relationship for softened concrete

7.3.4 *Material laws*

The stress and strain of concrete in the d-direction is assumed to obey the following material law proposed by Vecchio and Collins (1981) for the softened concrete

$$|\varepsilon_d| \le |\zeta\varepsilon_o| \qquad \sigma_d = \zeta f'_c\left[2\left(\frac{\varepsilon_d}{\zeta\varepsilon_o}\right) - \left(\frac{\varepsilon_d}{\zeta\varepsilon_o}\right)^2\right] \tag{7.8a}$$

$$|\varepsilon_d| > |\zeta\varepsilon_o| \qquad \sigma_d = -\zeta f'_c\left[1-\left(\frac{\varepsilon_d/\varepsilon_o-\zeta}{2-\zeta}\right)^2\right] \tag{7.8b}$$

Eqns (7.8a and b) are plotted in Figure 7.5(a). The stress f'_c is the maximum compressive stress of a non-softened standard cylinder, taken as positive (σd, εd and εo are negative for compression). The strain ε_o is defined as the strain at the maximum compressive stress of non-softened concrete and can be taken as -0.002. The factor ξ is a softening coefficient suggested to be

$$\zeta = \sqrt{\frac{\varepsilon_d}{(1-\mu)\varepsilon_d - \varepsilon_r}} \tag{7.8c}$$

The softening coefficient ξ, which is less than unity, is the reciprocal of the coefficient λ given in previous references (Vecchio and Collins, 1981; Hsu, 1984). The Poisson ratio μ in Eqn (7.8c) is taken as 0.3.

The stress-strain relationship in the r-direction can be expressed by

$$\varepsilon_r \le \varepsilon_{cr} \quad \sigma_r = E_c\varepsilon_r \tag{7.9a}$$

where E_c is the initial modulus of elasticity of concrete, taken to be $-2f'_c/\varepsilon_o$ with ε_o=-0.002, ε_{cr} is the strain at cracking of concrete taken to be f_{cr}/E_c and f_{cr} is the stress at cracking of concrete assumed to be $4\sqrt{f'_c}$, where f'_c and f_{cr} are expressed in psi

$$\varepsilon_r > \varepsilon_{cr} \qquad \sigma_r = f_{cr}\Big/\left(1+\sqrt{\frac{\varepsilon_r-\varepsilon_{cr}}{0.005}}\right) \tag{7.9b}$$

Eqns (7.9a and b) are plotted in Figure 7.5(b).

The stress-strain relationships for the longitudinal and transverse steel bars are assumed to be elastic-perfectly plastic

$$\varepsilon_l \ge \varepsilon_{ly} \qquad f_l = f_{ly} \tag{7.10a}$$
$$\varepsilon_l < \varepsilon_{ly} \qquad f_l = E_s\varepsilon_l \tag{7.10b}$$
$$\varepsilon_t \ge \varepsilon_{ty} \qquad f_t = f_{ty} \tag{7.10c}$$
$$\varepsilon_t < \varepsilon_{ty} \qquad f_t = E_s\varepsilon_t \tag{7.10d}$$

where E_s is the modulus of elasticity of steel bars, f_{lr}, f_{ty} are yield stresses of longitudinal and transverse steel bars, respectively and ε_{ly}, ε_{ty} are yield strains of longitudinal and transverse steel bars, respectively.

The general equations of the softened truss model theory, Eqns (7.4), (7.7–7.10) are described in a summary paper (Hsu, 1988). The equations for deep beams, Eqns (7.5) and (7.6), are given in a separate paper (Mau and Hsu, 1987b).

7.3.5 *Solution algorithm*

Eqns (7.6) to (7.10) are to be solved for a pair of given p and v. However,

the effective transverse compression p and the effective shear stress v are not independent. They are related by a factor that is dependent on the shear-span-to-height ratio a/h. Using Eqns (7.1) and (7.2), one obtains

$$p=Kv \tag{7.11}$$

where $K=2d_v/h \qquad 0<a/h\leq 0.5$ (7.12a)

$$K=\frac{d_v}{h}\left[\frac{4}{3}\left(\frac{h}{a}-\frac{1}{2}\right)\right] \qquad 0.5<a/h\leq 2 \tag{7.12b}$$

$$K=0 \qquad a/h>2 \tag{7.12c}$$

Using Eqn (7.11), Eqns (7.6 b and c) and solving the resulting equation for σ_r:

$$\sigma_r=\frac{\sigma_d\,(K\sin\alpha\cos\alpha-\sin^2\alpha)-\rho_t E_s \varepsilon_t}{K\sin\alpha\cos\alpha+\cos^2\alpha} \qquad \varepsilon_t<\varepsilon_{ty} \tag{7.13a}$$

$$\sigma_r=\frac{\sigma_d\,(K\sin\alpha\cos\alpha-\sin^2\alpha)-\rho_t f_{ty}}{K\sin\alpha\cos\alpha+\cos^2\alpha} \qquad \varepsilon_t\geq\varepsilon_{ty} \tag{7.13b}$$

where ε_t is determined from Eqn (7.7b).

Using Eqns (7.10a or b) and (7.7a), the remaining equilibrium condition Eqn (7.6a) can be used to solve for the angle α

$$\cos^2\alpha=\frac{\sigma_r+\rho_l E_s \varepsilon_r}{\sigma_r-\sigma_d+\rho_l E_s(\varepsilon_d-\varepsilon_r)} \qquad \varepsilon_l<\varepsilon_{ly} \tag{7.14a}$$

$$\cos^2\alpha=\frac{\sigma_r+\rho_l f_{ly}}{\sigma_r-\sigma_d} \qquad \varepsilon_l\geq\varepsilon_{ly} \tag{7.14b}$$

The five Eqns (7.8a or b), (7.8c), (7.9a or b), (7.13a or b) and (7.14a or b) include six unknowns: σ_d, σ_r, ε_d, ε_r, α, and ξ. When one unknown is given, the other five can be solved. The solution of the five simultaneous equations follows a simple iterative procedure. With the help of a computer, this procedure is used to trace the response history of the shear element and to locate the maximum shear sustained by the shear element. The tracing procedure is controlled by the compression strain ε_d, the magnitude of which increases monotonically from zero.

1. Select a value for ε_d
2. Assume a value of ε_r
3. Calculate σ_r, using Eqn (7.9a or b)
4. Calculate ξ, using Eqn (7.8c)
5. Calculate σ_d, using Eqn (7.8a or b)
6. Solve for α, using Eqn (7.14a or 14b) and check el to make sure the correct Eqn (7.14) has been used.
7. Calculate σ_r using Eqn (7.13a) or (b) and check ε_t to make sure the correct Eqn (7.13) has been used.

8. Compare the two values of σ_r obtained in step 3 and step 7. If they are within a small error, the assumed value of ε_r is accepted and the solution procedure continues at step 10.
9. If the error in σ_r is too large, iteration continues from step 2 to step 8 by sweeping through possible values of ε_r.
10. Calculate γ_{lt} [Eqn (7.7c)] and v [Eqn (7.6c)].
11. Select another εd with a suitable increment and repeat step 1 to step 10. In this way, the loading history of v vs. γ_{lt} can be traced and the maximum shear stress can be determined. The maximum shear stress is defined as the shear strength v_n.

7.3.6 *Accuracy*

A total of 64 test specimens are available in the literature to compare with the proposed theory. They were reported by Smith and Vansiotis (1982), Kong, Robins and Cole (1970), and de Paiva and Siess (1965). The basic data are listed in Table 7.1. The specimens were selected because they satisfy the following conditions: i) the test specimen must fail in web shear mode, not in bearing or flexural modes; ii) the test specimen must contain at least a minimum amount of transverse web reinforcement specified in the ACI Code (1989) to render the truss model applicable; iii) the span-depth ratio *a/h* must be less than 2; and iv) the test specimens must be simply supported at the bottom surface and the loads acting on the top surface of the beam.

In calculating the longitudinal steel ratio of the shear element, the longitudinal steel reinforcement provided at the bottom and the top of the beam is also included. This is because the expansion of the element in the longitudinal direction due to shear is restrained by the longitudinal steel in the top and bottom bars. Thus tests on beams with no horizontal web reinforcements can still be used for comparison. The effective depth of the shear element d_v is taken as the distance between the centre of the compression steel and the centre of the tension steel. When compression steel reinforcement is not provided, the depth d' is estimated as 0.1d.

The theoretical values of the normalised shear strength, $(v_n/f'_c)_T$, are computed according to the procedure outlined in the previous section. The results are listed in Table 7.2. Using the ratio of calculated shear strength to test shear strength R_T as an indicator, the mean and standard deviation of this ratio for the 64 data are 1.028 and 0.094, respectively. The agreement between theory and test is quite good. A comparison of the theoretical and experimental shear strengths is also presented in Figure 7.6.

The sensitivity of the shear strength to the magnitude of the effective transverse compression is studied using the available test specimens. The available test specimens are divided into nine groups based on the different *a/h* ratios ranging from 0.33 to 1.29. These nine groups are identified in Table 7.1 as SA, SB, SC, K30, K25, K20, K15, K10, and PS. As the effective

Table 7.1 Basic data of the test specimens

No.	Speci.	Group	ρ_w %	ρ_{vt} %	ρ_c %	ρ_t %	ρ_t %	f_{ty} psi	f_{ty} psi	E_s ksi	f_c' psi	L in	a' in	a in	x in	h in	d in	b in
1	1A1-10	SA	1.94	0.23	0.10	2.15	0.28	62500	63430	27000	2710	28	10.0	12.0	8.0	14	12.0	4
2	1A3-11	SA	1.94	0.45	0.10	2.36	0.28	62500	63400	27000	2615	28	10.0	12.0	8.0	14	12.0	4
3	1A4-12	SA	1.94	0.68	0.10	2.46	0.28	62500	63400	27000	2330	28	10.0	12.0	8.0	14	12.0	4
4	1A4-51	SA	1.94	0.68	0.10	2.46	0.28	62500	63430	27000	2980	28	10.0	12.0	8.0	14	12.0	4
5	1A6-37	SA	1.94	0.91	0.10	2.67	0.28	62500	63430	27000	3050	28	10.0	12.0	8.0	14	12.0	4
6	2A1-38	SA	1.94	0.23	0.10	2.15	0.63	62500	63430	27000	3145	28	10.0	12.0	8.0	14	12.0	4
7	2A3-39	SA	1.94	0.45	0.10	2.36	0.63	62500	63430	27000	2865	28	10.0	12.0	8.0	14	12.0	4
8	2A4-40	SA	1.94	0.68	0.10	2.46	0.63	62500	63430	27000	2950	28	10.0	12.0	8.0	14	12.0	4
9	2A6-61	SA	1.94	0.91	0.10	2.67	0.63	62500	63430	27000	2775	28	10.0	12.0	8.0	14	12.0	4
10	3A1-42	SA	1.94	0.23	0.10	2.15	1.25	62500	63430	27000	2670	28	10.0	12.0	8.0	14	12.0	4
11	3A3-43	SA	1.94	0.45	0.10	2.36	1.25	62500	63430	27000	2790	28	10.0	12.0	8.0	14	12.0	4
12	3A4-45	SA	1.94	0.68	0.10	2.46	1.25	62500	63430	27000	3020	28	10.0	12.0	8.0	14	12.0	4
13	3A6-46	SA	1.94	0.91	0.10	2.67	1.25	62500	63430	27000	2890	28	10.0	12.0	8.0	14	12.0	4
14	1B1-04	SB	1.94	0.23	0.10	2.15	0.24	62500	63430	27000	3200	33	12.5	14.5	10.5	14	12.0	4
15	1B3-29	SB	1.94	0.45	0.10	2.36	0.24	62500	63430	27000	2915	33	12.5	14.5	10.5	14	12.0	4
16	1B4-40	SB	1.94	0.68	0.10	2.46	0.24	62500	63430	27000	3020	33	12.5	14.5	10.5	14	12.0	4
17	1B6-31	SB	1.94	0.91	0.10	2.67	0.24	62500	63430	27000	2830	33	12.5	14.5	10.5	14	12.0	4
18	2B1-05	SB	1.94	0.23	0.10	2.15	0.42	62500	63430	27000	2780	33	12.5	14.5	10.5	14	12.0	4
19	2B3-06	SB	1.94	0.45	0.10	2.36	0.42	62500	63430	27000	2755	33	12.5	14.5	10.5	14	12.0	4
20	2B4-07	SB	1.94	0.68	0.10	2.46	0.42	62500	63430	27000	2535	33	12.5	14.5	10.5	14	12.0	4
21	2B4-52	SB	1.94	0.68	0.10	2.46	0.42	62500	63430	27000	3160	33	12.5	14.5	10.5	14	12.0	4
22	2B6-32	SB	1.94	0.91	0.10	2.67	0.42	62500	63430	27000	2865	33	12.5	14.5	10.5	14	12.0	4
23	3B1-08	SB	1.94	0.23	0.10	2.15	0.63	62500	63430	27000	2355	33	12.5	14.5	10.5	14	12.0	4
24	3B1-36	SB	1.94	0.23	0.10	2.15	0.77	62500	63430	27000	2960	33	12.5	14.5	10.5	14	12.0	4
25	3B3-33	SB	1.94	0.45	0.10	2.36	0.77	62500	63430	27000	2755	33	12.5	14.5	10.5	14	12.0	4
26	3B4-34	SB	1.94	0.68	0.10	2.46	0.77	62500	63430	27000	2790	33	12.5	14.5	10.5	14	12.0	4
27	3B6-35	SB	1.94	0.91	0.10	2.67	0.77	62500	63430	27000	2995	33	12.5	14.5	10.5	14	12.0	4
28	4B1-09	SB	1.94	0.23	0.10	2.15	1.25	62500	63430	27000	2480	33	12.5	14.5	10.5	14	12.0	4
29	1C1-14	SC	1.94	0.23	0.10	2.15	0.18	62500	63430	27000	2790	40	16.0	18.0	14.0	14	12.0	4
30	1C3-02	SC	1.94	0.45	0.10	2.36	0.18	62500	63430	27000	3175	40	16.0	18.0	14.0	14	12.0	4
31	1C4-15	SC	1.94	0.68	0.10	2.46	0.18	62500	63430	27000	3290	40	16.0	18.0	14.0	14	12.0	4
32	1C6-16	SC	1.94	0.91	0.10	2.67	0.18	62500	63430	27000	3160	40	16.0	18.0	14.0	14	12.0	4
33	2C1-17	SC	1.94	0.23	0.10	2.15	0.31	62500	63430	27000	2880	40	16.0	18.0	14.0	14	12.0	4
34	2C3-03	SC	1.94	0.45	0.10	2.36	0.31	62500	63430	27000	2790	40	16.0	18.0	14.0	14	12.0	4
35	2C3-27	SC	1.94	0.45	0.10	2.36	0.31	62500	63430	27000	2800	40	16.0	18.0	14.0	14	12.0	4
36	2C4-18	SC	1.94	0.68	0.10	2.46	0.31	62500	63430	27000	2965	40	16.0	18.0	14.0	14	12.0	4
37	2C6-19	SC	1.94	0.91	0.10	2.67	0.31	62500	63430	27000	3010	40	16.0	18.0	14.0	14	12.0	4
38	3C1-20	SC	1.94	0.23	0.10	2.15	0.56	62500	63430	27000	3050	40	16.0	18.0	14.0	14	12.0	4
39	3C3-21	SC	1.94	0.45	0.10	2.36	0.56	62500	63430	27000	2400	40	16.0	18.0	14.0	14	12.0	4
40	3C4-22	SC	1.94	0.68	0.10	2.46	0.56	62500	63430	27000	2650	40	16.0	18.0	14.0	14	12.0	4
41	3C6-23	SC	1.94	0.91	0.10	2.67	0.56	62500	63430	27000	2755	40	16.0	18.0	14.0	14	12.0	4
42	4C1-24	SC	1.94	0.23	0.10	2.15	0.77	62500	63430	27000	2840	40	16.0	18.0	14.0	14	12.0	4
43	4C3-04	SC	1.94	0.45	0.10	2.36	0.63	62500	63430	27000	2690	40	16.0	18.0	14.0	14	12.0	4
44	4C3-28	SC	1.94	0.45	0.10	2.36	0.77	62500	63430	27000	2790	40	16.0	18.0	14.0	14	12.0	4
45	4C4-25	SC	1.94	0.68	0.10	2.46	0.77	62500	63430	27000	2685	40	16.0	18.0	14.0	14	12.0	4
46	4C6-26	SC	1.94	0.91	0.10	2.67	0.77	62500	63430	27000	3080	40	16.0	18.0	14.0	14	12.0	4
47	4D1-13	–	1.94	0.23	0.10	2.67	0.42	62500	63430	27000	2330	58	23.0	25.0	21.0	14	12.0	4
48	1-30	K30	0.52	0.00	0.00	0.52	2.45	41600	40600	29000	3120	27	8.5	10.0	7.0	30	28.5	3
49	1-25	K25	0.63	0.00	0.00	0.63	2.45	41600	40600	29000	3560	27	8.5	10.0	7.0	25	23.5	3
50	1-20	K20	0.80	0.00	0.00	0.80	2.45	41600	40600	29000	3080	27	8.5	10.0	7.0	20	18.5	3
51	1-15	K15	1.09	0.00	0.00	1.09	2.45	41600	40600	29000	3080	27	8.5	10.0	7.0	15	13.5	3
52	1-10	K10	1.73	0.00	0.00	1.73	2.45	41600	40600	29000	3140	27	8.5	10.0	7.0	10	8.5	3
53	2-30	K30	0.52	0.00	0.00	0.52	0.86	41600	44000	29000	2785	27	8.5	10.0	7.0	30	28.5	3
54	2-25	K25	0.63	0.00	0.00	0.63	0.86	41600	44000	29000	2700	27	8.5	10.0	7.0	25	23.5	3
55	2-20	K20	0.80	0.00	0.00	0.80	0.86	41600	44000	29000	2880	27	8.5	10.0	7.0	20	18.5	3
56	2-15	K15	1.09	0.00	0.00	1.09	0.86	41600	44000	29000	3300	27	8.5	10.0	7.0	15	13.5	3
57	2-10	K10	1.73	0.00	0.00	1.73	0.86	41600	44000	29000	2920	27	8.5	10.0	7.0	10	8.5	3
58	5-30	K30	0.52	0.61	0.00	1.13	0.61	40600	40600	29000	2690	27	8.5	10.0	7.0	30	28.5	3
59	5-25	K25	0.63	0.61	0.00	1.24	0.61	40600	40600	29000	2790	27	8.5	10.0	7.0	25	23.5	3
60	5-20	K20	0.80	0.61	0.00	1.41	0.61	40600	40600	29000	2920	27	8.5	10.0	7.0	20	18.5	3
61	5-15	K15	1.09	0.61	0.00	1.70	0.61	40600	40600	29000	3180	27	8.5	10.0	7.0	15	13.5	3
62	5-10	K10	1.73	0.61	0.00	2.34	0.61	40600	40600	29000	3270	27	8.5	10.0	7.0	10	8.5	3
63	G33S-12	PS	1.67	0.00	0.92	2.59	1.09	47300	32000	29000	2890	20	6.0	8.0	4.0	9	8.0	3
64	G33S-32	PS	2.58	0.00	0.83	3.41	1.09	44200	32000	29000	2910	20	6.0	8.0	4.0	9	8.0	3

transverse compression is assumed to be a function of *a/h* ratio, the magnitude of the transverse compression may be changed individually for each group to see its effect on the calculated shear strength. The non-dimensionalised factor *K,* which varies from approximately 1.6 to 0 as calculated from Eqn (7.12), is taken as the benchmark value and a variation of *K,* designated as ΔK, is introduced up to ±0.25 (Figure 7.7). The resulting variation of the calculated

Table 7.2 Experimental and computed results

Specimen Number	ζ	α, deg	$\left(\frac{v_n}{f_c'}\right)_T$	L/d	d_v	ω_ℓ	ω_t	K	$V_{n,\,test}$ lb	$\left(\frac{v_n}{f_c'}\right)_F$	R_T	R_F
1	0.56	44.2	0.288	2.33	11.0	0.496	0.066	0.70	36250	0.296	0.95	0.97
2	0.57	44.0	0.294	2.33	11.0	0.564	0.068	0.70	33350	0.298	1.01	1.03
3	0.58	44.0	0.304	2.33	11.0	0.660	0.076	0.70	31750	0.300	0.98	0.97
4	0.56	43.8	0.286	2.33	11.0	0.516	0.060	0.70	38430	0.292	0.98	0.99
5	0.56	43.6	0.287	2.33	11.0	0.547	0.058	0.70	41385	0.291	0.93	0.94
6	0.56	46.0	0.290	2.33	11.0	0.427	0.127	0.70	39230	0.300	1.02	1.06
7	0.58	45.8	0.301	2.33	11.0	0.515	0.139	0.70	38350	0.300	0.99	0.99
8	0.58	45.6	0.300	2.33	11.0	0.521	0.135	0.70	38650	0.300	1.01	1.01
9	0.59	45.5	0.308	2.33	11.0	0.601	0.144	0.70	36400	0.300	1.03	1.01
10	0.60	47.6	0.313	2.33	11.0	0.503	0.297	0.70	36200	0.300	1.01	0.97
11	0.61	47.4	0.313	2.33	11.0	0.529	0.284	0.70	38830	0.300	0.99	0.95
12	0.60	47.3	0.310	2.33	11.0	0.509	0.263	0.70	40140	0.300	1.02	0.99
13	0.61	47.0	0.316	2.33	11.0	0.577	0.274	0.70	37800	0.300	1.06	1.01
14	0.48	39.5	0.241	2.75	11.0	0.420	0.048	0.49	33150	0.236	1.02	1.00
15	0.50	39.9	0.255	2.75	11.0	0.506	0.052	0.49	32275	0.240	1.01	0.96
16	0.50	39.7	0.253	2.75	11.0	0.509	0.050	0.49	31550	0.239	1.06	1.01
17	0.52	39.8	0.262	2.75	11.0	0.590	0.054	0.49	34475	0.242	0.94	0.87
18	0.53	42.3	0.272	2.75	11.0	0.483	0.096	0.49	29000	0.274	1.15	1.16
19	0.54	42.0	0.275	2.75	11.0	0.535	0.097	0.49	29500	0.275	1.13	1.13
20	0.55	42.0	0.282	2.75	11.0	0.607	0.105	0.49	28350	0.281	1.11	1.10
21	0.53	41.7	0.266	2.75	11.0	0.487	0.084	0.49	33700	0.266	1.10	1.10
22	0.54	41.6	0.276	2.75	11.0	0.582	0.093	0.49	32650	0.272	1.07	1.05
23	0.56	43.8	0.294	2.75	11.0	0.571	0.170	0.49	29400	0.291	1.04	1.03
24	0.55	44.3	0.283	2.75	11.0	0.454	0.165	0.49	35735	0.291	1.03	1.06
25	0.56	44.1	0.291	2.75	11.0	0.535	0.177	0.49	35600	0.291	0.99	0.99
26	0.56	43.9	0.291	2.75	11.0	0.551	0.175	0.49	34850	0.291	1.03	1.02
27	0.56	43.6	0.289	2.75	11.0	0.557	0.163	0.49	36350	0.291	1.02	1.05
28	0.59	45.9	0.307	2.75	11.0	0.542	0.320	0.49	34500	0.291	0.97	0.92
29	0.41	33.7	0.200	3.33	11.0	0.482	0.041	0.29	26750	0.192	0.92	0.88
30	0.40	32.8	0.190	3.33	11.0	0.465	0.036	0.29	27750	0.187	0.96	0.94
31	0.40	32.6	0.188	3.33	11.0	0.467	0.035	0.29	29450	0.185	0.92	0.91
32	0.41	32.7	0.194	3.33	11.0	0.528	0.036	0.29	27500	0.187	0.98	0.95
33	0.45	36.9	0.225	3.33	11.0	0.467	0.068	0.29	27900	0.216	1.02	0.98
34	0.47	36.9	0.232	3.33	11.0	0.529	0.070	0.29	23300	0.218	1.22	1.15
35	0.47	36.9	0.231	3.33	11.0	0.527	0.070	0.29	25925	0.218	1.10	1.03
36	0.46	36.4	0.226	3.33	11.0	0.519	0.066	0.29	28000	0.215	1.05	1.00
37	0.46	36.2	0.227	3.33	11.0	0.554	0.065	0.29	27900	0.214	1.08	1.01
38	0.51	41.2	0.257	3.33	11.0	0.441	0.116	0.29	31650	0.253	1.09	1.07
39	0.54	41.1	0.277	3.33	11.0	0.615	0.148	0.29	28100	0.255	1.04	0.96
40	0.53	40.9	0.270	3.33	11.0	0.580	0.134	0.29	28700	0.255	1.10	1.04
41	0.53	40.6	0.269	3.33	11.0	0.606	0.129	0.29	30850	0.255	1.06	1.00
42	0.53	42.6	0.272	3.33	11.0	0.473	0.172	0.29	32950	0.255	1.03	0.97
43	0.53	41.5	0.272	3.33	11.0	0.548	0.149	0.29	28900	0.255	1.12	1.04
44	0.54	42.3	0.276	3.33	11.0	0.529	0.175	0.29	34250	0.255	0.99	0.91
45	0.55	42.1	0.280	3.33	11.0	0.573	0.182	0.29	34300	0.255	0.96	0.88
46	0.54	41.7	0.272	3.33	11.0	0.542	0.159	0.29	35850	0.255	1.03	0.96
47	0.46	36.1	0.231	4.83	11.0	0.716	0.114	0.29	19650	–	1.20	–
48	0.53	62.3	0.215	0.95	25.7	0.069	0.319	1.71	53700	0.236	0.96	1.06
49	0.53	62.1	0.216	1.15	21.2	0.074	0.279	1.69	50400	0.244	0.97	1.09
50	0.58	60.1	0.263	1.46	16.7	0.108	0.323	1.67	42600	0.300	0.95	1.08
51	0.54	55.2	0.271	2.00	12.2	0.147	0.323	1.08	36900	0.289	0.82	0.88
52	0.58	48.7	0.299	3.18	7.7	0.229	0.317	0.51	20100	0.280	1.07	1.00
53	0.57	62.5	0.238	0.95	25.7	0.078	0.136	1.71	56000	0.253	0.91	0.97
54	0.60	61.5	0.265	1.15	21.2	0.097	0.140	1.69	50400	0.286	0.90	0.97
55	0.62	60.6	0.285	1.46	16.7	0.116	0.131	1.67	48400	0.300	0.85	0.89
56	0.49	54.7	0.248	2.00	12.2	0.137	0.115	1.08	31400	0.275	0.95	1.05
57	0.55	45.4	0.283	3.18	7.7	0.246	0.130	0.51	22400	0.292	0.85	0.87
58	0.72	59.6	0.328	0.95	25.7	0.171	0.092	1.71	53800	0.300	1.26	1.15
59	0.72	59.0	0.330	1.15	21.2	0.180	0.089	1.69	46800	0.300	1.25	1.13
60	0.71	58.2	0.332	1.46	16.7	0.196	0.085	1.67	38800	0.300	1.25	1.13
61	0.60	50.2	0.305	2.00	12.2	0.217	0.078	1.08	28600	0.300	1.24	1.22
62	0.50	40.5	0.255	3.18	7.7	0.291	0.076	0.51	17500	0.272	1.09	1.17
63	0.61	46.5	0.315	2.50	7.3	0.424	0.121	0.67	19000	0.300	1.04	0.99
64	0.62	45.8	0.324	2.50	7.3	0.518	0.120	0.67	22800	0.300	0.90	0.83

shear strength is represented by the mean calculated-to-test shear strength ratio in Figure 7.8. This Figure shows that the mean values change by less than ±5% from the benchmark value at ΔK=0, except in groups SB and SC when K is small. For these two groups, K is equal to 0.49 (SB) and 0.29 (SC) while the mean values change by more than ±10%.

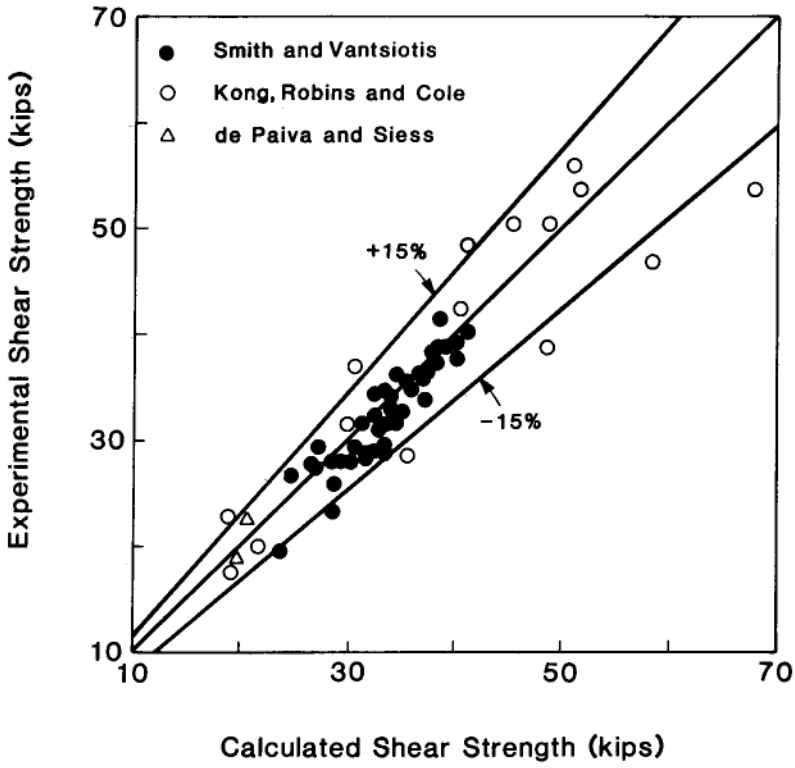

Figure 7.6 Comparison of calculated and experimental shear strength

7.4 Parametric study

Parametric studies will now be carried out to investigate the variation of shear strength with respect to the important factors involved. A close examination of the governing Eqns (7.6)–(7.10) reveals that the normalised shear strength v_n/f'_c is mainly affected by the two dimensionless parameters $\rho_l f_{ly}/f'_c$ and $\rho_t f_{ty}/f'_c$. Together with the parameter a/h inherent in K, these three parameters represent the amount of longitudinal reinforcement, the amount of transverse reinforcement, and the geometry of the beam, respectively. The first two parameters may be called the longitudinal reinforcement index and the transverse reinforcement index.

7.4.1 *Shear-span-to-height ratio*

The four curves in Figure 7.9 show the variation of the shear strength with respect to the shear-span-to-height ratio. Because each curve represents a different amount of reinforcement in the beam the four curves together cover the practical range of longitudinal and transverse reinforcement ratios. For transverse reinforcement, the minimum percentage is 0.0025

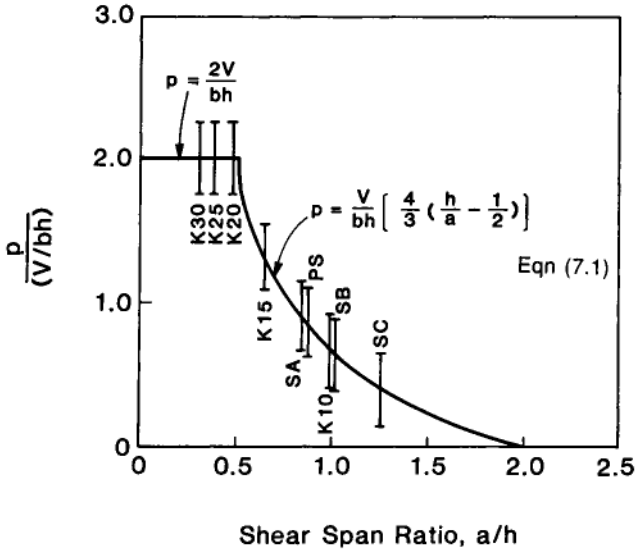

Figure 7.7 Variation of effective transverse compression (?K=±0.25)

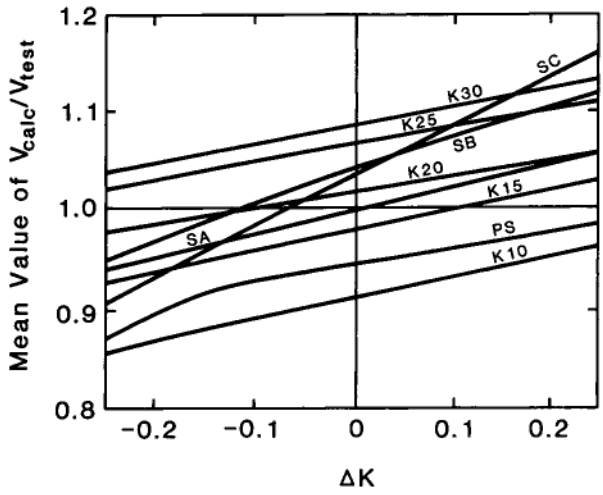

Figure 7.8 Sensitivity of shear strength to effective transverse compression

based on the ACI Building Code. For longitudinal reinforcement, the minimum is 0.0060, which is approximately the sum of the minimum web steel ratio (0.0025) and the minimum flexural steel ratio ($200/f_{ly}$). Figure 7.9 indicates that the shear strength ratio v_n/f'_c generally decreases with increasing a/h ratio. The rate of decrease is larger for the two cases with

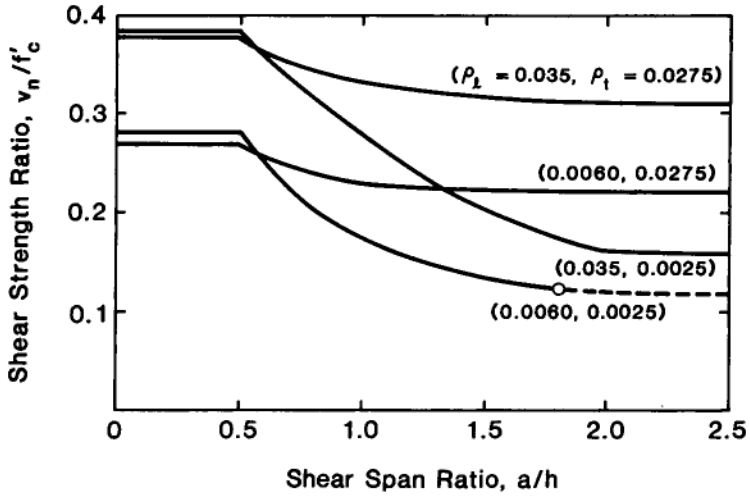

Figure 7.9 Effect of shear-span ratio on shear strength

low ratio of transverse reinforcement (0.0025). The dotted part of a curve represents the region where the present iterative algorithm fails to converge to a solution. This is due mainly to a very small amount of reinforcement.

7.4.2 *Longitudinal reinforcement*

The effect of the longitudinal reinforcement index $\rho_l f_{ly}/f'_c$ on the shear strength ratio v_n/f'_c is shown in Figure 7.10 for six combinations of shear span

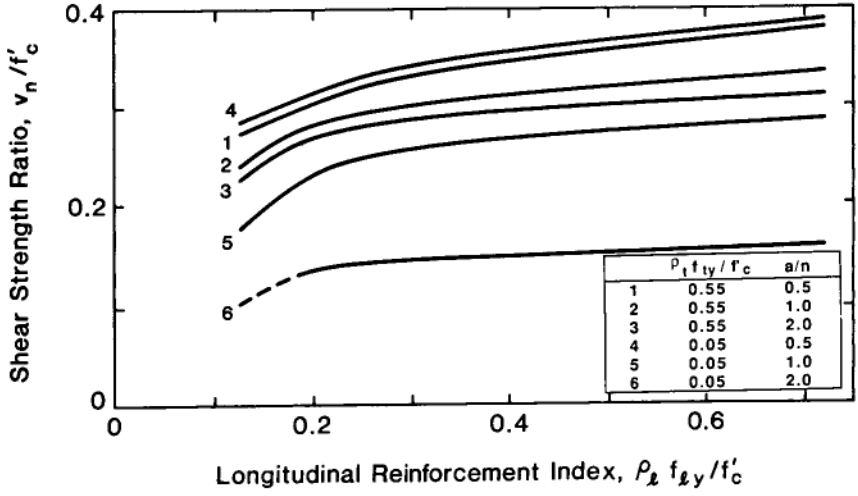

Figure 7.10 Effect of longitudinal reinforcement index on shear strength

ratios *a/h* and transverse reinforcement indices $\rho_t f_{ty}/f'_c$. For all six cases, the shear strength ratio increases with the increase of longitudinal reinforcement index. This means that the longitudinal steel is effective for *a/h* ratios from 0.5 to 2 and with transverse reinforcement indices from 0.05 to 0.55. The effectiveness is relatively large when the longitudinal reinforcement index varies from 0.1 to 0.3 but becomes gradually smaller at higher range.

7.4.3 *Transverse reinforcement*

The variation of shear strength ratio as a function of the transverse reinforcement index is shown in Figure 7.11 for six combinations of shear span ratios and longitudinal reinforcement indices. For large *a/h* ratios of 1.0 and 2.0 (cases 2,3,5 and 6), v_n/f'_c increases with the increase of $\rho_t f_{ty}/f'_c$ especially in the low range. For small *a/h* ratio of 0.5 (cases 1 and 4), however, v_n/f'_c decreases slightly with the increase of $\rho_t f_{ty}/f'_c$. This is because under large effective transverse compression, (i.e. small *a/h* ratio) more transverse reinforcement leads to relatively less compressive strain ε_d and this in turn leads to more softening of the concrete according to Eqn (7.8c)

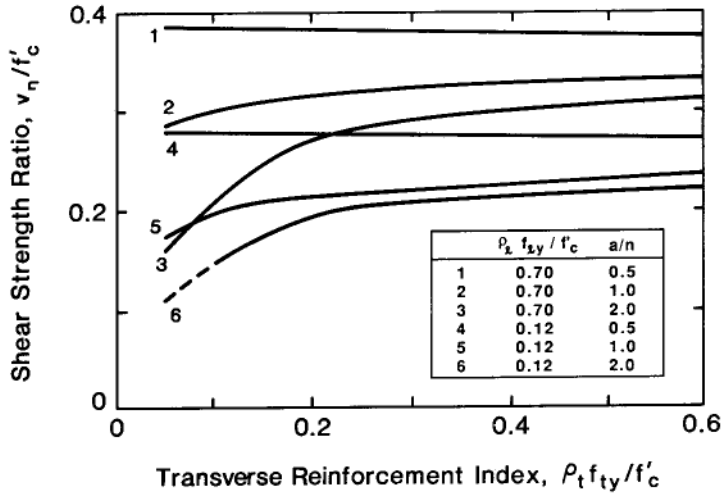

Figure 7.11 Effect of transverse reinforcement index on shear strength

The ineffectiveness of the transverse reinforcement in the range of low *a/h* ratios can also be observed from the tests of Kong *et al.* (1970). Three pairs of their test specimens with *a/h* ratios less than 0.5 are listed in Table 7.3.

In each pair of beams (1–30 versus 2–30; 1–25 versus 2–25, and 1–20 versus 2–20), the *a/h* ratio and the longitudinal steel percentage are identical, but the transverse steel percentage ρ_t differs greatly, 0.0245 versus 0.0086. It can be seen that the three beams with lower ρ_t (0.0086) all have

experimental maximum shear forces equal to or greater than those of the corresponding beams with higher ρ_t (0.0245).

In view of the theory and the above tests, it seems reasonable to state that the effectiveness of transverse reinforcement decreases when *a/h* ratio decreases from 2 to 0.5. When $a/h \leq 0.5$ an increase of transverse reinforcement beyond the ACI Code minimum requirement, ρ_t=0.25%, is not effective in increasing the shear strength of deep beams.

Table 7.3 Effect of tensverse reinforcement at low *a/h* ratios

Specimens	$\frac{a}{h}$	ρ_l	ρ_t	f_c' psi	$V_{n,\,test}$ lb
1-30	0.33	0.0052	0.0245	3120	53,700
2-30	0.33	0.0052	0.0086	2785	56,000
1-25	0.40	0.0063	0.0245	3560	50,400
2-25	0.40	0.0063	0.0086	2700	50,400
1-20	0.50	0.0080	0.0245	3080	42,600
2-20	0.50	0.0080	0.0086	2880	48,400

1 psi = 6984.8 N/m^2; 1 lb = 4.448 N.

7.5 Explicit shear strength equation

7.5.1 *Derivation of equation*

The accuracy of the theoretical results confirms the usefulness of the theoretical model. However, the solution procedure is too complicated to be used in design. An explicit formula suitable for practical design is presented in this section. The formula is derived from the three equilibrium Eqns (7.6a-c) alone. Recognising that the three quantities σ_t, $\rho_l f_l$, and $\rho_t f_t$ may be estimated, the shear capacity v may be expressible in terms of these three quantities by eliminating the other unknowns σ_d and α from Eqns (7.6a-c). This is achieved by the following manipulation.

Utilizing the identity $\sin^2\alpha+\cos^2\alpha=1$, one may rewrite Eqns (7.6a and b) as

$$(\sigma_d-\sigma_r)\cos^2\alpha=-\rho_l f_l-\sigma_r \qquad (7.15a)$$

$$(\sigma_d-\sigma_r)\sin^2\alpha=-K_v-\rho_t f_t-\sigma_r \qquad (7.15b)$$

Eqn (7.6c) may be squared to become

$$(\sigma_d-\sigma_r)^2\sin^2\alpha\cos^2\alpha=v^2 \qquad (7.15c)$$

Multiplying Eqn (7.15a) by Eqn (7.15b) and subtracting the result from Eqn (7.15c) gives:

$$v^2-(\rho_l f_l+\sigma_r)(K_v+\rho_t f_t+\sigma_r)=0 \qquad (7.16)$$

This is a quadratic equation in v and a solution for v gives an explicit expression

$$v = \frac{1}{2}\left[K(\rho_l f_l + \sigma_r) + \sqrt{K^2(\rho_l f_l + \sigma_r)^2 + 4(\rho_l f_l + \sigma_r)(\rho_t f_t + \sigma_r)}\right] \quad (7.17)$$

Assuming the yielding of steel, the variables $\rho_l f_l$ and $\rho_t f_t$ in Eqn (7.17) can be non-dimensionalized by using the definition of the reinforcement index, ω

$$\omega_l = \rho_l f_l / f'_c = \rho_l f_y / f'_c \quad (7.18a)$$
$$\omega_t = \rho_t f_t / f'_c = \rho_t f_y / f'_c \quad (7.18b)$$

Also

$$C = \sigma_r / f'_c \quad (7.18c)$$

Dividing Eqn (7.17) f'_c by and substituting ω_l, ω_t and C from Eqn (7.18) into (7.17) results in an explicit and non-dimensional formula

$$\frac{v_n}{f'_c} = \frac{1}{2}\left[K(\omega_l + C) + \sqrt{K^2(\omega_l + C)^2 + 4(\omega_l + C)(\omega_t + C)}\right] \quad (7.19)$$

The shear strength v_n is controlled by the yielding of the steel if ω_l and ω_t are limited to a maximum value as follows:

$$\omega_l \le C_l \quad (7.20a)$$
$$\omega_t \le C_t \quad (7.20b)$$

If the reinforcement indices exceed the limiting value, the shear strength may not be controlled by the yielding of the steel. In such cases, Eqn (7.19) is still applicable with the upper limits of Eqn (7.20) in effect, except the result may be slightly on the conservative side.

The parametric studies show that the shear strength tends to increase only slightly beyond certain value, Figures 7.10 and 7.11. Thus, for all practical purposes, the shear strength may also be limited by

$$v_n / f'_c \le C_s \quad (7.20c)$$

The four constants *C, C_l, C_t* and C_s can be obtained by calibration with the test data of Table 7.1.

7.5.2 *Calibration*

To calibrate the four constants, the experimental data compiled in Table 7.1 will be used. These data were for simply-supported deep beams loaded by concentrated forces. All the beams had vertical web reinforcements. Of the 64 specimens compiled, one is for a beam with *a/h*=1.79 (*L/d*=4.83) and all the others have *a/h*<1.3 (*L/d*≤3.3). As it is not reasonable to calibrate a formula with only one test in that range of *a/h,* it is decided to drop that single test and limit the applicability of the formula to *a/h*<1.3 or *L/d*≤3.3. The listed reinforcement ratio for the horizontal web steel ?v_l is based on the

vertical spacing of the steel, S_2 and width of beam b, while the reinforcement ratio for the total horizontal steel ρ_l is based on the total steel area and the effective cross-sectional area, bd.

For any given set of the C values the ratio of the calculated shear strength to the experimental shear strength R_F for each test is determined. The mean value and the coefficient of variation of this ratio for the 63 tests are then computed. A search for the least coefficient of variation leads to the following set of C values: C=0.03, C_l=0.26, C_t=0.12 and C_s=0.3.

Substituting these constants into Eqn (7.19) gives the explicit formula proposed for shear strength design:

$$\frac{v_n}{f'_c} = \frac{1}{2}\left[K(\omega_l + 0.03) + \sqrt{K^2(\omega_l + 0.03)^2 + 4(\omega_l + 0.03)(\omega_t + 0.03)}\right] \leq 0.3 \tag{7.21}$$

with the limitations $\omega_l = \rho_l f_y / f'_c \leq 0.26$ and $\omega_t = \rho_t f_t / f'_c \leq 0.12$. The coefficient K, representing the shear span effect, is given in Eqn (7.12). The shear strength V_n is then obtained from Eqn (7.2).

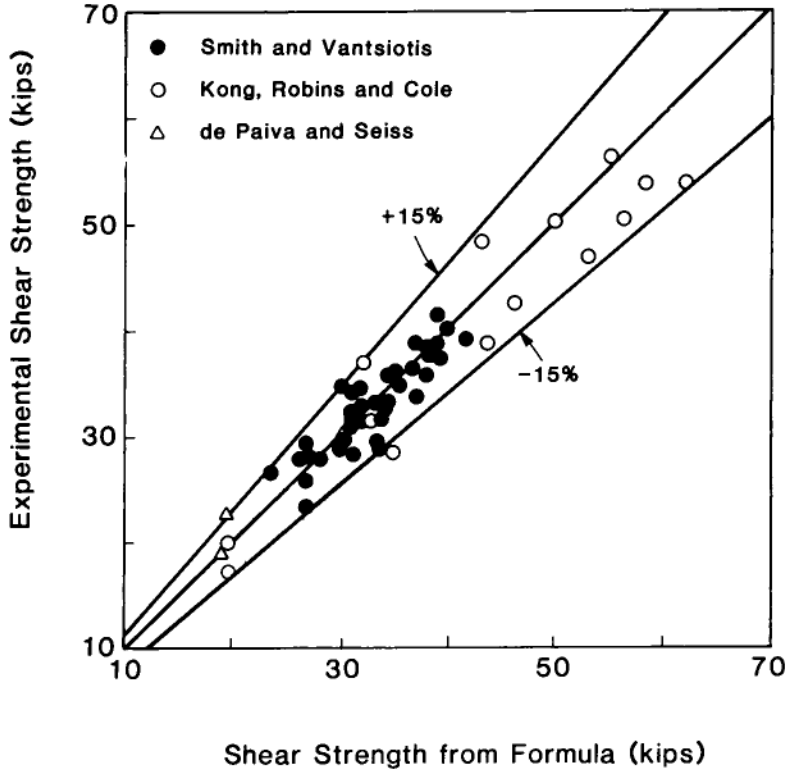

Figure 7.12 Comparison of proposed explicit formula (Eqn 7.21) with tests

The computed normalised shear strength $(v_n/f'_c)_F$ and R_F values are given in Table 2. The mean value of R_F for Eqn (7.21) is 1.008 and the coefficient of variation is 0.082. Also shown in Table 7.2 is the ratio for the theoretical shear strength from the softened truss model to the experimental shear strength R_T The mean value and the coefficient of variation of R_T for the 63 specimens are 1.025 and 0.092, respectively. It is observed that the proposed explicit formula gives as good a prediction as the more rigorous and complicated theory. The shear strengths calculated from Eqn (7.21) and Eqn (7.2) are plotted in Figure 7.12 against the experimental shear strengths for the 63 specimens. It is seen that only one of the data points falls slightly below the lower 15% line. Eqn. (7.21) has also been compared to other empirical formulas found in literature (Mau and Hsu, 1989). The comparison shows that the proposed explicit formula has the least coefficient of variation.

7.6 Conclusions

i) The softened truss model theory is shown to predict with reasonable accuracy the shear strength of simply-supported beams with transverse web reinforcement and having shear-span to height ratio *(a/h)* between 0.33 and 2.

ii) Three non-dimensionalised parameters are identified as having major effect on the shear strength of deep beams. They are the shear span ratio, the transverse reinforcement index, and the longitudinal reinforcement index. The present theory predicts that the effectiveness of transverse reinforcement decreases when the *a/h* ratio decreases from 2 to 0.5. For small *a/h* ratio below 0.5, the transverse reinforcement is ineffective in increasing the shear strength.

iii) An explicit formula is proposed for shear strength design. This non-dimensional formula expresses the shear strength ratio as a function of shear span ratio, (through K), longitudinal reinforcement index and transverse reinforcement index. This formula has been calibrated to the available test data in the following range: $0.95 \le L/d \le 3.3$, $0 \le \rho_{vl} = A_{vl}/bS_2 \le 0.0091$, $0.0018 \le \rho_t \le 0.0245$. The compression steel ratio is within 0.92% and the concrete cylinder compression strength is close to 3000 psi (21 MN/m^2).

References

American Concrete Institute Committee 318. (1989) *Building Code Requirements for Reinforced Concrete.* ACI 318–89, American Concrete Institute, Detroit.

Collins, M. (1973) Torque-twist characteristics of reinforced concrete beams, In *Inelasticity and Non-Linearity in Structural Concrete.* University of Waterloo Press, Waterloo Ontario: 211

Han, K.J. and Mau, S.T.(1988) Membrane behaviour of r/c shell element and limits on the reinforcement *J. Struct. Mechcs, Am. Soc. Civ. Engrs* **114** No. 2: 425.

Hagai, T. (1983) Recent plastic and truss theory on the shear failure of reinforced concrete members *Proc. Colloquium of Shear Analysis of RC Structures.* Japan Concrete Institute, Tokyo: 29–83.

Hsu, T.T.C. (1984) *Torsion of Reinforced Concrete.* Van Nostrand Reinhold, New York
Hsu, T.T.C. and Mo, Y.L. (1985a) Softening of concrete in torsional members—theory and tests, *J. Am. Concr. Inst.* **82** No. 3: 290.
Hsu, T.T.C. and Mo, Y.L (1985b) Softening of concrete in torsional members—design recommendations, *J. Am. Concr. Ins.* **82** No. 4: 443.
Hsu, T.T.C. and Mo, Y.L. (1985c) Softening of concrete in torsional members—Prestressed Concrete, *J. Am. Concr. Inst.* **82** No. 5: 603.
Hsu, T.T.C. and Mo, Y.L. (1985d) Softening of concrete in low-rise shear walls, *J. Am. Concr. Inst.* **82** No. 6: 883.
Hsu, T.T.C. Mau, S.T., and Chen, B. (1987) Theory of shear transfer strength of reinforced concrete *Am. Concr. Inst.* **84** No. 2: 149.
Hsu, T.T.C. (1988) Softened truss model for shear and torsion, *Am. Concr. Inst. Struct. J.* **85** No. 6: 624–635.
Kong, F.-K., Robins, P.J. and Cole, D.F. (1970) Web reinforcement effects on deep beams *J. Am. Concr. Inst.* **67** No. 12: 1010.
Lampert, P. and Thurlimann, B. (1968) *Torsionsversuche an Stahlbetonbalken* (Torsion tests of reinforced concrete beams), Bericht Nr. 6506–2; (1969) *Torsion-Biege-Versuche an Stahlbetonbalken* (Torsion-bending tests on reinforced concrete beams), Bericht Nr. 6506–3, Institut fur Baustatik, ETH, Zurich, (in German)
Mau, S.T. and Hsu, T.T.C. (1986) Shear design and analysis of low-rise structural walls. *J. Am. Concr. Inst.* **83** No. 2: 306.
Mau, S.T. and Hsu, T.T.C. (1987a) Shear behaviour of reinforced concrete frame wall panels with vertical load *Am. Concr. Inst. J.* **84** No. 3: 228.
Mau, S.T. and Hsu T.T.C. (1987b) Shear strength prediction for deep beams with web reinforcement *Am. Concr. Inst. J.* **84** No. 6: 513.
Mau, S.T. and Hsu, T.T.C. (1989) A formula for the shear strength of deep beams. *Am. Concr. Inst. Struct. J.* **86** No. 5: 516.
Morsch, E. (1902) *Der eisenbetonbau, seine Anwendung und Theorie.* 1st ed., Wayss and Freytag, A.G., Im Selbstverlag der Firma, Neustadt a.d. Haardt, (1906) *Der Eisenbetonbau, seine Theorie und Anwendung,* 2nd ed. Verlag von Konrad Wittmer, Stuttgart (1909) 3rd ed. translated into Enlgish by E.P.Goodrich, McGraw-Hill, New York.
de Paiva, H.A.Rawdon and Siess, C.P. (1965) Strength and behaviour of deep beams in shear. *J. Struct. Engng Div., Am. Soc. Civ. Engrs.* **91** ST 5: 19
Rausch, E. (1929) *Design of reinforced concrete in torsion* (Berechnung des Eisenbetons gegen Verdrehung), Technische Hochschule, Berlin, (in German) A second edition published in 1938. The third edition (1953) was titled *Drillung (Torsion), Schub und Scheren in Stahlbetonbau,* Deutcher Ingenieur- Verlag GmbH, Dusseldorf.
Ritter, W. (1899) *Die Bauweise Hennebique, Schweize. Bauzeitung,* Zurich.
Robinson, J.R., and Demorieux, J.M. (1972) *Essais de Traction-Compression sur Modèles d'ame de Poutre en Béton Armé* IRABA Report, Institut de Recherches Appliquées du Béton Armé Part 1, June 1968, and Part 2, *Resistance Ultimate due Béton de L'ame de Poutres en Double Té en Béton Armé,* May, 1972.
Smith, K.N. and Vansiotis, A.S. (1982) Shear strength of deep beams, *J. Am. Concr. Inst.* **79** No. 3: 201.
Vecchio, F. and Collins, M.P. (1981) Stress-strain characteristics of reinforced concrete in pure shear. *IABSE Colloquium, Advanced Mechanics of Reinforced Concrete,* Delft, Final report: 211.

8 Shear strength prediction—plastic method

M.W.BRAESTRUP, Rambull and Hannemann, Denmark

Notation

A_c	cross-sectional area of concrete perpendicular to steel area A_s
A_s	cross-sectional area of steel reinforcement
a	clear span between load and support platens
b	width of beam
c	distance from bottom face of beam to centroid of reinforcement
d	effective depth of beam; $d=h-c$
f_c	cylinder strength of concrete
f_c^*	effective compressive strength of concrete
f_y	yield stress of reinforcement
h	total depth of beam
l	shear span between point load and support reaction
r	geometrical ratio of smeared reinforcement, $r=A_s/A_c$
s	length of support platen
s_1	minimum support platen length to attain flexural capacity
T	force in longitudinal reinforcement
T_y	yield force of longitudinal reinforcement; $T_y=A_sf_y$
t	length of load platen
tl	minimum length of load platen
V	applied point load
v	relative displacement rate in yield line
x	width of triangular region in biaxial compression
y	depth of triangular region in biaxial compression
y_o	value of y corresponding to yielding of reinforcement, $y_o=h\phi/v\leq h/2$
α	inclination of relative displacement rate
ß	inclination of yield line (or chord)
γ	inclination of reinforcement relative to yield line
Δ	thickness of deforming zone idealised as yield line
ε_1	first principal strain rate
ε_2	second principal strain rate
ε_s	strain rate in reinforcement
η	relative rotation rate of rigid parts
θ	inclination of compressive concrete strut
V	effectiveness factor, $v=f_c^*/f_c$
ρ	geometrical ratio of long- itudinal reinforcement, $\rho=T_y/bhf_y$
σ	compressive concrete stress
σ_1	first principal concrete stress
σ_2	second principal concrete stress
σ_s	tensile stress in reinforcement
σ_v	vertical component of compressive concrete stress, $\sigma_v=\sigma\sin^2\theta$
τ	shear stress in concrete
ϕ	mechanical degree of reinforcement $\phi=T_y/bhf_c$

8.1 Introduction

The capacity of a slender beam subjected to concentrated loading is governed by either the strength in flexure of the maximum moment section or the strength in shear of the span. For a deep beam, however, the ultimate load is determined by the transfer of forces between load and support. Consequently, the capacity—whether it be termed flexural or shear—depends upon the detailing of loading and support.

For a simply supported beam under point loading the shear span l is defined as the distance between the lines of action of the load and the support reaction. If, on the other hand, the beam is indirectly loaded and built in at the support, it is the clearance $a=l-s/2-t/2$ (Figure 8.7) between the edges of the load and support platens which is given. Some cases, e.g. corbels, are hybrid, in the sense that the known span is the distance $l-s/2$ between the point load and the edge of the support.

Each of these cases can be solved by plastic analysis, and some solutions are derived in the present chapter. By way of introduction, a brief review is first given of the theory of plasticity, and the corresponding material description of structural concrete is presented.

The application of plastic methods to concrete structures has a fairly long history, but deep beams have not been the subject of much dedicated effort. Nielsen (1971) derived some solutions for deep beams considered as wall elements, and corbels were treated by B.C.Jensen (1979). Beam shear in general has been covered extensively, *cf.* Braestrup and Nielsen (1983), Nielsen (1984). The solutions given in this chapter were originally derived by J.F. Jensen (1981), but the formulation presented here is somewhat different.

Attention is restricted to beams under point loading. Deep beams subjected to a uniformly distributed load are most efficiently treated by the plasticity theory for plane elements, and reference is made to Nielsen (1984), *cf.* also J.F.Jensen (1981).

8.2 Plasticity theory

8.2.1 *Limit analysis*

To assess the strength of a structure under load designers have always, knowingly or unknowingly, made use of two fundamental principles of nature:

i) If there is any manner in which a structure can possibly collapse under a given load, then it will do so.
ii) If there is any manner in which a structure can possibly carry a given load, then nature will find it.

The first principle implies that if we can identify just one mode which can lead to collapse, with due account taken of the strengths of the

materials and members involved, then we know that the structure is unsafe under the given load.

The second principle implies that if we can identify just one way of transferring the load down through the structure, without overstressing any materials or members, then we know that the structure is safe under the given load.

These intuitive principles of structural behaviour are not particularly operational, but in the theory of plasticity they are refined and substantiated into the three theorems of limit analysis:

i) *The upper bound theorem,* stating that any load corresponding to which we can find a kinematically admissible failure mechanism is greater than or equal to the collapse load,
ii) *The lower bound theorem,* stating that any load corresponding to which we can find a statically admissible stress distribution is less than or equal to the collapse load;
iii) *The uniqueness theorem,* stating that the lowest upper bound and the highest lower bound coincide, and constitute the exact collapse load of the structure.

The first complete formulation of the limit analysis theorems was given by Gvozdev (1938), but his work was not known and credited in the West until 1960. The statement of the theorems i)-iii) was formulated by Drucker, Prager and Greenberg (1952), based upon work by Hodge and Prager (1948) and Hill (1950).

8.2.2 *Rigid, perfectly plastic model*

The limit analysis theorems can be rigorously proved under certain idealised assumptions of material behaviour. Materials complying with these are called plastic, the simplest example being comprised of the class of rigid, perfectly plastic materials. The structural response of a rigid, perfectly plastic body is described by a set of statical quantities Q_i, called the generalised stresses, and a set of kinematical quantities q_i, called the generalised strain rates, such that the inner product: $D=Q_i q_i$ constitutes the rate of internal work per unit element of the body. The scalar D is called the dissipation.

In order to estimate the collapse load of a rigid, perfectly plastic body it is not necessary to insist that the q_i be considered as rates or increments, and the distinction from conventional small strains is merely academic.

A yield function $f_k(Q_i)$ is a scalar function of the generalised stresses such that stress states for which $f_k(Q_i) >0$ cannot be sustained by the body and $f_k(Q_i^o)=0$ for at least one stress state $Q_i=Q_i^o$. A set of yield functions constitutes a *yield condition:* $f_k(Q_i)\leq 0$. The frontier of the set of allowable stress states defined by the yield condition is called the yield surface with the equation: $F(Q_i)=0$.

A supporting plane to the yield surface is a plane in stress space with the equation: $\pi(Q_i)=0$ where $\pi(Q_i)$ is a linear yield function.

A rigid, perfectly plastic body can now be defined as a body with the following properties:

i) There exists a *convex yield surface* $F(Q_i)=0$ such that non- zero strain rates qi° are only possible for stress states Q_i^o for which $F(Q_i^o)=0$
ii) The strain rates q_i^o are governed by the *associated flow rule,* which may be expressed: $q_i^o=\lambda\delta\pi/\delta Q_i$, where λ is a non-negative constant and $\pi(Q_i)=0$ is a supporting plane to the yield surface through the point $Q_i=Q_i^o$.

The associated flow rule is also called the *normality condition,* because if the strain rates q_i are represented as a vector in generalised stress space, q_i^o is an outwards directed normal to the yield surface at the corresponding stress point $Q_i=Q_i^o$ if the point is regular. If the yield surface is not differentiable at $Q_i=Q_i^o$ the direction of q_i^o is confined by the normals to the adjoining parts of the yield surface.

It appears from the above that the limit analysis theorems reflect sound engineering concepts of structural response, but that the formal proof is based upon the assumption of plastic material behaviour, in particular the conditions of convexity and normality. For a more comprehensive review of the theory of plasticity reference is made to standard textbooks, e.g. Martin (1975).

8.3 Structural concrete plane elements

8.3.1 *Concrete modelling*

In many reinforced concrete structures, including deep beams, the concrete can reasonably be assumed to be in a state of plane stress. This means that the principal stresses $\sigma_i=(\sigma_1, \sigma_2)$ may be taken as generalised stresses, the corresponding generalised strain rates being the principal strain rates $\varepsilon_i=(\varepsilon_1, \varepsilon_2)$.

The uniaxial strength of concrete in compression is termed and, assuming that the strength in biaxial compression is independent of the lateral stress, two yield functions have been identified: $f_1=-f_c^*-\sigma_1$ and $f_2=-f_c^*-\sigma_2$. The tensile strength of concrete is small and unreliable, and is prudently neglected in plastic analysis of plane elements. Thus we have the additional yield functions: $f_3=\sigma_1$ and $f_4=\sigma_2$.

The four yield functions $f_k(\sigma_1, \sigma_2)\leq 0$ constitute a yield condition for concrete in plane stress, and the corresponding yield locus in the principal stress plane is shown in Figure 8.1, which also indicates the associated flow rule.

The well-known square yield locus of Figure 8.1 corresponds to a more comprehensive material model for concrete, know as the Coulomb failure criterion, modified by a zero tension cut-off. The modified Coulomb criterion (also with a non-zero tension cut-off) was introduced

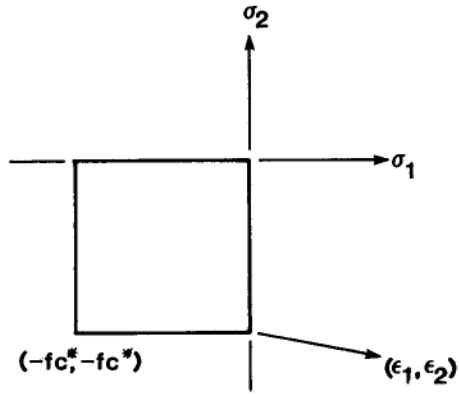

Figure 8.1 Square yield locus for concrete in plane stress.

into plastic analysis by Chen and Drucker (1969), and has been widely used for analysis and design of concrete structures, *cf.* B.C.Jensen (1977), International Association of Bridge and Structure Engineering (IABSE) (1978, 1979), Marti (1980), Braestrup and Nielsen (1983), Nielsen (1984).

The principal reservations concerning the applicability of plasticity to structural concrete are based upon the facts that concrete does not exhibit rigid, perfectly plastic behaviour, and the associated flow rule overestimates the dilatancy of concrete at failure. The latter objection appears to be inconsequential for ultimate load estimation, whereas the former has significant practical implications.

Figure 8.2 shows a typical stress-strain curve for a cylindrical concrete specimen under compression. The shape of the falling branch is debatable,

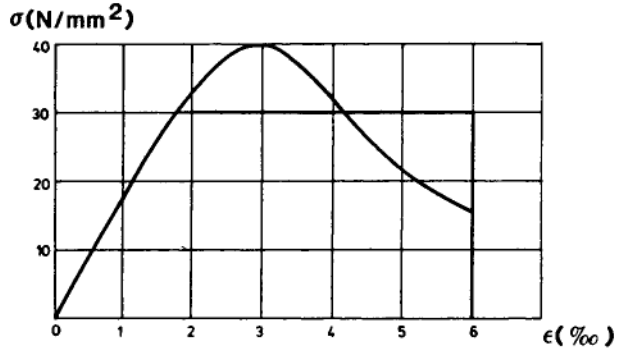

Figure 8.2 Stress-strain curve for concrete in compression.

but it is obvious that concrete does not possess any pronounced yield plateau, which would normally be required to justify the use of plasticity.

The simplest way of accounting for the shape of the stress-strain curve is to represent the uniaxial concrete strength not by the peak stress (cylinder strength) f_c, but by a reduced effective strength f_c^*. The ratio $v=f_c^*/f_c$ is called the effectiveness factor and its value must be assessed by comparing test results with the predictions of plastic analysis. It appears that the effectiveness factor is primarily a measure of concrete ductility, *cf.* Exner (1979), but as it is the only empirical factor of the theory it will have to absorb all other model uncertainties as well. The introduction of such an empirical calibration factor is by no means novel; in classical flexural analysis it is known as a stress block factor.

8.3.2 *Reinforcement modelling*

The reinforcing bars are assumed to resist forces in their axial direction only, dowel action being neglected. Thus the response of the reinforcement is described by the axial steel stress σ_s. For convenience the strength of compression reinforcement is also neglected, as the contribution is normally small in comparison with that of the surrounding concrete. The yield stress of the reinforcing steel is termed f_y and the yield condition $f_k(\sigma_s)\leq 0$ is then defined by the two yield functions: $f_1=\sigma_s-f_y$ and $f_2=-\sigma_s$. The one-dimensional yield locus is visualised in Figure 8.3.

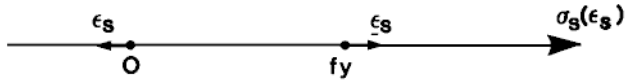

Figure 8.3 One-dimensional yield locus for reinforcement.

The reinforcement is assumed to be either concentrated in lines (stringers) or distributed over the section (smeared). In the latter case the bars are assumed to be parallel and sufficiently closely spaced.

The tensile strength of a stringer is the yield force $T_y=A_sf_y$, where A_s is the cross-sectional steel area. The strength of smeared reinforcement is described by the equivalent yield stress rf_y, where r is the geometrical reinforcement ratio $r=A_s/A_c$, A_c being the area of the section of concrete perpendicular to the bars of area A_s.

The actions of reinforcement in different directions are assumed to be independent, and generally problems with bond and anchorage are neglected. Perfect bond is therefore assumed in upper bound analysis, whereas lower bound analysis may assume any stress transfer, including complete slip.

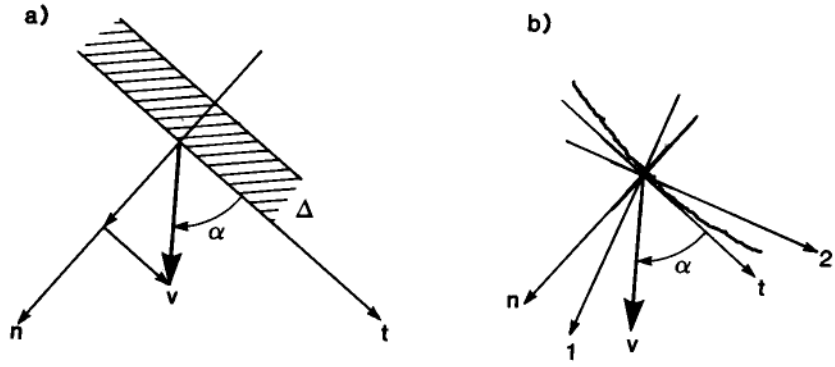

Figure 8.4 Yield line in plain concrete.

8.3.3 *Yield lines*

A yield line in a plane concrete element is the mathematical idealisation of a narrow zone with high strain rates, separating two rigid parts of the body, Figure 8.4a. The relative displacement rate of the rigid parts is v, inclined at the angle α to the yield line. Assuming the straining to be homogeneous over the depth Δ, we find the principal strain rates:

$$\varepsilon_1=(v/2\Delta)(1+\sin\alpha),\ \varepsilon_2=-(v/2\Delta)(1-\sin\alpha)$$

The principal directions of strain rate, which coincide with the principal directions of stress, are indicated in Figure 8.4b. The first principal axis bisects the angle between the displacement vector and the yield line normal.

For $-\pi/2\le\alpha\le\pi/2$ we have $\varepsilon_1\ge 0$ and $\varepsilon_2\le 0$ and according to the associated flow rule the only state of stress in the concrete for which such deformations can occur is $(\sigma_1,\sigma_2)=(0,f-f_c^*)$ *cf.* Figure 8.1. The rate of internal work (dissipation) per unit length of the yield line is:

$$D_c=b\Delta(\sigma_2\varepsilon_1+\sigma_2\varepsilon_2)=\frac{1}{2}bvf_c^*(1-\sin\alpha)$$

$$\text{for } -\pi/2\le\alpha\le\pi/2$$

Here *b* is the thickness of the element. The dissipation in the yield line is independent of the assumed depth Δ of the deforming zone.

The concept of yield lines introduced in this section should not be confused with cracks. Cracking of concrete may result from a number of reasons, including changes in temperature or humidity, and is not necessarily accompanied by any appreciable deformations. Under loading cracks tend to form perpendicular to the direction of first principal stress. Thus a yield line will only coincide with the crack direction if it is perpendicular to the relative displacement rate, *cf.* Figure 8.4.

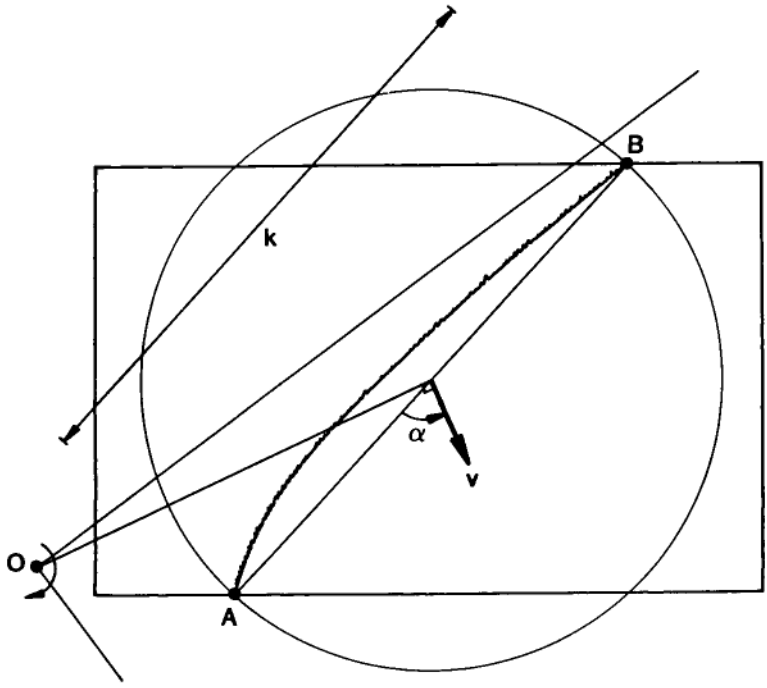

Figure 8.5 Hyperbolic yield line in concrete element.

During a loading history leading to collapse the principal axes of stress in the concrete are likely to change directions, and at failure the latest formed cracks will generally be at an angle to the yield line. This implies that shear stresses are transferred across the yield line, by friction or aggregate interlock in old cracks and by crushing zones between cracks.

The transfer of shear in yield lines is expressed by the rate of work dissipated, which depends upon the inclination a of the displacement rate, Figure 8.4. For pure separation ($\alpha=\pi/2$) the dissipation reduces to $D_c=0$ reflecting the assumption of zero tensile concrete strength. However, as soon as tangential deformation is introduced ($\alpha<\pi/2$) the resistance increases proportionally with the compressive concrete strength, corresponding to a failure stress $\tau=f_c^*/2$ for pure shearing ($\alpha=0$). For pure crushing ($\alpha=-\pi/2$) the compressive resistance is $\sigma=f_c^*$

In the general case a yield line will be a curve AB separating the element into two rigid parts, the relative movement of which is a rotation about a point O in the plane of the element (Figure 8.5). By calculus of variation it was shown by J.F.Jensen (1981, 1982) that the optimal shape of the yield line, leading to a stationary value of the total dissipation, is a hyperbola with orthogonal asymptotes through O. The corresponding rate of internal work is:

$$W_c = \frac{1}{2} kbvf_c^*(1 - \sin\alpha) \tag{8.1}$$

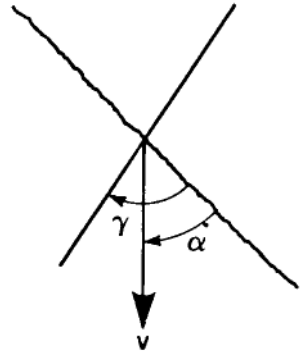

Figure 8.6 Yield line in crossed by reinforcing bar.

Where k is the length of the chord AB, and the magnitude v and inclination α of the displacement rate are measured at the midpoint of the chord (Figure 8.5).

The centre of rotation O must be outside the circle with diameter AB, otherwise the hyperbola is replaced by straight yield lines OA and OB, one with pure separation ($\alpha=\pi/2$) the other with pure crushing ($\alpha=-\pi/2$). If O is at infinity the yield line reduces to the straight line AB, with constant v and α.

Suppose a reinforcement stringer intersects a yield line at the angle γ where $0\leq\gamma=\pi$ and $\gamma=0$ corresponds to the same direction as $\alpha=0$ (Figure 8.6). The strain rate ε_s is then: $\varepsilon_s=(v/\Delta)\sin\gamma\cos(\gamma-\alpha)$. The rate of internal work is determined by the flow rule and the yield condition (Figure 8.3):

$$W_s=vT_y\cos(\gamma-\alpha) \qquad \text{for } \gamma-\alpha\leq\pi/2 \tag{8.2}$$
$$W_s=0 \qquad \text{for } \gamma-\alpha\geq\pi/2$$

If the yield line is intersected by a band of smeared reinforcement the contribution to the rate of internal work per unit length of the yield line is:

$$D_s=bvrf_y\cos(\gamma-\alpha)\sin\gamma \quad \text{for } \gamma-\alpha\leq\pi/2 \tag{8.3}$$
$$D_s=0 \qquad \text{for } \gamma-\alpha\geq\pi/2$$

The factor $\sin\gamma$ takes account of the fact that the reinforcement ratio r is defined per unit area perpendicular to the direction of the reinforcing bars.

8.4 Shear strength of deep beams

Consider a rectangular beam of width b and depth h, subjected to a point load V. The shear span l is defined as the distance between the point load and the support reaction. The term a denotes the clearance between the support and load platens, the lengths of which are s and t respectively (Figure 8.7).

The effective concrete strength is $f_c^*=vf_c$, and the yield force of the longitudinal reinforcement is T_y. The mechanical reinforcement degree is introduced: $\Phi=T_y/bhf_c$. The effective depth to the centroid of the reinforcement is termed $d=h-c$, and the beam is assumed to be in a state of plane stress.

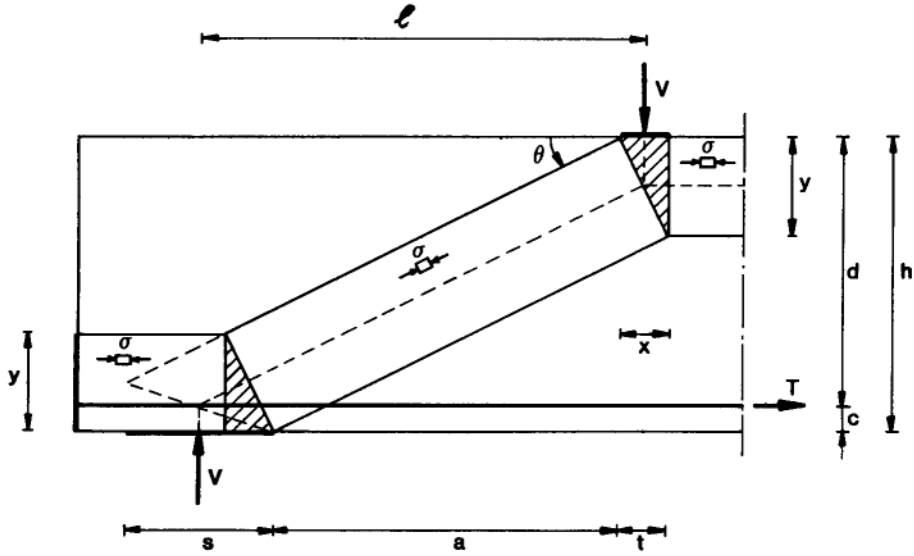

Figure 8.7 Stress distribution for beam with point loading.

8.4.1 *Lower bound analysis*

The statically admissible stress distribution shown in Figure 8.7 consists of a concrete strut running between the load and the support at the inclination θ. The compressive stress in the strut is σ and the triangular shaded areas are under biaxial hydrostatic compression. The force in the reinforcement is T.

The width x and depth y of the regions in biaxial compression are determined by the equations of vertical and horizontal equilibrium:

$$V=bx\sigma \tag{8.4}$$

$$T=by\,\sigma \tag{8.5}$$

The lengths s and t of the load and support platens are assumed to be necessary and sufficient to ensure equilibrium with the applied load. If the physical dimensions of the platens are greater it will not affect the validity of the solution as a lower bound. The required length of the load platen is determined by the size of the triangular region, (i.e. $t=x$).

The reinforcement is assumed to be anchored behind the support, symbolised by an anchor plate in Figure 8.7, resulting in a compressive concrete force T distributed over the depth y. If the reinforcement is not cocentral with the concrete compression (i.e. $y>2c$) this gives rise to a moment, which must equal the moment delivered by the support reaction. Hence: $V(s/2-x/2)=T(y/2-c)$, from which the required length s of the support platen is determined. This is equivalent with the geometrical relation:

$$\cot\theta=y/x=(s-x)/(y-2c) \tag{8.6}$$

which can also be deduced from Figure 8.7.

Although the stress distribution of Figure 8.7 formally satisfies equilibrium, the detailed load transfer at the support is left unexplained. Figure 8.8 shows a more consistent stress distribution at the support for the case where the reinforcement is concentrated in a single stringer (in Figure 8.7 the reinforcement may in principle be located anywhere in the beam section, as long as the effective depth to the centroid is $d=h-c$). The shaded areas are under the biaxial hydrostatic compression a and the vertical stress over the central part of the support platen is $\sigma_v=\sigma\sin^2\theta$, the inclined concrete stresses being transferred to the reinforcement by bond shear.

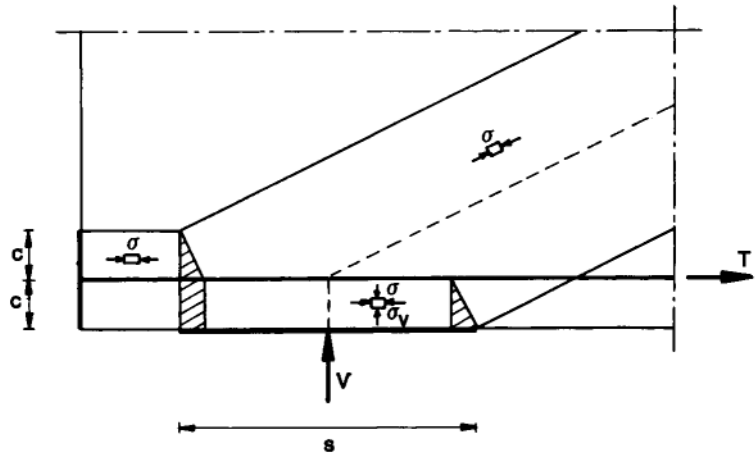

Figure 8.8 Alternative stress distribution at support.

The stress distributions mentioned are topical for $y>2c$. If $y\leq 2c$ it is possible to place the concrete compression symmetrically about the reinforcement centroid, and the stress distribution at the support is modified as shown in Figure 8.9.

Figure 8.7 yields an expression for the strut inclination:

$$\cot\theta=y/x=l/(h-c-y/2) \tag{8.7}$$

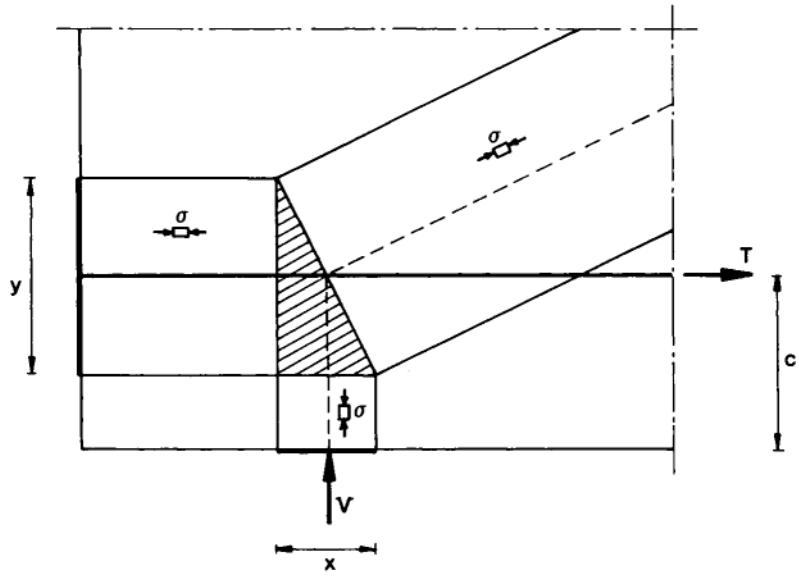

Figure 8.9 Stress distribution at support for $y=2c$.

Hence with Eqns (8.4) and (8.5), $V=T(d-T/2b\sigma)$, which expresses moment equilibrium at the loaded section. The classical flexural failure load $V=V_F$ is found by putting $T=T_Y$ and $\sigma=f_c^*=\nu f_c$, and introducing $\Phi=T_Y/bhf_c$:

$$V_F = \frac{1}{2} b\nu f_c (h/l)\,(2d - h\Phi/\nu)\,\Phi/\nu \tag{8.8}$$

However, the flexural solution fails to account for the transfer of forces from load to support, which requires a closer examination of the stress distribution. It appears that the highest load is obtained with the maximum compressive stress in the concrete ($\sigma=f_c^*$) whereas it is not always optimal to have maximum force in the reinforcement ($T=T_Y$).

Inspection of Figure 8.7 shows that if the parameters l, h, c and t are given, one of the quantities s and y is necessary and sufficient to define the stress distribution. Thus the lower bound is determined either by the strength T_y of the reinforcement or by the length s of the load platen. In the former case we have:

$$y = T_y/bf_c^* = h\Phi/\nu = y_o$$

whereas in the latter case $y<y_o$, which means that the reinforcement is not yielding. The strut inclination θ satisfies the geometrical relation:

$$\cot\theta = y/x = (a+x)/(h-y) \tag{8.9}$$

which also expresses moment equilibrium of the strut. Solving for x and using Eqns (8.4) and (8.5), we find the lower bound solution:

$$V = \frac{1}{2}(\sqrt{(ba\sigma)^2 + 4T(bh\sigma - T)} - ba\sigma) \tag{8.10}$$

The highest lower bound is determined by maximising with respect to the statical parameters s and T. It appears that:

$$\partial V/\partial\sigma > 0$$
$$\partial V/\partial T \gtrless 0 \quad \text{for } T \gtrless bh\sigma/2$$

Therefore the highest lower bound is obtained with the maximum concrete stress (i.e.s=f_c^*). For $T_y \le bhf_c^*/2$ the highest lower bound is obtained with the maximum reinforcement force (i.e. $T=T_y$). Inserting into Eqn (8.10) and introducing and $\Phi=T_y/bhf_c$, we find:

$$V = \frac{1}{2}b\nu f_c(\sqrt{a^2 + 4h^2\Phi(\nu - \Phi)/\nu^2} - a)$$

For $\Phi \le \nu/2$. For $T_y \ge \frac{1}{2}bhf_c^*$ the highest lower bound is obtained with $T = \frac{1}{2}bhf_c^*$, whence:

$$V = \frac{1}{2}b\nu f_c(\sqrt{a^2 + h^2} - a)$$

For $\Phi \ge \nu/2$. In this case the beam is over-reinforced, in the sense that the longitudinal reinforcement is not yielding at failure of the beam.

The lower bound solution may be written:

$$V = \frac{1}{2}b\nu f_c(\sqrt{a^2 + 4y_o(h - y_o)} - a) \tag{8.11}$$

With $y_o=h\Phi/\nu \le h/2$. It is understood that y_o is replaced by $h/2$ if $\Phi > \nu/2$.

The minimum dimensions of the load and support platens to ensure validity of Eqn (8.11) can now be determined. The required length $t=t_1$ of the load platen is:

$$t_1 = x = \frac{1}{2}(\sqrt{a^2 + 4y_o(h - y_o)} - a) \tag{8.12}$$

The required length of the support platen is determined by Eqn (8.6):

$$s_1 = x + (y_o - 2c)y_o/x \tag{8.13}$$

Inserting Eqn (8.12) we find:

$$s_1 = \frac{h - 2c}{2(h - y_o)}(\sqrt{a^2 + 4y_o(h - y_o)} + a) - a \tag{8.14}$$

It is assumed in the following that $c < y_o/2$, otherwise the required support length reduces to $s_1=x$ (Figure 8.9). It is further assumed that the load platen

is sufficiently long ($t=t_1$), otherwise the solution is either trivial ($V = btf_c^*$) or governed by the analysis below.

If the support platen is shorter than required ($s<s_1$) then the depth y of the concrete compression is determined by Eqn (8.6). From Figure 8.7 we find the geometrical relation: $\cot\theta=y/x=(a+s)/(h-2c)$. Solving for y, inserting into Eqns (8.6) and using Eqn (8.4) we find the lower bound solution:

$$\mathbf{V} = b\nu f_c \frac{(h-2c)\,(2ac+hs)}{(a+s)^2+(h-2c)^2} \tag{8.15}$$

By Eqns (8.11) and (8.15) the lower bound solution is given in terms of the clearance *a*. In most design situations, however, it is the distance *l* between load and reaction which is given. Exceptions are formed e.g. by cases of indirect loading and built-in support.

When the capacity is governed by the reinforcement the load is found in terms of the span *l* from Eqn (8.8):

$$\mathbf{V} = \frac{1}{2} b\nu f_c\,(2h-2c-y_o)\,y_o/l \tag{8.16}$$

With $y_o=h\Phi/\nu\le h/2$. The relationship between *l* and *a* is (Figure 8.7): $l=a+s/2+t/2$. Inserting $s=s_1$ from Eqn (8.14) and $t=t_1$ from Eqn (8.12), we find:

$$l = \frac{2(h-c)-y_o}{4(h-y_o)}\left(\sqrt{a^2+4y_o(h-y_o)}+a\right) \tag{8.17}$$

Eqn (8.16) is identical with Eqn (8.11) by virtue of Eqn (8.17).

The limiting size of the load platen $t_1=x=V/bvf_c$ as a function of *l* is found from Eqn (8.16):

$$t_1=x=(2h-2c-y_o)y_o/2l$$

Inserting into Eqn (8.13) we find the minimum size s_1 of the load platen:

$$s_1 = \frac{(2h-2c-y_o)^2\,y_o+4l^2\,(y_o-2c)}{2l\,(2h-2c-y_o)} \tag{8.19}$$

When the capacity is governed by the support length the load is found in terms of *l* by solving Eqns (8.7) and (8.6) for $x=V/bvf_c$. Elimination of *y* yields the cubic equation:

$$x^3-2x^2\,(2l+s)+x[(2l+s)^2+4(h-c)(h-2c)] \\ -4(h-2c)\,[2lc+s(h-c)]=0 \tag{8.20}$$

Eqn (8.20) has one real root, which may be expressed analytically, but the result is not particularly illuminating, and Eqn (8.20) is most easily solved by iteration.

Example
Consider a beam with span $l=3h/2$, reinforcement strength $y_o=h\Phi/v=h/3$ and level of reinforcement $c=h/12$ corresponding to $d=0.92/h$. From Eqn (8.16) we find the solution: $V/bvf_c=x=h/6=0.167h$ and Eqn (8.19) gives $s_l=h/2$. The geometry of the considered beam is shown in Figure 8.7, and we note that attainment of the flexural capacity requires a substantial length of the support platen.

If more realistically we assume $s=t=h/6$, the solution is found from Eqn (8.20): $V/bvf_c=x=0.108h$ corresponding to a reduction by 35%. If, on the other hand, the level of the reinforcement is increased to $c=h/6$, corresponding to $d=0.83h$, we find from Eqn (8.16): $V/bvf_c=x=0.148h$. This is a reduction of 11% only, and the attainment of this flexural capacity requires no oversize support platen, as we now have $s_l=x$ by Eqn (8.13).

8.4.2 *Upper bound analysis*

The kinematically admissible failure mechanism shown in Figure 8.10 consists of a straight yield line running at the inclination ß from the edge of the load platen to the edge of the support platen. The relative displacement rate is v, inclined at the angle α to the yield line.

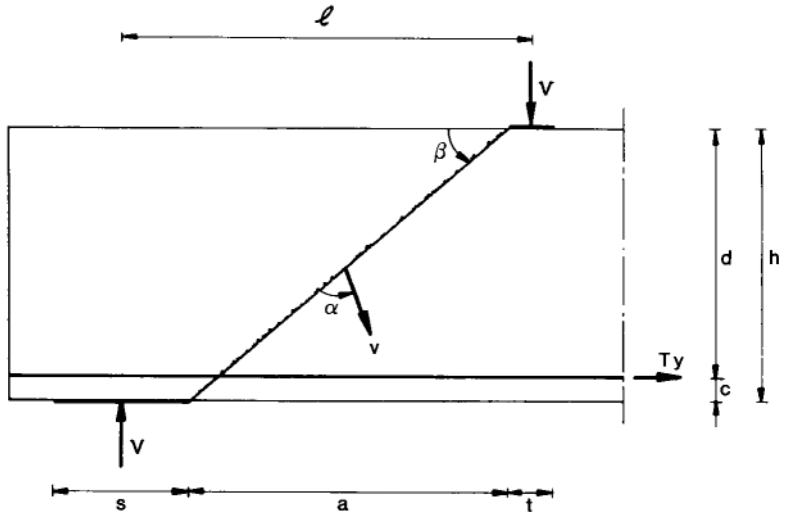

Figure 8.10 Failure mechanism for beam with point loading.

We assume that the reinforcement is not compressed, i.e. $\alpha \geq \pi/2-ß$ or $\alpha+ß \geq \pi/2$. The rate of external work done by the load is $W_E=V \sin(\alpha+ß)$. The rate of internal work dissipated in the mechanism is:

$$W_I = \frac{1}{2} b \frac{h}{\sin \beta} v f_c^* (1 - \sin \alpha) - v T_y \cos(\alpha + \beta)$$

where the contributions from the web concrete and from the reinforcement are calculated by Eqns (8.1) and (8.2), respectively.

The work equation $W_E=W_I$ gives the upper bound solution:

$$V=\frac{bhf_c^*(1-\sin(\alpha+\beta)\cos\beta+(bhf_c^*-2T_y)\cos(\alpha+\beta)\sin\beta}{2\sin(\alpha+\beta)\sin\beta} \qquad (8.21)$$

The lowest upper bound is determined by minimising with respect to the variable angle α. A minimum is found for $dV/d(\alpha+ß)=0$, which gives:

$$h\cos(\alpha+\beta)=-(bhf_c^*-2T_y)\sin\beta \qquad (8.22)$$

Inserting into Eqn (8.21) and introducing $f_c^*=\nu f_c$, $\phi=T_y/bhf$ and cot ß=a/h we find:

$$V=\frac{1}{2}b\nu f_c\left(\sqrt{a^2+4h^2\phi(\nu-\phi)/\nu^2}-a\right)$$

for $\phi\le\nu/2$. The validity range arises from the condition $\alpha+ß\ge\pi/2$, together with Eqn (8.22).

For $\alpha+ß\le\pi/2$ we have $dV/d(\alpha+ß)\le0$ which means that the lowest upper bound is obtained with $\alpha+ß=\pi/2$. This is the case also if a contribution to the rate of internal work is assigned to compressed reinforcement *cf.* Eqn (8.2). Thus we get:

$$V=\frac{1}{2}b\nu f_c\left(\sqrt{a^2+h^2}-a\right)$$

for $\phi\ge\nu/2$. The situation $\alpha+ß=\pi/2$ corresponds to a relative displacement rate which is perpendicular to the beam axis (Figure 8.10), in which case the longitudinal reinforcement does not yield, (i.e. the beam is over-reinforced).

The upper bound solution is seen to be identical with the lower bound solution, Eqn (8.11). This means that the flexural capacity, Eqn (8.16), is the exact plastic solution if we have $t=t_1$ given by Eqn (8.18), and $s=s_1$ given by Eqn (8.19). For $t>t_1$ and/or $s>s_1$ (and unchanged shear span 1), the lowest upper bound will exceed the highest lower bound.

Figure 8.11 shows an alternative, flexural mechanism, consisting of a clockwise rotation ? of the beam end about a point O at the distance y below and the distance x outside the inside edge of the load platen. The rate of external work done by the load is: $W_E=V(a+s/2+x)\eta$. The rate of internal work dissipated in the mechanism is:

$$W_I=\frac{1}{2}bf_c^*(x^2+y^2)\eta+T_y(h-c-y)\eta$$

The work equation $W_E=W_I$ gives the upper bound solution:

$$V=\frac{bf_c^*(x^2+y^2)+2T_y(h-c-y)}{2a+s+2x} \qquad (8.23)$$

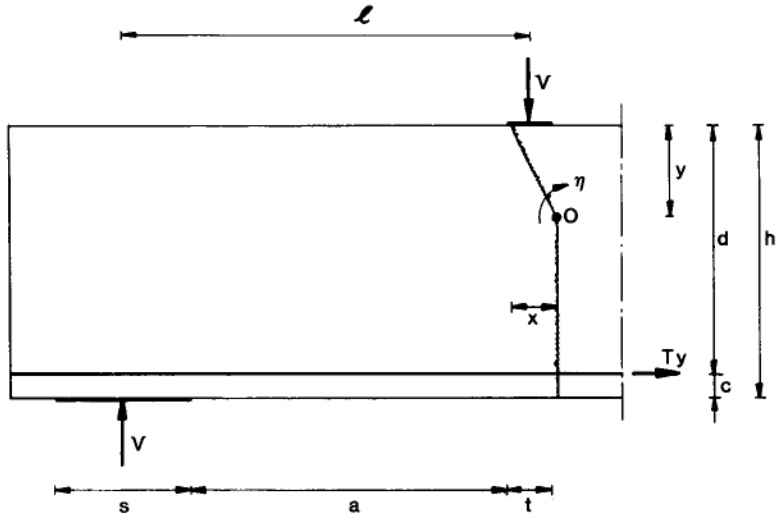

Figure 8.11 Rotational failure mechanism.

The lowest upper bound is determined by minimising with respect to the variables x and y. The condition $\delta V/\delta y=0$ gives $y = T_y/bf_c^* = y_o$, whereupon the condition $\delta V/\delta x=0$ yields:

$$2x = \sqrt{(2a+s)^2 + 4y_o(2h-2c-y_o)} - (2a+s)$$

Inserting into Eqn (8.23), we find:

$$V = \frac{1}{2}bf_c^*\left[\sqrt{(2a+s)^2 + 4y_o(2h-2c-y_o)} - (2a+s)\right]$$

Therefore $V = bxf_c^*$ and $l=a+s/2+x/2$ whereupon this solution is also seen to be identical with the flexural capacity, Eqn (8.16).

In the failure mechanism of Figure 8.10 the reinforcement may be located anywhere in the section, as long as the effective depth to the centroid is $d=h-c$, whereas the mechanism of Figure 8.11 requires that the reinforcement is located in the tension zone of depth $h-y_o$. Figure 8.12 shows a failure mechanism without yielding of the reinforcement for the case that the reinforcement is concentrated in a single stringer at the effective depth $d=h-c$.

The failure mechanism of Figure 8.12 consists of a hyperbolic yield line through the edges of the load and support platens, the inclination of the chord being ß. Relative to the loaded beam section the beam end is rotating counterclockwise at the rate η about a point O located outside the beam at the level of the reinforcement. The relative displacement rate at the midpoint of the chord is:

$$v=\eta r=\eta(h/2-c)/\sin(\alpha+ß-\pi/2)$$

where α is the inclination of v relative to the chord.

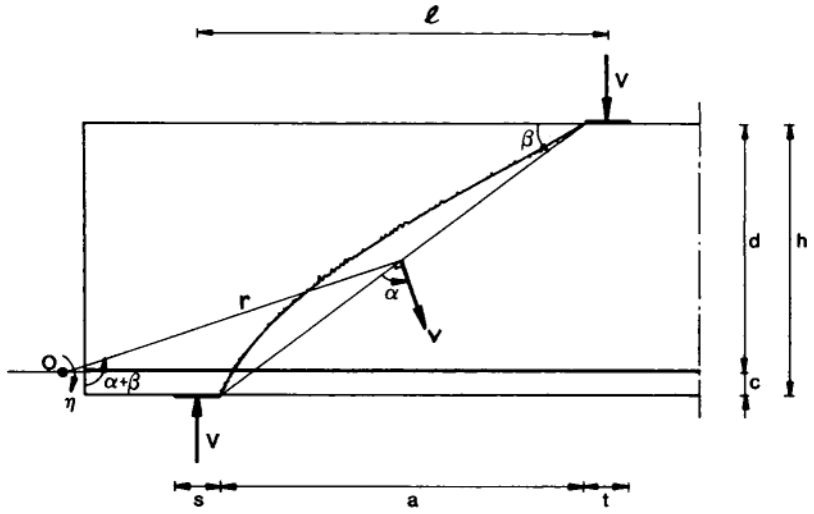

Figure 8.12 Failure mechanism with hyperbolic yield line.

The rate of external work is found by considering the displacement rate of the support reaction relative to the mid section of the beam:

$$W_E = v \cdot \eta(-(h/2 - c)\tan(\alpha+ß) - a/2 - s/2)$$

The rate of internal work is found from Eqn (8.1):

$$W_I = \frac{1}{2}\frac{h}{\sin\beta} b v f_c^* (1 - \sin\alpha)$$

$$= -\frac{1}{2} b f_c^* \frac{h}{\sin\beta} \eta \frac{h - 2c}{2\cos(\alpha+\beta)} (1 - \sin\alpha)$$

The reinforcement does not contribute to the rate of internal work because the relative displacement rate is perpendicular to the reinforcement at the intersection with the yield line.

The work equation $W_E = W_I$ gives the upper bound solution:

$$V = \frac{1}{2} b f_c^* \frac{h(h-2c)}{\sin\beta} \frac{1 - \sin\alpha}{(a+s)\cos(\alpha+\beta) + (h-2c)\sin(\alpha+\beta)} \qquad (8.24)$$

The lowest upper bound solution is determined by minimising with respect to the variable angle α. The condition $dV/d\alpha = 0$ gives:

$$\frac{1 - \sin\alpha}{\cos\alpha} = \frac{(a+s)\sin\beta - (h-2c)\cos\beta}{(a+s)\cos\beta + (h-2c)\sin\beta}$$

Inserting into Eqn (8.24) and introducing $f_c^* = \nu f_c$ and cotß=a/h we recover Eqn (8.15). Thus also in this case is the upper bound solution identical with the lower bound.

8.4.3 *Experimental evidence*

There exists a wealth of published shear test results, which have been compared with the plastic solution, albeit exclusively with the flexural capacity prediction in the 'shear strength' formulation, Eqn (8.11). Nielsen and Braestrup (1978) reported a series of five rectangular, simply supported, prestressed beams under two-point loading. The beam parameters were: depth h: 360 mm, concrete cylinder strength f_c:55 N/mm^2, degree of reinforcement ϕ:0.21 (including both bottom and top strands), and shear span ratio *a/h:* 0.5, 1.0, 2.0, 3.0 and 4.0. The latter beam failed in flexure, whereas shear failure was obtained for the four beams with lower shear span ratios.

The ultimate loads of all five beams were in excellent agreement with Eqn (8.11), with an effectiveness factor ν=0.46, thus the beams were close to being over-reinforced. Comparison with a number of over-reinforced beams ($\phi \geq \nu/2$) from the literature showed some scatter around the prediction corresponding to ν=0.6.

It appears that in comparing with test results, as well as in practical applications of the solution, the crux of the matter is the assignment of a value to the effectiveness factor. As mentioned in Section 8.3.1 the reduced effective concrete strength reflects the limited ductility of concrete, which depends primarily on the strength level f_c. In addition, however, the effectiveness factor must account for other neglected features, notably the size effect, the tensile concrete strength, and the state of stress at failure.

The amount of stress redistribution increases with the flatness of the compressive concrete strut, wherefore the effectiveness factor is expected to be a decreasing function of the shear span ratio *a/h*. On the other hand, the neglect of the tensile concrete strength leads to an underestimation of the rate of internal work in the yield line (Figure 8.10), which is greater for flatter yield lines, where the relative displacement rate is closer to the yield line normal. Consequently, the tensile strength leads to an increased effectiveness factor for higher shear span ratios, cancelling out the above effect.

The development of cracking that eventually leads to failure is basically a fracture mechanics phenomenon, which is scale dependent. The effectiveness factor is therefore a decreasing function of the absolute dimensions of the beam, e.g. represented by the depth *h*.

Finally, experience shows a beneficial influence of the reinforcement, possibly due to dowel action, in addition to the dependence upon the reinforcement degree Φ. Hence the effectiveness factor is also an increasing function of the geometrical reinforcement ratio $\rho = A_s/A_c$.

A comprehensive investigation of published test results has been carried out by G.W.Chen (1988). The conclusion is that the effectiveness factor for rectangular, non-prestressed beams can be expressed by the formula:

$$\nu = (1 - 0.25h)(2 - 0.4a/h)(2 + 100\rho)0.60/\sqrt{f_c} \qquad (8.25)$$

where h is measured in m and f_c in N/mm^2, and we have the restrictions:

$$h \leq 1 \text{ m}, \; a/h \leq 2.5, \; \rho \leq 0.02$$

Chen (1988) compared the strength prediction of Eqn (8.11), with v given by Eqn (8.25), with a large number of beam test results (including deep beams and corbels) and found very good agreement. Eqn (8.25) is complicated for practical use, and a safe and reasonably good estimate may be obtained by taking:

$$\nu = 2.0/\sqrt{f_c} \tag{8.26}$$

8.4.4 *Shear reinforcement*

In the analysis so far attention has been given only to beams without secondary reinforcement in the shear span. As the flexural capacity is not influenced by the introduction of shear reinforcement, the latter is seen to be efficient in two cases only i) beams with insufficient support length ($s<s_1$) ii) over-reinforced beams ($\phi>\nu/2$). This above statement is, however, in need of qualification, (see Section 8.5).

The latter case has been investigated (Braestrup and Nielsen, 1983). Considering the failure mechanism of Figure 8.10 we note that a uniformly distributed stirrup reinforcement of strength rf_y will give rise to a corresponding contribution to the rate of internal work, resulting in the upper bound solution:

$$V = \tfrac{1}{2} b \nu f_c \left(\sqrt{a^2 + 4y_o(h - y_o)} - a\right) + barf_y \tag{8.27}$$

with $y_o = h\phi/\nu \leq h/2$.The over-reinforced case is obtained by putting $y_o = h/2$, and a coinciding lower bound can then be found, J.F.Jensen (1981). Eqn (8.27) is only topical for low shear span ratios, the range depending upon the amount of shear reinforcement. For

$$a/h \geq \frac{\nu f_c - rf_y}{2\sqrt{rf_y(\nu f_c - rf_y)}}$$

the strength is given by the general plastic solution for beam shear (the web crushing criterion), Nielsen (1969), Braestrup (1974):

$$V = bh\sqrt{rf_y(\nu f_c - rf_y)} \tag{8.28}$$

with $rf_y \leq \nu f_c/2$. Eqn (8.28) is a coinciding upper and lower bound.

Braestrup (1980) gave a catalogue of solutions for beams with all combinations of longitudinal and web reinforcement (vertical or inclined stirrups) under concentrated or distributed loading.

8.5 Conclusion

In the preceding sections coinciding lower and upper bound solutions have been presented for deep beams subjected to point loading. Basically, the analysis shows that the ultimate load is determined by the flexural capacity, expressed in terms of the clearance a by Eqn (8.11), and in terms of the span l by Eqn (8.16). Note, however, that when the compression zone reaches mid-depth ($y_o=h/2$) the beam becomes over-reinforced. Thus for $\phi>\nu/2$ the ultimate load is governed by the strength of the inclined compression strut, which is found by putting $y=h/2$ irrespective of the yield force of the reinforcement.

On the other hand, the attainment of the flexural capacity requires a certain relationship between the length s of the support platen and the level c of the reinforcement centroid $s\geq s_1$ where s_1 is given by Eqn (8.14) in terms of a, and by Eqn (8.19) in terms of l. For $s<s_1$ the reinforcement does not yield, and the ultimate load is determined in terms of a by Eqn (8.15), and in terms of l by Eqn (8.20) (By solving for $x=V/bvf_c$).

The latter case $s<s_1$ corresponds to the generally observed shear failure, and it typically arises when the reinforcement is placed close to the bottom face of the beam. The stress distribution is shown in Figure 8.7, except that the length of the support platen will normally be designed according to the load (i.e. $s=x$) The capacity is determined by the inclined concrete strut, and as the stresses are concentrated at the extremities the collapse mode may also be classified as bearing failure.

The result is a significant loss of load-carrying capacity, unless the support platen is very large. As shown by the example in Section 8.4.1 it is beneficial to increase the cover to the reinforcement, the small loss in flexural capacity being offset by a large gain in shear strength.

Shear failure of deep beams is, however, also observed in cases where the load is governed by the flexural capacity. This is due to the fact that the effectiveness factor for the concrete is smaller for the sliding failure of the shear mechanism (Figure 8.10) than for the crushing failure of the flexural mechanism (Figure 8.11). For larger shear span ratios this effect is drowned by the influence of the neglected tensile concrete strength, wherefore slender beams are likely to fail in flexure, (*cf.* the discussion in Section 8.4.3).

The lower effectiveness factor for shear failure means that the introduction of shear reinforcement is also beneficial for deep beams which nominally attain their flexural capacity. The strength may be estimated by Eqn (8.27), but this upper bound is not backed by a lower bound solution for $\phi<\nu/2$.

The well known observation that horizontal web reinforcement has little or no effect on the shear strength is readily explained by the fact that the relative displacement rate at failure is close to the vertical.

It may be concluded that the theory of plasticity for structural concrete gives an insight into the behaviour of deep beams at failure, in addition to providing reasonable predictions of the ultimate loads.

References

Braestrup, M.W. (1974) Plastic analysis of shear in reinforced concrete. *Mag. Concr. Res.* **26,** No. 89: 221.

Braestrup, M.W. (1980) Shear capacity of reinforced concrete beams. *Arch Inzyn. Lad.* **26,** No. 2: 295.

Braestrup, M.W. and Nielsen, M.P. (1983) Plastic methods of analysis and design, In *Handbook of Structural Concrete* Ch.20 (Ed: F.K.Kong *et al*.) Pitman, London.

Chen, G.W. (1988) *Plastic analysis of shear in beams, deep beams and corbels* Technical University of Denmark, Department of Structural Engineering, Report R 237.

Chen, W.F. And Drucker, D.C. (1969) Bearing capacity of concrete blocks or rock, *J.Engng Mchs. Am. Soc. Civ. Engrs.* **95,** EM 4: 955.

Drucker, D.C., Prager, W. and Greenberg, H.J. (1952) Extended limit design theorems for continuous media. *Q. Appl.* Math. **9**: 381.

Exner, H. (1979) On the effectiveness factor in plastic analysis of concrete. *Internat. Assoc. Bridge and Struct. Engng:* 35

Gvozdev, A.A. (1938) The determination of the value of the collapse load for statically indeterminate systems undergoing plastic deformation. *Svornik trudov konferentsii po plasticheskim deformatsiyam,* Academy of Sciences, Moscow/Leningrad: 19. [In Russian, English translation: *Int. J.Mech. Sci.* **1,** 1960:322].

Hill, R. (1950) *The mathematical theory of plasticity,* Clarendon Press, Oxford.

Hodge, P.G. and Prager, W. (1948) A variational principle for plastic materials with strain-hardening. *J. Math. Phys.* **27,** No. 1, 1.

IABSE. (1978) *Plasticity in Reinforced Concrete. Introductory Report.* Internat. Assoc. Bridge and Struct. Engineering, Reports of the Working Commissions **28.**

IABSE. (1979) *Plasticity in Reinforced Concrete. Final Report,* Internat. Assoc. Bridge and Struct. Engineering, Reports of the Working Commissions **29.**

Jensen, B.C. (1977) *Some applications of plastic analysis to plain and reinforced concrete.* Technical University of Denmark, Institute of Building Design, Copenhagen, Report No. 123.

Jensen, B.C. (1979) Reinforced concrete corbels—some exact solutions, *Internat. Assoc. Bridge and Struct. Engng:* 293.

Jensen, J.F. (1981) *Plastic solutions for reinforced concrete discs and beams* [In Danish], Technical University of Denmark, Department of Structural Engineering, Report R 141.

Jensen, J.F. (1982) Discussion of K.O.Kemp, M.T.Al-Safi: An upper-bound rigid-plastic solution for the shear failure of concrete beams without shear reinforcement. *Mag. Concr. Res.* **34,** No. 119: 100.

Marti, P. (1980) *Zur plastischen Berechnung von Stahlbeton,* Eidgenössiche Technische Hochschule, Institut für Baustatik und Konstruktion, Zürich, Bericht Nr 104.

Martin, J.B. (1975) *Plasticity: fundamentals and general results.* MIT Press, Cambridge, Mass.

Nielsen, M.P. (1969) On shear reinforcement in reinforced concrete beams [In Danish,], Discusssion, *Bygningsstat. Medd.,* **40** No. 1: 60.

Nielsen, M.P. (1971) On the strength of reinforced concrete discs, *Acta Polytech. Scand., Civ. Engng. Bldg Constr. Ser.,* No. 70.

Nielsen, M.P. and Braestrup, M.W. (1978) Shear strength of prestressed concrete beams without web reinforcement. *Mag. Concr. Res.* **30,** No. 104: 119.

Nielsen, M.P. (1984) *Limit analysis and concrete plasticity,* Prentice- Hall, Englewood Cliffs, NJ.

9 Finite element analysis

Y.K.CHEUNG and H.C.CHAN, University of Hong Kong

Notation

A	cross-sectional area of a member
a, b	dimension of a side of a rectangle
a_i, b_i, c_i	expressions of the nodal coordinates as defined in Zienkiewicz (1971)
B	strain-displacement relationship function
d	diameter of a circular section
D	stress-strain elasticity relationship
ds, dv	differential of a surface, volume
E	modulus of elasticity
F	element nodal forces
G	shear modulus
H	weight coefficient in Gauss numerical integration
$\mathbf{I}$	2×2 identity matrix
J	Jacobian operator
$\overline{J}$	coefficient in the inverted Jacobian matrix
k	stiffness of an element
l	length of a member
$N_i, N_j,$ Nm	shape functions with respect to nodes i, j and m
P	applied load
ΔP	load increment
q	uniformly distributed surface load
R	residual nodal forces in an element due to excess stress
$\boldsymbol{R}$	load vector of an element
ST	strain rotational transformation matrix
t	thickness of an element
T	rotational transformation matrix
u, v	displacement components in the x- and y-directions
x, y	co-ordinates in the x-, y- reference axes
x', y'	local co-ordinates (as a distinction between the global co- ordinates x, y)
X, Y	force component in the x-, y-direction
$\varepsilon\ \gamma$	strains
δ	displacement vector of an element
Δ	area of a triangular element
$\Delta\ \delta$	increment in displacement
$\xi\ \eta$	natural co-ordinates
$\xi'\ \eta'$	first derivative of ξ, η
θ	angle between the local x' -axis and the global x-axis
ν	Poisson's ratio
σ	stress
ϕ	an expression in terms of ξ, η for $\sigma N/\sigma x$
ψ	an expression in terms of ξ, η for $\sigma N/\sigma y$

Subscripts

i, j, m	suffix to denote the node number of a node
r, s	suffix to denote the identity number of a node

Note: Commonly used symbols are self-explanatory and are not defined here again. Most symbols have been defined as they appear in the text and they are better understood within the text. The repeated use of a symbol at different sections with different meanings is unavoidable as the same symbol may be commonly used in different subjects.

9.1 Introduction

In current design practice, structural analysis for reinforced concrete frames is generally based on the assumption that plane sections remain plane after loading and the material is homogeneous and elastic. Therefore, linear elastic methods of analysis are normally adopted for the design of simple reinforced concrete beams and frames to obtain the member forces and bending moments that will enable the design and detailing of the sections to be carried out, despite the fact that reinforced concrete is not a homogeneous and elastic material (British Standard BS 8110:1985).

However, the elementary theory of bending for simple beams may not be applicable to deep beams even under the linear elastic assumption. A deep beam is in fact a vertical plate subjected to loading in its own plane. The strain or stress distribution across the depth is no longer a straight line, and the variation is mainly dependent on the aspect ratio of the beam. (Figure 9.1).

The analysis of a deep beam should therefore be treated as a two-dimensional plane stress problem, and two-dimensional stress analysis methods should be used in order to obtain a realistic stress distribution in deep beams even for a linear elastic solution. There are several methods available for the analysis of deep beams that are either simply supported or continuous.

The classifical analytical method is based on the classical theory of elasticity and it relies on finding a solution for the biharmonic differential equation of Airy's stress function satisfying all boundary conditions. But in the practical situation, a mathematical solution is not always possible.

The finite difference technique may be used to solve the differential equation to obtain a numerical solution if the analytical solution is not readily available. Both methods are more suitable for deep beams with rectangular shapes, straight top and bottom soffits, prismatic constant cross-section and with uniform material properties (Timoshenko and Goodier, 1951)

The finite element method is a much more versatile tool compared with the former methods. It can be used to analyse variable thickness deep beams with curved, stepped or inclined edges. Edge stiffening, openings and loading at any location of the beam can be easily dealt with; and the different properties of the constituent materials, concrete and steel, can be separately represented. By incorporating a known constitutive law and an iterative procedure, the non-homogeneous and non-linear nature of the composite construction can be accounted for (Zienkiewicz, 1971).

9.2 Concept of finite element method

The finite element method can be regarded as an extension of the displacement method for beams and frames to two and three dimensional continuum problems, such as plates, shells and solid bodies. The actual continuum is replaced by an equivalent idealised structure composed of discretised elements connected together at a finite number of nodes.

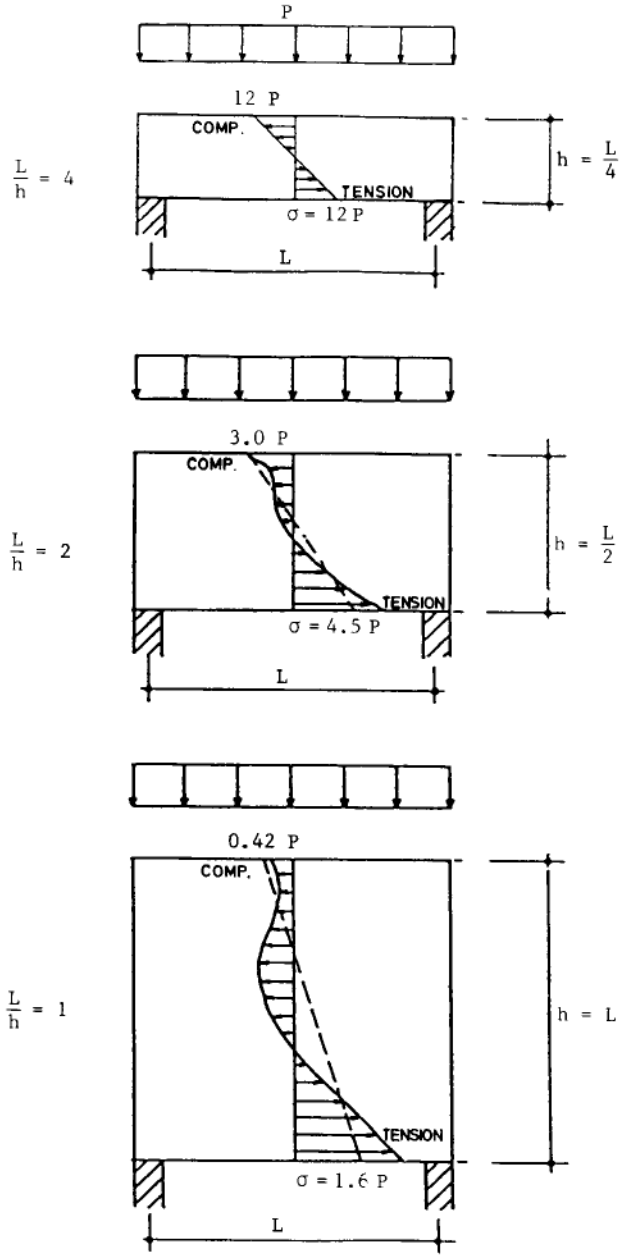

Figure 9.1 Distribution of horizontal stress in beams with various span to depth ratio.

By assuming displacement fields of stress patterns within an element it is possible to derive a stiffness matrix relating the nodal forces to the nodal displacements of an element. The global stiffness matrix of the structure, which is the assemblage of all the elements, is then obtained by combining the individual stiffness matrices of all the elements in the proper manner. If conditions of equilibrium are applied at every node of the idealised structure, a set of simultaneous equations can be formed, the solution of which gives all the nodal displacements, which in turn are used to calculate all the internal stresses (Ghali, Neville and Cheung, 1971).

In applying the finite element method to a problem, it is first necessary to discretise the continuum, that is to subdivide the continuum into small areas of triangular or rectangular shapes. Obviously, it is clear and more straightforward to use triangular elements to model a structure with inclined or curved edges.

9.3 Triangular plane stress elements

Let us therefore first of all derive the stiffness matrix of a triangular element which is the simplest element available in two-dimensional stress analysis.

Consider a triangular element ijm with nodal co-ordinates (x_i, y_i), (x_j, y_j) and (x_m, y_m) respectively as shown in Figure 9.2.

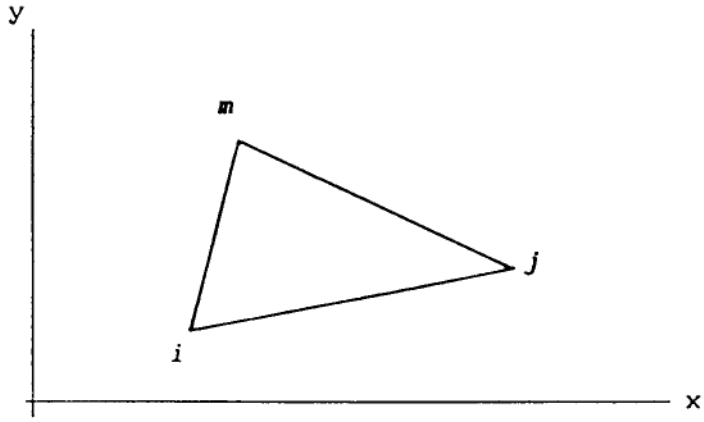

Figure 9.2 Triangular element.

The displacement at any point can be defined by two internal displacement components in the *x*- and *y*-directions, *u(x, y)* and *v(x, y)*. Assuming a linear displacement field the displacements *u* and *v* can be expressed in terms of the nodal displacements and the shape functions N_i, N_j and N_m.

$$\begin{aligned} u &= N_i U_i + N_j U_j + N_m u_m \\ v &= N_i v_i + N_j v_j + N_m v_m \end{aligned} \tag{9.1}$$

in which $N_i=(a_i+b_ix+c_iy)/2\Delta$ etc. for (i, j, m) is simply the area co-ordinate which takes up the value of unity at node i and the value of zero at the edge opposite to node i, where

$$\left.\begin{aligned} a_i &= x_i y_m - x_m y_j \\ b_i &= y_j - y_m \\ c_i &= -x_j + x_m \end{aligned}\right\} \quad \text{etc. for (i, j, m)} \tag{9.2}$$

$$\Delta = \frac{1}{2}\begin{vmatrix} 1 & x_i & y_i \\ 1 & x_j & y_j \\ 1 & x_m & y_m \end{vmatrix} \tag{9.3}$$

In matrix form

$$\begin{aligned} \begin{Bmatrix} u \\ v \end{Bmatrix} &= \begin{bmatrix} \mathbf{I}N_i & \mathbf{I}N_j & \mathbf{I}N_m \end{bmatrix} \{\delta\} \\ &= \begin{bmatrix} N_i & 0 & N_j & 0 & N_m & 0 \\ 0 & N_i & 0 & N_j & 0 & N_m \end{bmatrix} \begin{Bmatrix} u_i \\ v_i \\ u_j \\ v_j \\ u_m \\ v_m \end{Bmatrix} \end{aligned} \tag{9.4}$$

It follows that the strains will be obtained from the derivatives of the displacements as follows

$$\left.\begin{aligned} \varepsilon_x &= \frac{\delta u}{\delta x} = (b_i u_i + b_j u_j + b_m u_m)/2\Delta \\ \varepsilon_y &= \frac{\delta v}{\delta y} = (c_i v_i + c_j v_j + c_m v_m)/2\Delta \\ \gamma_{xy} &= \frac{\delta u}{\delta y} + \frac{\delta v}{\delta x} = [(c_i u_i + c_j u_j + c_m u_m) + (b_i v_i + b_j v_j + b_m v_m)]/2\Delta \end{aligned}\right\} \tag{9.5}$$

or written in matrix form

$$\{\varepsilon\} = \begin{Bmatrix} \varepsilon_x \\ \varepsilon_y \\ \gamma_{xy} \end{Bmatrix} = \begin{Bmatrix} \dfrac{\delta u}{\delta x} \\ \dfrac{\delta v}{\delta y} \\ \dfrac{\delta u}{\delta y} + \dfrac{\delta v}{\delta x} \end{Bmatrix} = \frac{1}{2\Delta} \begin{bmatrix} b_i & 0 & b_j & 0 & b_m & 0 \\ 0 & c_i & 0 & c_j & 0 & c_m \\ c_i & b_i & c_j & b_j & c_m & b_m \end{bmatrix} \begin{Bmatrix} u_i \\ v_i \\ u_j \\ v_j \\ u_m \\ v_m \end{Bmatrix}$$

$$\{\varepsilon\} = [B]\{\delta\} \tag{9.6}$$

in which

$$[B] = \begin{bmatrix} B_i & B_j & B_m \end{bmatrix} = \frac{1}{2\Delta} \begin{bmatrix} b_i & 0 & b_j & 0 & b_m & 0 \\ 0 & c_i & 0 & c_j & 0 & c_m \\ c_i & b_i & c_j & b_j & c_m & b_m \end{bmatrix} \tag{9.7}$$

$$[B_i] = \frac{1}{2\Delta} \begin{bmatrix} b_i & 0 \\ 0 & c_i \\ c_i & b_i \end{bmatrix} \quad \text{etc. for (i, j, m)} \tag{9.8}$$

The stresses in the element are obtained by multiplying the strains by the material elasticity properties

$$\{\sigma\} = [D]\{\varepsilon\} \tag{9.9}$$

For isotropic materials

$$[D] = \frac{E}{1-\nu^2} \begin{bmatrix} 1 & \nu & 0 \\ \nu & 1 & 0 \\ 0 & 0 & \dfrac{1-\nu}{2} \end{bmatrix} \tag{9.10}$$

and in order to prepare for the more general case in non-linear analysis, the more general form for orthotropic materials is given by

$$[D] = \frac{1}{1-\nu_x\nu_y} \begin{bmatrix} E_x & \nu_y E_x & 0 \\ \nu_x E_y & E_y & 0 \\ 0 & 0 & (1-\nu_x\nu_y)G \end{bmatrix} \tag{9.11}$$

or

$$[D] = \begin{bmatrix} E_x & E_n & 0 \\ E_n & E_y & 0 \\ 0 & 0 & G_n \end{bmatrix} \tag{9.12}$$

Where E_x, E_y, E_n and G_n are the material properties which should take the appropriate values at different stress-strain level according to the constitutive law adopted.

The stresses caused by the element nodal displacements are then related by the following relation

$$\{\delta\} = \begin{Bmatrix} \sigma_x \\ \sigma_y \\ \tau_{xy} \end{Bmatrix} = [D]\{\varepsilon\} = [D][B]\{\delta\} \tag{9.13}$$

From virtual work principle, it can be established that the element nodal forces induced by the nodal displacements are given by

$$\{F\} = \int\int [B]^T [D][B]\, t\, dx\, dy\, \{\delta\} \tag{9.14}$$

where t denotes the thickness of the element and hence the stiffness matrix of the element is

$$[k] = \int\int [B]^T [D][B]\, dx\, dy\, t \tag{9.15}$$

Since all the terms are constant, the integral $\iint dx\, dy$ over the whole area of the element is just its area Δ. Hence

$$\{F\} = [B]^T [D][B]\, t\, \Delta \{\delta\} = [k]\{\delta\} \tag{9.16}$$

where

$$\{k\} = [B]^T [D][B]\, t \cdot \Delta \tag{9.17}$$

or written in terms of the sub-matrices

$$[k] = \begin{bmatrix} k_{ii} & k_{ij} & k_{im} \\ k_{ji} & k_{jj} & k_{jm} \\ k_{mi} & k_{mj} & k_{mm} \end{bmatrix} \tag{9.18}$$

The coefficients of the stiffness sub-matrix can be expressed explicitly, e.g. for the case of isotropic medium

$$[k_{rs}] = \frac{Et}{4(1-\nu^2)\Delta} \begin{bmatrix} b_r b_s + \frac{1-\nu}{2} c_r c_s & \nu b_r c_s + \frac{1-\nu}{2} c_r b_s \\ \nu c_r b_s + \frac{1-\nu}{2} b_r c_s & c_r c_s + \frac{1-\nu}{2} b_r b_s \end{bmatrix}; \begin{matrix} (r = \text{i, j, m} \\ s = \text{i, j, m}) \end{matrix} \tag{9.19}$$

and for the general case

$$[k_{rs}] = \frac{t}{4\Delta} \begin{bmatrix} E_x b_r b_s + G_n c_r c_s & E_n b_r c_s + G_n c_r b_s \\ E_n c_r b_s + G_n b_r c_r & E_y c_r c_s + G_n b_r b_s \end{bmatrix}, \begin{matrix} (r = \text{i, j, m} \\ s = \text{i, j, m}) \end{matrix} \tag{9.20}$$

Hence, the forces at a node i are given by

$$\{F_i\} = \begin{Bmatrix} X_i \\ Y_i \end{Bmatrix} = \begin{bmatrix} k_{ii} & k_{ij} & k_{im} \end{bmatrix} \begin{Bmatrix} \delta_i \\ \delta_j \\ \delta_m \end{Bmatrix} \tag{9.21}$$

where $\begin{Bmatrix}\delta_i\\ \delta_j\\ \delta_m\end{Bmatrix}$ are the displacement vectors of the nodes of the triangular element

and

$$\{\delta_i\} = \begin{Bmatrix} u_i \\ v_i \end{Bmatrix}, \qquad \text{etc. for (i, j, m)}$$

9.4 Rectangular plane stress elements

Another type of finite element commonly used for the analysis of deep beams is the rectangular element. However, right-angled rectangular elements are not suitable for beams with inclined or curved edges, and it is more convenient to use the quadrilateral element, which must be formulated through the use of natural co-ordinates (ξ, η) and co-ordinate transformation techniques.

9.4.1 *Isoparametric quadrilaterals*

Based on some mathematical manipulation, regular shaped elements can be distorted into desired irregular shapes with either straight or curved edges which can then be made to coincide nearly with the curved boundary of a structure. In general a one-to-one correspondence must exist between points on the original element and those on the distorted one. The co-ordinates of a point on the parent element and on the distorted one are related by means of interpolation functions or shape functions. If the same shape functions are used to represent the relationships of the displacements as well as the geometric co-ordinates system, the procedure is known as the isoparametric finite element formulation (Zienkiewicz, 1971).

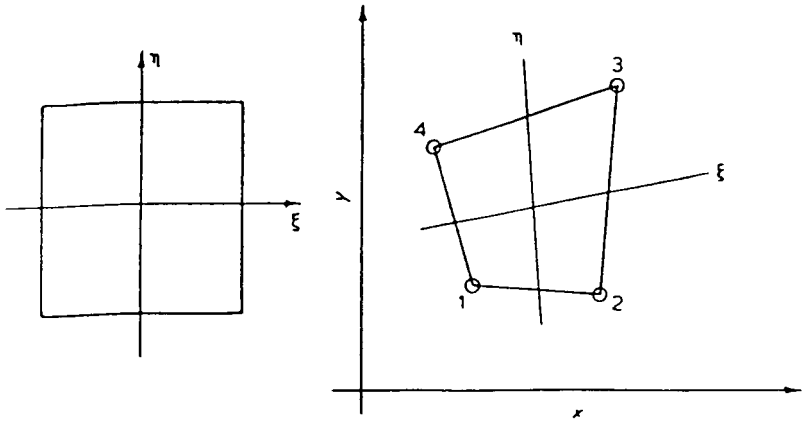

Figure 9.3 Natural co-ordinates of a parent square element and element co-ordinates of a quadrilateral.

For example, the co-ordinates of a point *(x, y)* in a quadrilateral can be expressed in terms of the co-ordinates at the four nodes and the shape functions as

$$\left\{ \begin{array}{l} x = N_1 x_1 + N_2 x_2 + N_3 x_3 + N_4 x_4 \\ y = N_1 y_1 + N_2 y_2 + N_3 y_3 + N_4 y_4 \end{array} \right\} \tag{9.22}$$

in which the N_s are the shape functions given in terms of the natural co-ordinates (ξ, η)) of the corresponding point in the parent square element.

$$\left\{ \begin{array}{l} N_1 = \frac{1}{4}(1-\xi)(1-\eta) \\ N_2 = \frac{1}{4}(1+\xi)(1-\eta) \\ N_3 = \frac{1}{4}(1+\xi)(1+\eta) \\ N_4 = \frac{1}{4}(1-\xi)(1+\eta) \end{array} \right\} \tag{9.23}$$

If the same shape functions are used to relate the displacements

$$\left\{ \begin{array}{l} u = N_1 u_1 + N_2 u_2 + N_3 u_3 + N_4 u_4 \\ v = N_1 v_1 + N_2 v_2 + N_3 v_3 + N_4 v_4 \end{array} \right\} \tag{9.24}$$

the quadrilateral element is called iso-parameteric.

As before, the strains are given by

$$\{\varepsilon\} = \begin{Bmatrix} \varepsilon_x \\ \varepsilon_y \\ \gamma_{xy} \end{Bmatrix} = \begin{Bmatrix} \frac{\delta u}{\delta x} \\ \frac{\delta v}{\delta y} \\ \frac{\delta u}{\delta y} + \frac{\delta v}{\delta x} \end{Bmatrix} = \begin{bmatrix} \frac{\delta N_1}{\delta x} & 0 & \frac{\delta N_2}{\delta x} & 0 & \frac{\delta N_3}{\delta x} & 0 & \frac{\delta N_4}{\delta x} & 0 \\ 0 & \frac{\delta N_1}{\delta y} & 0 & \frac{\delta N_2}{\delta y} & 0 & \frac{\delta N_3}{\delta y} & 0 & \frac{\delta N_4}{\delta y} \\ \frac{\delta N_1}{\delta y} & \frac{\delta N_1}{\delta x} & \frac{\delta N_2}{\delta y} & \frac{\delta N_2}{\delta x} & \frac{\delta N_3}{\delta y} & \frac{\delta N_3}{\delta x} & \frac{\delta N_4}{\delta y} & \frac{\delta N_4}{\delta x} \end{bmatrix} \{\delta\}$$

$$= [B_1 \;\; B_2 \;\; B_3 \;\; B_4]\{\delta\} = [B]\{\delta\} \tag{9.25}$$

with

$$[B_i] = \begin{bmatrix} \frac{\delta N_i}{\delta x} & 0 \\ 0 & \frac{\delta N_i}{\delta y} \\ \frac{\delta N_i}{\delta y} & \frac{\delta N_i}{\delta x} \end{bmatrix}; \qquad (i=1,2,3,4) \tag{9.26}$$

Because the strains are given by the differentials of the displacements with respect to x and y whereas the displacements have now been expressed as functions of ξ and η, the relation between the derivatives in the two co-ordinate systems has to be established and this is done by the chain rule for differentiation to give the Jacobian operator or Jacobian transformation matrix as follows:

$$\frac{\delta N_i}{\delta \xi} = \frac{\delta N_i}{\delta x}\frac{\delta x}{\delta \xi} + \frac{\delta N_i}{\delta y}\frac{\delta y}{\delta \xi}$$
$$\frac{\delta N_i}{\delta \eta} = \frac{\delta N_i}{\delta x}\frac{\delta x}{\delta \eta} + \frac{\delta N_i}{\delta y}\frac{\delta y}{\delta \eta} \tag{9.27}$$

or put in matrix form

$$\begin{Bmatrix} \frac{\delta N_i}{\delta \xi} \\ \frac{\delta N_i}{\delta \eta} \end{Bmatrix} = \begin{bmatrix} \frac{\delta x}{\delta \xi} & \frac{\delta y}{\delta \xi} \\ \frac{\delta x}{\delta \eta} & \frac{\delta y}{\delta \eta} \end{bmatrix} \begin{Bmatrix} \frac{\delta N_i}{\delta x} \\ \frac{\delta N_i}{\delta y} \end{Bmatrix} = [J] \begin{Bmatrix} \frac{\delta N_i}{\delta x} \\ \frac{\delta N_i}{\delta y} \end{Bmatrix} \tag{9.28}$$

where

$$[J] = \begin{bmatrix} \frac{\delta x}{\delta \xi} & \frac{\delta y}{\delta \xi} \\ \frac{\delta x}{\delta \eta} & \frac{\delta y}{\delta \eta} \end{bmatrix} = \begin{bmatrix} \sum_{i=1}^{4} \frac{\delta N_i}{\delta \xi} x_i & \sum_{i=1}^{4} \frac{\delta N_i}{\delta \xi} y_i \\ \sum_{i=1}^{4} \frac{\delta N_i}{\delta \eta} x_i & \sum_{i=1}^{4} \frac{\delta N_i}{\delta \eta} y_i \end{bmatrix} \tag{9.29}$$

$$= \begin{bmatrix} \frac{\delta N_1}{\delta \xi} & \frac{\delta N_2}{\delta \xi} & \frac{\delta N_3}{\delta \xi} & \frac{\delta N_4}{\delta \xi} \\ \frac{\delta N_1}{\delta \eta} & \frac{\delta N_2}{\delta \eta} & \frac{\delta N_3}{\delta \eta} & \frac{\delta N_4}{\delta \eta} \end{bmatrix} \begin{bmatrix} x_1 & y_1 \\ x_2 & y_2 \\ x_3 & y_3 \\ x_4 & y_4 \end{bmatrix} = \begin{bmatrix} J_{11} & J_{12} \\ J_{21} & J_{22} \end{bmatrix}_{(\xi, \eta)} \tag{9.30}$$

The proper differentials are obtained by inversion of $[J]$, which is possible only when there is a one-to-one correspondence between the natural and the local co-ordinates. In general $[J]$ becomes singular for a quadrilateral with a re-entrant corner.

$$\begin{Bmatrix} \frac{\delta N_i}{\delta x} \\ \frac{\delta N_i}{\delta y} \end{Bmatrix} = [J]^{-1} \begin{Bmatrix} \frac{\delta N_i}{\delta \xi} \\ \frac{\delta N_i}{\delta \eta} \end{Bmatrix} = \begin{bmatrix} \bar{J}_{11} & \bar{J}_{12} \\ \bar{J}_{21} & \bar{J}_{22} \end{bmatrix} \begin{Bmatrix} \frac{\delta N_i}{\delta \xi} \\ \frac{\delta N_i}{\delta \eta} \end{Bmatrix} = \begin{Bmatrix} \phi_i \\ \psi_i \end{Bmatrix} \tag{9.31}$$

Therefore

$$[B_i] = \begin{bmatrix} \frac{\delta N_i}{\delta x} & 0 \\ 0 & \frac{\delta N_i}{\delta y} \\ \frac{\delta N_i}{\delta y} & \frac{\delta N_i}{\delta x} \end{bmatrix} = \begin{bmatrix} \phi_i & 0 \\ 0 & \psi_i \\ \psi_i & \phi_i \end{bmatrix} \tag{9.32}$$

The stiffness matric will be given as before by

$$[k] = \int_v [B]^T [D] [B] \, dv = \iint [B]^T [D] [B] \, dx \cdot dy \cdot t$$

$$= \int_{-1}^{1} \int_{-1}^{1} [B]^T [D] [B] \, |J| \, d\xi \cdot d\eta \cdot t \tag{9.33}$$

or in terms of the stiffness sub-matrices

$$[k] = \begin{bmatrix} k_{11} & k_{12} & k_{13} & k_{14} \\ k_{21} & k_{22} & k_{23} & k_{24} \\ k_{31} & k_{32} & k_{33} & k_{34} \\ k_{41} & k_{42} & k_{43} & k_{44} \end{bmatrix} \tag{9.34}$$

in which each of the stiffness sub-matrix is given by

$$[k_{rs}] = \int_{-1}^{1} \int_{-1}^{1} [B_r]^T [D] [B_s] \, |J| \, d\xi \cdot d\eta \cdot t \; ; \quad (r = 1, 2, 3, 4; \quad s = 1, 2, 3, 4) \tag{9.35}$$

An explicit solution of $[J]^{-1}$ and the subsequent integrals are generally not obtainable and numerical integration technique has to be resorted to. Gaussian integration is one of the processes commonly used for this purpose.

$$[k_{rs}] = \sum_{j=1}^{n} \sum_{i=1}^{n} H_j H_i [B_r]_{ji}^T [D] [B_s]_{ji} \, |J| \cdot t \tag{9.36}$$

Where H_j and H_i are the weight coefficients corresponding to the specified Gauss points (ξ_j, η_i) and n is the number of Gauss points in each direction.

Table 9.1 Gaussian point natural co-ordinates and weight coefficients

Number of Gauss points $n \times n$	Gaussian point natural coordinate ξ or η	Weight coefficient H_i or H_j
2 x 2	–0.5773502692	1.0
	0.5773502692	1.0
3 x 3	–0.7745966692	0.5555555555
	0.0	0.8888888889
	0.7745966692	0.5555555555

9.4.2 *Equivalent load vector*

The equivalent load vector at the nodes due to the effect of uniformly distributed element surface load is

$$\{R_s\} = \int_s [N^T]\{q\}\, dS = \int_{-1}^{1}\int_{-1}^{1} [N^T]\{q\}\,|J|\, d\xi \cdot d\eta$$
$$= \sum_{j=1}^{n}\sum_{i=1}^{n} H_j H_i [N_r]_{ji}^T \{q\}\,|J| \qquad (9.37)$$

9.4.3 *Stiffness matrix of rectangle with sides* $2a \times 2b$

For example, consider a rectangle with sides 2a×2b as shown in Figure 9.4.

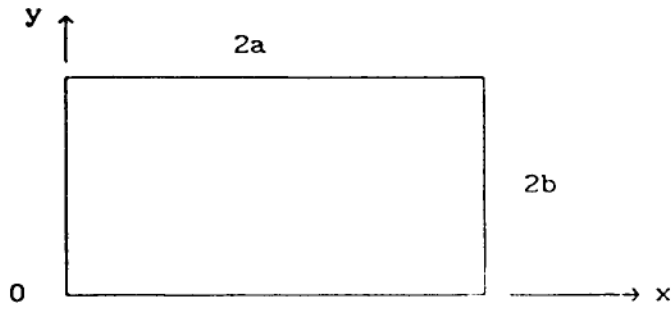

Figure 9.4 Rectangular element.

The Jacobian transformation matrix is

$$[J] = \tfrac{1}{4}\begin{vmatrix} -(1-\eta) & (1-\eta) & (1+\eta) & -(1+\eta) \\ -(1-\xi) & -(1+\xi) & (1+\xi) & (1-\xi) \end{vmatrix} \begin{vmatrix} 0 & 0 \\ 2a & 0 \\ 2a & 2b \\ 0 & 2b \end{vmatrix}$$

$$= \tfrac{1}{4}\begin{vmatrix} \{(1-\eta)2a + (1+\eta)2a\} & \{(1+\eta)2b - (1+\eta)2b\} \\ \{-(1+\xi)2a + (1+\xi)2a\} & \{(1+\xi)2b + (1-\xi)2b\} \end{vmatrix} = \begin{vmatrix} a & 0 \\ 0 & b \end{vmatrix}$$

$$|J| = a.b, \qquad [J]^{-1} = \frac{1}{a.b}\begin{vmatrix} b & 0 \\ 0 & a \end{vmatrix} = \begin{vmatrix} \frac{1}{a} & 0 \\ 0 & \frac{1}{b} \end{vmatrix}$$

$$\begin{Bmatrix} \frac{\delta N_i}{\delta x} \\ \frac{\delta N_i}{\delta y} \end{Bmatrix} = [J]^{-1}\begin{Bmatrix} \frac{\delta N_i}{\delta \xi} \\ \frac{\delta N_i}{\delta \eta} \end{Bmatrix} = \begin{Bmatrix} \frac{1}{a}\,\frac{1}{4}\,\xi_i'\,(1+\eta_i'\eta) \\ \frac{1}{b}\,\frac{1}{4}\,\eta_i'\,(1+\xi_i'\xi) \end{Bmatrix} = \begin{Bmatrix} \phi_i \\ \psi_i \end{Bmatrix}$$

in which for i=1, 2, 3, 4
ξ'_i=-1, 1, 1, -1 and
η'_j=-1, -1, 1, 1 respectively

$$[B_i] = \begin{bmatrix} \frac{\delta N_i}{\delta x} & 0 \\ 0 & \frac{\delta N_i}{\delta y} \\ \frac{\delta N_i}{\delta y} & \frac{\delta N_i}{\delta x} \end{bmatrix} = \begin{bmatrix} \phi_i & 0 \\ 0 & \psi_i \\ \psi_i & \phi_i \end{bmatrix}$$

$$[B_r]^T [D] [B_s] = \begin{bmatrix} \phi_r & 0 & \psi_r \\ o & \psi_r & \phi_r \end{bmatrix} \begin{bmatrix} E_x & E_n & 0 \\ E_n & E_y & 0 \\ 0 & 0 & G_n \end{bmatrix} \begin{bmatrix} \phi_s & 0 \\ 0 & \psi_s \\ \psi_s & \phi_s \end{bmatrix}$$

$$= \begin{bmatrix} (\phi_r E_x \phi_s + \psi_r G_n \psi_s) & (\phi_r E_n \psi_s + \psi_r G_n \phi_s) \\ (\psi_r E_n \phi_s + \phi_r G_r \psi_s) & (\psi_r E_y \phi_s + \phi_r G_n \phi_s) \end{bmatrix}$$

Substituting into

$$[k_{rs}] = \int_{-1}^{1} \int_{-1}^{1} [B_r]^T [D] [B_s] \mid J \mid d\xi \cdot d\eta \cdot t$$

gives the stiffness coefficients in the stiffness matrix.
To find $[k_{11}]$

$$\phi_1 = -\frac{1}{4a}(1-\eta) \qquad \psi_1 = -\frac{1}{4b}(1-\xi)$$

$$\int_{-1}^{1}\int_{-1}^{1} \phi_1 \phi_1 \, d\xi d\eta = \frac{1}{16a_2} \quad \int_{-1}^{1}\int_{-1}^{1} (1-\eta)^2 \, d\xi d\eta = \frac{1}{3a^2}$$

$$\int_{-1}^{1}\int_{-1}^{1} \psi_1 \psi_1 \, d\xi d\eta = \frac{1}{16b^2} \quad \int_{-1}^{1}\int_{-1}^{1} (1-\xi)^2 \, d\xi d\eta = \frac{1}{3b^2}$$

$$\int_{-1}^{1}\int_{-1}^{1} \phi_1 \psi_1 \, d\xi d\eta = \frac{1}{16ab} \quad \int_{-1}^{1}\int_{-1}^{1} (1-\eta)(1-\xi) \, d\xi d\eta = \frac{1}{4ab}$$

$$k_{11} = t \begin{bmatrix} \frac{b}{3a} E_x + \frac{a}{3b} G_n & -\frac{1}{8} E_n - \frac{1}{8} G_n \\ -\frac{1}{8} E_n - \frac{1}{8} G_n & \frac{a}{3b} E_y + \frac{b}{3a} G_n \end{bmatrix}$$

To find $[k_{21}]$

$$\phi_1 = \frac{1}{4a}(1-\eta) \qquad \psi_1 = -\frac{1}{4b}(1-\xi)$$

$$\phi_2 = \frac{1}{4a}(1-\eta) \qquad \psi_2 = -\frac{1}{4b}(1+\xi)$$

$$\int_{-1}^{1}\int_{-1}^{1}\psi_2\phi_1\,d\xi d\eta = -\frac{1}{16a^2}\int_{-1}^{1}\int_{-1}^{1}(1-\eta)^2\,d\xi d\eta = -\frac{1}{3a^2}$$

$$\int_{-1}^{1}\int_{-1}^{1}\psi_2\psi_1\,d\xi d\eta = \frac{1}{16b^2}\int_{-1}^{1}\int_{-1}^{1}(1-\xi^2)\,d\xi d\eta = \frac{1}{6b^2}$$

$$\int_{-1}^{1}\int_{-1}^{1}\phi_2\psi_1\,d\xi d\eta = -\frac{1}{16ab}\int_{-1}^{1}\int_{-1}^{1}(1-\eta)(1-\xi)\,d\xi d\eta = -\frac{1}{4ab}$$

$$\int_{-1}^{1}\int_{-1}^{1}\psi_2\phi_1\,d\xi d\eta = \frac{1}{16ab}\int_{-1}^{1}\int_{-1}^{1}(1+\xi)\,1-\eta)\,d\xi d\eta = \frac{1}{4ab}$$

$$k_{21} = t\begin{bmatrix} -\frac{b}{3a}E_x + \frac{a}{6b}G_n & -\frac{1}{4}E_n + \frac{1}{4}G_n \\ \frac{1}{4}E_n - \frac{1}{4}G_n & \frac{a}{6b}E_y - \frac{b}{3a}G_n \end{bmatrix}$$

and similarly for other stiffness sub-matrices.

For the case of isotropic elasticity

$$[D] = \begin{bmatrix} E_x & E_n & 0 \\ E_n & E_y & 0 \\ 0 & 0 & G_n \end{bmatrix} = \frac{E}{1-\nu^2}\begin{bmatrix} 1 & \nu & 0 \\ \nu & 1 & 0 \\ 0 & 0 & \frac{1-\nu}{2} \end{bmatrix}$$

The full stiffness matrix for the rectangular element with sides $2a \times 2b$ is

$$[k] = \frac{Et}{1-\nu^2}\left[\begin{array}{cccc} \frac{1}{3}\frac{b}{a} + \frac{1-\nu}{6}\frac{a}{b} & & & \\ \frac{1+\nu}{8} & \frac{1}{3}\frac{a}{b} + \frac{1-\nu}{6}\frac{b}{a} & & \text{Symmetric} \\ -\frac{1}{3}\frac{b}{a} + \frac{1-\nu}{12}\frac{a}{b} & \frac{1-3\nu}{8} & \frac{1}{3}\frac{b}{a} - \frac{1-\nu}{6}\frac{a}{b} & \\ -\frac{1-3\nu}{8} & \frac{1}{6}\frac{b}{a} - \frac{1-\nu}{6}\frac{b}{a} & -\frac{1-\nu}{8} & \frac{1}{3}\frac{a}{b} + \frac{1-\nu}{6}\frac{b}{a} \\ \hline -\frac{1}{6}\frac{b}{a} - \frac{1-\nu}{12}\frac{a}{b} & -\frac{1+\nu}{8} & \frac{1}{6}\frac{b}{a} - \frac{1-\nu}{6}\frac{a}{b} & \frac{1-3\nu}{8} \\ -\frac{1+\nu}{8} & -\frac{1}{6}\frac{a}{b} - \frac{1-\nu}{12}\frac{b}{a} & -\frac{1-3\nu}{8} & -\frac{1}{3}\frac{a}{b} + \frac{1-\nu}{12}\frac{b}{a} \\ \frac{1}{6}\frac{a}{b} - \frac{1-\nu}{6}\frac{a}{b} & -\frac{1-3\nu}{8} & -\frac{1}{6}\frac{b}{a} - \frac{1-\nu}{12}\frac{a}{b} & \frac{1+\nu}{8} \\ \frac{1-3\nu}{8} & -\frac{1}{3}\frac{a}{b} + \frac{1-\nu}{12}\frac{b}{a} & \frac{1+\nu}{8} & -\frac{1}{6}\frac{a}{b} - \frac{1-\nu}{12}\frac{b}{a} \end{array}\right]$$

		Symmetric	
$\frac{1}{3}\frac{b}{a}+\frac{1-\nu}{6}\frac{a}{b}$			
$\frac{1+\nu}{8}$	$\frac{1}{3}\frac{a}{b}+\frac{1-\nu}{6}\frac{b}{a}$		
$\frac{1}{3}\frac{b}{a}+\frac{1-\nu}{12}\frac{a}{b}$	$\frac{1-3\nu}{8}$	$\frac{1}{3}\frac{b}{a}+\frac{1-\nu}{6}\frac{a}{b}$	
$-\frac{1-3\nu}{8}$	$\frac{1}{6}\frac{b}{a}-\frac{1-\nu}{6}\frac{b}{a}$	$-\frac{1-\nu}{8}$	$\frac{1}{3}\frac{a}{b}+\frac{1-\nu}{6}\frac{b}{a}$

9.5 Elastic stress distribution in deep beam by finite element method

If it is only required to obtain a pattern of the stress distribution in a deep beam for preliminary study or design purpose, one can proceed by assuming the reinforced concrete beam as an elastic isotropic plate, discretising the beam with triangular and/or rectangular elements, assembling the element stiffness matrices and setting up equilibrium equations for the nodes. The nodal displacements can be solved and the element principal stresses calculated. Figure 9.5 shows the distribution of the magnitude and direction of the principal stresses in a simply supported deep beam with a span/depth ratio of 2.0 subjected to a uniformly distributed load applied at the top.

9.6 Finite element model for cracked reinforced concrete

However, the linear elastic solutions and stress distributions will have little meaning once cracking of concrete occurs, and a more sophisticated finite element model which can make a realistic representation of reinforced concrete and take into account the actual complexity of the construction should be employed.

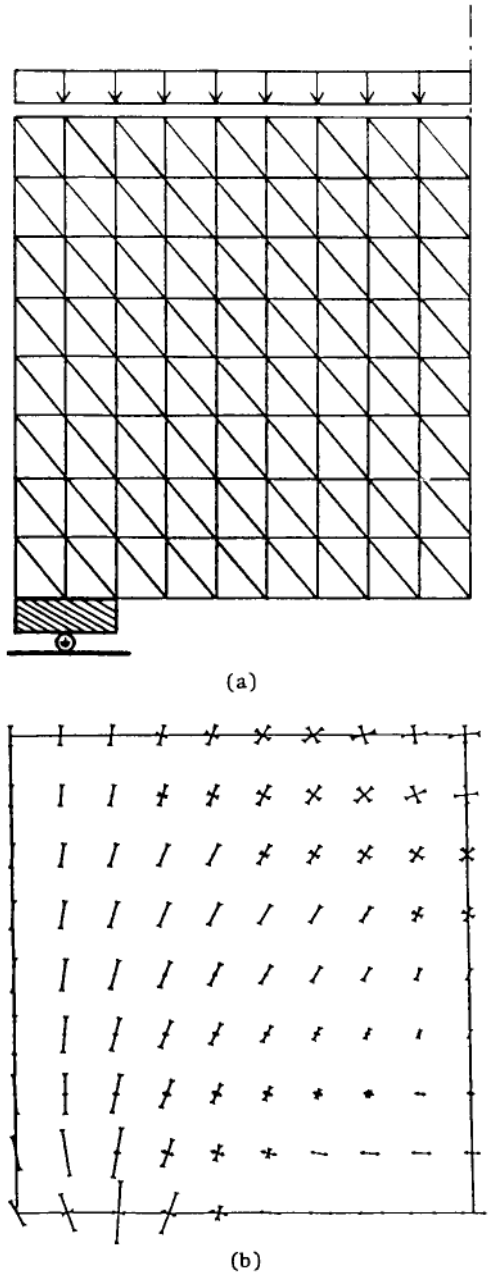

Figure 9.5 (a) Idealisation by triangular element; (b) Elastic stress distribution of a simply supported deep beam with span/depth ratio of 2.0 subjected to a uniformly distributed load applied at top.

In a more realistic numerical model, it is necessary to take into account:

i) the composite nature of the construction—the reinforced concrete section is composed of two different materials, concrete and steel, with intrinsically different properties;
ii) the non-homogeneous and non-linear behaviour of concrete—concrete is a mixture of aggregates and mortar and is highly non-homogeneous; the stress-strain relationship for concrete varies with many variables and is non-linear under load;
iii) the possible relative slip between steel reinforcement and concrete and the effect of the bond stress;
iv) the low tensile strength of concrete—as a result of which progressive cracking of the concrete section will occur under increasing load;
v) other time-dependent effects of the materials such as shrinkage and creep.

In view of the great complexities involved in such a problem, it is virtually impossible to obtain an exact analytical solution for the distribution of stresses throughout a reinforced concrete member by direct application of the classical theories of continuum mechanics. Approximate numerical methods must be resorted to and the finite element method is apparently one of the most appropriate approaches. In order to deal with the composite material, it is necessary that separate finite elements are used to represent individually the steel bars and the concrete in a reinforced concrete section (Ngo and Scordelis, 1967).

9.7 Modelling of reinforcing steel bars

For the steel bars, whether tension or compression main steel, distribution bars or stirrups, it is possible to use either the triangular or the rectangular element, as described in the previous sections, to model them.

If triangular or rectangular elements are used, the circular section of a bar of diameter d is taken as an equivalent square with sides $\sqrt{\pi}\, d/2$ and the thickness of concrete at the steel level is reduced accordingly (Nilson, 1968).

Reinforcing steel bars can also be modelled in a much simpler manner by bar elements or line elements (Figure 9.6).

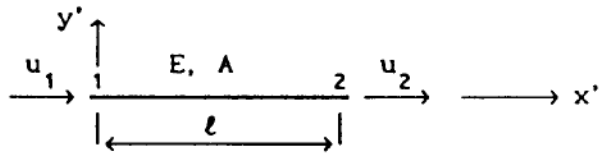

Figure 9.6 Bar element

For a bar element as shown in Figure 9.6 the displacement function is

$$u = [(1 - \frac{x'}{l}) \ , \ \frac{x'}{l}] \begin{Bmatrix} u_1 \\ u_2 \end{Bmatrix} \tag{9.38}$$

By the method already explained earlier, the stiffness of the bar is

$$[k] = \frac{EA}{l} \begin{bmatrix} 1 & -1 \\ -1 & 1 \end{bmatrix} \tag{9.39}$$

For simplicity, it is sometimes assumed that the bar elements are connected to the planar elements in such a way that the bar elements do not occupy any cross-sectional area of the planar elements and they are interconnected at the nodes with perfect bonding (Nam and Salmon, 1974).

9.8 Point element or linkage element

At low stress level, perfect bonding between steel and concrete may exist. As the stresses in the steel and concrete increase, cracking as well as breaking of the bond will occur and there will be bond slip between the bar and concrete (Ngo and Scordelis, 1967)

In order to account for the slip between concrete and steel a point element or linkage (Figure 9.7) element may be used to connect the steel and concrete elements. This can be considered to consist of two springs with appropriate stiffnesses arranged in orthogonal directions, parallel to the axes along the longitudinal direction of the bar and the normal direction. These springs are considered to have negligible lengths and only their mechanical

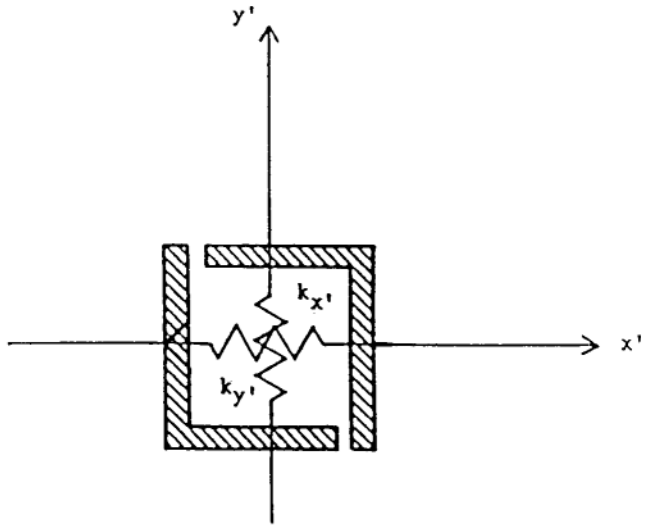

Figure 9.7 Linkage element

properties are significant in the analysis. Therefore a point element is assumed to have no physical dimensions (Ngo and Scordelis 1967). The stiffness matrix of the linkage element is

$$\begin{Bmatrix} \sigma_{x'} \\ \sigma_{y'} \end{Bmatrix} = \begin{bmatrix} k_{x'} & 0 \\ 0 & k_{y'} \end{bmatrix} \begin{Bmatrix} u \\ v \end{Bmatrix} \tag{9.40}$$

For generality, the reference x' axis of the linkage element or bar element may be oriented at any angle θ with the horizontal axis of the beam. The usual rotational transformation matrix

$$[T] = \begin{bmatrix} \cos\theta & \sin\theta \\ -\sin\theta & \cos\theta \end{bmatrix} \qquad \text{and its transpose } [T^{\mathrm{T}}]$$

should be applied to the displacement, force and stiffness matrices.

9.9 Discrete cracking model

Wherever relative movement such as slip or crack is anticipated, a linkage element may be introduced at the nodal point at which a steel element is connected to a concrete element or between the adjacent concrete elements which are triangular or quadrilateral finite elements (Ngo and Scordelis, 1967). A discrete cracking model will then result (Figure 9.8).

The spring in the linkage element parallel to the longitudinal axis of the bar represents the bonding between the steel and concrete elements. It will

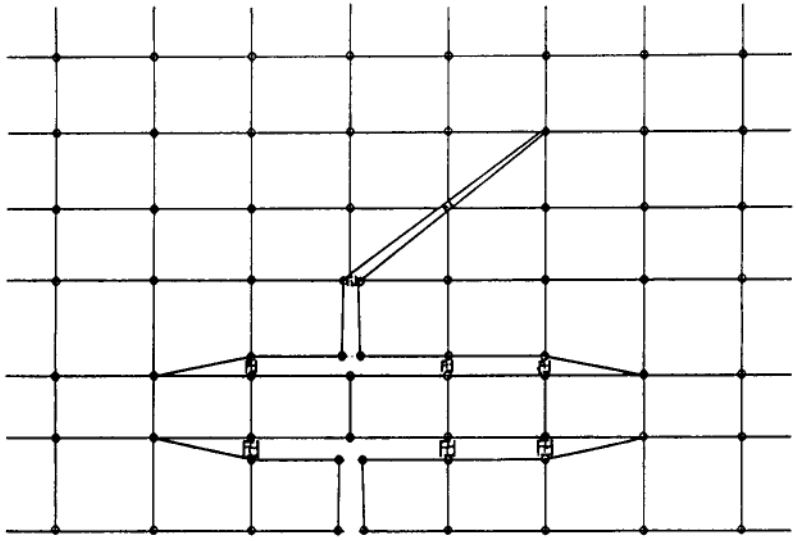

Figure 9.8 Discrete cracking model

permit a certain amount of slippage to take place during the transfer of stress from steel to concrete. The amount of slippage at various stress levels will depend on the assumed characteristics of the spring.

The true relationship between bond slip and bond stress is a complex one which is affected by many factors. From their study of bond stress-slip relationships, Mirza and Houde (1979) proposed the bond spring stiffness modulus as

$$\frac{\text{d(stress)}}{\text{d(slip)}} = 1.95\times 10^{6} - 4.70\times 10^{9}s + 4.17\times 10^{12}s^{2} - 1.32\times 10^{15}s^{3} \qquad (9.41)$$

where s is slip in inch and pound force units. For simplicity a linear relationship between bond slip and bond stress could be assumed for k_x (Ngo and Scordelis, 1967).

The spring in the linkage element normal to the direction of the bar represents the effect of the relation of bond stress and normal separation. This effect depends not only on the adhesion and the mechanical interlocking between the steel and concrete, but also on how well the surrounding concrete is holding the steel from vertical separation. The vertical spring stiffness k_y is even more difficult to determine. It is reasonable to stipulate that under normal conditions the vertical separation is very small and its effect may be neglected. Hence the spring in the normal direction to the bar is assumed to be very stiff and k_y is arbitrarily taken to be a very large value. This means that the steel element is rigidly connected to the concrete element in the normal direction of the bar (Ngo and Scordelis, 1967).

In the case when a point element is used to define a crack between two concrete elements the spring stiffness should be an appropriate representation of the relationship between the tensile stress and strain as well as the aggregate interlocking force of concrete (Nilson, 1982).

9.10 Smeared cracking model

Since the use of a discrete cracking model is not sufficiently flexible with regard to the location of crack development and also involves the complications of a bond-slip relationship which has not been definitely established yet, some investigators prefer not to use a linkage element at all but to put up with the assumption that perfect bond exists between concrete and reinforcement in their analysis (Valliappan and Doolan, 1972) leading to what is called a smeared cracking model (Figure 9.9).

In this approach, the cracked concrete is assumed to remain a continuum, and the effect of the cracks is assumed to spread over the entire element or a portion of it. After the first crack has occurred, the concrete will become orthotropic with one axis being oriented along the direction of the crack. This model has the advantage that cracks are allowed to form anywhere in the structure as the stresses reach the limiting

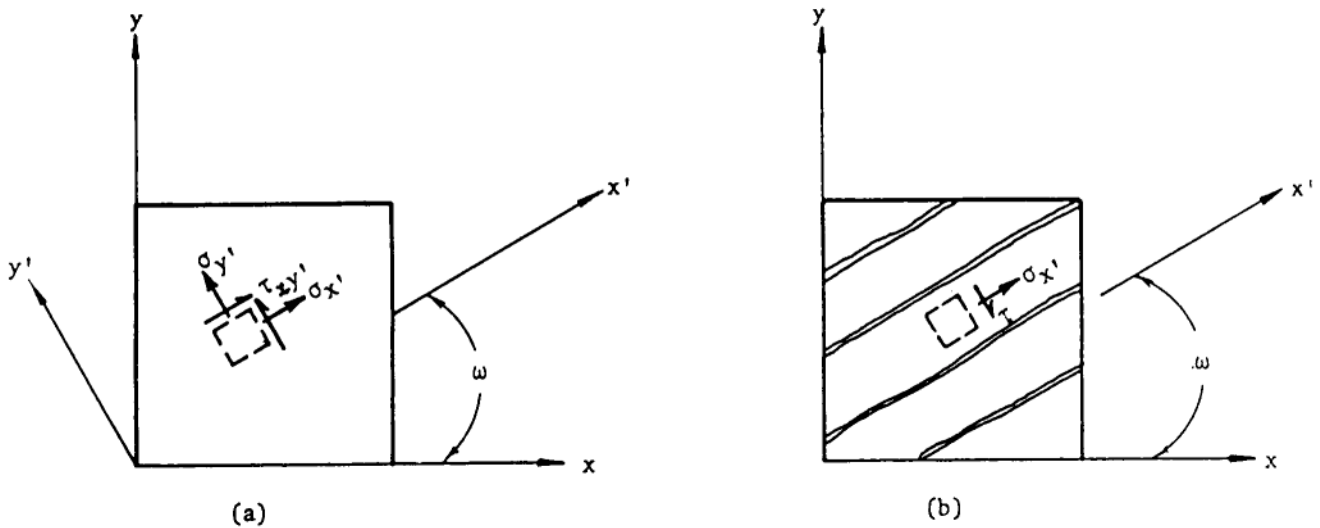

Figure 9.9 Smeared crack model showing stress distribution (a) just before cracking: (b) just after cracking

value and the same delineated model with the node numbers can be retained throughout the entire non-linear analysis.

9.11 Modelling of constitutive relationships of concrete

In non-linear finite element analysis of reinforced concrete structures, the stress-strain relationships of concrete under various conditions are required. A great deal of research work has been done in this field in recent years and there are several proposals commonly used in the finite element analysis of reinforced concrete structures.

Liu, Nilson and Slate (1972) assumed concrete to be orthotropic with two tangential moduli of elasticity which vary according to the state of stress and strain in each principal direction. They proposed the following incremental constitutive relations in the form of an elasticity matrix:

$$\begin{bmatrix} d\sigma_1 \\ d\sigma_2 \\ d\sigma_{12} \end{bmatrix} = \begin{bmatrix} \lambda' \dfrac{E'_{1b}}{E'_{2b}} & \lambda'\nu & 0 \\ \lambda'\nu & \lambda' & 0 \\ 0 & 0 & \dfrac{E'_{1b}E'_{2b}}{E'_{1b}+E'_{2b}+2E'_{2bv}} \end{bmatrix} \begin{bmatrix} d\varepsilon_1 \\ d\varepsilon_2 \\ d\varepsilon_{12} \end{bmatrix} \tag{9.42}$$

in which E'_{1b} and E'_{2b} the two tangential moduli, are given by

$$E'_{ib} = \frac{\left(1 - \left(\dfrac{\varepsilon_i}{\varepsilon_p}\right)^2\right)}{\left[1 + \left(\dfrac{1}{1-\nu\alpha_i}\dfrac{E}{E_s} - 2\right)\left(\dfrac{\varepsilon_i}{\varepsilon_p}\right) + \left(\dfrac{\varepsilon_i}{\varepsilon_p}\right)^2\right]^2} \tag{9.43}$$

and $$\lambda' = \frac{E'_{1b}}{\dfrac{E'_{1b}}{E'_{2b}} - \nu^2} \tag{9.44}$$

Tasuji, Slate and Nilson (1978) suggested the following expression for the biaxial stress-strain relationship for plain concrete:

$$\sigma = \frac{E\varepsilon}{(1-\nu k)\left[1 + \left(\dfrac{1}{1-\nu k}\dfrac{E}{E_s} - 2\right)\left(\dfrac{\varepsilon}{\varepsilon_p}\right) + \left(\dfrac{\varepsilon}{\varepsilon_p}\right)^2\right]} \tag{9.45}$$

where σ is principal stress, ε is principal strain, E is the uniaxial elastic modulus, ν is Poisson's ratio, k is the ratio of principal stresses, σ_p is the

ultimate stress, ε_p is strain at ultimate stress and $E_s=\sigma_p/\varepsilon_p$ is the secant modulus at ultimate load.

Kotsovos (1984) proposed that if the internal compressive state of stress is known, the non-linear behaviour of concrete can be described by using linear material properties. Thus the strains (ε_1, ε_2, ε_3) corresponding to a given state of applied principal stresses (σ_1, σ_2, σ_3) can be related by Hooke's law as follows:

$$\begin{aligned} E\varepsilon_1&=(\sigma_1+s_1)-\nu(\sigma_2+s_{2+}\sigma_3+s3)\\ E\varepsilon_2&=(\sigma_2+s_2)-\nu(\sigma_3+s_{3+}\sigma_1+s_1)\\ E\varepsilon_3&=(\sigma_3+s_3)-\nu(\sigma_1+s_1+\sigma_2+s_2)\end{aligned} \tag{9.46}$$

where E is modulus of elasticity, v is Poisson's ratio and (s_1, s_2, s_3) are the principal stress components of the internal compressive state of stress. Details of these expressions are given in the corresponding references. A number of other proposals can be found in the literature [9.6, 9.18–21] (Chen and Han, 1988, Han and Chan, 1987; Chen and Chan, 1975, Kupfer and Gerstle, 1973 Darwin and Pecknold 1977).

9.12 Constitutive relationship of steel bars

The steel bars are generally assumed to take axial forces only. Hence, the stress-strain relationship under uniaxial loading is required and the most commonly adopted model is the bilinear curve with a linearly elastic and a perfectly plastic branch. The same relationship is assumed for compression as well as for tension. This is similar to that specified in Figure. 2.2 of BS

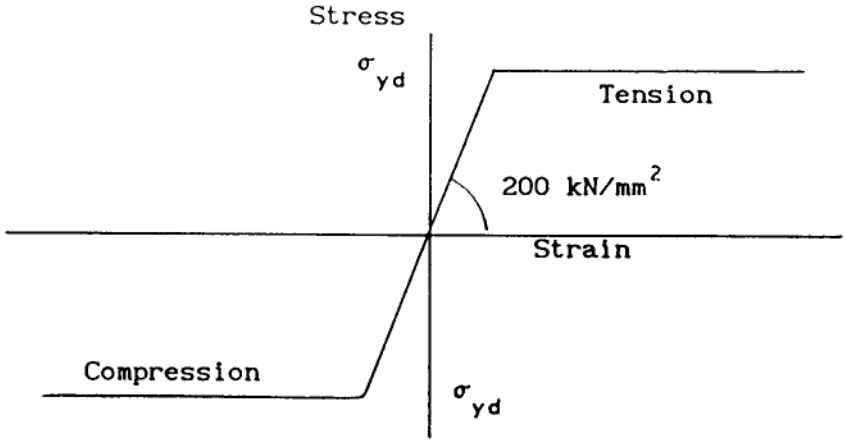

Figure 9.10 Stress-strain curve for steel reinforcement

8110 1985. However, it has been pointed out that the plastic range of the curve should be given a slight inclination to facilitate computation (Kotsovos, 1984) (Figure 9.10).

9.13 Cracking in concrete and yielding in steel

Concrete has a very limited tensile strength. If the principal tensile stress in the concrete exceeds its tensile capacity, cracks will develop in the direction perpendicular to the appropriate principal stress. The tensile stress that fictitiously existed just prior to cracking has to be removed and transferred to other parts of the structure. This is done by working out the equivalent nodal forces in the element due to the excess stress and treating them as additional external loads in the next cycle of iteration in non-linear analysis (Zienkiewicz, 1971; Valliappan and Doolan, 1972).

$$\{R\} = \Sigma \int_v [B^T] \{\sigma_{ex}\} \, dv \tag{9.47}$$

Similarly, if the stress value exceeds the yield strength of the material, the excess stress is also to be removed and transferred in the same manner. In this case only the portion of the stress exceeding the yield stress is removed; whereas in the case of cracking, all of the normal stress perpendicular to the crack becomes excess stress.

9.14 Stiffness of cracked element

Once yielding or cracking has started to form and develop in an element, the material elasticity matrix will be different and its stiffness will decrease. The element which has cracked should have its stiffness reduced before going further with the analysis.

For a quadrilateral element, direct integration cannot be performed on the cracked element because the stiffness function is no longer continuous. Only approximate integrations are possible with cracked elements.

In the smeared cracking model, it is assumed that the concrete becomes anisotropic with one of the material axis x' being oriented along the direction of the crack. The modulus of elasticity along the direction perpendicular to the crack will be reduced to zero whereas the modulus of elasticity along the direction of the crack may remain to take its appropriate value under uncracked condition. Hence, the elasticity matrix $[D_{x'}]$ should be modified to

$$\begin{bmatrix} E_{x'} & 0 & 0 \\ 0 & 0 & 0 \\ 0 & 0 & \lambda G \end{bmatrix}$$

in which x' is parallel to the crack. The introduction of the cracked shear factor $\lambda(0<\lambda\leq 1)$ will enable the effective shear modulus to be estimated realistically (Liu and Scordelis, 1975; Suidan and Schnobrich, 1973) The new elasticity matrix is now at an angle of rotation, say ?, with regard to the global axis. Hence

$$[D_x]=[ST]\,[D_{x'}]\,[ST]^T \tag{9.48}$$

in which

$$[\,ST\,]=\begin{bmatrix} \cos^2\omega & \sin^2\omega & -2\sin\omega\cos\omega \\ \sin^2\omega & \cos^2\omega & 2\sin\omega\cos\omega \\ \sin\omega\cos\omega & -\sin\omega\cos\omega & \cos^2\omega-\sin^2\omega \end{bmatrix} \tag{9.49}$$

is the strain rotational transformation matrix.

The Gaussian integration points are used as check points to assess cracking or plasticity, assuming that the elastic coefficient matrix [**D**] varies continuously throughout the element.

An alternative method is to use four corner nodes as the check points (Nam and Salmon, 1974). If cracking or yielding is present at a node, necessary adjustment to elasticity coefficients and computation of excess stress are made. Interpolation by the Lagrangian interpolation formula is used to get the appropriate values at the Gaussian integration points. These values are used to determine the cracked element stiffness and the unbalanced nodal forces.

9.15 Solution procedure

With all these techniques, a realistic numerical model for reinforced concrete structures can be built up. Now it depends on the degree of sophistication of the solution required which different numerical procedures should be followed.

If the applied loading is small compared with the ultimate load, it may be assumed that the structure behaved elastically and a linear elastic analysis can be performed to give the elastic stress distribution in the steel and in different parts of the concrete. If nearly full ultimate loading is considered then it is necessary to have the non-linear stress-strain relationships, tensile cracking strength and bond stress-slip relationship and so on established and a non-linear analysis can then be performed.

The major steps in the linear and non-linear analysis at a typical load increment are:

Linear analysis:

i) Subdivision of the deep beam and representing different parts by appropriate types of finite elements
ii) Generation of the element stiffness

iii) Assembly of the structure stiffness
iv) Assembly of the load vector
v) Solution for the nodal displacements
vi) Determination of the element stresses

Additional steps in each load increment of the *non-linear analysis:*

vii) Check for cracking, yielding, and failure
viii) Determination of the unbalanced nodal forces
ix) Check for convergence
x) If new crack appears: repeat steps ii)–iii) and then followed by steps
x) If yielding only occurs: repeat steps iv)–ix)
xi) Stop when failure occurs or when full loading has been applied.

The linear solution procedure is well-known (Ghali, Neville and Cheung, 1971) and needs no further explanation.

Three different approaches are commonly used to solve a non-linear problem, namely: incremental procedure, iterative procedure, and mixed procedure.

9.15.1 *Increment procedure*

The total load is divided into a number of equal or unequal load increments. At each step only one increment of load is added to the structure each time. At each stage of loading the stiffness of the structure may have a different value depending on the deformation reached and the constitutive law adopted for the material as well as the method for estimating the stiffness at that stage. After the application of the (*i*-l)th load increment ΔP_{i-1} and the determination of the stress σ_{i-1}, the elasticity matrix $[D_{i-1}]$ can be determined from the stress-strain relationship and hence the new stiffness $[K_i]$ can be estimated. The *i*th increment of displacement can then be determined from

$$[K_i]\{\Delta\delta_i\} = \{\Delta P_i\} \tag{9.50}$$

It is obvious that in the incremental procedure (Figure 9.11) a series of linear solutions is used to yield the continuous non-linear solution. In fact the non-linear curve is approximately represented by a number of short linear segments.

The total load and displacement at any stage is given by the sum of the increments of all the loads and displacements of the previous stages.

$$\{P_r\} = \sum_{i=1}^{r} (\Delta P_i) \qquad \text{and} \qquad \{\delta_r\} = \sum_{i=1}^{r} (\Delta\delta_i) \tag{9.51}$$

This method has the advantage that it is simple to apply but the accuracy is rather low unless the load increments are very small. However, the method has a serious drawback that at each step the stiffness matrix has to be re-assembled and the solution procedure for the linear equations has to be performed each time. This is uneconomical in terms of computational efforts.

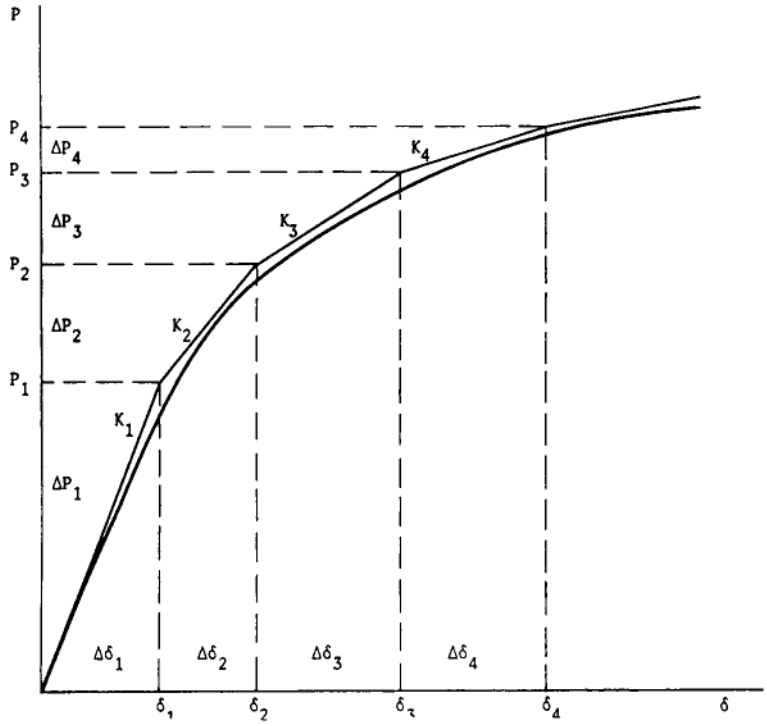

Figure 9.11 Incremental procedure

9.15.2 *Iterative procedure*

In the iterative procedure, the total load is applied to the structure and then the displacement is adjusted in accordance with the constitutive laws until equilibrium is attained.

In general, the finite element method for structural analysis results in a system of simultaneous equations as follows

$$\mathbf{[K]}\{\delta\}+\{P\}=0 \tag{9.52}$$

in which **[K]** is the assembled stiffness matrix which may vary according to the state of stress and strain, or in other words, it may depend on the displacement $\{\delta\}$ reached. If the coefficients of **[K]** depend on the unknown displacements $\{\delta\}$ the problem is non-linear and therefore direct solution of Eqn (9.52) is generally impossible and an iterative method should be used.

During any step in the iteration process, before satisfactory convergence is reached, the equilibrium condition as set out by the system of Eqns (9.52) will not be satisfied. A set of unbalanced residual forces will remain on the structure given by

$$\{\boldsymbol{R}\}=[\mathbf{K}(\{\delta\})]\{\delta\}+\{\mathrm{P}\}\neq 0 \tag{9.53}$$

The residual force vector ***{R}*** can be considered as a measure of the deviation from the equilibrium state.

To implement this iterative procedure, first of all, solve for the first approximate displacements $\{\delta_1\}$ using the initial stiffness $[K_o]$ and the initial total load $[P_o]$

$$\{\delta_1\}=[K_o]^{-1}\ \{P_o\} \tag{9.54}$$

and work out the strain $\{\varepsilon_1\}$ from $\{\varepsilon\}=[B]\ \{\delta^e\}$.

Suppose that it is possible to express the nonlinear stress-strain relationship of the material by

$$\{\sigma\}=f(\{\varepsilon\}) \tag{9.55}$$

If the tangential elasticity matrix $[D_o]$ is used and an initial stress $\{\sigma_{01}\}$ is introduced

$$\{\sigma_1\}=\mathbf{[D_0]}\ \{\varepsilon_1\}-\{\sigma_{01}\} \tag{9.56}$$

where $\{\sigma_{01}\}$ is the initial stress as shown in Figure 9.11. Therefore

$$\{\sigma_{01}\}=[D_0]\ \{\varepsilon_1\}-f(\{\varepsilon_1\})=\{\sigma_{e1}\}-\{\sigma_1\} \tag{9.57}$$

where $\{\sigma_{e1}\}=\boldsymbol{[D_0]}\ \{\varepsilon_1\}$ is the elastic stress. The excess initial stress $\{\sigma_{01}\}$ corresponding to $\{\varepsilon_1\}$ can then be obtained.

The initial stress in an element may be considered as the difference in stress between the non-linear stress actually exists in the element due to the deformation and the elastic stress.

The unbalanced residual forces on the structure are the assembly of all the element residual forces given by

$$\{R_1\}=\sum \iint [B]^{\mathrm{T}}\{\sigma_{01}\}\,t\cdot \mathrm{d}x\cdot \mathrm{d}y \tag{9.58}$$

Hence it is now possible to make an adjustment to the displacement as follows:

$$\{\Delta\delta_1\}=[K_0]^{-1}\ \{R_1\} \tag{9.59}$$

Therefore $\{\delta_2\}=\{\delta_1\}+\{\Delta\delta_1\}$ (9.60)

The procedure is repeated until $\{\Delta\delta_n\}$ is sufficiently close to zero. Here, in this case, a constant stiffness $[K_0]$ has been employed in one stage of iteration and the method is thus called the initial stiffness method.

One distinctive advantage of this method is that the same stiffness matrix is used at each step of iteration (Figure 9.12) Once the stiffness matrix is inverted, it only involves a small amount of computing effort in each subsequent iteration step for determination of $\{\Delta\delta_1\}$. But the rate of convergence is slow. Other methods with variable stiffness matrix ***[K]*** such as the secant stiffness method and Newton-Raphson method may have a

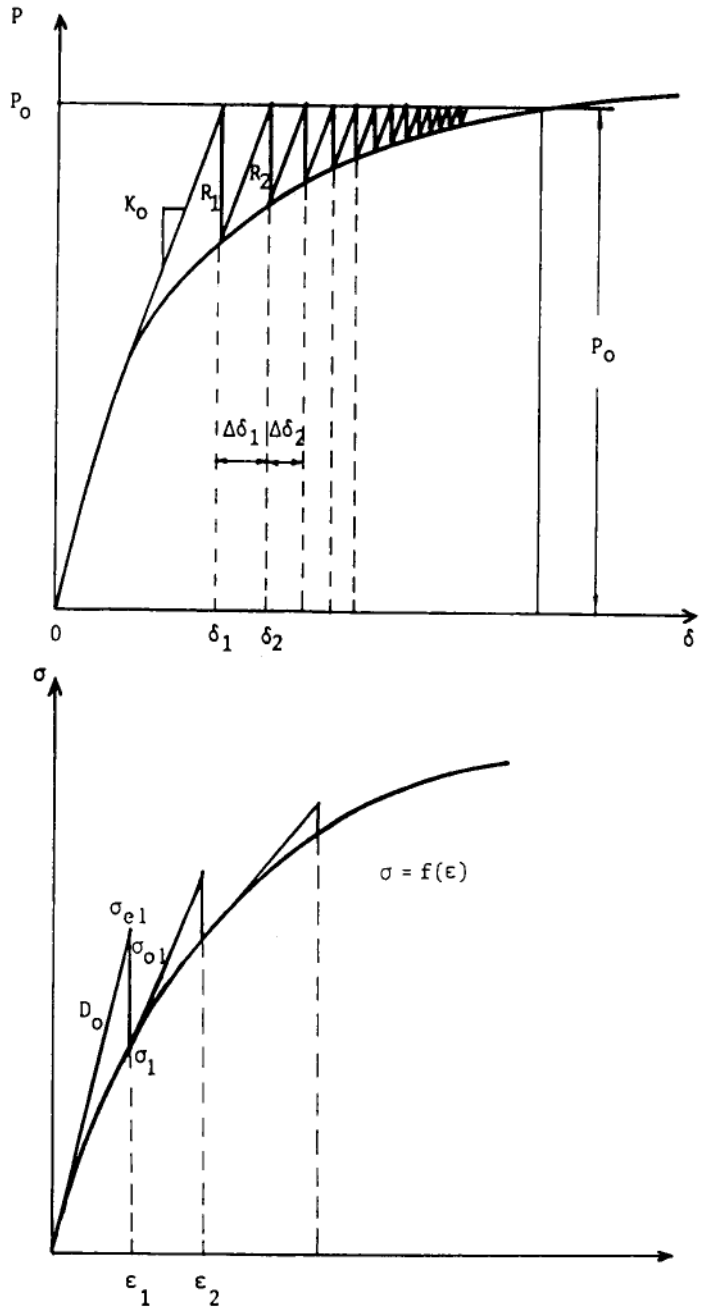

Figure 9.12 Iterative procedure.

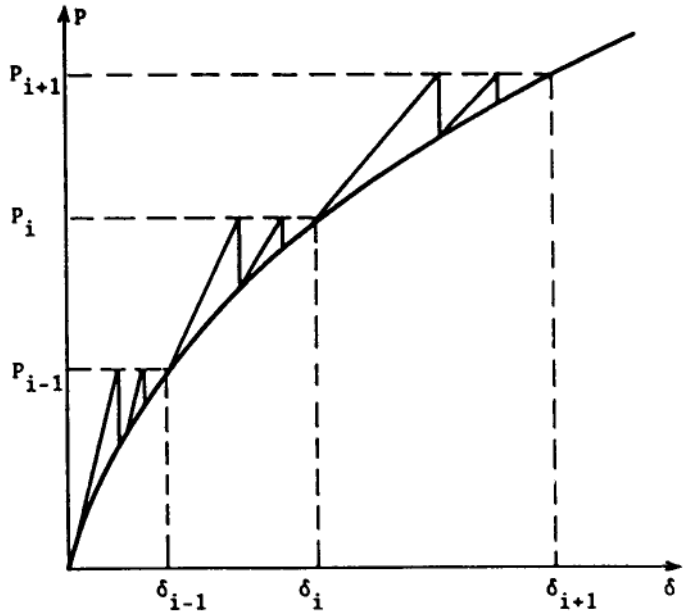

Figure 9.13 Mixed procedure

faster convergence rate but only at the expense of having to re-assemble and solve a new system of linear equations at each iteration.

9.15.3 *Mixed procedure*

In practice, usually both the incremental and iterative procedures are used together. The total load will be divided into a number of load increments. At every increment of load, iterative procedure is applied until convergence is obtained under that load increment. The accumulated load, displacement, stress and strain arrived at up to that stage are stored and become the starting values for the next load increment and the same procedure is repeated till the full load has been applied. For non-linear analysis of reinforced concrete structures, experience seems to indicate that relatively small load increments with fairly frequent updating of the stiffness for just a few iteration steps are required to produce the best results. The mixed procedure is illustrated in Figure 9.13.

9.15.4 *Flow chart of the non-linear analysis procedure*

In short, the non-linear analysis procedure in fact consists of a series of linear solutions in an iterative process which is based on the initial stiffness method or Newton-Raphson (tangential stiffness) method and the residual force concept. It also requires the use of constitutive laws describing the

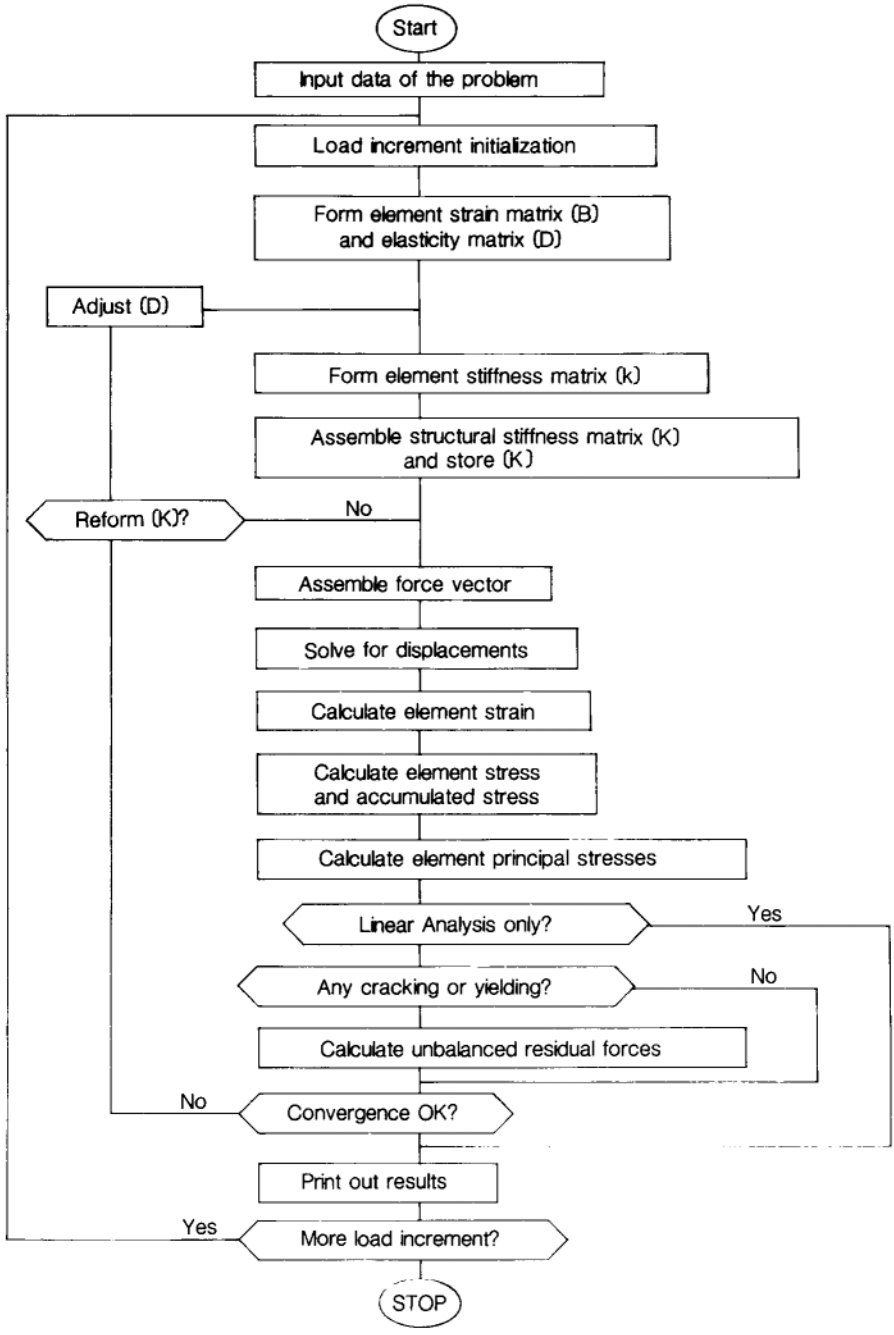

Figure 9.14 Flow chart for linear and non-linear analysis of reinforced deep beams

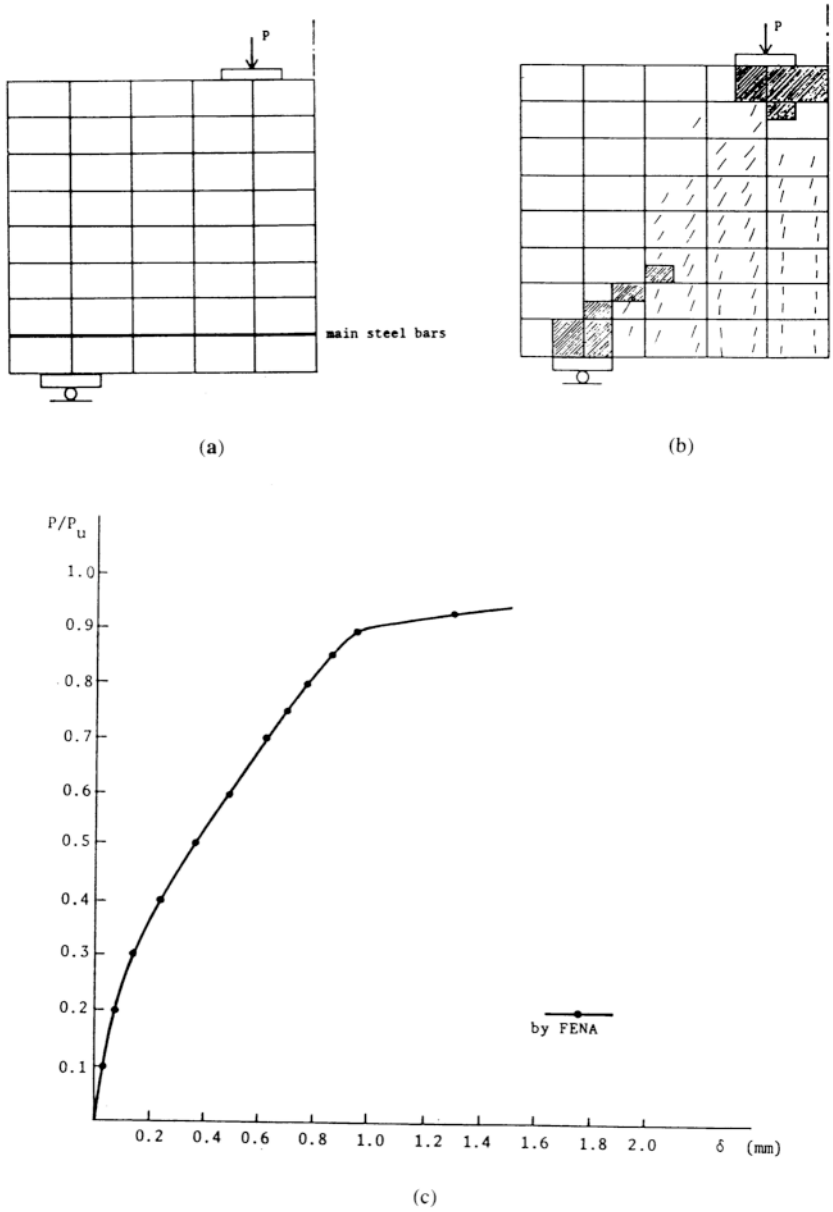

Figure 9.15 (a) Idealisation by rectangular and bar elements; (b) smeared crack pattern at 70% ultimate load; (c) load vs deflection at mid-span of a simply supported deep beam under nonlinear analysis.

strength and deformational properties of concrete and steel. Such laws form the basis for the evaluation of residual forces and the elasto-plastic material matrix ***[D]*** used in the linear solution technique. The flow chart in Figure 9.14 shows the organisation of the finite element nonlinear analysis procedure.

9.16 Example of non-linear analysis of reinforced concrete deep beams

Dimensions and properties of example beam:
A concrete beam 480 mm deep, 1000 mm long and 100 mm thick.
Distance between centre-lines of simple supports=800 mm
Two concentrated loads at 100 mm from either side of the centre-line of the beam were applied at top
Shear span to depth ratio=300/480=0.625
Concrete: compressive strength=25 Mpa
tensile strength=2.2 Mpa
modulus of elasticity=26 kN/mm^2
Poisson's ratio=0.2
Main reinforcement: Two ϕ—14 mild steel bars at bottom
Steel: yield stress=300 Mpa
modulus of elasticity=200 kN/mm^2
Half of the beam was idealised by 5×8=40 rectangular elements and 5 bar elements as shown in Figure 9.15a. The crack pattern arrived at after the total load reached 70% of the ultimate load is shown in Figure 9.15b. The full curve showing the load versus the deflection at mid-span is shown in Figure 9.15c.

References

Structural Use of Concrete, British Standard Institution. (1985) BS8110, BSI, London.
Chen, A.C.T. and Chan W.F. (1975) Constitutive relations for concrete. ASCE *J. Engng. Mechcs. Div. Am. Soc. Civ. Engrs.* **101** No. EM4, Aug.
Chen, W.F. and Han, D.J (1988) *Plasticity for Structural Engineers.* Springer-Verlag, New York.
Darwin, D. and Pecknold, D.A. (1977) Nonlinear biaxial stress strain law for concrete *Am. Soc. Civ. Engrs.* Engineering Mechanics Division, April.
Ghali, A., Neville, A.M. and Cheung, Y.K. (1972) *Structural Analysis.* Chapman and Hall, London
Han, D.J. and Chan W.F. (1987) Constitutive modelling in analysis of concrete structures, *J. Engng. Mechcs. Am. Soc. Civ. Engrs.* **113,** No.4, Apr.: 577,
Hinton, E. and Owen, D.R.J. (1986) *Computational Modelling of Reinforced Concrete Structures,* Pineridge Press, Swansea.
Kotsovos, M.D. (1984) Behaviour of reinforced concrete beams with a shear span to depth ratio between 1.0 and 2.5 *Am. Concr. Inst. J.* **81** May-June: 279.
Kupfer, H. and Gerstle K.H. (1973) Behaviour of concrete under biaxial stresses, *J. Engng. Mechcs Div. Am. Soc. Civ. Engrs,* Aug.
Liu, T.C.y., Nilson A.H. and Slate, P.O. (1972) Biaxial stress strain relations for concrete, *J. Struct. Div., Am. Soc. Civ. Engrs,* May.
Liu, C.S. and Scordelis, A. (1975) Nonlinear Analysis of RC Sheels of General form. *J. Struct. Div. Am. Soc. Civ. Engrs:* 523.

Mirza, S.M. and Houde, J. (1979) Study of bond stress-slip relationships in reinforced concrete. *Am. Concr. Inst. J.* **76** Jan: 19.
Nam, C.H. and Salmon, C.G. (1974) Finite element analysis of concrete beams. *J. Struct. Engng. Div., Am. Soc. Civ. Engrs* ST12, Dec: 2419
Ngo, D. and Scordelis, A.C. (1967) A.C. (1967) Finite element analysis of reinforced concrete beams, *Am. Concr. Inst. J.* **64** Mar.: 152.
Nilson, A.H. (1968) Nonlinear analysis of reinforced concrete by the finite element method. *Am. Concr. Inst. J.* Sept. : 757.
Nilson, A.H. (1985) *State-of-the-Art Report on Finite Element Analysis of Reinforced Concrete.* Special Publication, *Am. Soc. Civ. Engrs,* New York.
Suidan, M. and Schnobrich, W.C. (1973) Finite element analysis of reinforced concrete, J. Struct. *Div. Am. Soc. Civ. Engrs* **99,** No. ST10, Oct.
Tasuji, M.E., Slate F.O. and Nilson, A.H. (1978) Stress-strain response and fracture of concrete in biaxial loading. *Am. Concr. Inst. J.* **75** July: 306.
Timoshenko, S. and Goodier, J.N. (1951) *Theory of Elasticity,* McGraw-Hill, New York.
Valliappan, S. and Doolan T.F. Nonlinear stress analysis of reinforced concrete. *J. Struct. Div. Am. Soc. Civ. Engrs.* ST4, Apr.: 885.
Zienkiewicz, O.C. (1971) *The Finite Element Method in Engineering Science,* McGraw-Hill, London.

10 Stability and strength of slender concrete deep beams

F.K.KONG and H.H.A.WONG, University of Newcastle upon Tyne and Ove Arup and Partners

Notation

A	area under concrete stress-strain curve
A_{si}	area of ith layer of reinforcement
b	breadth of column section; thickness of deep beam
b_{eff}	effective column width
c	width of bearing
d_i	depth of $_i$th layer of reinforcement measured from top of more compressed fibre (Fig. 10.10 and 10.11)
e	effective load eccentricity, defined as $0.6e_1+0.4e_2$
e_1 (e_2)	bottom (top) eccentricity of reaction (load)
e_{add}	lateral deflection
EI'	flexural stiffness of equivalent panel
E_{si}	modulus of elasticity of ith layer of reinforcement
f_{si}	stress of ith layer of reinforcement
f_{yi}	yield stress of ith layer of reinforcement
h	overall depth of column section; overall height of deep beam
h_e, L_e	effective height and length of equivalent panel
h_p, L_p	height and width of equivalent panel
k_2	ratio of centroidal distance measured from the more highly compressed face to the neutral axis
L	overall length of deep beam
M	resistance moment
M_t	external moment
N	total axial force
N_c	axial force contributed by concrete
N_{crit}	total axial force at instability failure
N_h, N_v	mean equivalent horizontal and vertical stresses
N_{her}, N_{ver}	critical horizontal and vertical stresses
P	ultimate load
$1/r_m$	curvature at critical section
R	ratio of measured to predicted buckling load. Subscripts to *R:* SR, SP TP stand for CIRIA Guide's supplementary rules, single-panel and two-panel methods respectively; EC1 to EC4 stands for Case 1 to 4 of equivalent-column method
x	neutral axis depth of column section; clear shear span of deep beam
x_t	total shear span of deep beam (Fig. 10.3)
$[x/h]_{yci}$, ($[x/h]_{yti}$)	neutral axis depth ratios at which ith layer of reinforcement yields in compression (tension)

α	total axial force ratio, $N/(f_{cu}bh)$ (Eqns 10.3 and 10.19)	ε'_c	concrete strain at the extreme fibre of the least highly compressed face for an uncracked section
α_c	concrete axial force ratio, $N/(f_{cu}bh)$	ε_{cu}	ultimate concrete strain
α_{max}	total axial force ratio at ultimate condition	ε_{si}	steel strain of ith layer of reinforcement
α_{unity}	total axial force ratio at $\varepsilon_c/\varepsilon_{cu}=1$ and $x/h=1$	ε_{yi}	steel yield strain of ith layer of reinforcement
β	resistance moment ratio, $M/(f_{cu}bh^2)$	$[\varepsilon_c/\varepsilon_{cu}]_{min}$	minimum concrete strain ratio below which Eqn 10.23 is not solvable
β_t	external moment ratio, $M_t/(f_{cu}bh^2)$	$[\varepsilon_c/\varepsilon_{cu}]_{x/h}=1$	concrete strain ratio at $x/h=1$
ε	concrete strain	ρ_i	steel ratio of ith layer of reinforcement, A_{si}/bh
ε_c	concrete strain at the extreme fibre of the more highly compressed face	τ	shear stress

10.1 Introduction

In the past three decades, much of the research on the ultimate load behaviour of reinforced concrete beams has been concentrated on their bearing, flexural and shear strengths (Albritton, 1965; C & CA, 1969; CIRIA, 1977, Kong, 1986a). At a recent lecture given at Ove Arup and Partners, (Kong, 1986b; Whittle, 1986), it became clear that deep beam buckling is a failure criterion that needs to be considered in design. Indeed, with the expected advances in materials technology (ACI Committee 363, 1984; Clarke and Pomeroy, 1985; Kong *et al,* 1983) deep beam designers will find it possible to use much smaller cross sections in the future. This would clearly allow more slender deep beams. As with other thin- walled and slender members such as thin plates and slender columns, stability rather than strength requirements will probably dictate the design of slender deep beams. Of the four main deep beam design documents, namely, the Canadian Building Code CAN3-A23.3-M84 (CSA, 1984), the American Building Code ACI 318–83 (1983), the CEB-FIP Model Code (1978) and the CIRIA Guide No. 2 (1977), the only one that gives direct recommendations on the buckling strength of concrete deep beams is the CIRIA Guide. However, because of the lack of experimental data, the CIRIA's buckling recommendations had to be based on theoretical studies and engineering judgement; at the end of the CIRIA Guide's Appendix C: *Buckling strength of deep beams,* it is pointed out that 'there is no experimental evidence to substantiate these procedures' (CIRIA, 1977).

This chapter explains the behaviour of slender concrete deep beams and presents recent test results which show that the CIRIA Guide (1977)

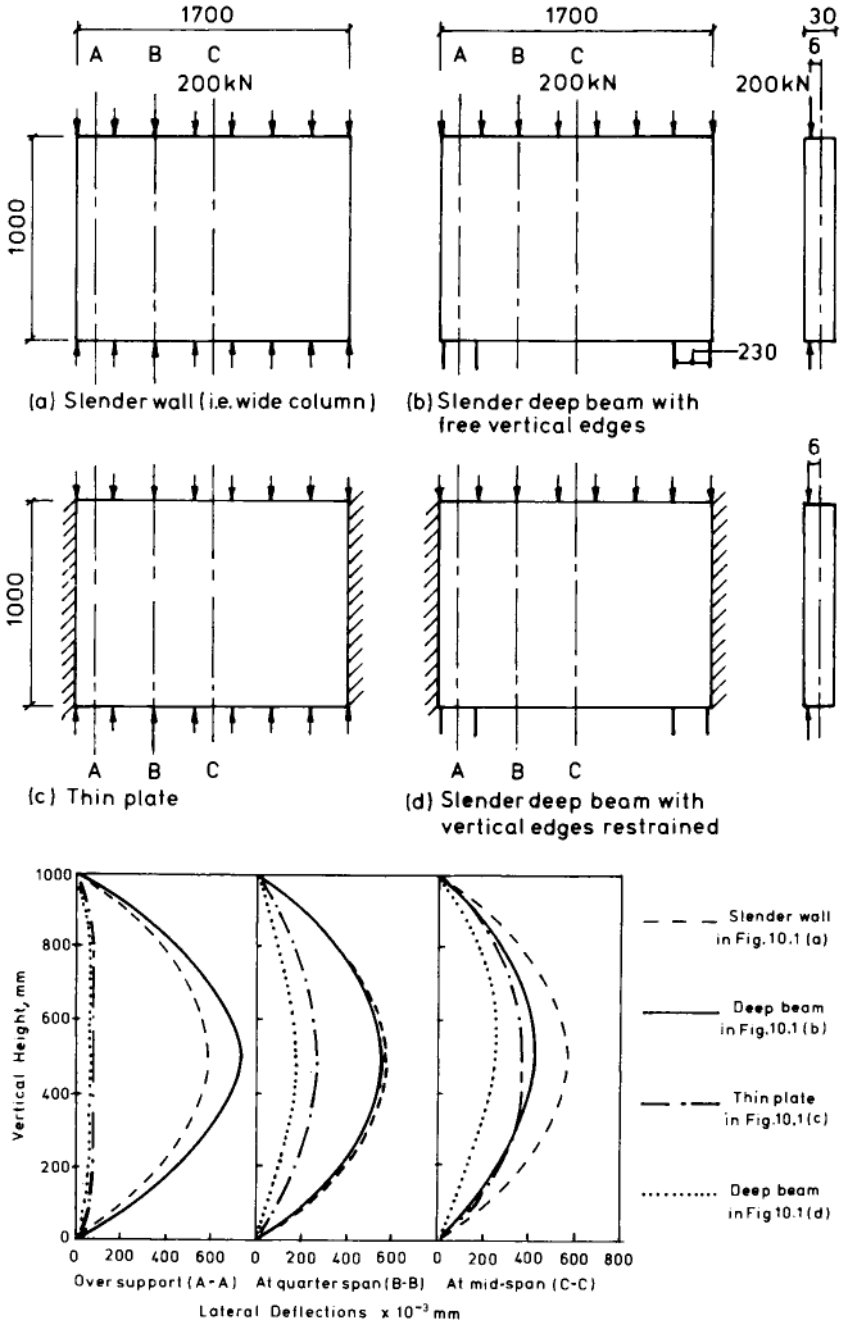

Figure 10.1 Slender wall, thin plate, slender deep beams-comparison of elastic behaviour.

methods are very conservative. An equivalent-column method is also proposed for more accurate prediction of deep beam buckling loads.

10.2 Slender deep beam behaviour

10.2.1 *Elastic behaviour*

There is very little information on the elastic behaviour of slender deep beams in the literature (Albritton, 1965; Andrews, 1978; CIRIA, 1977). It is reasonable to expect that the buckling behaviour of a slender deep beam with free vertical edges is comparable to that of a slender wall (Figure 10.1a and b). Similarly, the buckling behaviour of a slender deep beam with lateral restraint along four edges can be expected to be comparable to that of a thin plate (Figures 10.1 c and d). Using the finite element program PAFEC, the specimens shown in Figure 10.1 were modelled by three layers of Brick elements, and their lateral deflections were determined and compared.

Figure 10.1e shows that the maximum deflections of the wall (i.e. wide column) in Figure 10.1a and those of the deep beam in Figure. 10.1b always occurred at around mid-height. Figure 10.1e also shows that the mid-height deflections of the column were practically the same at Sections A-A, B-B, and C-C, but those of the deep beam decreased markedly from A-A to C-C: over the support (Section A-A), the mid-height deflection of the deep beam was about 20% higher than that of the column; at the quarter-span (Section B-B), the mid-height deflection of the deep beam and that of the column were almost the same; at mid-span (Section C-C), the mid height deflection of the deep beam was about 20% less than that of the column. Therefore, Figure 10.1e suggests that, for a slender deep beam with unrestrained vertical edges (Figure 10.lb), buckling failure is likely to occur at mid-height by horizontal cracks, initialised from the vertical edges where the lateral deflections are maximum; this seemed to agree with the authors' tests (Wong, 1987a). Figure 10.1e shows that when the vertical edges of the slender deep beam in Figure 10.1 b were restrained (Figure 10.1d), its lateral deflections were considerably reduced, and were always less than those of the column in Figure 10.1a and the plate in Figure 10.1e. Figure 10.1e also shows that the buckling failure mode of the deep beam in Figure 10.1d would be in biaxial curvature, as that of the plate in Figure 10.1c.

The above comparison is based on elastic analysis, which assumes an isotropic material obeying Hooke's law, and hence provides no information on the post-cracking behaviour and inadequate guidance of the ultimate load behaviour under the influence of the slenderness effect.

10.2.2 *Ultimate load behaviour*

Experiments on slender concrete deep beams are comparatively difficult to carry out and require attention to details to prevent injury to personnel or

damage to equipment (Kong *et al,* 1986a; Wong, 1987a). Probably for this reason, experimental studies of the ultimate behaviour of slender deep beams are few (Albritton, 1965; C & CA 1969; Marshall, 1969; PCA, 1984). The first published results on the ultimate load behaviour of deep beams with high height/thickness ratios are probably the 4 beams tested by Besser and Cusens (1984) and the 38 beams tested by the authors (Kong *et al.,* 1986a). Of these reported results, one of Besser and Cusens and 30 of Kong failed by buckling. Though very few test data were previously available on slender deep beams, much is known about the behaviour of stocky deep beams. Hence, it would be helpful to describe the behaviour of slender deep beams, as observed in recent tests (Kong *et al.,* 1986a), with reference to that of the stocky concrete beams as explained elsewhere (Kong, 1986a; Kong and Singh, 1972; Kong *et al.,* 1975, 1986a). The general behaviour of top-loaded slender deep beams can be briefly summarised as follows:

i) On loading, the first cracks to form were the flexural cracks in the midspan region (Figure 10.2: cracks [1]). The flexural cracking load was typically 20–40% of the ultimate load and was somewhat lower than that for a stocky deep beam of comparable span to depth ratio,

ii) On further loading, long diagonal cracks (Figure 10.2: cracks [2]) would form, usually with a fairly loud noise. Typically these diagonal cracks initiated not at the soffit, but within the depth of the beam. These cracks were usually fairly long, even detected first by visual observation. Comparing with stocky deep beams, the first major diagonal cracks of slender deep beams tended to form at lower loads and to be more inclined to the horizontal. It was

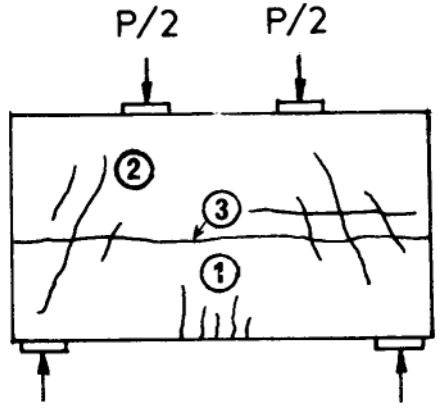

Figure 10.2 Typical sequence in which the cracks appeared in top-loaded slender deep beams

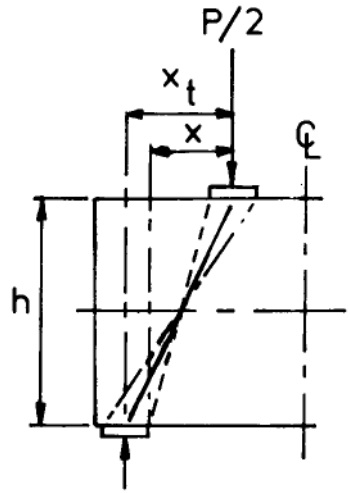

Figure 10.3 Representation of critical diagonal crack—dotted line for stocky deep beams; full and chain-dotted lines for slender deep beams

observed that the direction of the major diagonal cracks was generally between those of the solid line and the chain-dotted line in Figure 10.3 (Kong *et al.,* 1986c; Wong 1987a).

iii) As the load was further increased, the failure mode depended strongly on the height/thickness ratio *h/b* and the load-eccentricity/thickness ratio *e/b*. Generally speaking, the higher these ratios, the more likely it was that buckling failure would occur. Where the effective *e/b* ratio, defined as $0.4e_1/b+0.6e_2/b$ (Kong *et al.,* 1986a), did not exceed 0.03, none of the test beams failed by buckling even when the *h/b* ratio was high as 50. However, when the effective *e/b* ratio was 0.1 or more, even test beams of *h/b* ratio down to 25 failed by buckling. The buckling mode was characterised by prominent horizontal cracking, usually across the length of the beam (Figure 10.2: cracks [3]) and was accompanied by a significant reduction in the failure load.

10.3 Current design methods—CIRIA Guide 2 (1977)

As explained in Section 10.1, the CIRIA Guide is the only major deep beam design document that gives recommendations on the buckling strength of slender concrete deep beams. Other documents that provide guidance for the buckling design of slender concrete deep beams are the ACI Committee 533

Report (1971) and the Portland Cement Association's Report (PCA, 1979). Of these, the CIRIA Guide's coverage is the most comprehensive. The Portland Cement Association's recommendations apply only to a limited class of deep beam and the ACI Committee Report is even more restrictive in scope and now rather out-of-date. Because of space limitation, only the CIRIA's methods will be examined in the following sections. Detailed worked examples and comparison of the above-mentioned design documents for slender deep beams are given elsewhere (Kong *et al.,* 1987; Wong, 1987a).

In the CIRIA Guide, the deep beam buckling problem is approached in two stages (Figure 10.4). In stage 1, the CIRIA Guide's Simple Rules (Section 10.3.1 this chapter) is used to check whether the deep beam can be defined as a short braced wall or not. If the deep beam cannot be defined as a short braced wall, its load-carrying capacity is determined in stage 2 (Sections 10.3.2 and 10.3.3 this chapter). The CIRIA Guide is intended to be used in conjunction with CP110:1972 which has been replaced by BS 8110:1985. In the following sections, the BS 8110 clause numbers are used. The CIRIA buckling design methods are compared with authors' test results (Kong *et al.,* 1986a) in Section 10.6.

10.3.1 *CIRIA Guide Simple Rules*

The Simple Rules assume no reduction of capacity due to the slenderness of the section or to lack of adequate restraint, if every panel can be defined as a short braced wall in terms of Clause 3.9.1.2 of BS8110. Otherwise, the Supplementary Rules of Appendix C of the CIRIA Guide should be used to design the slender deep beam against buckling (Figure 10.4). For the purpose of assessing the slenderness limit of a panel in accordance with BS 8110, the CIRIA Guide gives the following recommendations for determining the effective height:

i) For a panel with effective lateral restraints at all four edges, its effective height is taken as 1.1 times the shortest distance between centres of parallel lateral restraint,
ii) For a panel with one or two opposite edges free, its effective height is taken as 1.5 times the distance between the centres of the parallel lateral restraints,
iii) For a panel with both rotational and lateral movements restrained, its effective height may be taken as the clear distance between restraints.

10.3.2 *CIRIA Guide Supplementary Rules*

When the CIRIA Guide's Simple Rules do not apply, it is necessary to treat the panel as a slender wall in accordance with Clause 3.9.1 of BS 8110:1985.

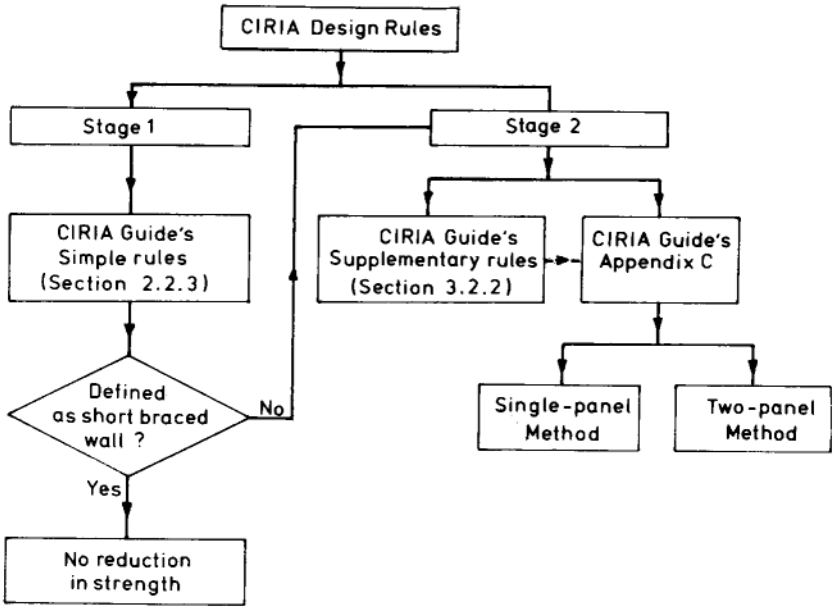

Figure 10.4 Flow diagram-CIRIA Guide's buckling recommendations

The Supplementary Rules for the design of slender deep beams can be summarised as follows:

Step 1: Determination of maximum compressive stresses.
Based on the elastic stress distribution in the deep beam, the greater of the maximum vertical and horizontal axial stresses are used to calculate the additional moments in Step 3.

Step 2: Calculation of effective height, h_e
The recommendations described in Section 10.3.1 are applicable when the following conditions a-c are satisfied; otherwise Appendix C of the CIRIA Guide should be used.

(a) The web panel is rectangular and braced.

(b) The web panel has effective lateral restraint on a minimum of two opposite edges.

(c) The nominal average shear stress (V/bh_a) is less than 50% of the average axial compressive stress in the vertical or horizontal direction of the panel, whichever is the greater, where V is the total shear force on a vertical section due to the applied loads, b is the thickness of deep beam, and h_a is the effective height of deep beam as defined in Clause 2.2.1 of the CIRIA Guide. The effective height h_e so obtained may have been calculated from either a vertical or horizontal dimension.

Step 3: Design of vertical and horizontal column strips.
The vertical and horizontal column strips of unit width are then designed as slender columns in accordance with BS 8110: Clause 3.8.3, with the additional moment for the horizontal strips to be taken as the greatest additional moment (see Step 1) calculated for the vertical strips.

10.3.3 *CIRIA Guide Appendix C: Single-Panel Method*

The Single-Panel Method is one of the two methods given in Appendix C of the CIRIA Guide for a more accurate estimate of the effective heights and effective lengths, using interaction diagrams to allow for the effects of the in-plane biaxial stresses due to bending and shear. The procedure for the Single-Panel Method is outlined below.

Step 1: Division of beam into panels.
The deep beam is divided into panels by adequate restraints. If there are lateral restraints at the top and bottom edges only, then the whole beam forms one panel. Each panel is to be considered individually in the following steps.

Step 2: Determination of equivalent panel.
If the actual panel is non-rectangular, it is to be replaced by a notional safe equivalent panel which comprises a rectangular plate, with its edges either simply supported or free. The width L_p (the height h_p) of the equivalent panel is taken as equal to the width (the height) of the actual panel at the point where the actual horizontal stress (the actual vertical stress) is at a maximum, as shown in Figure 10.5. Further recommendations are also given in the CIRIA Guide (1977) to take into account the effect of rotational restraint along the edges of the panel.

Step 3: Determination of equivalent applied stresses.
The equivalent applied stresses acting on the equivalent panel comprise linearly varying axial compressive stresses [N_v, N_h] applied to the edges and a constant shear stress τ. The equivalent applied stresses are chosen such that

(a) The axial stresses [N_v, N_h] produce compressive stresses within the panel that are at no point less than the actual stresses;
(b) The shear stress τ is equal to the algebraic mean of the actual average vertical shear stresses applied at the ends of the panel. Where the actual stresses are tensile, they should be treated as if they were zero.

Step 4: Determination of elastic critical stresses.
Depending upon the edge restraint, the critical axial and shear stresses are found, each in the absence of any other applied stresses from the charts given in the CIRIA Guide (1977). The effect of the shear stress and the in-plane biaxial stresses are then allowed for

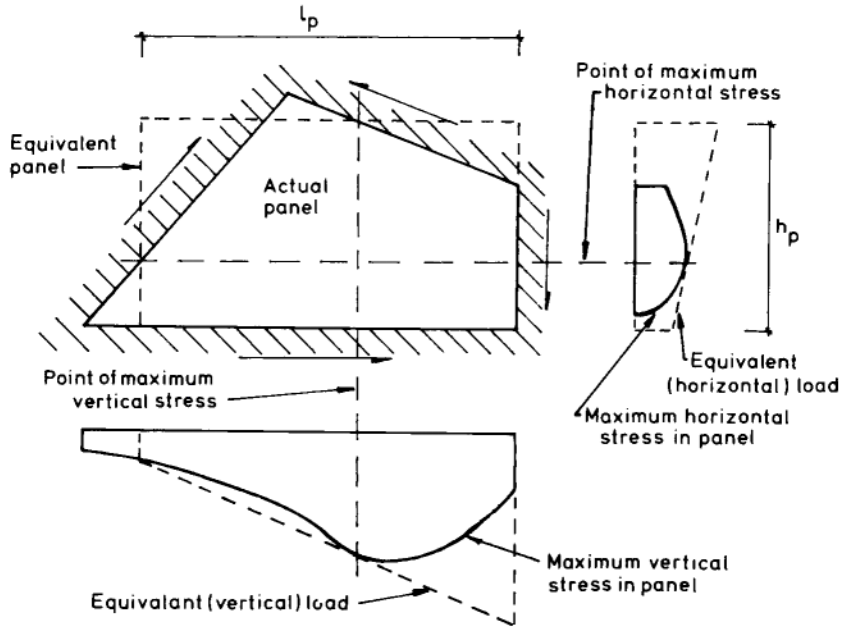

Figure 10.5 Equivalent panels and loads (after CIRIA (1977))

using the CIRIA Guide's interaction diagrams to give modified critical stresses N_{vcr} in the vertical direction and N_{hcr} in the horizontal direction in terms of EI', where EI' is the flexural stiffness of the equivalent panel.

Step 5: Determination of effective heights h_e and lengths L_e.

The effective heights and lengths are determined from the following formulae.

$$h_e^2 = \frac{\pi^2 EI'}{N_{vcr}} \tag{10.1a}$$

$$L_e^2 = \frac{\pi^2 EI'}{N_{hcr}} \tag{10.1b}$$

where N_{vcr} and N_{hcr} are the modified critical stresses determined in Step 4.

Step 6: Design of vertical and horizontal column strips.

The vertical and horizontal strips of unit width are then designed as slender columns (Wong and Kong, 1986; Kong and Wong, 1988), as if they were subjected to the *equivalent* axial stresses N_v and N_h respectively (see Step 3 above).

10.3.3.1 Comments on the Single-Panel Method

The Single-Panel Method is rather convenient to use, but may be too conservative where the actual stresses vary abruptly, e.g. when concentrated loads or reactions are applied. This is because the Single-Panel Method may require an unnecessarily large amount of reinforcement in areas of low stresses. In these cases, the CIRIA Guide recommends the use of the two-panel method.

10.3.4 *CIRIA Guide Appendix C: Two-Panel Method*

The Two-Panel Method is the second method in Appendix C of the CIRIA Guide (1977). The Two-Panel Method is rather similar to the Single-Panel Method, except that the former analyses and designs a braced panel as two individual panels. The design procedure for the Two-Panel Method may be outlined as follows.

Steps 1 and 2: As Steps 1 and 2 of the Single-Panel Method.

Step 3: Determination of equivalent applied stresses.
In the Two-Panel Method, the equivalent loads adopted to select the effective height and the effective length differ in the two panels. For Panel 1, the equivalent load consists of an upper-bound horizontal stress, a lower-bound vertical stress and a constant shear stress. For Panel 2, the equivalent load consists of a lower-bound horizontal stress, an upper-bound vertical stress and a constant shear stress. Some recommendations are given in the CIRIA Guide (1977) on the choice of the lower-bound and upper-bound equivalent stresses.

Step 4: The critical stresses are determined for the two panels as in Step 4 of the Single-Panel Method.

Step 5: Following Step 5 of the Single-Panel Method, the effective height h_e is calculated for Panel 1 and the effective length L_e is determined for Panel 2.

Step 6: The vertical and horizontal strips of unit width are designed as slender columns (Wong and Kong, 1986; Kong and Wong, 1988) using the *actual* axial stress distributions.

10.4 The equivalent-column method

The CIRIA Guide's methods for the buckling design of slender concrete deep beam consist essentially of replacing the deep beam by equivalent panels. CIRIA then uses (previously CP110) the slender column approach of BS 8110 for assessing the strength of the equivalent panels as slender columns. A close examination (Cranston, 1972; Kong *et al.,* 1986b; Kong and Wong, 1987; Wong 1987a) of the relevant BS 8110 and CP 110 Clauses shows that these are really intended for the material failure of slender columns and not for their instability failure. It will be shown (Section 10.6)

that the CIRIA methods could lead to designs with a factor of safety exceeding 60; the authors believe that BS8110's slender column recommendations are unsuitable for use in predicting the buckling loads of slender concrete deep beams. Though the CIRIA methods can be grossly inaccurate, the concept of an equivalent-column is attractive. In this section, a computer-aided method (Kong *et al.*, 1986b; Kong and Wong, 1987; Wong, 1987a) is presented for the detailed stability analysis of slender concrete columns. The method is applied to slender deep beams in Section 10.5 and compared with CIRIA's methods in Section 10.6.

10.4.1 *Theoretical background*

Consider the slender column in Figure 10.6a; let the moment-deflection (M–e_{add}) curve be as shown in Figure 10.6b. The total external moment M_t at the mid-height due to the load N is $M_t=N(e+e_{add})$.

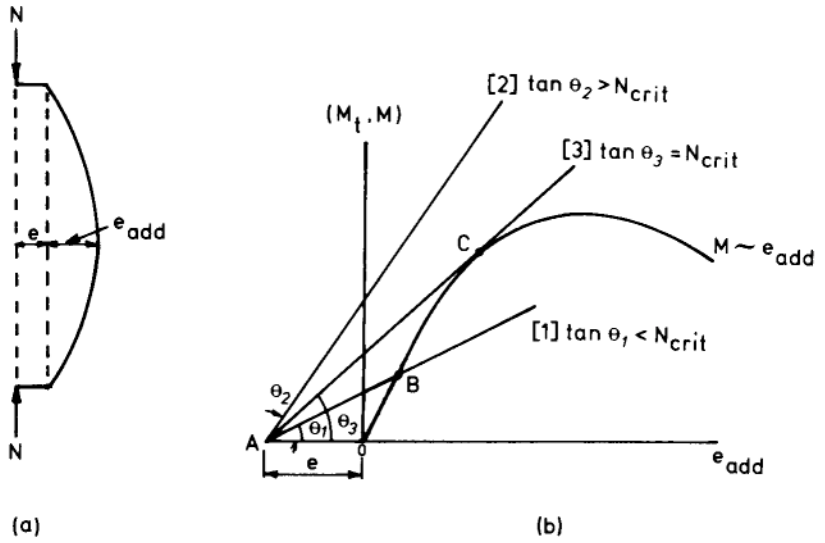

Figure 10.6 Simplified moment-deflection curve

For any given value of N, the relation between Mt and e_{add} can be represented on Figure 10.6b as a straight line having a slope equal to N and passing through the point A at a distance e to the left of the origin O. Suppose for the time being it is crudely assumed that the M–e_{add} curve is independent of the load N. Let N_{crit} be the value of N at which instability failure of the column occurs. Then a line such as Line 1, with a slope less than N_{crit}, will intersect the M–e_{add} curve. At the point of intersection, B, the external moment M_t [$=N(e+e_{add})$] is in equilibrium with the internal moment M. If this equilibrium is disturbed by slightly increasing e_{add}, then M_t becomes less than M. Hence the equilibrium at B is stable.

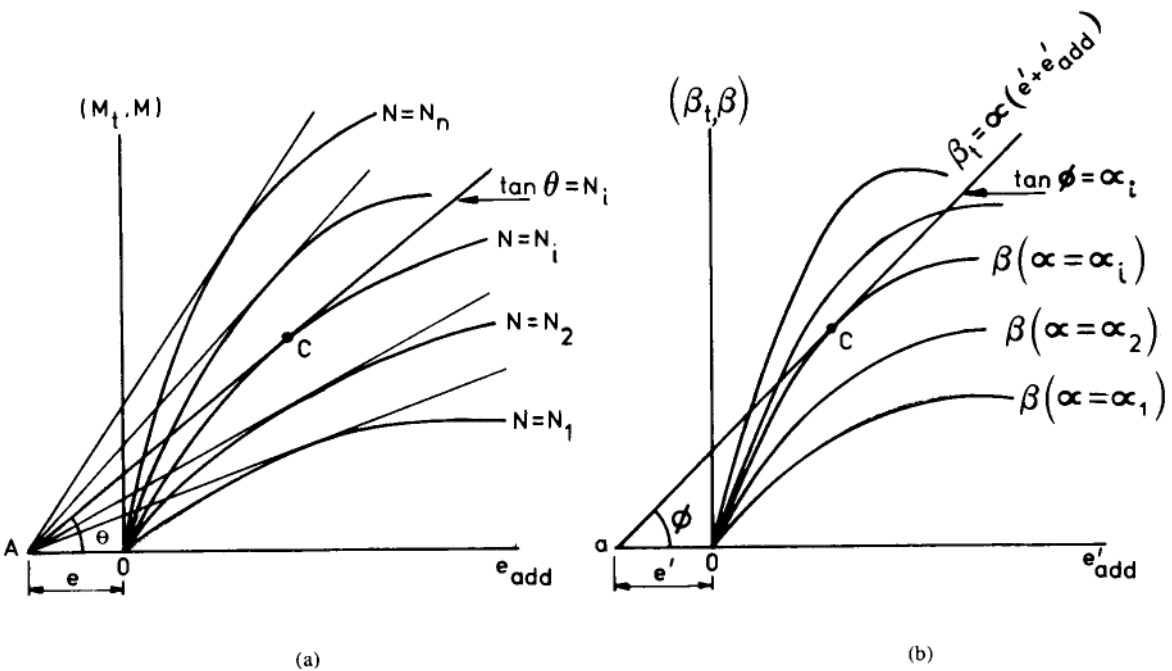

Figure 10.7 Typical moment-deflection curves

Line 2, having a slope exceeding N_{crit}, will not intersect the M–e_{add} curve. For such a line, the external moment M_t always exceeds the internal moment M, and equilibrium is impossible.

Line 3, having a slope equal to N_{crit}, will touch the M–e_{add} curve. At the tangent point C, equilibrium exists between Mt and M. The equilibrium is obviously unstable.

It can be concluded from the above that the instability load N_{crit} of a slender column is given by the slope of the line which touches the M–e_{add} curve. In practice, N_{crit} cannot be so readily found in this way, because the M–e_{add} curve is itself dependent on the value of N. However, we can proceed as follows.

A family of M–e_{add} curves are drawn for a range of values of N, as shown in Figure 10.7a. From the point A, straight lines are drawn tangential to these curves. The instability load N_{crit} is then obtained as the slope of the line which simultaneously satisfies the two requirements:

i) the line touches the M–e_{add} curve for $N=N_i$
ii) the line itself has a slope tan $\theta=N_i$

That is, $N_{crit}=N_i$

Consider again the equation $M_t=N(e+e_{add})$; for computer application, it is convenient to convert it into dimensionless form, by dividing throughout by $f_{cu}bh^2$:

$$\beta_t=\alpha[e'+e'_{add}] \tag{10.2}$$

where

$$\beta_t=\frac{M_t}{f_{cu}\,bh^2};\quad \alpha=\frac{N}{f_{cu}\,bh};\quad e'=\frac{e}{h};\quad e'_{add}=\frac{e_{add}}{h} \tag{10.3}$$

Figure. 10. 7a expressed in dimensionless form, becomes Figure 10.7b. The straight line a-c in Figure 10.7b simultaneously satisfies the two requirements:

i) the line touches the β–e'_{add} curve for $\alpha=\alpha_i$
ii) the line itself has a slope tan $\phi=\alpha_i$

Therefore, the critical value of α, namely α_{crit}, is given by α_i.
Hence the instability load is

$$N_{crit}=\alpha_{crit}f_{cu}bh=\alpha_i f_{cu}bh \tag{10.4}$$

It can be shown (Kong and Wong, 1987; Wong, 1988) that along any moment-deflection curve β–e'_{add}, the concrete strain ε_c, i.e. the concrete strain ratio $\varepsilon_c/\varepsilon_{cu}$, increases with e'_{add}. Therefore, with reference to Figure 10.7b, it should be noted that α_i is the correct instability load, only if at the point c on the β–e'_{add} curve the concrete ultimate strain ε_{cu} has not been reached. In Figure 10.8, the β–e'_{add} curve

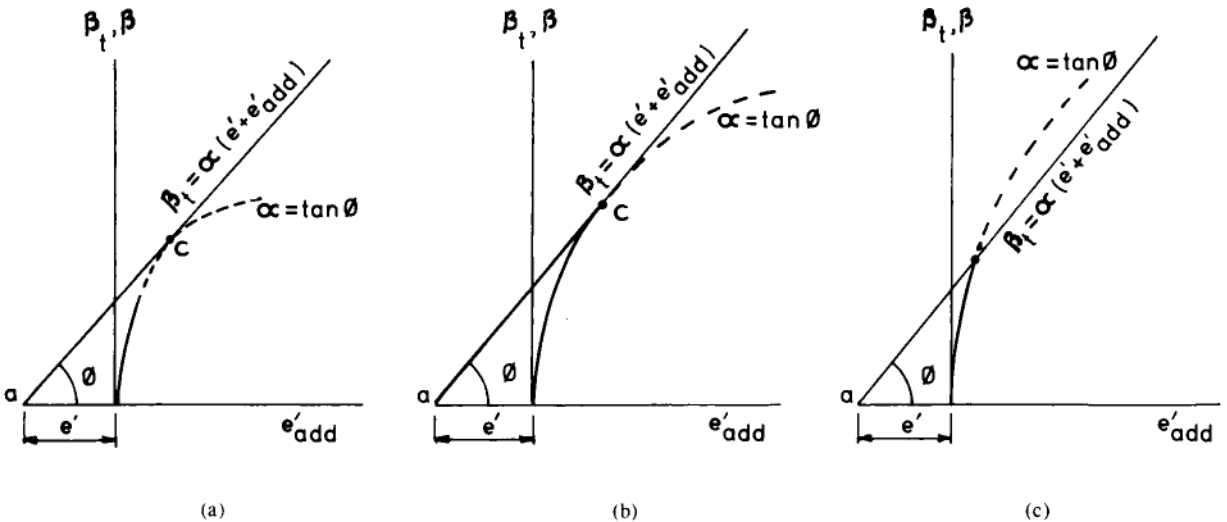

Figure 10.8 Column failures modes

is shown dotted where the maximum concrete strain exceeds ε_{cu}. Thus in Figure 10.8a, the column would have collapsed in material failure before the 'instability load' is attained; in Figure 10. 8b, the instability and material failures occur simultaneously; in Figure 10.8c, material failure occurs.

It is now clear that the major effort required by the method is to obtain the moment-deflection curves (Wong 1987b, 1988). The stability analysis described above can be carried out by three methods, listed below in order of increasing efficiency:

i) The graphical method (Section 10.4.2)
ii) The improved graphical method (Section 10.4.3)
iii) The analytical method (Section 10.4.4)

10.4.2 *Stability analysis of columns: graphical method*

10.4.2.1 Assumptions and sign convention The following assumptions and sign convention are adopted for the graphical method to be described here, and for the improved graphical method and the analytical method to be described in Section 10.4.3 and 10.4.4, respectively:

i) The strains in the concrete and the reinforcing steel are proportional to the distances from the neutral axis,
ii) Material failure (i.e. crushing of concrete) occurs when the concrete strain at the extreme compression fibre reaches a specified value ε_{cu}, which is taken to be 0.0035 as specified in BS 8110 (1985). (Users of other national Codes of Practice may of course use other values for ε_{cu} at their discretion),
iii) The tensile strength of the concrete is ignored,
iv) Compressive stresses and strains are taken to be positive, and tensile stresses and strains negative.

10.4.2.2 Stress-strain relationships Figure 10.9 shows the stress-strain relation for concrete and steel. Expressing the concrete stress f as function of the strain ratio $\varepsilon/\varepsilon_{cu}$ the area under the concrete stress-strain curve in Figure 10.9a between $\varepsilon=\varepsilon'_c$ and $\varepsilon=\varepsilon_c$ is

$$A = \int_{\varepsilon'_c}^{\varepsilon_c} f(\varepsilon/\varepsilon_{cu})\, d\varepsilon \qquad [N/mm^2] \tag{10.5}$$

and the corresponding centroidal distance ε_g (dimensionless; Figure 10.9a) is

$$\varepsilon_g = \frac{\int_{\varepsilon'_c}^{\varepsilon_c} f(\varepsilon/\varepsilon_{cu})\, \varepsilon\, d\varepsilon}{\int_{\varepsilon'_c}^{\varepsilon_c} f(\varepsilon/\varepsilon_{cu})\, d\varepsilon} \tag{10.6}$$

The stress-strain relation for steel in Figure 10.9b is that of BS 8110:1985 with the partial safety factor γ_m set to unity.

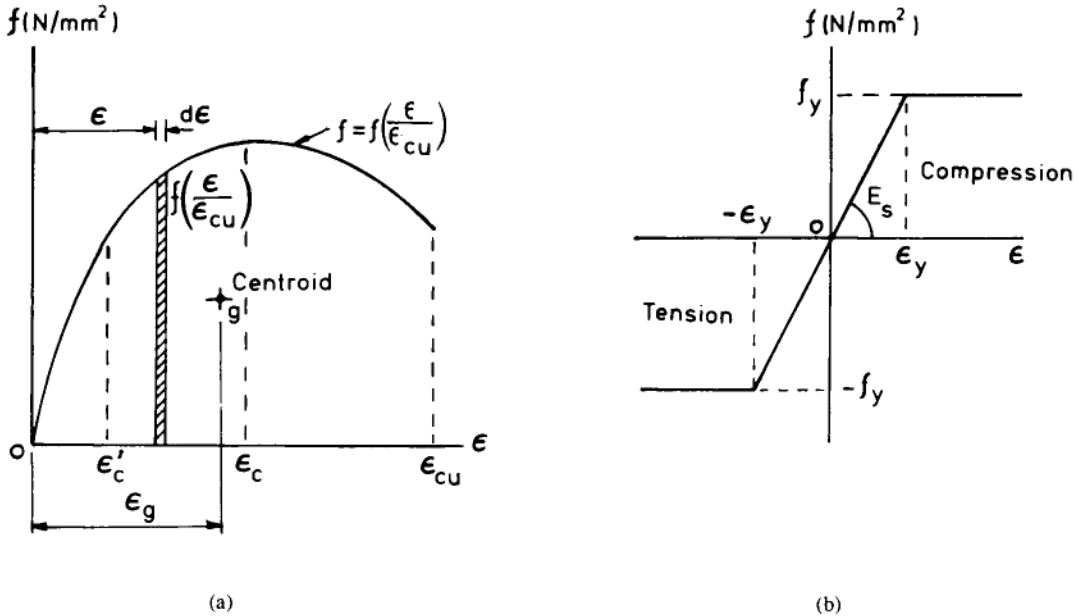

Figure 10.9 Stress-strain relations of concrete and steel: (a) concrete; (b) reinforcement

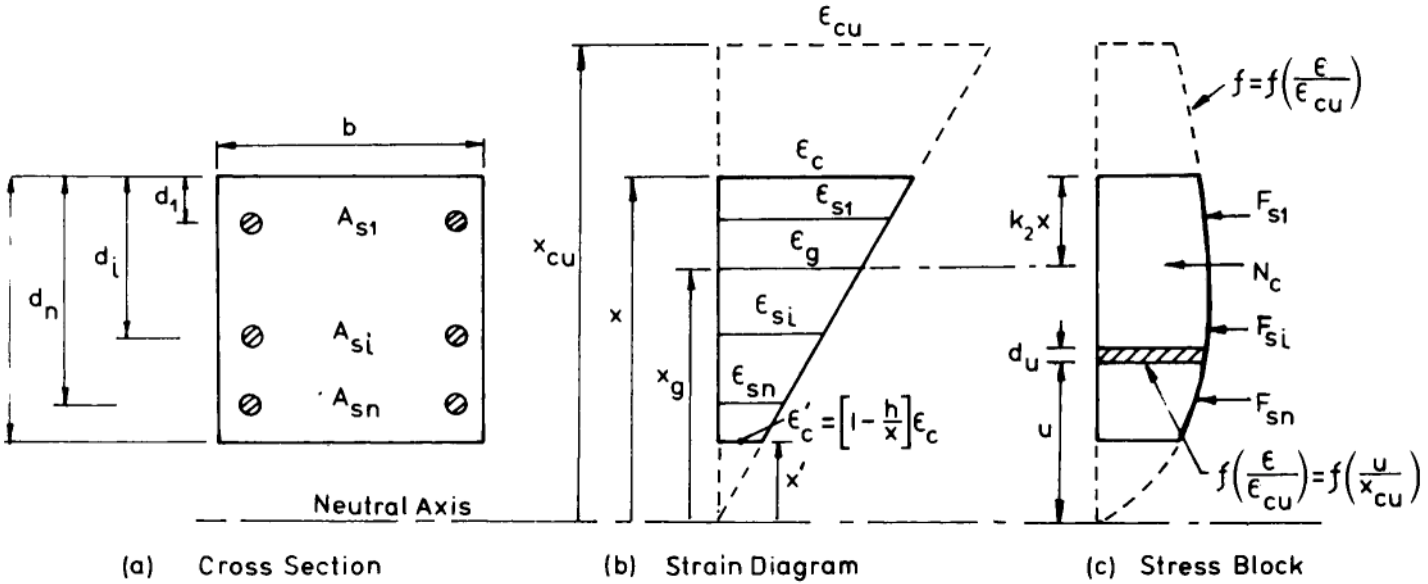

Figure 10.10 Uncracked column section

10.4.2.3 The column section Figure 10.10 refers to an uncracked section where, of course, $x/h \geq 1$. Referring to the concrete stress block in Figure 10.10c, the concrete compressive force is

$$N_c = b \int_{x'}^{x} f(\varepsilon/\varepsilon_{cu}) du \tag{10.7a}$$

It is seen from Figure 10.10b that $x_{cu}/\varepsilon_{cu}=x/\varepsilon_c=x'/\varepsilon'_c$; using these relations it is easy to show that Eqn 10.7a can be written as

$$N_c = b \frac{x}{\varepsilon_c} \int_{\varepsilon'_c}^{\varepsilon_c} f(\varepsilon/\varepsilon_{cu})\, d\varepsilon \tag{10.7b}$$

Including the contribution by n layers of steel, the total compressive force is

$$N = N_c + \sum_i f_{si} A_{si} \tag{10.8}$$

and the resistance moment about the mid-depth of the section is

$$M = N_c \left[\frac{h}{2} - k_2 x\right] + \sum_i f_{si} A_{si} \left[\frac{h}{2} - d_i\right] \tag{10.9}$$

where (Figures 10.10c and 10.9a)

$$k_2 = \frac{\varepsilon_c/\varepsilon_{cu} - \varepsilon_g/\varepsilon_{cu}}{\varepsilon_c/\varepsilon_{cu}} \tag{10.10}$$

Introduce the dimensionless parameter

$$\alpha_c = \frac{N_c}{f_{cu} bh} \tag{10.11}$$

and the dimensionless parameters a and ß (see Eqn 10.3). Then divide Eqns 10.7–10.9 by $f_{cu}bh$ to obtain:

$$\alpha_c = \frac{x/h}{\varepsilon_c} \int_{\varepsilon'_c}^{\varepsilon_c} \frac{f(\varepsilon/\varepsilon_{cu})}{f_{cu}} d\varepsilon \tag{10.12}$$

$$\alpha = \alpha_c + \sum_i \rho_i \frac{f_{si}}{f_{cu}} \tag{10.13}$$

$$\beta = \alpha_c \left[\frac{1}{2} - k_2 \frac{x}{h}\right] + \sum_i \rho_i \frac{f_{si}}{f_{cu}} \left[\frac{1}{2} - \frac{d_i}{h}\right] \tag{10.14}$$

where $\rho_i = \dfrac{A_{si}}{bh}$ and k_2 is defined in Eqn 10.10.

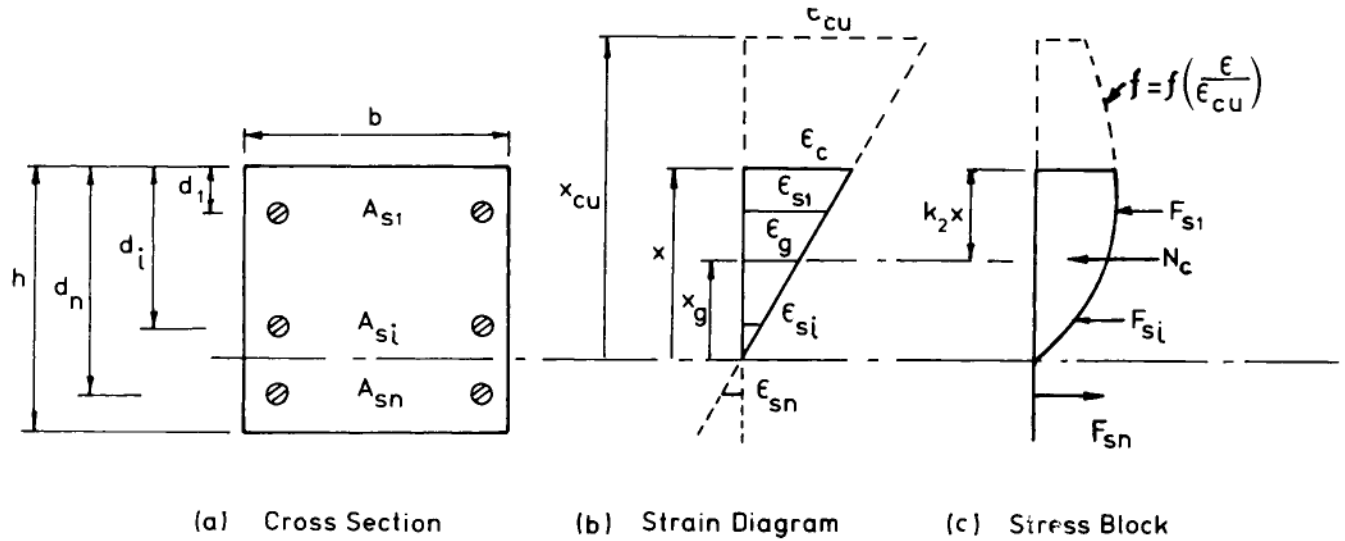

Figure 10.11 Cracked column section

Eqns 10.12 and 10.13 can also be applied to a cracked section where, of course, $x/h<1$ (Figure 10.11); note, however, that for a cracked section, the limit of integration ε'_c in Eqn 10.12 becomes zero. Therefore, for a cracked section, Eqn 10.12 becomes

$$\alpha_c = \frac{x/h}{\varepsilon_c} \int_0^{\varepsilon_c} \frac{f(\varepsilon/\varepsilon_{cu})}{f_{cu}} \, d\varepsilon \tag{10.15}$$

10.4.2.4 Calculation of α, ß *and* e'_{add} For any values assigned to ε_c and x, i.e. assigned to the pair $[\varepsilon_c/\varepsilon_{cu}, x/h]$, Eqn 10.12 or 10.15 can be used to calculate α_c. α is then calculated from Eqn 10.13 and ß from Eqn 10.14. It can be shown (Kong et al., 1986b; Kong and Evans, 1987) that the additional eccentricity

$$e_{add} = \frac{L^2}{n^2} \frac{1}{r_m}$$

where n^2 is the numerical constant which depends on the curvature distribution and

$$\frac{1}{r_m} = \frac{\varepsilon_c - \varepsilon'_c}{h} = \frac{\varepsilon_c}{x}$$

Therefore the lateral deflection parameter e'_{add} of Eqn 10.3 can be written as

$$e'_{add} = \frac{e_{add}}{h} = \frac{\varepsilon_{cu}}{n^2} \left[\frac{L}{h}\right]^2 \left[\frac{\varepsilon_c/\varepsilon_{cu}}{x/h}\right] \tag{10.16}$$

10.4.2.5 Preparation of β–e'_{add} *curves* The procedure for preparing the moment-deflection curves β–e'_{add} can be summarised as follows:

Step 1: With reference to Figure 10.9a, select a convenient value for the concrete strain ratio $\varepsilon_c/\varepsilon_{cu}$, say $\varepsilon_{c,1}/\varepsilon cu$.

Step 2(a): With reference to Figures 10.10b and c (and Figures 10.11b and c) select a convenient x/h value, and calculate the area A under the stress-strain curve and the centroidal strain ε_g from Eqns 10.5 and 10.6 respectively, noting that $\varepsilon'_c=\varepsilon_c[1-1/(x/h)]$ for $x/h\geq1$ (i.e. uncracked section; Figure 10.10), and $\varepsilon'_c=0$ for $x/h<1$ (i.e. cracked section; Figure 10.11).

Step 2(b): Calculate α, ß and e'_{add} from Eqns 10.13, 10.14 and 10.16 respectively.

Step 3: Repeat Step 2 with other x/h values until a sufficient number of points is obtained for plotting curve Ia in Figure 10.12a, curve Ib in Figure 10.12b and curve Ic in Figure 10.12c.

Step 4: Repeat Steps 1 to 3 with other strain ratios $\varepsilon_{c,2}/\varepsilon_{cu}$, $\varepsilon_{c,3}/\varepsilon_{cu}$…in stages up to $\varepsilon_{c,n}/\varepsilon_{cu}=\varepsilon_{cu}/\varepsilon_{cu}=1$.

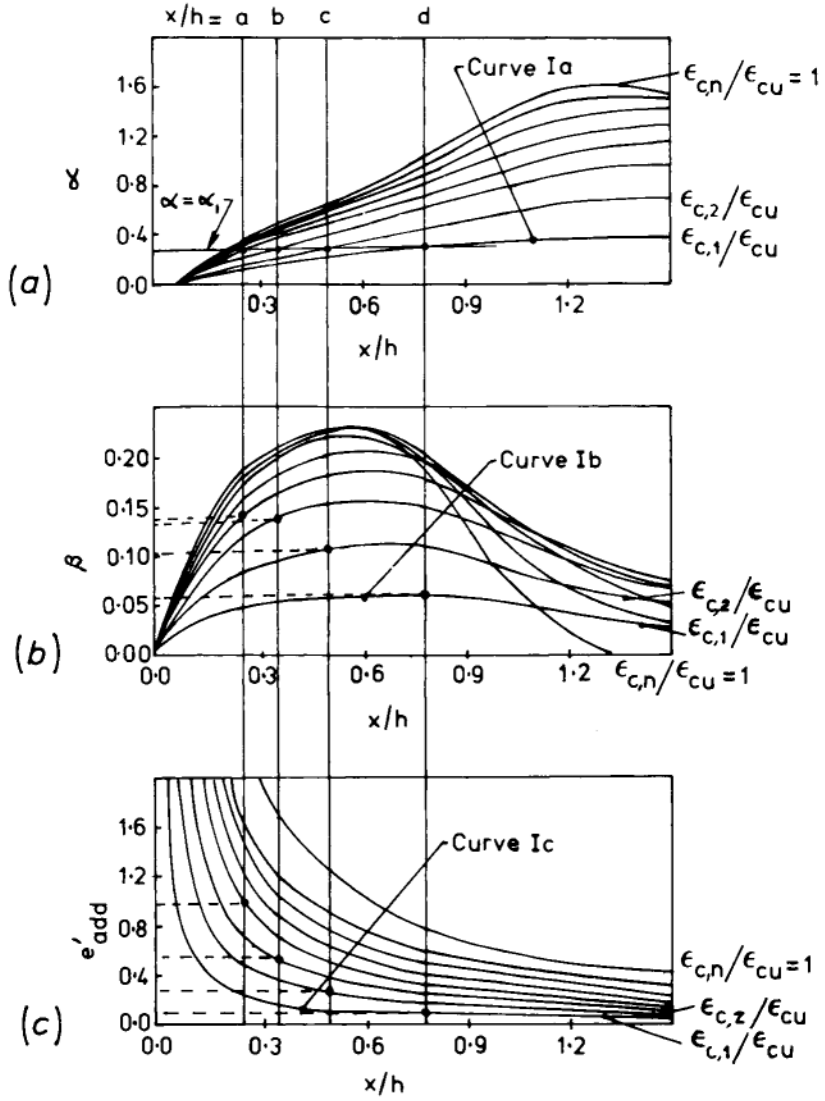

Figure 10.12 Relationship of α, ß, e'_{add} with *x/h* for various values *x/h*

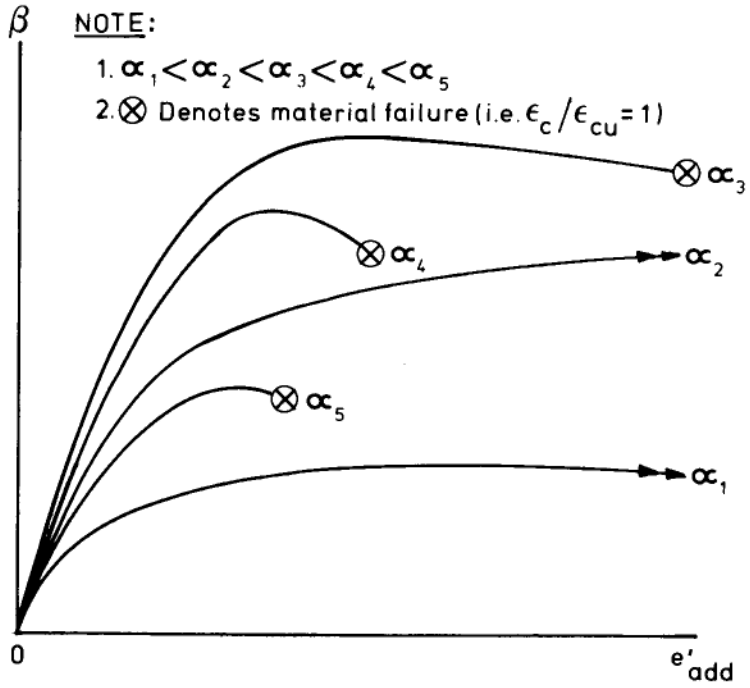

Figure 10.13 Typical ß–e'$_{add}$ curves for various values of α

Step 5: For a chosen α value, say α_1, read off *x/h*=a, b, c, d…, from Figure 10.12a. For *x/h*=a, b, c, d…, read off the corresponding values of β from Figure 10.12b and e'_{add} from Figure 10.12c.

Step 6: Repeat Step 5 for other α values. Then plot the moment-deflection curves (β–e'_{add}) for various α values, as shown in Figure 10.13.

The β–e'_{add} curves in Figure 10.13 can now be used to obtain the critical load of the column, using the procedure explained in Section 10.4.1 and Figure 10.7. It should be noted that the above steps can also be used to obtain moment-curvature curves (Wong, 1988). Details of the authors' computer program and worked examples of the method are given elsewhere (Kong *et al.,* 1986b; Wong 1987a).

10.4.3 *Stability analysis of columns: improved graphical methods*

10.4.3.1 Analytical expressions The basic concepts, as summarised in Sections 10.4.1 and 10.4.2 above, will now be extended to derive several analytical expressions which have powerful applications. First, it is convenient to express the parameters α and ß explicitly in terms of $\varepsilon_c/\varepsilon_{cu}$ and *x/h*.

Consider the strain compatibility conditions in Figures 10.10b and 10.11b. The steel strain ε_{si} is

$$\varepsilon_{si} = \varepsilon_c \left[1 - \frac{d_i/h}{x/h} \right] \tag{10.17}$$

and hence the steel stress f_{si} is

$$f_{si} = E_{si}\, \varepsilon_c \left[1 - \frac{d_i/h}{x/h} \right] \leq f_{yi} \tag{10.18}$$

where f_{yi} and E_{si} are the yield stress and Young's modulus, respectively, of the ith layer of steel. Therefore, ε_{si} and hence f_{si} are completely defined by the values assigned to ε_c and x/h in other words, they are completely defined by the values assigned to $\varepsilon_c/\varepsilon_{cu}$ and x/h. Substituting Eqn 10.18 into Eqns 10.13 and 10.14 and rearranging,

$$\alpha = \alpha_c + K_1 \frac{\varepsilon_c/\varepsilon_{cu}}{x/h} + K_2 \frac{\varepsilon_c}{\varepsilon_{cu}} + MM \tag{10.19}$$

$$\beta = \alpha_c \left[\frac{1}{2} - k_2 \frac{x}{h} \right] + K_3 \frac{\varepsilon_c/\varepsilon_{cu}}{x/h} + K_4 \frac{\varepsilon_c}{\varepsilon_{cu}} + NN \tag{10.20}$$

where α is defined by Eqns 10.12 (or 10.15) and k_2 is defined by Eqn 10.10; the values of K_1, K_2, K_3, K_4, MM and NN are defined in Eqn 10.21

$$K_1 = \sum_i \left[-\rho_i \frac{d_i}{h} \right] r_i \frac{E_{si}}{f_{cu}} \varepsilon_{cu} = \sum_i L_{1i}\, r_i \frac{E_{si}}{f_{cu}} \varepsilon_{cu} \tag{10.21a}$$

$$K_2 = \sum_i [\rho_i]\, r_i \frac{E_{si}}{f_{cu}} \varepsilon_{cu} = \sum_i L_{2i}\, r_i \frac{E_{si}}{f_{cu}} \varepsilon_{cu} \tag{10.21b}$$

$$K_3 = \sum_i \left\{ -\rho_i \frac{d_i}{h} \left[\frac{1}{2} - \frac{d_i}{h} \right] \right\} r_i \frac{E_{si}}{f_{cu}} \varepsilon_{cu} = \sum_i L_{3i}\, r_i \frac{E_{si}}{f_{cu}} \varepsilon_{cu} \tag{10.21c}$$

$$K_4 = \sum_i \left\{ \rho_i \left[\frac{1}{2} - \frac{d_i}{h} \right] \right\} r_i \frac{E_{si}}{f_{cu}} \varepsilon_{cu} = \sum_i L_{4i}\, r_i \frac{E_{si}}{f_{cu}} \varepsilon_{cu} \tag{10.21d}$$

$$MM = \sum_i m_i \tag{10.21e}$$

$$NN = \sum_i n_i \tag{10.21f}$$

where the values of r_i, m_i and n_i are as shown in Table 10.1.

Table 10.1 Summary of values of ri, mi and n_i

	Yield in tension[1]	Elastic tension or compression[2]	Yield in compression[3]
r_i	0	1	0
m_i	$-\rho_i [f_{yi}/f_{cu}]$	0	$\rho_i [f_{yi}/f_{cu}]$
n_i	$m_i [0.5 - d_i/h]$	0	$m_i [0.5 - d_i/h]$

1. Figure 10.16a. 2. Figure 10.16b and c. 3. Figure 10.16d.

For any given column section, Eqns 10.19, and 10.20 and 10.16 (and Table 10.1) show that the quantities α, ß and ϵ'_{add} are completely defined by the ratios x/h and $\varepsilon_c/\varepsilon_{cu}$. Substituting Eqn 10.12 into Eqn 10.19 to eliminate α_c and rearranging,

$$\frac{\dfrac{1}{\varepsilon_{cu}}\displaystyle\int_{\varepsilon'_c}^{\varepsilon_c} \frac{f\left(\dfrac{\varepsilon}{\varepsilon_{cu}}\right)}{f_{cu}}\,d\varepsilon}{\dfrac{\varepsilon_c}{\varepsilon_{cu}}}\left[\frac{x}{h}\right]^2 + \left[K_2\frac{\varepsilon_c}{\varepsilon_{cu}} + MM - \alpha\right]\left[\frac{x}{h}\right] + K_1\frac{\varepsilon_c}{\varepsilon_{cu}} = 0 \qquad (10.22)$$

That is,

$$a\left[\frac{x}{h}\right]^2 + b\left[\frac{x}{h}\right] + c = 0 \qquad (10.23)$$

where

$$a = \frac{\dfrac{1}{\varepsilon_{cu}}\displaystyle\int_{\varepsilon'_c}^{\varepsilon_c} \frac{f\left(\dfrac{\varepsilon}{\varepsilon_{cu}}\right)}{f_{cu}}\,d\varepsilon}{\dfrac{\varepsilon_c}{\varepsilon_{cu}}} \qquad (10.24a)$$

$$b = K_2\frac{\varepsilon_c}{\varepsilon_{cu}} + MM - \alpha \qquad (10.24b)$$

$$c = K_1\frac{\varepsilon_c}{\varepsilon_{cu}} \qquad (10.24c)$$

and K_1, K_2 and MM are defined by Eqns 10.21a, 10.21b and 10.21e respectively. Therefore, at any point on a moment-deflection curve for a specified value of α, the concrete strain ratio $\varepsilon_c/\varepsilon_{cu}$ and the neutral axis depth ratio x/h are related by Eqn 10.23. If the concrete strain ratio, say $[\varepsilon_c/\varepsilon_{cu}]_1$, at a certain point on a moment-deflection curve for a particular value of α can somehow be found, then the corresponding neutral axis depth ratio, say $[x/h]_1$, can be found by solving Eqn 10.23. Hence, the values of ß and e'_{add} at that point on the moment-deflection curve can be calculated by substituting the pair $\{[\varepsilon_C/\varepsilon_{cu}]_1, [x/h]_1\}$ into Eqns 10.20 and 10.16 respectively.

It is now clear that, for a given value of α, a complete β–e'_{add} curve can be constructed by the appropriate solution of Eqn 10.23 for different $\varepsilon_c/\varepsilon_{cu}$ ratios (see Section 10.4.3.3 later). Before the detailed procedure for preparing the whole family of β–e'_{add} curves is given, it is necessary to examine some of their properties.

10.4.3.2. Some properties of β–e'_{add} curves

With reference to Figures 10.14 and 10.15, the main properties relevant to constructing the β–e'_{add} curve may be summarised as follows (Kong and Wong, 1987):

i) On a β–e'_{add} curve for a given value of α (Figure 10.14), the neutral axis depth ratio x/h decreases with e'_{add} while the concrete strain ratio $\varepsilon_c/\varepsilon_{cu}$ increases with e'_{add} until $\varepsilon_c/\varepsilon_{cu}=1$, when the curve terminates (see point D in Figure 10.14).

ii) Consider again a typical β–e'_{add} curve for a given value of α, as shown in Figure 10.14. The figure is divided into two regions by the

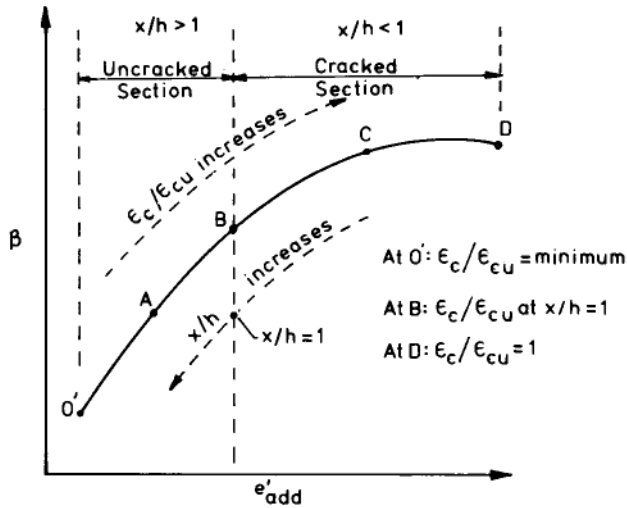

Figure 10.14 Variation of x/h and $\varepsilon_c/\varepsilon_{cu}$ along a typical β–e'_{add} curve

vertical line at x/h=1, which intersects the curve at *B*. To the left of *B*, x/h>1 and the column sections are uncracked; to the right of B, x/h<1 and the column sections are cracked. It turns out that the $\varepsilon_c/\varepsilon_{cu}$ value of a point is a useful reference. Let $[\varepsilon_c/\varepsilon_{cu}]_{x/h=1}$ denote the value of $\varepsilon_c/\varepsilon_{cu}$ at the point where x/h=1, i.e. at the point B. To the left of the line x/h=1, the $\varepsilon_c/\varepsilon_{cu}$ of any point (e.g. point A) will be less than $[\varepsilon_c/\varepsilon_{cu}]_{x/h=1}$. To the right of the line x/h=1, the $\varepsilon_c/\varepsilon_{cu}$ value of any point (e.g. point *C*) will be greater than $[\varepsilon_c/\varepsilon_{cu}]_{x/h=1}$. In other words we can test as follows:

On a β–e'_{add} curve for given value of α, the column section is uncracked (x/h>1) whenever $\varepsilon_c/\varepsilon_{cu}$ is less than $[\varepsilon_c/\varepsilon_{cu}]_{x/h=1}$; the section is cracked (x/h<1) whenever $\varepsilon_c/\varepsilon_{cu}$ is greater than $[\varepsilon_c/\varepsilon_{cu}]_{x/h=1}$. The value of $[\varepsilon_c/\varepsilon_{cu}]_{x/h=1}$ can be obtained from Eqn 10.23 using x/h=1 (Kong and Wong, 1987).

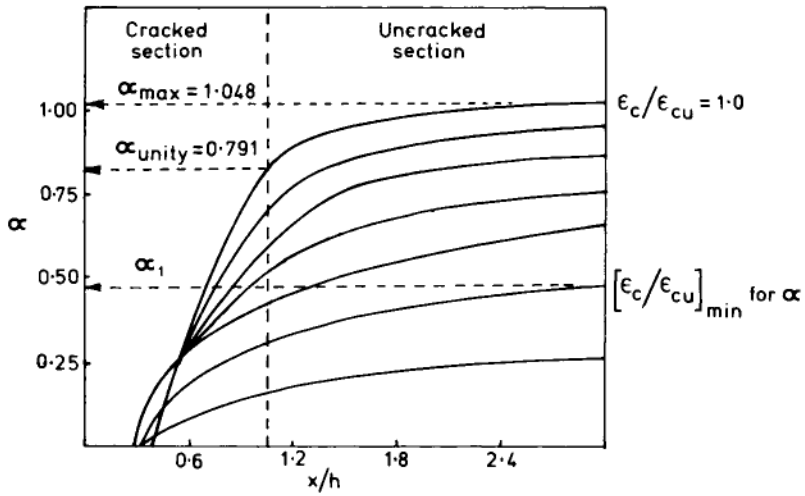

Figure 10.15 Typical a-x/h curves

iii) Figure 10.15 shows that for a given value of α there exists a minimum concrete strain ratio, referred to as $[\varepsilon_c/\varepsilon_{cu}]_{min}$, below which the β–e'_{add} curve does not exist. Since $[\varepsilon_c/\varepsilon_{cu}]_{min}$ is greater than zero, it follows that the β–e'_{add} curve does not start at the origin. In Figure 10.14 the curve is shown to start at a point 0', where $\varepsilon_c/\varepsilon_{cu}=[\varepsilon_c/\varepsilon_{cu}]_{min}$ for the α value of that particular curve. $[\varepsilon_c/\varepsilon_{cu}]_{min}$ can be obtained from Eqn 10.23 with a sufficiently large value of x/h (say x/h=5; see Figure 10.15).

iv) Figure 10.15 shows that at $\alpha=\alpha_{unity,}$ $\varepsilon_c/\varepsilon_{cu}$=1, and x/h=1 occur simultaneously. Following the arguments (i) and (ii) above, for

$\alpha \geq \alpha_{unity,}$ the entire β–e'_{add} curve corresponds to uncracked sections (i.e. curve *BCD* in Figure 10.14 does not exist). The value of α_{unity} can be found from Eqn 10.19 with $\varepsilon_c/\varepsilon_{cu}=1$ and $x/h=1$.

v) It is convenient, and sufficiently accurate, to consider that the strength capacity of a section is reached (i.e. $\alpha=\alpha_{max}$ in Figure 10.15) when the concrete strain reaches ε_{cu} simultaneously as the *nth* layer of reinforcement yields in compression. The value of α_{max} can be found from Eqn 10.19 with $\varepsilon_c/\varepsilon_{cu}=1$ and $x/h=[x/h]_{ycn}$, where $[x/h]_{ycn}$ is the x/h ratio at which the *nth* layer of reinforcement yields in compression (see Eqn 10.26b). When $\alpha>\alpha_{max}$, the section may be considered to have crushed; hence equilibrium is not possible and Eqn 10.23 is not solvable.

10.4.3.3 Solution of Equation 10.23 On a β–e'_{add} curve for any particular value of α, if the concrete strain ratio $\varepsilon_c/\varepsilon_{cu}$ is known at any point, then the corresponding value of x/h ratio at that point can be found by solving Eqn 10.23. Suppose for the time being, two simplifying assumptions are made:

Assumption (i) No reinforcement reaches its yield strength, i.e. $f_{si}<f_{yi}$ at all points on the β–e'_{add} curve for the particular value of α.

Assumption (ii) For any positive values assigned to α and $\varepsilon_c/\varepsilon_{cu}$, Eqn 10.23 is solvable for a real and positive root (i.e. for a real and positive x/h).

As a result of Assumption (i), $r_i=1$ and $m_i=0$ (see Table 10.1) and hence b and c become constant. Suppose the concrete strain ratio $\varepsilon_c/\varepsilon_{cu}$ at a certain point on a β–e'_{add} curve for a given value of α is known, then the corresponding x/h ratio at the point can be determined from Eqn 10.23 as follows:

Case 1: $\varepsilon_c/\varepsilon_{cu} \leq [\varepsilon_c/\varepsilon_{cu}]_{x/h=1}$
Reference to Figure 10.14 makes it clear that the point lies to the left of *B;* that is $x/h \geq 1$ and the section is *uncracked*. Hence, in Eqn 10.24a, the limit of integration ε'_c is itself a function of x/h (see Section 10.4.2.3). Therefore, in Eqn 10.23 the coefficient a is a function of x/h; the solution of Eqn 10.23 requires an iterative method, say the bisection method (Conte and Boor, 1980).

Case 2: $\varepsilon_c/\varepsilon_{cu} > [\varepsilon_c/\varepsilon_{cu}]_{x/h=1}$
The point now lies to the right of *B* in Figure 10.14; that is $x/h<1$ and the section is *cracked*. Hence, in Eqn 10.24a, $\varepsilon'_c=0$ (see Figure 10.11b). Eqn 10.23 is therefore a quadratic equation, the roots of which are

$$\frac{x}{h} = \frac{-b \pm [b^2 - 4ac]^{1/2}}{2a} \tag{10.25}$$

However, neither Assumption (i) nor Assumption (ii) is always true. In practice, some or all of the reinforcement may reach their yield strengths at certain values of α and $\varepsilon_c/\varepsilon_{cu}$. Therefore, for given values of α and $\varepsilon_c/\varepsilon_{cu}$, a trial and error procedure is required to determine the coefficients *b* and *c*, and hence *x/h* from Eqn 10.23.

With reference to (iii) and (v) of Section 10.4.3.2, Assumption (ii) is valid if, and only if, α is less than α_{max} and the concrete strain ratio $\varepsilon_c/\varepsilon_{cu}$ exceeds $[\varepsilon_c/\varepsilon_{cu}]_{min}$ for that value of α.

In practice, three cases should be considered:

Case A: Assumption (ii) is not valid.
If Assumption (ii) is not valid, there is no solution to Eqn 10.23. Indeed, the situation is unreal and there is no need to seek a solution.

Case B: Assumption (i) and (ii) are both valid.
Use procedure described in Case 1 or 2 above.

Case C: Assumption (i) is not valid; Assumption (ii) is valid.
A trial and error procedure is required to solved Eqn 10.23, until the root *x/h* satisfies both the compatibility condition and the equilibrium condition, as explained below.

Consider the column section in Figure 10.16. For a specified value of ε_c, i.e. $\varepsilon_c/\varepsilon_{cu}$, each layer of reinforcement may be in one of the following three conditions:

(i) Yield in tension, if $\dfrac{x}{h} \le \left[\dfrac{x}{h}\right]_{yti}$ (Figure 10.16a)

(ii) Elastic (tension or compression), if

$$\left[\frac{x}{h}\right]_{yti} < \frac{x}{h} < \left[\frac{x}{h}\right]_{yci} \qquad \text{(Figure. 10.16b and c)}$$

(iii) Yield in compression, if

$$\left[\frac{x}{h}\right]_{yci} \le \frac{x}{h} \qquad \text{(Fig. 10.16d)}$$

where $[x/h]_{yti}$ and $[x/h]_{yci}$ are, respectively, the neutral axis depth ratios, at which the ith layer of reinforcement yields in tension and compression; they are readily calculated from the geometry of Figure 10.16.

$$\left[\frac{x}{h}\right]_{yti} = \left[\frac{\varepsilon_c}{\varepsilon_c + \varepsilon_{yi}}\right]\frac{d_i}{h} \qquad (10.26a)$$

$$\left[\frac{x}{h}\right]_{yci} = \left[\frac{\varepsilon_c}{\varepsilon_c - \varepsilon_{yi}}\right]\frac{d_i}{h} \qquad (10.26b)$$

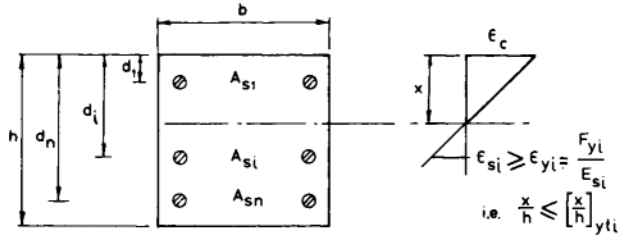

(a) A_{si} yield in tension.

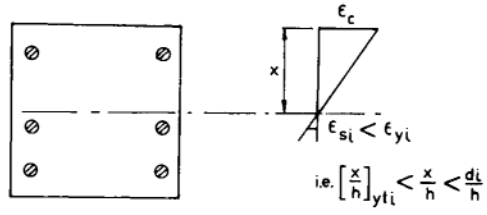

(b) A_{si} elastic in tension

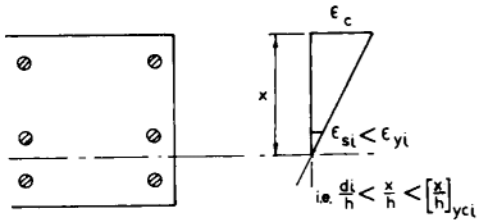

(c) A_{si} elastic in compression

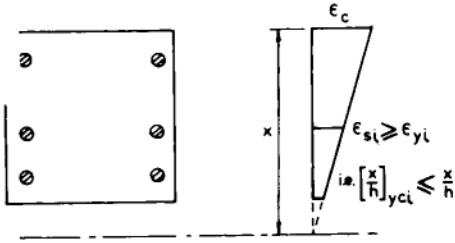

(d) A_{si} yield in compression

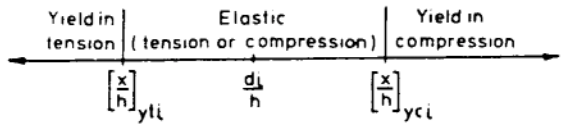

(e) 3 possible intervals of x/h for A_{si}

Figure 10.16 Column section—3 possible intervals of *x/h* for each layer of steel.

For a column section with a single layer of steel there are three possible conditions. By drawing simple sketches similar to those in Figure 10.16, the reader can verify that for two layers of steel there will be 3+2 conditions, for three layers there will be 3+2+2 and so on. Therefore, for a column section with n layers of steel, there will be

$$3+2(n\text{-}1)=2n+1$$

possible conditions, within which some, or all, of the reinforcement may reach their yield strengths. It follows that the values of the parameters K_1 to *NN*, and hence the coefficients *b* and *c*, have at most $2n+1$ possible combinations. The condition of compatibility is satisfied, if the root of Eqn 10.23 is within the *x/h* interval, where *b* and *c* are calculated. If the root of Eqn 10.23 so calculated satisfies Eqn 10.19, the condition of equilibrium is achieved.

10.4.3.4 Preparation of β–e'_{add} *curves—An interval technique* The procedure for preparing the moment-deflection (β–e'_{add}) curves may be summarised as follows.

Step 1: Determine α_{unity} and α_{max} (see (iv) and (v) of Section 10.4.3.2).

Step 2: Select a convenient positive α value, say α_1, such that $\alpha_1<\alpha_{max}$, where α_{max} is determined in Step 1.

Step 3: Determine the concrete strain ratio $\varepsilon_c/\varepsilon_{cu}$ at $x/h=1$, i.e. $[\varepsilon_c/\varepsilon_{cu}]_{x/h=1}$, for the α chosen in Step 2 (see (ii) of Section 10.4.3.2).

Step 4: Determine the initial portion of the β–e'_{add} curve for the *uncracked section* (i.e. curve 0'*AB* of Figure 10.14).

(a) With reference to Figure 10.9a, select a concrete strain ratio $\varepsilon_c/\varepsilon_{cu}$, such that $0<\varepsilon_c/\varepsilon_{cu}\leq[\varepsilon_c/\varepsilon_{cu}]_{x/h=1}$, where $[\varepsilon_c/\varepsilon_{cu}]_{x/h=1}$ is determined in Step 3.

(b) With reference to Figure 10.16 calculate, for each layer of steel, the ratios $[x/h]_{yti}$ and $[x/h]_{yci}$ from Eqns 10.26a and b. Therefore, for a section with n layers of reinforcement, there are 2n such *x/h* ratios.

(c) From the *x/h* ratios calculated in Step 4b, select those with values greater than or equal to 1. Then arrange the selected *x/h* ratios in ascending order. For example,

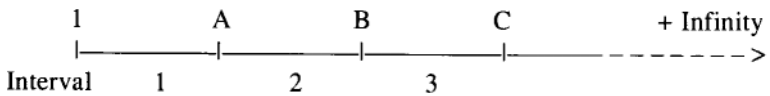

where *A, B, C* and so on are the selected *x/h* ratios.

(d) Choose an interval from Step 4c, say interval No.1: [1, A]. Calculate the values of *K1, K*$_2$ and *MM* from Eqns 10.21a, b and e, and the coefficients *b* and *c* of Eqn 10.23 from Eqns 10.24b and c. Then solve Eqn 10.23 as a non-linear equation, using an iterative method. If the root of Eqn 10.23 is positive and real, proceed to Step 4e; otherwise repeat Step 4d for other intervals of *x/h*. If Eqn 10.23 is not solvable in any one of the intervals of *x/h* determined in Step 4c, the selected concrete strain ratio $\varepsilon_c/\varepsilon_{cu}$ is less than the minimum possible value $[\varepsilon_c/\varepsilon_{cu}]_{min}$ for that chosen α (see (iii) of Section 10.4.3.2). Then return to Step 4a using a larger value of $\varepsilon_c/\varepsilon_{cu}$.

(e) If the root obtained in Step 4d is within the interval of *x/h* chosen in Step 4d, the condition of compatibility is satisfied; then proceed to Step 4f. Otherwise, return to Step 4d for other intervals of *x/h*.

(f) Calculate the force parameter, say α'_1 by substituting the pair $[\varepsilon_c/\varepsilon_{cu}, x/h]$ into Eqn 10.19 where the $\varepsilon_c/\varepsilon_{cu}$ is chosen in Step 4a and the *x/h* is the root of Eqn 10.23 as obtained in Step 4d and checked in Step 4e. The condition of equilibrium is considered satisfied if $|\alpha'_1,-\alpha_1|<$TOL, where a_1 is the axial force ratio chosen in Step 2 and TOL is a small number, say 1.0×10^{-4}. If the equilibrium is not satisfied, return to Step 4d for other intervals of *x/h*.

(g) For the $\varepsilon_c/\varepsilon_{cu}$ chosen in Step 4a and the *x/h* determined in Step 4d and checked in Steps 4e and 4f, calculate K_3, K_4 and *NN* from Eqns 10.21c, d and f. Then calculate the corresponding values of ß and e'_{add} from Eqns 10.20 and 10.16.

(h) Repeat Steps 4a to 4g for other concrete strain ratios $\varepsilon_c/\varepsilon_{cu}$ until sufficient pairs of [ß, e'_{add}] are obtained for plotting the initial portion of the moment-deflection curve, for instance, curve 0'*AB* of Figure 10.14.

Step 5: If the α value selected in Step 2 is less than α_{unity} (see (iv) of Section 10.4.3.2), proceed to Step 6. Otherwise, the moment-deflection curve determined in Step 4 represents the entire moment-deflection curve for the selected α value. Then return to Step 2 for other α values, if required.

Step 6: Determine the portion of the β–e'_{add} curve for the *cracked section* (i.e. curve *BCD* of Figure 10.14).

(a) With reference to Figure 10.9a, select a concrete strain ratio $\varepsilon_c/\varepsilon_{cu}$, such that $[\varepsilon_c/\varepsilon_{cu}]_{x/h=1}<\varepsilon_c/\varepsilon_{cu}\leq1$. Then calculate the coefficient a from Eqn 10.24a by putting $\varepsilon'_c=0$.

(b) With reference to Figure 10.16 calculate the 2n values of the *x/h* ratios from Eqns 10.26a and b as in Step 4b.

(c) From the *x/h* ratios calculated in Step 6b above, select those within the range [*x/h*=0; *x/h*=1]. Then arrange the selected *x/h* ratios in ascending order. For example,

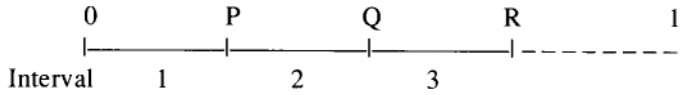

Where *P, Q, R* and so on are the selected *x/h* ratios.

(d) Choose an interval from Step 6c, say interval No.1: [0, P]. Calculate K_1, K_2 and *MM* from Eqns 10.21a, b and e and the coefficients *b* and c of Eqn 10.23 from Eqn 10.24b and c. Then determine the positive real root from Eqn 10.25.

(e) If the root obtained in Step 6d is within the interval of *x/h* chosen in Step 6d, the condition of compatibility is satisfied and proceed to Step 6f; otherwise, return to Step 6d for other intervals of *x/h*.

(f) Calculate the force parameter, say α'_1 by substituting the pair [$\varepsilon_c/\varepsilon_{cu}$, *x/h*] into Eqn 10.19 where $\varepsilon_c/\varepsilon_{cu}$ is chosen in Step 6a and the *x/h* is determined and checked in Step 6d and Step 6e, respectively. The condition of equilibrium is considered satisfied if $|\alpha'_1-\alpha_1|<TOL$, where α_1 is the axial force ratio chosen in Step 2 and TOL is a small number, say 1.0×10^{-4}. If the equilibrium condition is not satisfied, return to Step 6d for other intervals of *x/h*.

(g) For the $\varepsilon_c/\varepsilon_{cu}$ chosen in Step 6a, and the *x/h* determined in Step 6d and checked in Steps 6e and 6f, calculate K_3, K_4, and *NN* from Eqns 10.21c, d and f. Then calculate the corresponding values of ß and e'_{add} from Eqn 10.20 and 10.16.

(h) Repeat Steps 6a–6g for other concrete strain ratios $\varepsilon_c/\varepsilon_{cu}$ until sufficient pairs of [ß, e'_{add}] are obtained for plotting the second portion of the moment-deflection curve (i.e. the portion *BCD* of Figure 10.14).

Step 7: Repeat Steps 2–6 for other a values. Then plot the moment-deflection curves (ß–e'_{add}) for various α values, as shown in Figure 10.13.

Details of the authors' computer program and worked examples for the method are given elsewhere (Kong and Wong, 1987; Wong, 1987a).

10.4.4 *Stability analysis of columns: analytical method*

The two methods described in Sections 10.4.2 and 10.4.3 require manual manipulation of machine-generated curves, which would be a disadvantage when graphical facilities are not readily available or when substantial

amount of analysis is required. In this section, an analytical method is presented for the direct determination of the buckling load of slender columns.

10.4.4.1 Conditions of instability failures It is explained in Section 10.4.1 that, at the point c in Figure 10.7b, the column is in unstable equilibrium and the following two requirements are satisfied simultaneously:

i) the line *ac* touches the β–e'_{add} curve for $\alpha=\alpha_i$;
ii) the line *ac* itself has a slope $\phi=\alpha_i$

The requirements (i) and (ii) can be represented by the following expressions.

$$\left[\frac{d\beta}{de'_{add}}\right]_{c_1}=\left[\frac{d\beta_t}{de'_{add}}\right]_{a_1c_1}=\alpha_1 \tag{10.27a}$$

i.e.
$$\left[\frac{d\beta}{de'_{add}}\right]_{c_1}-\alpha_1=0 \tag{10.27b}$$

where $[d(\beta)/d(e'_{add})]_c$ is the slope of the β–e'_{add} curve for α_i at the point *c* in Figure 10.7b; $[d(\beta)/d(e'_{add})]_{ac}$ is the slope of the straight line *a-c*.

Also, at the point *c* in Figure 10.7b,

$$\beta_t=\beta$$

i.e.
$$\beta-\beta_t=0 \tag{10.28a}$$

or, from Eqn 10.2

$$\beta-\alpha_i\,[e'+e'_{add}]=0 \tag{10.28b}$$

Note that Eqn 10.27 guarantees that the line *a-c* having a slope α is tangential to the β–e'_{add} curve for α at c, and Eqn 10.28 guarantees that the point *a* is at a distance *e*' to the left of the origin 0 (see Figure 10.7b).

Next, consider Figure 10.17a. The line a_1-c_1 has a slope equal to α_1 and the point a_1 is at a distance e'_1 ($=e_1/h$) to the left of the origin 0. Suppose the line a_1-c_1 touches the β–e'_{add} curve for $\alpha=\alpha_1$ at c_1, then from Eqn 10.27.

$$\left[\frac{d\beta}{de'_{add}}\right]_{c_1}=\left[\frac{d\beta_t}{de'_{add}}\right]_{a_1c_1}=\alpha_1 \tag{10.29a}$$

i.e.
$$\left[\frac{d\beta}{de'_{add}}\right]_{c_1}-\alpha_1=0 \tag{10.29b}$$

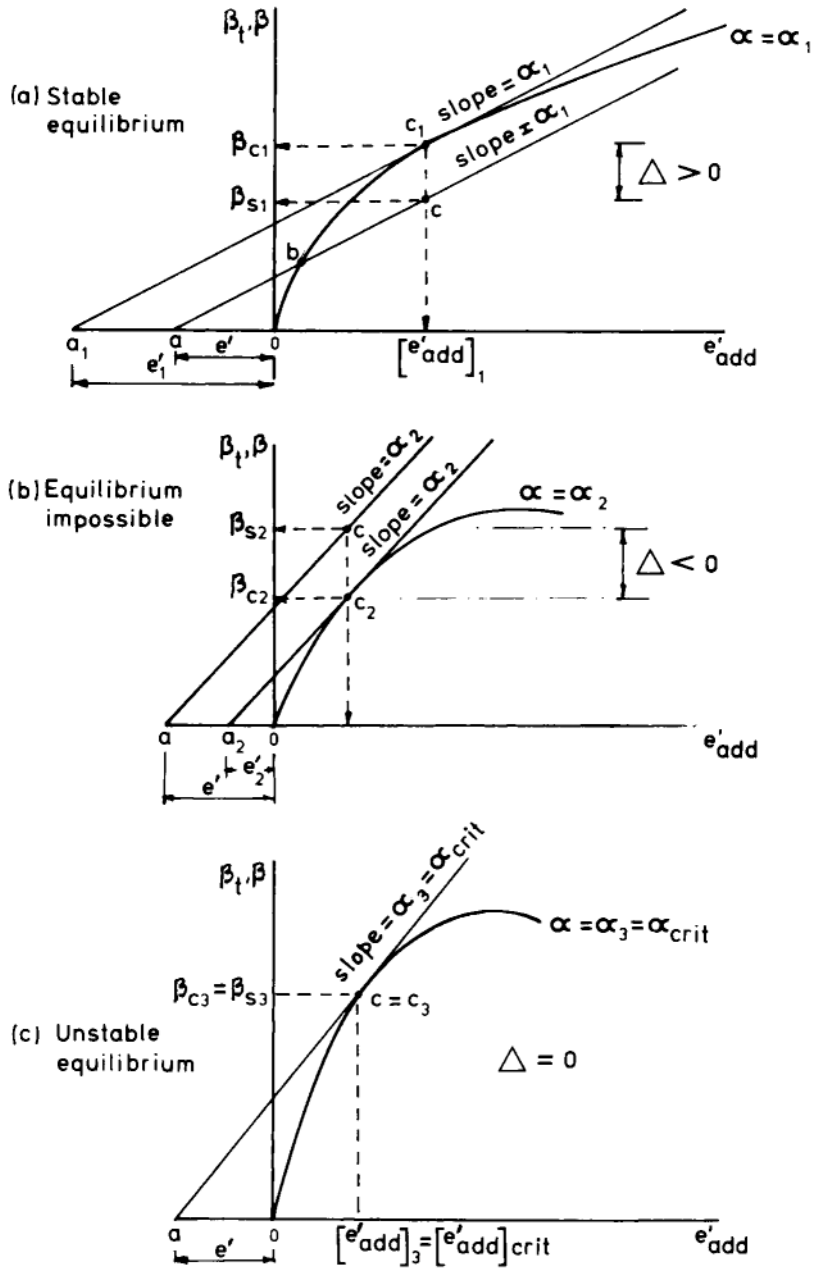

Figure 10.17 Stability analysis of column—an analytical method

where $[d(\beta)/d(e'_{add})]_{c_1}$ is the slope of the β–e'_{add} curve for α_1 at the point c_1 in Figure 10.17a; $[d(\beta_t)/d(e'_{add})]_{a_1c_1}$ is the slope of the straight line a_1-c_1.

Suppose the line *a*-*b*-*c* in Figure 10.17a is parallel to line a_1-c_1 and the point *a* is at a distance *e*' to the left of the origin 0, where $e' < e'_1$. It is clear from Figure 10.17a that the difference Δ between the values of ß at c_1 on the β–e'_{add} curve for a_1 and that at *c* on the line *a*-*b*-*c* is greater than zero. That is,

$$\Delta = \beta_{c_2} - \beta_{s_2} < 0 \tag{10.31a}$$

or, from Eqn 10.2,

$$\Delta = \beta_{c_2} - \alpha_2 [e' + (e'_{add})_2] < 0 \tag{10.31b}$$

where β_{c_1} is the value of ß on the β–e'_{add} curve for the value of α_1 at c_1; β_{s_1} is the value of ß on the line *a*-*c* at c.

Following the arguments in Section 10.4.1, it is clear that the column is in stable equilibrium at *b* (Figure 10.17a). That is, $\alpha_1 < \alpha_{crit}$.

In Figure 10.17b, the lines a_2-c_2 and *a*-*c* are parallel and have slopes equal to $\alpha 2$. The line a_2-c_2 touches the moment-deflection curve for α_2 at the point c_2; hence Eqn 10.27b holds at c_2. Since the line *a*-*c* is above the line a_2-c_2 (i.e. $e' > e'_2$) in Figure 10.17b, the difference Δ between the value of ß at c_2 on the β–e'_{add} curve for α_2 and that at *c* on the line *a*-*b*-*c* is less than zero. That is

$$\Delta = \beta_{c_2} - \beta_{s_2} < 0 \tag{10.31a}$$

or, from Eqn 10.2,

$$\Delta = \beta_{c_2} - \alpha_2 [e' + (e'_{add})_2] < 0 \tag{10.31b}$$

where β_{c_2} and β_{s_2} are as shown in Figure 10.17b.

In this case, the external moment M_t (i.e. $ß_t$ value on the line *a*-*c*) always exceeds the internal moment *M* (i.e. the ß value on the β–e'_{add} curve for α_2 in Figure 10.17b) and equilibrium is impossible. That is, $\alpha_2 > \alpha_{crit}$.

In Figure 10.17c, the line *a*-*c* having a slope equal to α_3 touches the β–e'_{add} curve for α_3 at c_3, (i.e. at c). The column is in unstable equilibrium, that is, $\alpha = \alpha_{crit}$. In this case,

$$\Delta = \beta_{c_3} - \beta_{s_3} = 0 \tag{10.32a}$$

or, from Eqn 10.2,

$$\Delta = \beta_{c_3} - \alpha_3 [e' + (e'_{add})_3] = 0 \tag{10.32b}$$

where β_{c_3} and β_{s_3} are shown in Figure 10.17c.

Before further discussion of the implication of Eqns 10.30, 10.31 and 10.32, it is helpful to define the general expression for Δ:

$$\Delta = \beta - \alpha [e' + e'_{add}] \tag{10.33}$$

where the pair [e'_{add}, ß] are the coordinates at a point on the β–e'_{add} curve for α.

With reference to Figure 10.17 and based on the above discussions, it can be concluded that the equilibrium of a slender column can be related to the value of Δ, calculated from Eqn 10.33 as follows.

Condition 1: Δ>0
This corresponds to stable equilibrium, as shown at the point *b* in Figure 10.17a.

Condition 2: Δ<0
This corresponds to the condition that equilibrium is impossible, as shown in Figure 10.17b.

Condition 3: Δ=0
This corresponds to unstable equilibrium, as shown at the point *c* in Figure 10.17c.

10.4.4.2 Analytical expressions for instability failures As explained in Section 10.4.4.1, the slope at a point on a β–e'_{add} curve for α is defined by the derivative $d(\beta)/d(e'_{add})$, where ß is given by Eqn 10.20. The derivative can be rewritten as

$$\frac{d\beta}{de'_{add}} = \frac{d\beta}{d\,[x/h]} \cdot \frac{d\,[x/h]}{de'_{add}} \tag{10.34}$$

Considering the derivatives $dß/d(x/h)$ and $d(x/h)/d(e'_{add})$ separately, it can be shown that (Wong, 1987a)

$$\frac{d\beta}{de'_{add}} = \frac{1}{B}\left\{\frac{d\alpha_c}{d\,[x/h]}\left[\frac{1}{2}\left(\frac{x}{h}\right)^2 - k_2\left(\frac{x}{h}\right)^3\right]\right.$$

$$\left. - k_2\alpha_c\left(\frac{x}{h}\right)^2 - K_3\left(\frac{\varepsilon_c}{\varepsilon_{cu}}\right)\right\} \tag{10.35}$$

where

$$B = -\left(\frac{\varepsilon_{cu}}{n^2}\right)\left(\frac{L}{h}\right)^2\left(\frac{\varepsilon_c}{\varepsilon_{cu}}\right) \tag{10.36}$$

and k_2, K_3, and α_c are as defined before.

If the value of the concrete strain ε_c and that of the neutral axis depth x (i.e. the values of the pair [$\varepsilon_c/\varepsilon_{cu}$, x/h] at a certain point on the β–e'_{add} curve for α are known, Eqn 10.35 can be used to calculate the slope of the β–e'_{add} curve at that point.

Suppose the slope at a point on the β–e'_{add} curve for a particular value of α is equal to α (Eqn 10.27), then substituting Eqn 10.19 (for α) and Eqn 10.35 (for) $d(\beta)/d(e'_{add})$ into Eqn 10.27b, and rearranging

$$\frac{1}{B}\left[\frac{d\alpha_c}{d[x/h]}\right]\left[k_2\left(\frac{x}{h}\right)^4-\frac{1}{2}\left(\frac{x}{h}\right)^3\right]+\alpha_c\left[\frac{k_2}{B}\left(\frac{x}{h}\right)^3+\left(\frac{x}{h}\right)\right]$$
$$+\left[K_2\left(\frac{\varepsilon_c}{\varepsilon_{cu}}\right)+\frac{K_3}{B}\left(\frac{\varepsilon_c}{\varepsilon_{cu}}\right)+MM\right]\left(\frac{x}{h}\right)+K_1\left(\frac{\varepsilon_c}{\varepsilon_{cu}}\right)=0 \qquad (10.37)$$

Substituting Eqn 10.5 into Eqn 10.12, the parameter α_c can be expressed as

$$\alpha_c=\frac{A}{\varepsilon_c f_{cu}}\left(\frac{x}{h}\right) \qquad (10.38)$$

where A is given by Eqn 10.5. Hence,

$$\frac{d\alpha_c}{d\,[x/h]}=\frac{A}{\varepsilon_c f_{cu}}+\left[\frac{x/h}{\varepsilon_c f_{cu}}\right]\frac{dA}{d\,[x/h]} \qquad (10.39)$$

Substituting Eqns 10.38 and 10.39 into Eqn 10.37, and rearranging,

$$a_5\left[\frac{x}{h}\right]^5+a_4\left[\frac{x}{h}\right]^4+a_3\left[\frac{x}{h}\right]^3+a_2\left[\frac{x}{h}\right]^2+a_1\left[\frac{x}{h}\right]+a_0=0 \qquad (10.40)$$

where

$$a_5=\left[\frac{k_2}{B\varepsilon_c f_{cu}}\right]\cdot\frac{dA}{d\,[x/h]} \qquad (10.41a)$$

$$a_4=\left[\frac{1}{2B\varepsilon_c f_{cu}}\right]\left[4Ak_2-\frac{dA}{d\,[x/h]}\right] \qquad (10.41b)$$

$$a_3=-\frac{A}{2B\varepsilon_c f_{cu}} \qquad (10.41c)$$

$$a_2=\frac{A}{\varepsilon_c f_{cu}} \qquad (10.41d)$$

$$a_1=K_2\frac{\varepsilon_c}{\varepsilon_{cu}}+\left[\frac{K_3}{B}\right]\frac{\varepsilon_c}{\varepsilon_{cu}}+MM \qquad (10.41e)$$

and

$$a_0=K_4\frac{\varepsilon_c}{\varepsilon_{cu}} \qquad (10.41f)$$

where A is defined by Eqn 10.5; B is defined by Eqn 10.36; k_2 is defined by Eqn 10.10; K_2, K_3, K_4 and MM are defined by Eqns 10.21b, c, d, and e, respectively.

For an *uncracked section* (i.e. $x/h\geq 1$), the area A (see Eqn 10.5) under the stress-strain curve in Figure 10.9a, between $\varepsilon=\varepsilon'_c=\varepsilon_c[1-1/(x/h)]$ and $\varepsilon=\varepsilon_c$, is completely defined by the concrete strain ε_c and the neutral axis depth x. Hence, for a given value of ε_c (i.e. of $\varepsilon_c/\varepsilon_{cu}$), the values of A and the

derivative $\{d(A)/d(x/h)\}$ (and hence the coefficients a_5, a_4, a_3, a_2) depend on the value of x (i.e. of x/h). It follows that, for a given value of $\varepsilon_c/\varepsilon_{cu}$, Eqn 10.40 is a non-linear equation in x/h, the solution of which requires an iterative procedure such as the bisection method (Conte and Boor, 1984).

For a *cracked section* (i.e. $x/h<1$), the area A (see Eqn 10.5) under the stress-strain curve in Figure 10.9a, between $\varepsilon=\varepsilon'_c=0$ and $\varepsilon=\varepsilon_c$, is completely defined by the concrete strain ε_c. For a given value of $\varepsilon_c/\varepsilon_{cu}$, A is constant and hence the derivative $d(A)/d(x/h)$ is equal to zero. It follows that the coefficient a_5 becomes zero and the coefficients a_4, a_3, a_2 become constant. Therefore, for a cracked section, Eqn 10.40 becomes a quartic equation (i.e. an algebraical equation of the fourth degree). That is,

$$a_4\left[\frac{x}{h}\right]^4+a_3\left[\frac{x}{h}\right]^3+a_2\left[\frac{x}{h}\right]^2+a_1\left[\frac{x}{h}\right]+a_0=0 \qquad (10.42)$$

where

$$a_4=\frac{aAk_2}{B\varepsilon_c f_{cu}} \qquad (10.43)$$

and a_3, a_2, a_1 and a_0 are as defined by Eqns 10.41c, d, e and f respectively.

Following the argument in Section 10.4.3.3, it should be noted that there are at most $2n+1$ possible combination of values for the coefficients $[a_1, a_0]$ (as they depend on K_2, K_3, K_4, MM) irrespective of whether the section is uncracked or cracked, where n is the number of layers of reinforcement.

It is now clear that Eqns 10.40 and 10.42 define the relationship between the concrete strain ε_c and the neutral axis depth x (i.e. $\varepsilon_c/\varepsilon_{cu}$ and x/h) at a point on a moment-deflecting β–e'_{add} curve, where the slope is equal to the values of α for constructing the β–e'_{add} curve. However, at that point on the β–e'_{add} curve it is not known whether the section is uncracked (i.e. $x/h\geq1$) or cracked (i.e. $x/h<1$). Therefore, for a given concrete strain ratio $\varepsilon_c/\varepsilon_{cu}$, a trial and error procedure similar to that described in Section 10.4.3.3 is required to determine the corresponding neutral axis depth ratio x/h at that point on the β–e'_{add} curve. Further details of solving Eqns 10.40 and 10.42 are given elsewhere (Wong, 1987a).

10.4.4.3 Procedure for determining column buckling loads

The procedure for determining column buckling loads can be outlined as follows:

Step 1: Select a convenient value for the concrete strain ratio $\varepsilon_c/\varepsilon_{cu}$ between the interval [0,1].

Step 2: Solve Eqn 10.27 (i.e. Eqn 10.40 or 10.42) for the correct value of x/h, as explained in Section 10.4.4.2.

Step 3: For a concrete strain ratio $\varepsilon_c/\varepsilon_{cu}$ selected in Step 1 and the neutral axis depth ratio x/h determined in Step 2, the values of α, ß, and e'_{add} are calculated from Eqn 10.19, 10.20 and 10.16, respectively. The

pair [e'_{add}, ß] so determined are the coordinates at a point on the β–e'_{add} curve for α, and the slope at the point is equal to α.

Step 4: Calculate the value of Δ from Eqn 10.33. There are three cases to consider:

(a) If Δ exceeds zero (i.e. Condition 1), the column is in stable equilibrium; instability failure would occur at a higher concrete strain ε_c (i.e. higher $\varepsilon_c/\varepsilon_{cu}$ ratio).
Repeat the calculations from Step 1 for a larger value of $\varepsilon_c/\varepsilon_{cu}$.

(b) If Δ is less than zero (i.e. Condition 2), it is impossible for the column to attain equilibrium; instability failure would occur at lower concrete strain ε_c (i.e. lower $\varepsilon_c/\varepsilon_{cu}$ ratio). Repeat the calculations from Step 1 for a smaller value of $\varepsilon_c/\varepsilon_{cu}$.

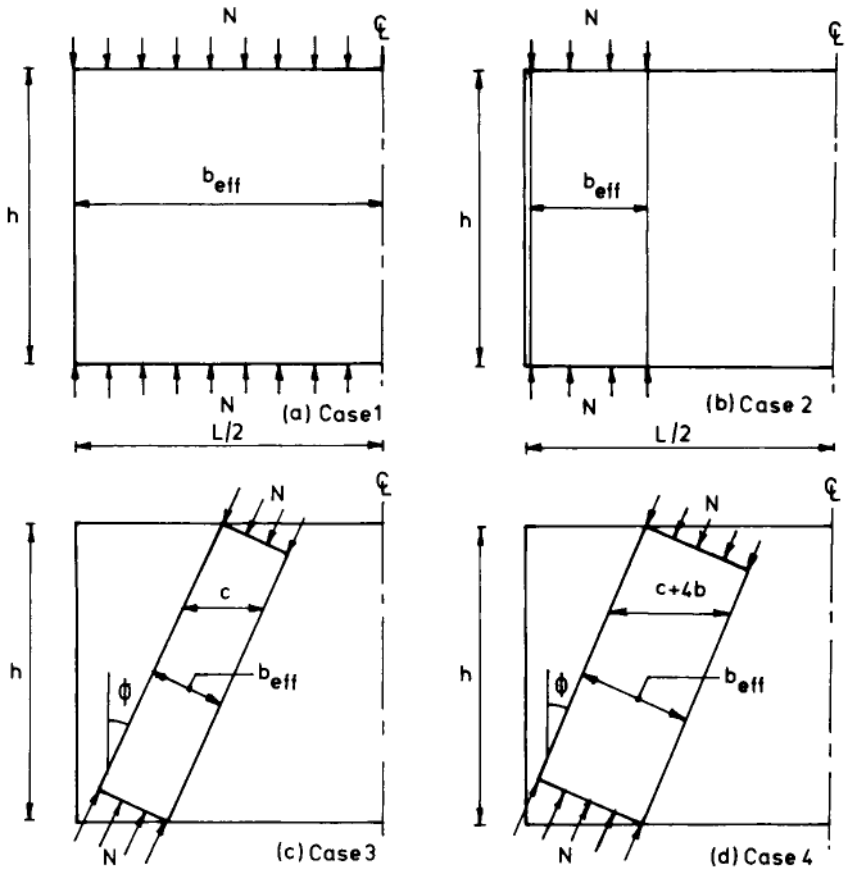

Figure 10.18 Equivalent-column method—effective column widths

(c) If Δ is equal to zero (i.e. Condition 3), or more realistically, if Δ is within a small tolerance of zero, 1.OE-4 say, then the column is considered to be at incipient instability failure. That is, the current value of α is equal to, or sufficiently close to α_{crit}. Hence the column buckling load N_{crit} can be calculated from Eqn 10.4.

The steps described above assume that instability failures always precede material failures. However, for a general computer program, the possibility of material failure should be considered. Because of space limitation it is not considered here.

10.5 Stability analysis of slender deep beams: the equivalent-column method

Based on the method presented in Section 10.4, the buckling strength of a deep beam is calculated as that of two 'equivalent columns', each joining a loading block to a support reaction block, as shown in Figure 10.18. Each column is of rectangular cross section b by b_{eff}, where b is the actual thickness of the deep beam and b_{eff} is the effective column width. As an exploratory investigation, four effective column widths will be considered:

Case 1: (Figure 10.18a). The effective width b_{eff} of each equivalent column is taken as $L/2$, where L is the overall length of the beam. The buckling load P of the deep beam is then taken as $2N$, where N is the buckling load of an equivalent column. Case 1 is equivalent to analysing the deep beam as a wide column.

Case 2: (Figure 10.18b) $b$eff is taken as c, where c is the width of each of the stiff bearing blocks at the loading and support points. $P=2N$, as in Case 1.

Case 3: (Figure 10.18c). Here the equivalent-column axis is the line joining the loading and support reaction points, inclined at an angle ϕ to the vertical. b_{eff} is taken as $c \cos \phi$. The buckling load P of the beam is taken as $2N \cos \phi$.

Case 4: (Figure 10.18d). Cae 4 is as Case 3, except that b_{eff} is taken as $(c+4b) \cos \phi$, where b is the beam thickness and $(c+4b)$ is the effective width recommended by Clause 14.2.4 of the ACI Code (ACI Committee 318, 1983) for walls under concentrated loads.

The effective reinforcement for each equivalent column is taken as the average amount of reinforcement in the direction of the equivalent-column axis.

10.6 Deep beam buckling: comparison with test results

Table 10.2 shows that the measured buckling loads of the authors' 38 test beams (Kong *et al.,* 1986a) together with the predictions by the CIRIA

Guide and the Equivalent-Column method of Section 10.4 this chapter. In Table 10.2, the predictions of the CIRIA Guide's Supplementary Rules supersede those published earlier (Kong *et al.,* 1986a; Kong and Wong, 1986) which were incorrect, as explained elsewhere (Kong *et al.,* 1987; Wong 1987a). The concrete stress-strain relationship used to calculate the equivalent-column loads is that proposed by Desayi and Krishnan (1964). With reference to Table 10.2, several observations can be made:

i) All the three CIRIA methods were safe and conservative. When used in conjunction with BS 8110, the mean factors of safety are: R_{SR}=35.63, R_{SP}=13.06 and R_{TP}=7.06. Therefore, the relative conservatism of the CIRIA Guide method was in the descending order: the supplementary rules, the single-panel method and the two-panel method. As shown in Table 10.2, the supplementary rules and the single-panel method were often too conservative, particularly for the very slender beams of *h/b* ratio of 33 or more, and could lead to factors of safety exceeding 60. The two-panel method gave the most realistic results; the R_{TP} values ranged from about 2 to 15, with many values in the region of 8.

ii) A closer scrutiny of Table 10.2 shows that the conservatism of the CIRIA methods increased sharply as the height/thickness ratio *h/b* increased, and decreased gradually as the load-eccentricity/thickness ratio *e/b* increased.

iii) Of the three methods given by CIRIA Guide, the supplementary rules are the easiest to use, the single-panel method is more difficult to use, and the two-panel method even more so. Table 10.2 shows that the two-panel method gave the most realistic results, while the supplementary rules gave the least realistic results. In practical design, therefore, it is worthwhile to move straight to the two-panel method, by-passing the supplementary rules and the single-panel method. Even when the deep beam is such that the easier to use supplementary rules are applicable, the supplementary rules should be used merely as a preliminary check of the adequacy of the deep beam against buckling failure.

iv) The 'equivalent-column' method generally gave comparatively better predictions than those obtained by the CIRIA Guide.

v) The last three columns of Table 10.2 show that Cases 2, 3 and 4 (mean R_{EC2}=2.65; R_{EC3}=3.03; R_{EC4}=2.02) lead to quite realistic results, indicating that the equivalent-column approach is potentially a useful tool for the buckling analysis and design of slender concrete deep beams. It should be noted that Cases 3 and 4 of Figure 10.18 suggests that the buckling strengths of slender deep beams would increase with the width *c* of the bearings, which is yet to be confirmed by tests (Wong, 1987a). The Case 1 results (mean R_{EC1}=0.72) show that the effective width b_{eff} in Figure 10.18a is too large, as expected.

Table 10.2 Buckling loads—comparison of test results with CIRIA Guide predictions and equivalent—column predictions.

+ Beam	Experimental failure load	CIRIA Guide used with BS 8110			Equivalent-column Method			
					Case 1	Case 2	Case 3	Case 4
	kN	R_{SR}	R_{SP}	R_{TP}	R_{EC1}	R_{EC2}	R_{EC3}	R_{EC4}
A-67-0.2	148	64.23	29.10	13.47	1.48	5.47	6.37	4.83
A-50-0.2	360	67.40	28.75	19.93	1.56	5.78	6.67	4.73
A-40-0.2	420	48.26	18.68	9.74	0.95	3.50	4.05	2.68
A-33-0.2	560	40.65	13.32	7.89	0.64	2.38	2.76	1.70
A-29-0.2	682	32.32	8.79	5.97	0.54	2.01	2.33	1.37
A-25-0.2	620	19.65	5.08	3.46	0.44	1.64	1.90	1.06
A-50-0.05	440							
A-40-0.05	534	Specimens failed in shear						
A-33-0.05	620							
B-67-0.2	120	52.00	23.55	10.91	1.18	4.38	4.83	3.76
B-50-0.2	146	29.10	13.47	6.13	2.28	8.41	9.35	6.82
B-40-0.2	340	38.98	15.05	7.86	0.74	2.75	3.02	1.99
B-33-0.2	560	40.87	13.53	7.95	0.68	2.53	2.77	1.74
B-29-0.2	420	21.90	7.00	4.20	0.51	1.90	2.11	1.25
B-25-0.2	700	21.59	5.12	3.73	0.42	1.56	1.69	0.96
B-50-0.05	460							
B-40-0.05	550	Specimens failed in shear						
B-33-0.05	692							
C-67-0.1	60	26.91	12.13	5.64	0.47	1.73	2.00	1.54
C-50-0.1	120	27.40	11.41	5.63	0.35	1.30	1.52	1.06
C-40-0.1	270	35.67	13.17	7.13	0.41	1.51	1.77	1.16
C-33-0.1	450	36.92	11.65	7.12	0.48	1.76	2.05	1.28
C-29-0.1	550	28.30	7.18	5.15	0.40	1.48	1.72	1.01
D-40-0.1	300	24.68	10.13	5.06	0.51	1.89	2.13	1.41
D-33-0.1	340	14.23	5.19	2.83	0.40	1.48	1.69	1.05
D-29-0.1	538	14.99	5.20	2.93	0.46	1.69	1.93	1.13
E-67-0.1		Specimen failed by vertical splitting						
E-50-0.1	200	51.02	21.26	10.49	0.67	2.46	2.86	2.01
E-40-0.1	502	74.02	27.36	14.81	0.86	3.18	3.70	2.43
E-33-0.1	440	40.66	13.04	7.86	0.57	2.11	2.47	1.51
E-29-0.1	700	39.46	9.47	7.13	0.49	1.82	2.12	1.24
E-25-0.1	560	19.74	4.04	3.28	0.31	1.15	1.33	0.74
E-67-0.2		Specimen damaged (accident)						
E-50-0.2	170	44.76	19.55	9.30	1.16	4.29	5.05	3.50
E-40-0.2	210	32.93	13.39	6.73	0.73	2.83	3.28	2.14
E-33-0.2	300	29.92	10.97	5.96	0.64	2.35	2.74	1.67
E-29-0.2	400	26.45	8.53	5.10	0.58	2.14	2.48	1.43
E-25-0.2	540	23.99	6.67	4.43	0.54	2.01	2.32	1.27
Mean		35.63	13.06	7.06	0.72	2.65	3.03	2.02
Standard Deviation		15.04	7.14	3.20	0.43	1.60	1.80	1.40

\+ Beam notation as defined elsewhere (Kong *et al.*, 1986a)

vi) Table 10.2 shows that the conservatism of the equivalent-column method tended to increase slightly with the *h/b* and *e/b* ratios.

10.7 Concluding remarks

Test data in the literature on the buckling strength of deep beams are few, probably because experiments on slender deep beams are comparatively difficult and hazardous to carry out. It is believed that the tests reported by the authors and their colleagues (Kong *et al.,* 1986a; Wong, 1987a) represent most of the experimental data available to date on slender concrete deep beams. These tests have revealed that the failure mode and the failure load of slender deep beams depended strongly upon the *h/b* and *e/b* ratios. More recent tests have also shown that the failure mode and the failure load of slender deep beams depended upon concrete strength, the amount and arrangement of web reinforcement (Wong, 1987a). The effects of other parameters such as lateral restraints, width of bearings, loading arrangements, creep buckling under long-term loading have yet to be studied.

The tests by the authors and their colleagues, which for the first time enabled the CIRIA's methods to be checked against experimental values, show that the CIRIA Guide methods could be very conservative, and suggest that the equivalent-column method is a potentially useful tool for the design and analysis of slender concrete deep beams. By choosing suitable effective widths, the equivalent-column method may be extended to cover slender deep beams with restrained vertical edges.

References

Albritton, G.E. (1965) Review of literature pertaining to the analysis of deep beams. Technical Report No. 1–701, U.S. Army Engineer Waterways Experimental Station, Vicksburg, Miss.

American Concrete Institute (1971) *Design of precast concrete wall panels.* ACI Committee 533 Proceedings of the American Concrete Institute, **68,** 7: 504.

American Concrete Institute. (1983, revised 1986) *Building code requirements for reinforced concrete.* ACI Committee 318. American Concrete Institute, Detroit.

American Concrete Institute (1984) *State-of-the-art report on the high strength concrete.* ACI Proceedings of the American Concrete Institute **81,** 4: 364.

Andrews. R.D. (1978) Buckling of concrete—a review. Transport and Road Research Laboratory, Crowthorne, Supplementary Report 430.

Beal, A.N. (1986) The design of slender columns. *Proc. Inst. Civ. Engrs.,* Part 2, **81:** 397.

Besser, I.I. and Cusens, A.R. (1984) Reinforced concrete deep beams panels with high depth/span ratios. *Proc. Inst. Civ. Engrs.* Part 2, **77:** 265.

British Standard Institution (1972) *The structural use of concrete.* CP110, BS1, London, Part 1.

British Standards Institution (1985) *The structural use of concrete* BS 8 110: 1985British Standards Institution. London, Part 1.

Canadian Standards Association (1984) *Design of concrete structures for buildings.* CAN3-A23. 3-M84, CSA, Rexdale.

Cement and Concrete Institution (1969) *Bibliography on deep beams.* Library Bibliography No. Ch. 71(3/69). Cement and Concrete Association. London.
Clarke, J.L. and Pomeroy, C.D. (1985) Concrete opportunities for the structural engineer. *Stru. Engr.* **63A** 2: 45–53
Cognini, S., Dezi, L. and Menditto, G., Speranzini, E. (1987). Viscoelastic moment-curvature diagrams. *Am. Con. Inst. Mat. J.* **84,** No.6, 519–524.
Comité Européen de Béton—Fédération Internationale de la Précontrainte. (1978) *Model code for concrete structures.* English Edition, Cement and Concrete Association, London.
Construction Industry Research and Information Association. (1977) *The design of deep beams in reinforced concrete.* CIRIA Guide 2. Ove Arup & Partners and CIRIA, London.
Conte, S.D. and Boor, C.D. (1980) Elementary numerical analysis-an algorithm approach. McGraw-Hill Kogakusha Ltd., Tokyo: 74, 81, 295–303.
Cranston, W.B. (1972). Analysis and design of reinforced concrete columns. Research Report 20, Cement and Concrete Association.
Desayi. P. and Krishnan, S. (1964) Equation for the stress-strain curve for concrete. *Proc. Am. Conc. Inst.* **61,** 3: 345.
Kong, F.K. (1986a). Reinforced concrete deep beams. Being Chapter 6 of *Concrete Framed Structures—Stability and Strength,* ed. Narayanan, R.Elsevier Applied Science Publishers, London: chap 6: 169.
Kong, F.K. (1986b) Reinforced concrete deep beams. Lecture delivered at Ove Arup and Partners, London, 3 October.
Kong, F.K. and Evans, R.H. (1987) *Reinforced and Prestressed Concrete.* Van Nostrand Reinhold (UK) Ltd., 3rd Edn.: 175, 273.
Kong, F.K. and Singh, A. (1972) Diagonal cracking and ultimate loads of lightweight concrete deep beams. *Proc. Am. Conc. Inst.* **69,** 8: 513.
Kong, F.K. and Wong, H.H.A. (1986) Computer modelling of the collapse behaviour of slender concrete deep beams. Proc. Res. Sem. *The Behaviour of Concrete Structures.* Cement and Concrete Association: 182.
Kong, F.K. and Wong, H.H.A. (1987) Buckling failure of slender concrete columns—a computer method of prediction. Proc. 1st Int. Conf. Struc. Failure, Singapore Conc. Inst. and Nanyang Technological Institute, Singapore: J15.
Kong, F.K. and Wong, H.H.A. (1988) Computer-aided design of concrete columns: an interval technique. Proc. 2nd Int. Conf. on Computer Applications in Concrete, Singapore Conc. Inst. and Nanyang Technological Institute, Singapore: L1.
Kong, F.K., Robins, P.J. and Cole, D.F. (1970) Web reinforcement effects on lightweight concrete deep beams. *Proc. Am. Conc. Inst.* **67,** 12: 1010.
Kong, F.K., Robins, P.J. and Sharp, G.R. (1975) The design of reinforced concrete deep beams in current practice. *Struc. Engr.* **53,** 4: 173.
Kong, F.K., Evans, R.H., Cohen, E. and Roll, F. (1983) *Handbook of Structural Concrete.* McGraw-Hill, New York.
Kong, F.K., Garcia, R.C., Paine, J.M., Wong, H.H.A., Tang, C.W.J., and Chemrouk, M. (1986a) Strength and stability of slender concrete deep beams. *Struc. Engr,* **64B,** 3: 49.
Kong, F.K., Paine, J.M. and Wong, H.H.A. (1986b) Computer-aided analysis and design of slender concrete columns. Proc. 1st Int. Conf. on Computer Applications in Concrete, Singapore Concrete Institute and Nanyang Technological Institute, Singapore: C68.
Kong, F.K., Tang, C.W.J., Wong, H.H.A. and Chemrouk, M, (1986c) Diagonal cracking of slender reinforced concrete deep beams. Proc. Res. Sem. *The Behaviour of Concrete Structures.* Cement and Concrete Association: 213.
Kong, F.K., Wong, H.H.A., Tang, C.W.J. and Chemrouk, M. (1987) Worked examples on the use of CIRIA Guide 2 to calculate the buckling strengths of slender concrete deep beams. Tech. Rep. 7/3 A. Dept. Civ. Eng., University of Newcastle upon Tyne.
Marshall, W.T. (1969) A survey of the problem of lateral instability in reinforced concrete beams. *Proc. Inst. Civ. Engrs.,* Part 2, 43: 397.
Portland Cement Association (1979) Tilt-up load-bearing walls—a design aid. PCA Publication No. EB074.02D., PCA, Illinois.
Portland Cement Association (1984) *Notes on ACI 318–83: Building code requirements for reinforced concrete with design applications.* 4th edn. PCA, Illinois: 18–1.
Whittle, R. (1986) *Deep beams: recent research at Newcastle University.* Report on the lecture delivered by F.K.Kong (1986b). Notes on Structures: 6, Ove Arup Parternship, London, 1.

Wong, H.H.A. (1987a) *Buckling and stability of slender reinforced concrete deep beams*. Ph.D, Thesis, University of Newcastle upon Tyne.
Wong, H.H.A. (1987b) Discussion of the paper by Beal (1986). *Proc. Inst. Civ. Engrs.* Part 2, **83:** 489.
Wong, H.H.A. (1988) Discussion of the paper of Cognini *et al* (1987). *Am. Conc. Inst. Mat. J.* **85.** 5: 472.
Wong, H.H.A. and Kong, F.K. (1986) Concrete codes—CP 110 and BS 8110. Verulam Letter. *Struc. Engr.* **64A** 12, 391.